RATIONAL DESIGN AND SYNTHESIS OF D-GALACTOSYL LYSOPHOSPHOLIPID AS SELECTIVE SUBSTRATES AND NON-ATP-COMPETITIVE INHIBITOR OF PHOSPHATIDYLINOSITOL PHOSPHATE KINASES

By

Mengxia Sun

A DISSERTATION

Submitted to
Michigan State University
in partial fulfillment of the requirements
for the degree of

Chemistry – Doctor of Philosophy

2022

ABSTRACT

Phosphatidylinositol phosphate kinases (PIPKs) produce lipid signaling molecules and have been attracting increasing attention as drug targets for cancer and viral infection. Given the potential cross-inhibition of kinases and other ATP-utilizing enzymes by ATP-competitive inhibitors, targeting the unique lipid substrate binding site represents a superior strategy for PIPK inhibition. Here, by taking advantage of the nearly identical stereochemistry between *myo*-inositol and D-galactose, we designed and synthesized a panel of D-galactosyl lysophospholipids, one of which was found to be a selective substrate of phosphatidylinositol 4-phosphate 5-kinase. Derivatization of this compound led to the discovery of a human PIKfyve inhibitor with an apparent IC_{50} of 6.2 μM, which significantly potentiated the inhibitory effect of Apilimod, an ATP-competitive PIKfyve inhibitor under clinical trials against SARS-CoV-2 infection and amyotrophic lateral sclerosis. Our results provide the proof of concept that D-galactose-based phosphoinositide mimetics can be developed into artificial substrates and new inhibitors of PIPKs. In addition, the activity loops of PIPKs were disordered in all crystal structures because of the membrane sensing mechanism. Here, through conjugation of a zebrafish PIP5Kα with maleimide functionalized lipid, the protein can be immobilized on nanodisc for structural characterization.

ACKNOWLEDGEMENTS

First and foremost, I would like to express my sincere gratitude to my advisor Dr. Xuefei Huang, for his continuous support throughout my PhD study. Dr. Huang is an intelligent and sagacious scientist at the chemistry-biology interface, especially in the carbohydrates field. He is a reliable advisor and mentor despite his incredibly busy schedule. I grateful for his leading into the carbohydrates study, appreciate his guidance in all the aspects of research as well as his encouragement to pursue innovative ideas.

I also would like to heartfelt thank my advisor and seconder reader Dr. Jian Hu for his invaluable guidance and support during my PhD study. As a chemistry student, I am deeply indebted to Dr. Hu for his guidance and patience during my study of molecular biology. His immense knowledge and experience have supported me to conquer all the difficulties in the research.

Besides, I would like to thank the rest of my doctoral committee, Dr. Jetze J. Tepe and Dr. Kevin D. Walker, for their insightful feedbacks, comments, and encouragement. I would also like to thank Dr. Dan Holmes, who trained me and provided me useful suggestions for NMR usage, and Dr. Anthony Schilmille in the Mass spectrometry& Metabolomics Core Facility, who trained me for high resolution mass spectrometry, ion-paired mass spectrometry, and tandem mass spectrometry. I also appreciate Dr. Dohun Pyeon and Canchai Yang for their help in the collaborative work, and Dr. Min Su from University of Michigan for generating Cryo-EM images.

I thank all the Huang group members: Dr. Jicheng Zhang, Dr. Changxin Huo, Dr. Peng Wang, Dr. Sherif Ramadan, Dr. Kedar Baryal, Dr. Jia Gao, Zibin Tan, Dr. Shuyao Lang, Dr. Zahra Rashidijahanabad, Dr. Hunter McFall-Boegeman, Dr. Kunli Liu, Shivangi Chugh, Chia-wei Yang, Po-han Lin, Dr. Tianlu Li, Dr. Xuanjun Wu, and Dr. Yuetao Zhao. Especially thank Dr. Weizhun

Yang, who gave me numerous useful suggestions for carbohydrates synthesis. I thank all the Hu lab members: Dr. Dexin Sui for his guidance in protein expression and purification, as well as all the other supports in molecular biology research, Dr. Chi Zhang for her supports in cell culture and confocal image, Dr. Yao Zhang for his help in nanodiscs construction, Dr. Tuo Zhang, Dr. Eziz Kuliyev, Yuhan Jiang, and Tianqi Wang. I also thank my friends for their support during this six-year life of PhD study.

Last but not least, I would like to thank my parents and my brother back in China, who have supported me all the time.

TABLE OF CONTENTS

LIST OF ABBREVIATIONS

Aß	Angiotensin-converting enzyme 2
ACE2	Alzheimer's disease
AD	Amyotrophic lateral sclerosis
ALS	Acute myeloid leukemia
AML	α-amino-3-hydroxy-5-methyl-4-isoxazolepropionic acid
AMPA	AMPA-type glutamate receptor
AMPAR	Antigen-presenting cell
APC	Amyloid precursor protein
APP	Adenosine triphosphate
ATP	tert-Butyloxycarbonyl
BOC	B-cell non-Hodgkin lymphoma
B-NHL	Chaperone containing TCP1
CCR	Conserved cysteine-rich
CCT	Cellular thermal shift assay
CETSA	Cation-independent mannose-6-phosphate receptor
CI-MPR	Charcot-Marie-Tooth syndrome
CMT4J	Central nervous system
CNS	Coronavirus disease 2019
COVID-2019	CP
Amyloid beta	CpG
	CRPC
	cryo-EM

CXCL10	Castration-resistant prostate cancer
DHPC	cryo-electron microscopy
DMPC	C-X-C motif chemokine ligand 10
DMPE	1,2-dihexanoyl-sn-glycero-3-phosphocholine
DMSO	1,2-Dimyristoyl-sn-glycero-3-phosphocholine
DRG	1,2-Dimyristoyl-sn-glycero-3-phosphoethanolamine
DS	Dimethyl sulfoxide
EGFR	Dorsal root ganglia
EMT	Down syndrome
ER	Epidermal growth factor receptor
FMDV	Mesenchymal transition
HDX	Edoplasmic reticulum
HTS	Foot-and-mouth disease virus
IFN-γ	Hydrogen–deuterium exchange
IL-12	High throughput screen
IL-23	Interferon gamma
IP_3	Interleukin 12
LAMP1	Interleukin 23
LC3	Inositol 1,4,5-trisphosphate
Cerebral palsy	Lysosomal-associated membrane protein 1
Cytosine–	Microtubule-associated proteins 1A/1B light chain 3B
guanine	LPS
dinucleotide	MAPK

MS	Mitogen-activated protein kinase
MTKI	Multiple sclerosis
MSP	Multi-tyrosine kinase inhibitor
mTOR	Membrane scaffold protein
NHS	Mammalian target of rapamycin
NFT	N-hydroxysuccinimide
OL	Neurofibrillary tangle
OLP	Oligodendrocyte
P21	OL precursor
PAMPs	Cyclin-dependent kinase inhibitor 1
PD-1	Pathogen-associated molecular pattern
$Pd(OH)_2$	Programmed cell death protein 1
PFF	Palladium hydroxide
PI	Fluorophore labeled preformed fibril
PI3K	Phosphatidylinositol
PI4K	Phosphoinositide 3-kinases
PIKfyve	Phosphatidylinositol 4-kinase
PI(3)P	FYVE finger-containing phosphoinositide kinase
$PI(3,4,5)P_3$	Phosphatidylinositol 3-phosphate
$PI(3,5)P_2$	Phosphatidylinositol 3,4,5-triphosphate
PI4P	Phosphatidylinositol 3,5-bisphosphate
Lipopolysacchari	Phosphatidylinositol 4-phosphate
de	$PI(4,5)P_2$

PI(5)P	Phosphatidylinositol 4,5-biphosphate
PIPK	Phosphatidylinositol 5-phosphate
PIP4K	Phosphatidylinositol phosphate kinase
PIP5K	phosphatidylinositol 5-phosphate 4-kinase
PKCε	Phosphatidylinositol 4-phosphate 5-kinase
PLC	Protein kinase Cε
PLS	Phospholipase C
PPIn	Primary lateral sclerosis
PRR	Phosphoinositides
PTEN	Pattern recognition receptor
RA	Phosphatase and tensin homolog
ROS	Rheumatoid arthritis
SAR	Reactive oxygen species
SARS-CoV-2	Structure–activity relationship
SHIP	Severe acute respiratory syndrome coronavirus 2
SLE	Src homology 2 domain containing inositol polyphosphate 5-phosphatase 1
sulfo-SMCC	Systemic lupus erythematosus
TBDPS	Sulfosuccinimidyl-4-(N-maleimidomethyl) cyclohexane-1-carboxylate
TEM	*tert*-butyldiphenylsilyl
TFA	Transmission electron microscopy
TGN	Trifluoroacetic acid
Th1	Trans-Golgi network
	Type 1 T helper cell

TLC	Thin-layer chromatography
TLR	Toll-like receptor
TMPRSS2	Transmembrane protease, serine 2
TRPML	Transient receptor potential cation channel
VSV	Enveloped vesicular stomatitis virus
WMI	White matter injury

Chapter 1 A Review of the Research Progress of Phosphatidylinositol Phosphate Kinases (PIPKs) and Their Inhibitors

1.1. Introduction

In 1949, Jordi Folch discovered a mixture of phosphatides when studying the brain extracts[1], which was the very first time that scientists became aware of phosphatidylinositols (PIs). Later in 1950s, the signaling function of PIs and phosphoinositides (PPIns) were discovered by Hokin and Hokin[2-5]. However, little was known about these phospholipids, until the discovery that PPIns were the source of second messengers responsible for the transduction of signals from extracellular into intracellular space[6]. Starting from then, more attention has been directed to the PPIns. Moreover, with the discovery and functional characterization of other rare PPIns, as well as PPIn-binding proteins and PPIn-metabolizing enzymes, this field has dramatically advanced.

Although only accounting for less than 1% of total phospholipids, PPIns play significant physiological roles in cellular and subcellular processes. PIs, as the precursor of PPIns, are synthesized primarily in the endoplasmic reticulum (ER) and then delivered to membranes of other subcellular compartments, via either vesicular transports or PI-transfer proteins[7]. Then, the reversible phosphorylation of the 3-, 4- and/or 5-positions on inositol ring results in the generation of seven naturally occurring PPIns. The generation of these different PPIns is spatially and temporally regulated by phosphoinositide kinases, phosphatases and phospholipases (**Fig 1.1**)[7].

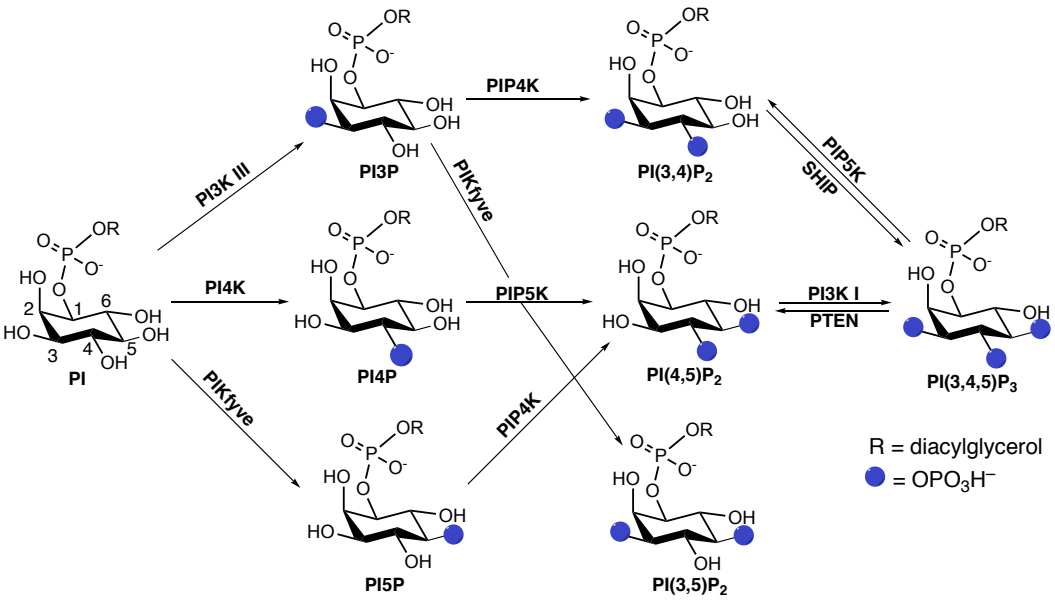

Figure 1.1. Interconversion of phosphoinositides and the enzymes involved in the transformations. Kinases: PI3K, phosphoinositide 3-kinases; PI4K, phosphatidylinositol 4-kinase; PIP4K, phosphatidylinositol 5-phosphate 4-kinase; PIP5K, phosphatidylinositol 4-phosphate 5- kinase; PIKfyve, FYVE finger-containing phosphoinositide kinase. Phosphatases: PTEN, Phosphatase and tensin homolog; SHIP, Src homology 2 domain containing inositol polyphosphate 5-phosphatase 1.

Each of the seven PPIns has a unique subcellular distribution with a predominant localization in subset of membranes (**Figure 1.2**). For example, the phosphatidylinositol 3-phosphate [PI(3)P] is concentrated in early endosome, whereas the phosphatidylinositol 3,5-bisphosphate [PI(3,5)P_2] is enriched in late endosomes and lysosomes. Moreover, because of the tightly controlled subcellular localization of the phosphoinositide kinases and phosphatases, the PPIns are spatially restricted and maintained at a steady-state level locally. Therefore, the PPIns subcellular distribution has been characterized as a code for organelle identity. Because of that, the PPIn interconversion is also used for subcellular compartment communication. Meanwhile, the changes of PPIns cellular level occur in a precise and reversible manner, which are affected by cellular changes and environmental stimuli. The diverse intracellular distribution and the complex synthesis pathways, together with the acute sense of the membrane dynamics and cellular

environment, make these phospholipids optimal mediators of signaling events in all cellular compartments.

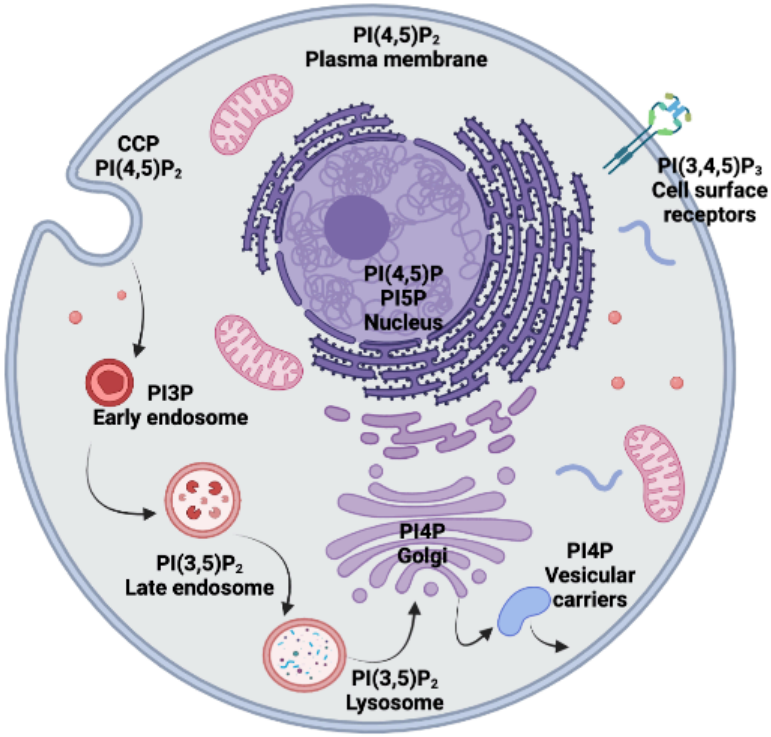

Figure 1.2. Predominant subcellular localization of phosphoinositides in a eukaryotic cell. Major organelles are shown and labeled. CCP: clathrin-coated pits.

As a second messenger, phosphatidylinositol 4,5-biphosphate [$PI(4,5)P_2$] is known to play an important role in signal transduction at the plasma membrane, where it transduces cellular signals through its metabolites (IP_3 and DAG after PLC hydrolysis) or fluctuations of its own levels[7]. $PI(4,5)P_2$ participates in the recruitment and activation of a wide variety of actin regulatory proteins at the plasma membrane, through cooperating with small GTPases, to regulate membrane cytoskeleton, cell shape, motility, and internalization pathways, such as endocytosis and phagocytosis. Indeed, the retention of $PI(4,5)P_2$ level at the plasma membrane is related to endocytosis, as it works as an important co-receptor for the recruitment and regulation of endocytic

proteins to the plasma membrane. And the rapid dissociation of endocytic factors following internalization require the removal of $PI(4,5)P_2$ from endocytic membranes. Meanwhile, phagocytosis requires $PI(4,5)P_2$ to stimulates actin nucleation, which means that binding of foreign particles to cell surface receptors produces $PI(4,5)P_2$, triggering the local polymerization of actin to initiate engulfing particles for cellular uptake. After that, mediated by phospholipase C (PLC), the metabolism of $PI(4,5)P_2$ triggers the release of actin and the fusion of phagosomes with endosome/lysosome compartment

PI3P is mainly localized at early endosomes and involved in endosomal trafficking. Meanwhile, PI3P is also found on autophagosomal membrane and related to autophagy regulation. In neural cells, PI3P is important in mediating neurotransmitters by regulating the level of cell surface receptors. In Alzheimer's disease patients, PI3P has been found to be selectively deficient in their brains, which may explain the role of PI3P played in neurodegeneration. In contrast, $PI(3,5)P_2$, one of the phosphorylation products of PI3P, is enriched in late endosomal and lysosomal membranes. The balance of synthesis and degradation of $PI(3,5)P_2$ is tightly regulated to allow this scarce PPIn to play important roles in mediating membrane trafficking, endocytic vesicle fission/fusion, and intracellular ion channel function.

Another important PPIn is $PI(3,4,5)P_3$, which is produced by phosphorylation of the 3-position of $PI(4,5)P_2$ by class I phosphoinositide 3-kinases (PI3K). As the product of PI3K and the activator of the serine/threonine-specific protein kinase (AKT) pathway, $PI(3,4,5)P_3$ plays key roles in regulating cell proliferation, differentiation, migration and metabolic changes. $PI(3,4,5)P_3$ can be broken down by phosphatase and tensin homolog (PTEN) via dephosphorylation, through which it regulates the cell cycle and other cellular events. Accordingly, PI3K hyperactivation and PTEN disfunction are linked to tumorigenesis.

In sum, the PPIns play their unique roles in cellular functions and aberration in cellular levels and subcellular distributions of PPIns is closely related to cell disfunctions, which may lead to diseases. Therefore, the lipid kinases which produce and/or process PPIns are vital for cell proper function. The three lipid kinase families responsible for biosynthesis of the PPIns are PI3K, phosphatidylinositol 4-kinase (PI4K), and PIPK. As my thesis work has been focusing on the PIPK family, I will review the PIPKs in terms of their roles played in diseases and the progress in the development of their inhibitors in this chapter.

The PIPK family members are responsible for the synthesis of phosphatidylinositol bisphosphates (PIP_2) from the singly phosphorylated PIs (**Figure 1.1 & Figure 1.3**). Phosphatidylinositol 4-phosphate 5-kinase (PIP5K, type I) produces the majority of $PI(4,5)P_2$ using PI4P as the substrate; phosphatidylinositol 5-phosphate 4-kinase (PIP4K, type II) generates $PI(4,5)P_2$ using PI5P as the substrate, possibly contributing to vesicular production of $PI(4,5)P_2$; and the third family member FYVE finger-containing phosphoinositide kinase (PIKfyve, type III) phosphorylates PI3P to produce $PI(3,5)P_2$, a phosphoinositide with very low abundance but critically involved in endosomal trafficking.

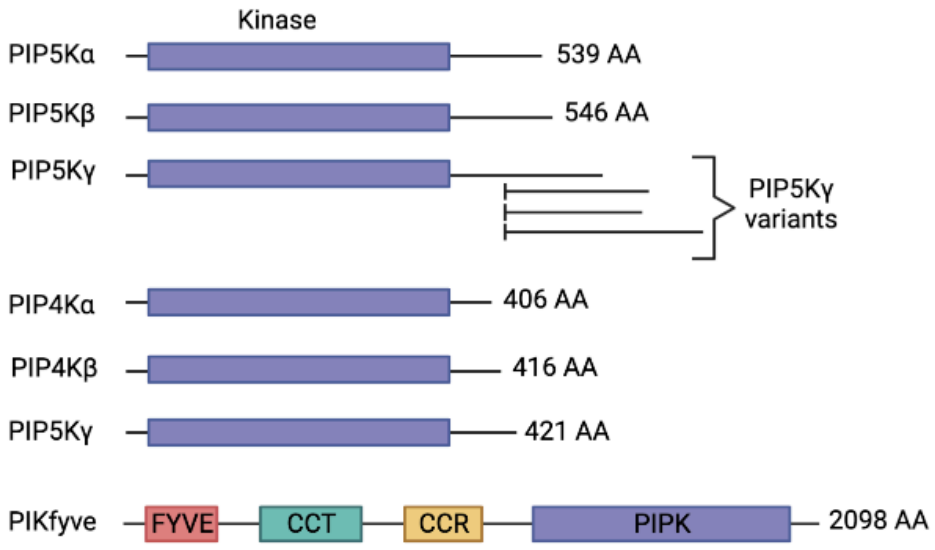

Figure 1.3. Domain organization of human PIP kinases[8]. Regulatory and catalytic regions (purple region) of each enzyme are shown. PIP5K, Phosphatidylinositol 4-phosphate 5- kinase; PIP4K, phosphatidylinositol 5-phosphate 4-kinase; PIKfyve, FYVE finger-containing phosphoinositide kinase; FYVE, FYVE zinc finger domain; CCT, chaperone-containing TCP1 domain; CCR, conserved cysteine-rich domain.

1.2.Type I PIPK - PIP5K

PIP5K is the major PIPK responsible for synthesis of PI(4,5)P_2 *in vivo*. To a lesser extent, PIP5K can also phosphorylate PI and PI3P at the 5-position to form PI5P and PI(3,5)P_2, respectively. Due to the substrate promiscuity of PIPKs, the phosphorylation of PI(3,4)P_2 at 5-position *in vivo* and phosphorylation of PI5P at 4-position *in vitro* were also observed[9]. There are three isoforms of PIP5K, i.e., PIP5Kα, PIP5Kβ and PIP5Kγ, which are encoded by three distinct genes *PIP5KA*, *B*, *C*, respectively. PIP5Kα and PIP5Kβ each has a molecular mass of approximately 64 kDa, while the size of PIP5Kγ varies depending on the splice variants (**Figure 1.3**)[10]. All the three PIPK proteins have a well-conserved kinase domain. Within the catalytic domain, all the three isoforms also contain a segment called the activation loop, which differs in

sequence among PIPKs and determines the substrate specificity[9-11]. By swapping the activation loop of PIP5K and PIP4K, the substrate specificity also switched[11].

The subcellular localization of different PIP5K isoforms has been characterized. The PIP5Kα is localized to the plasma membrane, Golgi complex and the membrane ruffling[10], whereas PIP5Kβ is found on vesicles in the perinuclear region as well as plasma membrane. In terms of PIP5Kγ, it is mainly localized at the focal adhesions through interaction with talin. Through the regulation of the local $PI(4,5)P_2$ production, PIP5Ks play crucial roles in numerous cellular functions, including regulation of the actin cytoskeleton, cell-cell adhesion, endo-, exo-, and phagocytosis, stress response, cell growth and apoptosis[10].

1.2.1. PIP5K and diseases

The PIP5K dysfunction has been linked with many diseases, such as cancer, viral infection, and neuronal disorders. As the major lipid kinase responsible for $PI(4,5)P_2$ synthesis and the precursor of $PI(3,4,5)P_3$, PIP5Ks are the upstream regulators of PI3K/Akt signaling pathway[12], and thus are involved in PI3K/Akt regulated cell growth and apoptosis. Meanwhile, clathrin-mediated endocytosis needs the local $PI(4,5)P_2$ production for its initiation[13]. Therefore, PIP5K plays a role in the viral and bacterial infections, because many viruses and bacteria hijack the clathrin-mediated endocytosis pathway for entry[14].

1.2.1.1. Cancer

The hyperactivation of PI3K/Akt in many types of cancer leads to the loss of PTEN and overexpression of PI3K (**Figure 1.4**)[12]. Many studies have been carried out to develop inhibitors of PI3K or agonist of PTEN for the treatment of cancer. However, little is known about how PIP5K, an upstream factor of PI3K/AKT pathway, contributes to the development and growth of cancer until recently. In 2014, Persson's group discovered that overexpression of PIP5Kα is

associated with poor prognosis in prostate cancer and correlated with an elevated level of the androgen receptor[15]. It has been observed that overexpression of PIP5Kα in PNT1A nonmalignant cells resulted in increased Akt activity and cell survival, as well as an invasive malignant phenotype; whereas siRNA-mediated knockdown of PIP5K1α in aggressive PC-3 cells led to reduced Akt activity and inhibition in tumor growth in xenograft mice[15]. These results suggested that PIP5Kα is a druggable target for cancer treatment, the inhibition of which may reduce the formation of tumor by blocking the PIP5Kα-associated PI3K/Akt and the downstream survival, proliferation, and invasion pathways.

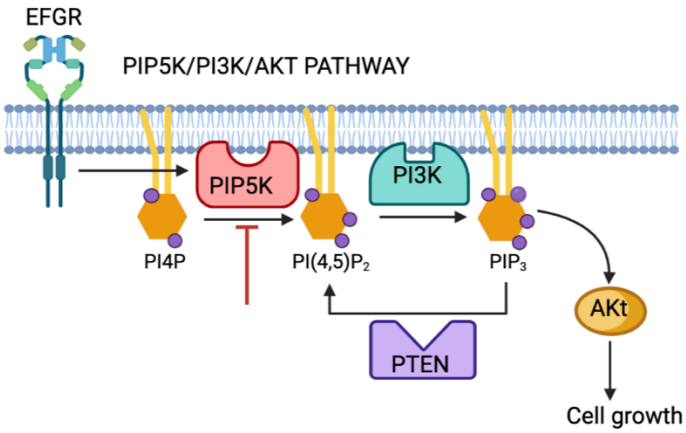

Figure 1.4. Schematic of downstream signaling pathway of PIP5K for cell growth[15].

Heretofore, although considerable progress has been made to improve the treatment of prostate cancer, one-third of treated prostate cancer patients experience disease recurrence and progress into castration-resistant prostate cancer (CRPC). Because of the increasing expression of androgen receptor (AR) variants lacking the ligand binding-domain, CRPC no longer responds to traditional anti-androgen therapies, like Enzalutamide (MDV3100) [16]. In 2016, Persson's group discovered that the expression level of one of the AR variants AR-V7 was positively correlated with that of PIP5Kα in tumor specimens from prostate cancer patients and that pharmacological

inhibition of PIP5Kα suppressed the growth and invasiveness of xenograft tumors overexpressing AR-V7[16]. This study provided a potential therapeutic strategy for treatment of CRPC.

Besides prostate cancer, PIP5Ks are related to breast cancer progression and metastasis. Because of the frequent occurrence of tumor relapse and metastasis, breast cancer, the most malignancies in woman, still needs significant studies to understand the underlying mechanism of metastasis and develop therapeutic strategies. In 2010, Yamaguchi et al. found that, in breast cancer cells, the formation of invadopodia requires $PI(4,5)P_2$. Invadopodia has the ability to degrade extracellular matrix (ECM), whose formation is related to the metastasis of breast cancer[17]. By using a real-time quantitative PCR analysis, they also confirmed that PIP5Kα is the dominant isoform expressed in MDA-MB-231 breast cancer cells, which is responsible for the synthesis of $PI(4,5)P_2$ and invadopodia formation. In addition, PIP5Kγ regulates focal adhesion assembly and cell migration, which is also critical for breast cancer metastasis. Chen and colleagues found that, upon stimulating by epidermal growth factor (EGF) and hepatocyte growth factor (HGF), PIP5Kγ could be phosphorylated, and the phosphorylation level was positively correlated with tumor grade[18], whereas deletion of PIP5Kγ inhibited cell proliferation, cell migration and invasion. All these results indicated that, PIPKIγ alone or as the downstream receptor of EGF and HGF, participates in breast cancer progression and can be a potential therapeutic target. Consistently, Anderson's group reported a Kaplan-Meier survival analysis, which showed significant inverse correlation between strong PIP5Kγ expression and overall patient survival[19]. Also, pharmacological inhibition of PIP5Kγ or knockdown suppressed the growth and invasiveness of MDA-MB-231 xenografts, indicating that PIP5K γ might be a potential target for the treatment of triple-negative and ER^+ breast cancer[20].

As a matter of fact, PIP5Ks play more sophisticated roles in regulation of cancer progression then we ever thought. PIP5Ks have been linked to facilitate Warburg effect in colorectal cancer. Warburg effect, also known as aerobic glycolysis, is a reprogrammed metabolism in cancer cells, which ferments glucose to lactate to provide cells intermediary glucose metabolites for generating cellular building blocks, facilitating rapid proliferation, and avoiding apoptosis. Thus, Warburg effect has emerged as a hallmark of cancer[21]. In 2020, Peng et al. reported that PIP5Kγ was substantially upregulated in colorectal cancer, and its expression level negatively correlated with prognosis. Genetic silencing and pharmacological inhibition of PI5PKγ suppressed colorectal cancer glycolysis and xenograft tumor growth[22]. Mechanically, PIP5Kγ acts as an upstream regulator that reinforced glycolysis by activating the PI3K/AKT/mTOR/c-Myc-HIF1α axis.

1.2.1.2. Immune regulation

As the primary generator of $PI(4,5)P_2$, PIP5Ks are critical regulators of T cell activation. The immune system was affected by PIP5K via the production of $PI(4,5)P_2$ in two ways. Firstly, as a key regulator of the actin cytoskeleton, $PI(4,5)P_2$ controls the T cell polarization, migration, adhesion to antigen-presenting cells (APC), co-stimulation and signaling in the immunological synapse. Secondly, through the hydrolysis of $PI(3,4,5)P_3$, the product of PI3K catalyzed phosphorylation of $PI(4,5)P_2$, activates the signaling pathways regulating cytokine production, cell cycle, survival, and metabolism [23]. A typical case is the PIP5Kγ mediated programmed cell death protein 1(PD-1) expression in triple negative breast cancer cells, reported by Ling's group in 2017. PD-1 is a protein that down-regulates the immune system and promotes self-tolerance by suppressing T cell inflammatory activity. PD-L1 activates the immune checkpoint pathway by binding to PD-1 on the surface of immune cells. Studies have shown that, in cancer cells, the

expression level of PD-L1 was elevated, which induced the T-cell exhaustion and immune suppression, leading to the survival of cancer cells. Ling and coworkers found that, by deletion of PIP5Kγ, the expression level of PD-L1 was suppressed, typically through the downregulation of the activity of NF-κB pathway in these cells[24].

1.2.1.3. Viral infection

The clathrin-mediated endocytosis starts from the assembly of clathrin-coated pits (CCPs) at the plasma membrane, where CCPs invaginate to form clathrin-coated vesicles (CCVs) upon capturing transmembrane receptor (**Figure 1.5**)[25, 26]. PI(4,5)P_2 is critical for CCP initiation and nucleation, whose depletion has been shown to inhibit clathrin-dependent endocytosis[25, 26]. As the major PIPK kinase responsible for synthesis of PI(4,5)P_2 in plasma membrane, PIP5K exhibited potential antiviral and antibacterial infection properties. Va´zquez-Calvo et al. discovered that the expression of kinase dead mutant (KD) PIP5kα can impair the entry and infection of enveloped vesicular stomatitis virus (VSV) and non-enveloped foot-and-mouth disease virus (FMDV), whose infection used a well characterized clathrin mediated endocytic route[14]. Likewise, Shi et al. demonstrated that, local production of PI(4,5)P_2 by PIP5K was critical for the internalization of *Staphylococcus aureus* by host cells[27].

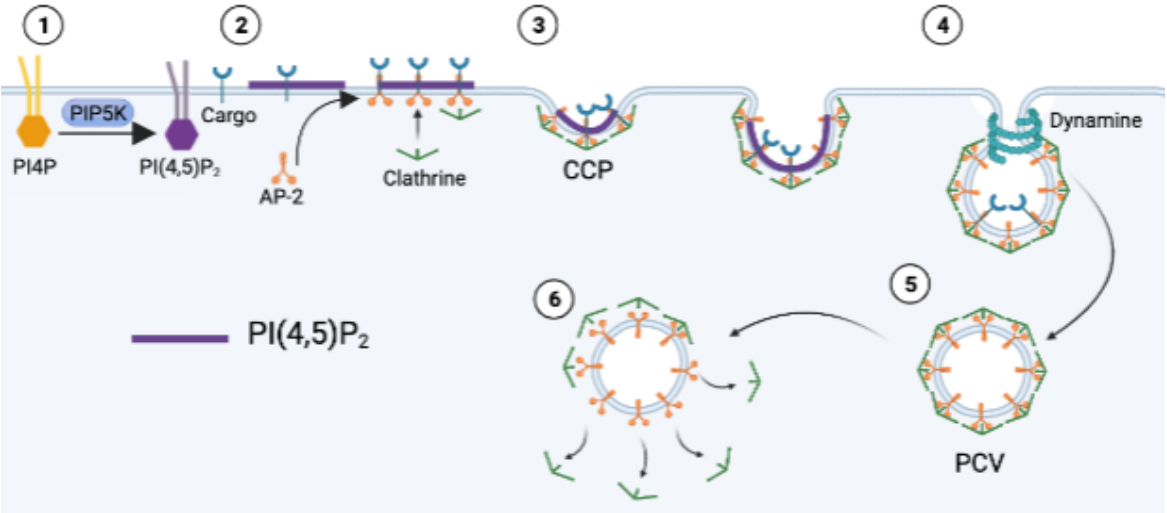

Figure 1.5. Schematic of PIP5K mediated clathrin-dependent endocytosis[10]. During endocytosis, PIP5K is recruited to the AP-2 complex, where it is activated to produce $PI(4,5)P_2$. The produced $PI(4,5)P_2$ promotes the clustering of AP-2 complexes, and further recruits clathrin for endocytic cups formation. After fission, the $PI(4,5)P_2$ level on vesicle is reduced, which leads to the dissociation of the AP-2 complexes and clathrin coat.

1.2.1.4.Neuronal development

Oligodendrocytes (OLs) play a critical role in the production and the assembly of the myelin sheath, whose dysfunction can result in several neurological disorders, including multiple sclerosis (MS) in adults and cerebral palsy (CP) in children. Although OLs have a robust capacity for regeneration, in white matter injury (WMI), the differentiation of OL precursors (OLPs) into OLs is suppressed by Wnt signaling[28-31]. Meanwhile, the clustering of Wnt receptor complexes into signalosomes (Frizzled/LRP/Dishevelled/Axin complexes) was regulated by Daam2 and PIP5K. The signalosome formation is a critical step for the initiation, amplification, and maintenance of Wnt signaling, Lee et al. have found that the direct interaction between Daam2 and PIP5K promoted the phosphorylation of LRP6 by $PI(4,5)P_2$, and the phosphorylated LRP6 further facilitated the clustering of Wnt receptor complexes into signalosomes (**Figure 1.6a**)[32].

Thus, this Daam2-PIP5K interaction can be a potential therapeutic target for increasing OL generation after WMI.

The traditional method for the treatment of chronic pain is targeting the pronociceptive receptors in dorsal root ganglia (DRG) neurons, which were usually activated upon tissue inflammation and nerve injury[33]. However, drugs that inhibit pronociceptive receptors, like protein kinase Cε (PKCε) and mitogen-activated protein kinases (MAPKs), have modest to no efficacy in treating different pains. Thus, to overcome the limitations in targeting individual pronociceptive receptors, an alternative strategy is to attack on a point where different signaling pathways converge. One such convergence point is PIP5Kγ, which is responsible for the synthesis of $PI(4,5)P_2$ in DRG neurons, and the PLC-mediated hydrolysis of $PI(4,5)P_2$ further regulates the nociceptive sensitization (**Figure 1.6b**)[34]. In 2014, Zylka's group found that PIP5Kγ was highly expressed in DRG neurons, and it generated at least half of all $PI(4,5)P_2$ in DRG neurons[35]. The studies in mouse models also revealed that the insufficiency of PIP5Kγ reduced pronociceptive receptor signaling in DRG neurons, which led to a reduced thermal and mechanical hypersensitivity of chronic pain. Therefore, these studies suggested that PIP5Kγ might be a therapeutic target for chronic pain.

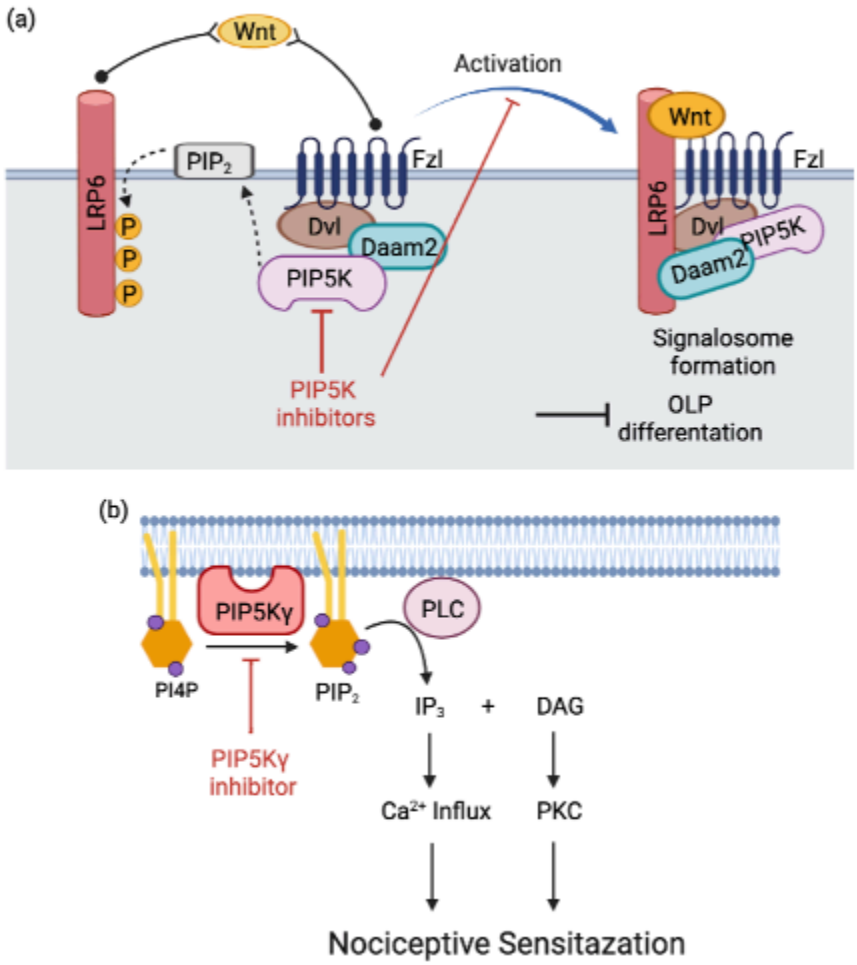

Figure 1.6. Model of PIP5K function in Wnt signaling and Nociceptive sensitization. (a). Model of PIP5K function in Wnt signaling and remyelination[32]. Daam2 associates with PIP5K, which facilitates the phosphorylation of LRP6 and finally promotes the clustering of Wnt receptor complex into signalosomes. The signalosomes formation results in the Wnt signal transduction, which suppress the OLP differentiation after WMI. However, pharmacologically inhibition of PIP5K can decrease the generation of $PI(4,5)P_2$ and disrupt the clustering of Wnt receptor complexes. (b). Model of PIP5kγ in generation of PIP2 which is hydrolyzed by PLC for the downstream pronociceptive receptor activation[35]. The Ca^{2+} influx and PKC activation contribute to nociceptive sensitization.

1.2.2. PIP5K inhibitors

So far, to the best of our knowledge, only four PIP5K inhibitors have been reported. The first PIP5K inhibitor was discovered by Zylka's group during their study about PIP5K and pain signaling. Zylka and coworkers found that, in nociceptive DRG neurons, PIP5Kγ is the major

PIP5K responsible for local production of $PI(4,5)P_2$, whose hydrolysis by PLC initiate the pain-producing receptors signaling. Although the results were confirmed using genetic methods, Zylka and coworkers also identified a small molecule inhibitor, UNC3230 (**1**) (**Scheme 1.1**), which selectively inhibited PIP5Kγ, providing a complimentary method for target validation [35]. UNC3230 (**1**) was identified using a high-throughput microfluidic mobility shift assay, in which, the fluorescein conjugated PI4P was incubated with recombinant human PIP5Kγ, with or without the presence of inhibitors, and then the product formation was measured using a microfluidic mobility shift assay[35]. After screening more than 5,000 compounds (a kinase-focused library), UNC3230 (**1**), [5-(cyclohexanecarboxamido)-2-(phenylamino) thiazole-4-carboxamide] was identified as a selective inhibitor of PIP5Kγ, with an IC_{50} value of 41 nM[35]. The *in vivo* test also demonstrated that UNC3230 (**1**) can lower the $PI(4,5)P_2$ level in DRG neurons and attenuate hypersensitivity.

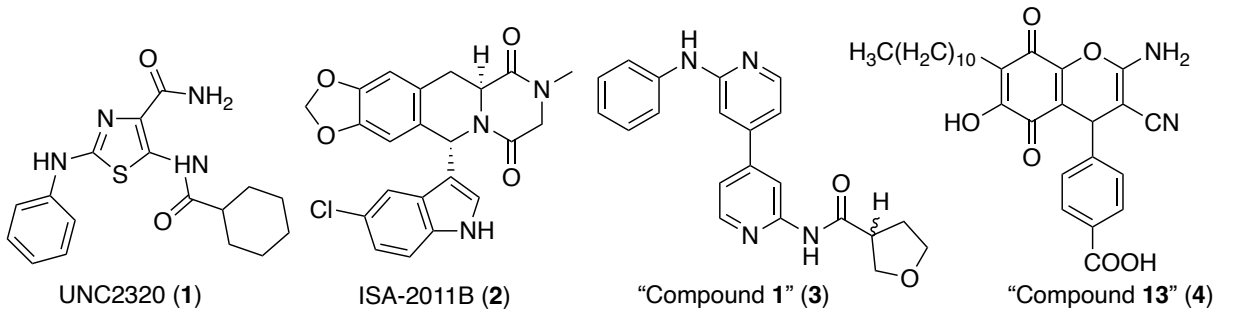

Scheme 1.1. PIP5K inhibitors.

Later in the same year, Persson's group reported another PIP5Kα inhibitor ISA-2011B (**2**) (**Scheme 1.1**), a diketopiperazine fused C-1 indol-3-yl substituted 1,2,3,4-tetrahydroisoquinoline derivative[15]. ISA-2011B (**2**) was firstly synthesized in Sterner's lab, and its initial proliferation assay against various types of aggressive cancer cell lines displayed a strong inhibitory effect[36].

To identify the binding target of ISA-2011B (**2**), Persson's group applied ISA-2011B (**2**) to a comprehensive high-throughput kinase profiling, in which ISA-2011B (**2**) was screened across 460 kinases[15]. This high throughput screen (HTS) displayed the highest binding affinity to PIP5Kα, an upstream factor of PI3K/ AKT pathway. To further validate the target and the relationship between the target and disease, human prostate cancer cell PC-3 cell was treated with ISA-2011B (**2**) due to its high expression of PIP5Kα. Upon treatment, the elevated proliferation and invasion of PC-3 cells were inhibited. Moreover, ISA-2011B (**2**) also exhibited a significant suppression of prostate tumor growth in xenograft mice. Further studies in the same group demonstrated that, the expression of androgen receptor was positively correlated with PIP5K1α in prostate tumor cells, and the resistance of prostate cancer to antiandrogen therapies can be overcame by inhibition of PIP5K1α[16]. In 2019, Persson's group found that, by inhibition of PIP5kα with ISA-2011B (**2**), the tumor growth and invasiveness were suppressed in a triple-negative breast cancer xenograft mouse model[20].

Similarly, by screening the AstraZeneca compound collection via HTS, Smith et al. discovered "compound **1**" (**3**) (**Scheme 1.1**) as a pan-isoform inhibitor of PIP5K, with IC_{50}s of 1.7 μM, 1.0 μM, and 0.67 μM for PIP5Kα, β, and γ, respectively[37]. In addition, "compound **13**" (**4**) (**Scheme 1.1**), 4-(2-amino-3-cyano-6-hydroxy-5,8-dioxo-7-undecyl-5,8-dihydro-4H-chromen-4-yl) benzoic acid, was identified via an in-silico prescreening[38]. Compound（**4**) exhibited a potent inhibitory effect to PIP5Kα with an IC_{50} value of 1.55 μM and a substrate-competitive mode of action.

1.3. Type II PIPK - PIP4K

Before 1997, it was believed that $PI(4,5)P_2$ was exclusively generated by PIP5K. Unexpectedly, Rameh et. al. found that a new type of PIPK, type II PIPK (PIP4K), was also

capable of generating $PI(4,5)P_2$ by phosphorylation of PI5P at the 4-position[39]. The function of PIP5K and PIP4K are nonredundant, even though both of them are capable of producing $PI(4,5)P_2$. However, the major pathway of generating $PI(4,5)P_2$ is still through the activity of PIP5K[7]. It was confirmed by the cellular level of PI5P, which is only about 1-2% of PI4P level[40]. Therefore, unlike PIP5K, whose role is to maintain the $PI(4,5)P_2$ level, the $PI(4,5)P_2$ level was not impacted when PIP4K was knocked down. Human genome encodes three isoforms of PIP4K, named as PIP4Kα, PIP4Kβ and PIP4Kγ, whose molecular weights are all around 45 kDa (**Figure 1.3**). All the 3 isoforms are highly expressed in the brain. Meanwhile, PIP4Kα, β and γ isoforms are also expressed in peripheral blood cells, muscle tissue and the kidney, respectively[41]. The sub-cellular localization of the kinase isoforms varies wildly. PIP4Kα is predominantly present in the cytoplasm and the plasma membrane, while PIP4Kβ is primarily in the nucleus, cytoplasm, and plasma membrane. PIP4Kγ is predominantly in a not well-defined endomembrane compartment[41]. Gene silencing studies in model organisms revealed a critical role PIP4K played in regulation of cell growth and development, immune function, and tumor growth control[40].

1.3.1. PIP4K and diseases

Early studies have suggested a role PIP4K played in regulation of receptor-activated PI3K signaling activated by cell surface receptors[39, 42]. However, at that time, the mechanism through which PIP4K regulates cell signaling was not defined. In general, PIP5K regulates the PI3K/Akt signaling pathway through production of $PI(4,5)P_2$, whereas PIP4K, modulating the minor pool of $PI(4,5)P_2$, would not be able to work in the same way. Indeed, recent studies in Drosophila found that the cellular level of PIP_3 was elevated in PIP4K knockout cells, which can be rescued by re-introducing the PIP4K protein to the plasma membrane[43]. Similarly, increased PIP_3 production after insulin stimulation was much greater in PIP4K depleted cells compared with control cells.

Moreover, consistent with the increasing level of PIP_3, the $PI(4,5)P_2$ level was also elevated in cells lacking PIP4K. All the results suggested a negative correlation between PIP4K activity and PI3K/Akt signaling through the suppression of $PI(4,5)P_2$ production (**Figure 1.7**). The PI3K/Akt signaling pathway has been identified in regulation of cell growth and apoptosis, whose dysregulation is closely related to tumorigenesis. Accordingly, in 2013, Keune et al. reported a correlation of low PIP4Kβ expression and reduced breast cancer patient survival[44]. In addition, they found that, in normal cells (MCF10A), shRNA knockdown of PIP4Kβ led to a decreased expression of the tumor suppressor protein E-cadherin (CDH1), while enhancing TGF-β–induced epithelial to mesenchymal transition (EMT), a process required during the development of metastasis[44].

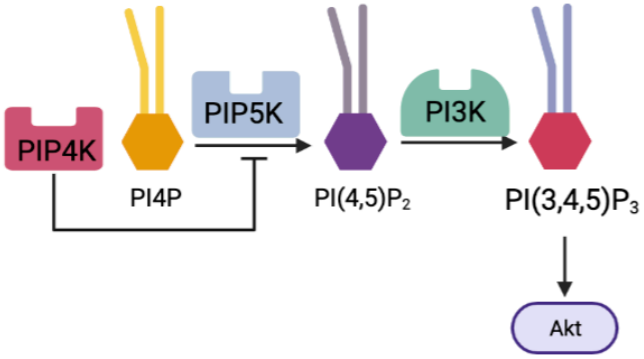

Figure 1.7. PIP4K regulation of PIP5K activity.

1.3.1.1. Cancer

As the most common leukemia, acute myeloid leukemia (AML) develops rapidly and become fetal within weeks without treatment. Also, because of the low survival rate and high relapse rate, the development of new targeted therapies is badly in need. With the knowledge on the importance of PI signaling in leukemic hematopoiesis, Jude et al. hypothesize that proteins regulating interconversion of PI derivatives may play significant roles in leukemia. Therefore, in

2014, they performed a targeted knockdown screen of the genes that encode PI modulating proteins in human AML cells and found that PIP4Kα is required to sustain proliferation of AML cells, since its knockdown resulted in cell cycle arrest and apoptosis[45]. Moreover, no adverse impact was observed in normal hematopoietic cells with PIP4Kα knockdown. Regarding why PIP4Kα knockdown results in inhibition of cell growth, one putative mechanism is through the activation of mTOR pathway and the downstream factors p21, a cyclin-dependent kinase inhibitor[45]. The knockdown of PIP4Kα activates mTOR and subsequently activates p21, which lead to cell cycle arrest. Thus, PIP4Kα is seen as a novel candidate therapeutic target in myeloid malignancy. Later in 2019, Machado-Neto's group reported that the expression levels of PIP4Kα and PIP4Kγ, but not PIP4Kβ, were positively related to the outcomes of AML patients[46]. Thus, this study provides additional evidence that PIP4Kα and PIP4Kγ are involved in AML.

The triple negative, Her2 and Claudin-low subtype of breast cancers generally have poorer prognosis than other subtypes of breast cancers. There have been studies showing that PIP4Kβ was highly expressed in Her2 positive breast tumors. One explanation of this correlation is the close location of the genes encoding PIP4Kβ (*PIP4KB*) and Her2 (*ERBB2*). As a result, *PIP4KB* gene is often amplified as part of the *ERBB2* amplicon[47]. In 2013, Cantley's group found high levels of PIP4Kα, PIP4Kβ, or both enzymes in a number of breast cancer cell lines and, more importantly, they proved that these kinases are essential for the growth of tumors cells in the absence of p53, since knocking down of these genes results in impaired glucose metabolism and enhanced levels of ROS leading to cell senescence[48].The study on p53 knockout mouse revealed that germline deletion of both alleles of PIP4Kα and one allele of PIP4Kβ on the background of $p53^{-/-}$ resulted in a viable mouse with a dramatic reduction of tumor growth compared to p53

knockout mouse[48]. These exciting observations further demonstrated that PIP4Kα and β are potential targets for treatment of breast cancer.

However, as discussed before, PIP4K is a negative regulator of PI3K/Akt signaling pathway, which suppress the activity of PIP5K for $PI(4,5)P_2$ production. Therefore, PIP4K is a potent tumor suppressor protein. However, in AML, triple negative and HER2+ breast cancer cells, the expression of PIP4K was elevated, and studies suggested a critical role PIP4K played in tumorigenesis. This apparent paradox of PIP4K still holds many of its secrets, which needs to be discovered.

1.3.1.2. Type 2 diabetes

Type 2 diabetes is an impairment where the body has an elevated blood sugar level and is unable to manage it. Under normal circumstances, when blood sugar increases in bloodstream, pancreas release insulin to trigger blood sugar uptake into cells for usage and storage. However, cells respond poorly to insulin in type 2 diabetes patients, also referred to as insulin resistant. In turn, pancreas tend to make more insulin to keep the blood sugar level under control. However, over time, the insulin resistance gets worse, and the pancreas is no longer able to make enough insulin, and the blood sugar remains at high levels, and ultimately leads to disorders of the circulatory, nervous, and immune systems.

The phosphoinositides are known to play important roles in insulin response through regulation of the PI3K/Akt pathway. Depletion of Akt leads to an impaired insulin signaling in mice. However, as the upstream effector of the PI3K/Akt pathway, little is known about the physiological role of PIP4Ks in insulin response. In 2004, Cantley's group generated $PIP4K\beta^{-/-}$ mice and observed an insulin hypersensitivity phenomenon[49]. These mice also exhibited reduced body weights compared to wild type littermates. These results, for the first time, indicate that

PIP4Kβ plays a role in regulating insulin sensitivity and could be the therapeutic target for the treatment of type 2 diabetes.

An interesting question is through what mechanism PIP4K regulates the insulin response. Prior to the aforementioned PIP4Kβ$^{-/-}$ mice study, Lewis C. Cantley et al. has reported that the expression of PIP4K reduced rather than increased PIP_3 level, and subsequently decreased activation of Akt, in cells stimulated with insulin[42]. This might explain why PIP4Kβ$^{-/-}$ mice have hypersensitivity toward insulin. Further evidence was provided by the same group in 2019, where they showed that the loss of PIP4Ks result in an increase of $PI(4,5)P_2$ and a subsequent increase in insulin stimulated production of $PI(3,4,5)P_3$[50]. They also demonstrated that the suppression of PIP5K activity, in the presence of PIP4Ks, is produced by an allosteric binding of N-terminal motif VMLFPDD of PIP4K to PIP5K[50]. A similar negative regulatory role of PIP4K played in controlling PIP3 production was also discovered by Sharma et al[43]. Moreover, they also demonstrated that, in Drosophila, loss of PIP4K enhanced the sensitivity of cells to insulin signaling, which can ameliorate the insulin resistance phenotypes[43]. All the results suggest that PIP4Ks could be the pharmacological target for regulating insulin resistant.

1.3.2. PIP4K inhibitors

Compared to PIP5K, more PIP4K inhibitors were identified in the recent decade, which covered all the 3 PIP4K isoforms. In 2013, Simeonov's group designed a homogeneous 1536-well luciferase-coupled bioluminescence assay for PIP4Kα, through which they screened a library of bioactive compounds and identified an ATP-competitive PIP4Kα inhibitor I-OMe-AG-538 (**5**) (**Scheme 1.2**), with an IC_{50} of 1 μM[51]. Later in 2015, Kitagawa et al. identified a novel compound a131 (**6**) (**Scheme 1.2**), which selectively killed Ras-activated cancer cells through mitotic catastrophe, while protecting normal cells from apoptosis.[52]. Then, a mass spectrometry based

cellular thermal shift assay (MS-CETSA) was applied to identify the cellular target of a131 (**6**). After screening more than 8000 proteins, PIP4K was identified as the most promising target. *In vitro* assay also validates that, a131(**6**) inhibited the kinase activity of purified PIP4Kα with an IC_{50} value of 1.9 μM[52]. Further evidence indicated that the inhibition of cancer cell by a131 (**6**) was via a cross-activation between the Ras/Raf/MEK/ERK and PI3K/AKT/mTOR pathways, which was mediated by a Ras-PIK3IPI-PI3K signaling network[52]. Another 2 potent and highly selective PIP5Kα inhibitors, Bay-091 (**7**) and BAY-297 (**8**) (**Scheme 1.2**), were identified via HTS and subsequent SAR optimization by Lemos et al in 2021[53]. The cellular target engagement of Bay-091 (**7**) and BAY-297 (**8**) were also validated by CETSA in THP-1 cells, where both compounds exhibited a dose-dependent thermal shift.

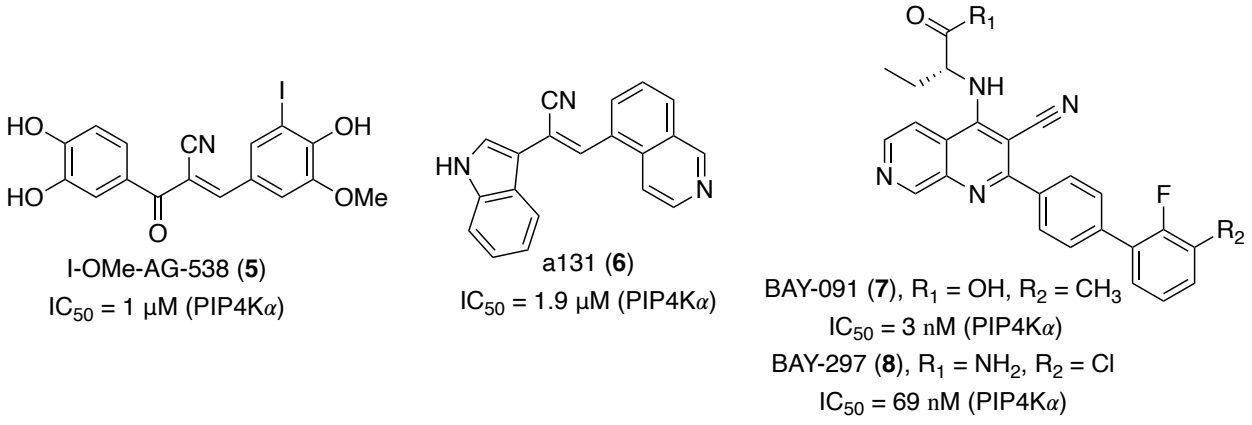

Scheme 1.2. PIP4K**α** selective inhibitors.

To the best of our knowledge, so far, only one PIP5Kβ selective inhibitor was discovered. To identify the inhibitors of PIP5Kβ, Voss et al. screened a library containing 115,000 substances via HTS, and identified a series of pyrimidine-2,4-diamine derivatives as hits for further SAR and optimization[49]. Finally, SAR088 (**9**) (**Scheme 1.3**) was identified as a PIP5Kβ inhibitor with an IC_{50} value of 2.18 μM[49]. Furthermore, the subsequent enzymatic and cellular assays indicated that

SAR088 (**9**) is a potent and selective PIP5Kβ inhibitor for the treatment of insulin resistance and diabetes.

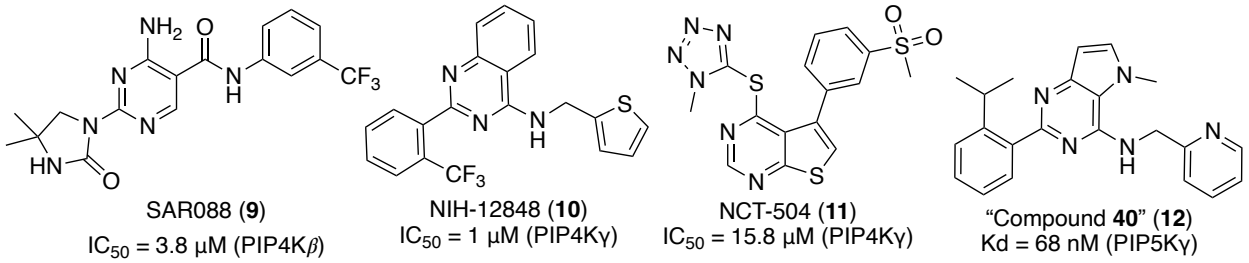

Scheme 1.3. PIP4K**β** selective and PIP4K**γ** selective inhibitors.

In 2015, Irvine's group reported a PIP4Kγ inhibitor, NIH-12848 (**10**) (**Scheme 1.3**), through a kinome profiling study[54]. The *in vitro* assay showed that NIH-12848 (**10**) selectively inhibited PIP4Kγ with an IC_{50} of approximately 1 μM but did not inhibit PI5P4Kα or PIP4Kβ up to 100 μM. Moreover, the hydrogen–deuterium exchange (HDX)-MS study revealed that NIH-12848 (**10**) putatively interacts with the PI5P binding site rather than the ATP-binding site[54].

In addition to substrate-competitive inhibitor, two allosteric PIP5Kγ inhibitors were discovered. One of them is NCT-504 (**11**) (**Scheme 1.3**), a 5-phenylthieno [2,3-d] pyrimidine derivative, which was initially discovered through a high-throughput phenotypic screen and then optimized via medicinal chemistry for treatment of Huntington' disease. However, at that time, the cellular target of NCT-504 (**11**) was unclear. Then, in 2017, because of the presence of a kinase activity associated analog thienopyrimidine, AI-Ramahi et al. screened NCT-504 (**11**) against a panel of 442 human kinases and found its single kinase target PIP4Kγ[55]. The inhibition effect of NCT-504 (**11**) against PIP4Kγ was further validated using the DiscoverX binding assay with a dissociate constant of 354 nM, as well as an inhibition assay against the phosphorylation of the natural substrate PI5P by the purified PIP4Kγ with an IC_{50} of 15.8 μM[55]. What is noteworthy is that, in the presence of NCT-504 (**11**) without PI5P, the intrinsic ATP hydrolysis of PIP4Kγ

remained, which means that NCT-504 (**11**) is an allosteric inhibitor binding outside the ATP-binding pocket.

The other allosteric inhibitor is "compound **40**" (**12**) (**Scheme 1.3**), a selective small molecule PI5P4Kγ inhibitor, which was found during the optimization of NIH-12848 (**10**) for better potency and physicochemical properties[56]. NIH-12848 (**10**) is an isoform selective and non-ATP competitive PIP4k inhibitor, which was proposed to bind to the substrate binding site of PIP4Kγ, while having a poor solubility (<5 μM) due to its high lipophilicity (clog P 6.5)[54]. To maximize the inhibition efficiency and decrease the lipophilicity, SAR was carried out, where the trifluoromethyl substitution on phenyl was replaced with an isopropyl group, the thiophene was replaced by a pyridine, and the quinazoline was replaced by a pyrrolopyrimidine[56]. The newly generated "compound **40**" (**12**), in addition to the preserved isoform selectivity, displayed a good potency (K_d = 68 nM) and a submicromolar cellular target engagement, as well as a higher permeability and a moderate microsomal stability. Moreover, the complex crystal structure with PIP4Kγ was also solved at the resolution of 2.4 Å, where "compound **40**" (**12**) displayed two different binging modes (**Figure 1.8),** including an allosteric binding mode and an ATP site binding mode[56].

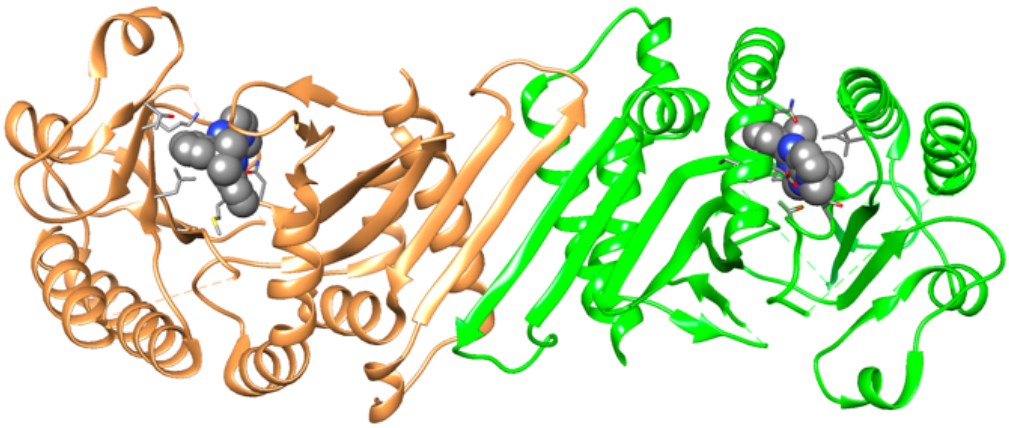

Figure 1.8. Crystal structure of PIP4kγ dimer bound with "compound **40**" (**12**) (dark gray). at ATP binding site (orange chain) and allosteric site (green chain), respectively[56] (PDB: 7QIE).

Besides isoform specific inhibitors, another category of PIP4K inhibitor is pan-PIP4K inhibitors. In 2019, a collaborative work of Lewis C. Cantley' group and Nathanael S. Gray's group discovered a covalent pan-PI5P4K inhibitor THZ-P1-2 (**13**) (**Scheme 1.4**)[57]. The development of THZ-P1-2 (**13**) was inspired by a previously developed covalent JNK inhibitor, JNK-IN-7[58], which also exhibited an inhibitory activity against PIP4Ks and the labeling of cysteine residue of PIP4K on mass spectrometry. Guided by the biochemical kinase assays and cellular pulldown assay, the structure of JNK-IN-7 was optimized to form the covalent pan-PIP4K inhibitor THZ-P1-2 (**13**), with IC_{50} of 0.95 μM to PIP4Kα and 5.9 μM to PIP4Kβ[57]. Then, protease digestion and tandem mass spectrometry were carried out to identify the specific residue that was covalently labeled by THZ-P1-2 (**13**). The result indicated that, Cys293 on PI5P4Ka, Cys307 and Cys318 on PI5P4Kb, and Cys313 on PI5P4Kg, were covalently modified by THZ-P1-2 (**13**) (**Figure 1.9**)[57]. Those residues are on a conserved disordered loop outside the ATP-binding pocket. The DiscoverX KINOMEscan profiling revealed an off-target, PIKfyve. At the same time, Gray's lab performed further structure-guided optimization and structure−activity relationship (SAR)

study of THZ-P1-2 (**13**), which resulted in a more potent and selective inhibitor, "compound **30**" (**14**) (**Scheme 1.4**)[59]. The KINOMEscan profiling of "compound **30**" (**14**) showed loss of almost all off-targets seen with THZ-P1-2 (**13**), including PIKfyve.

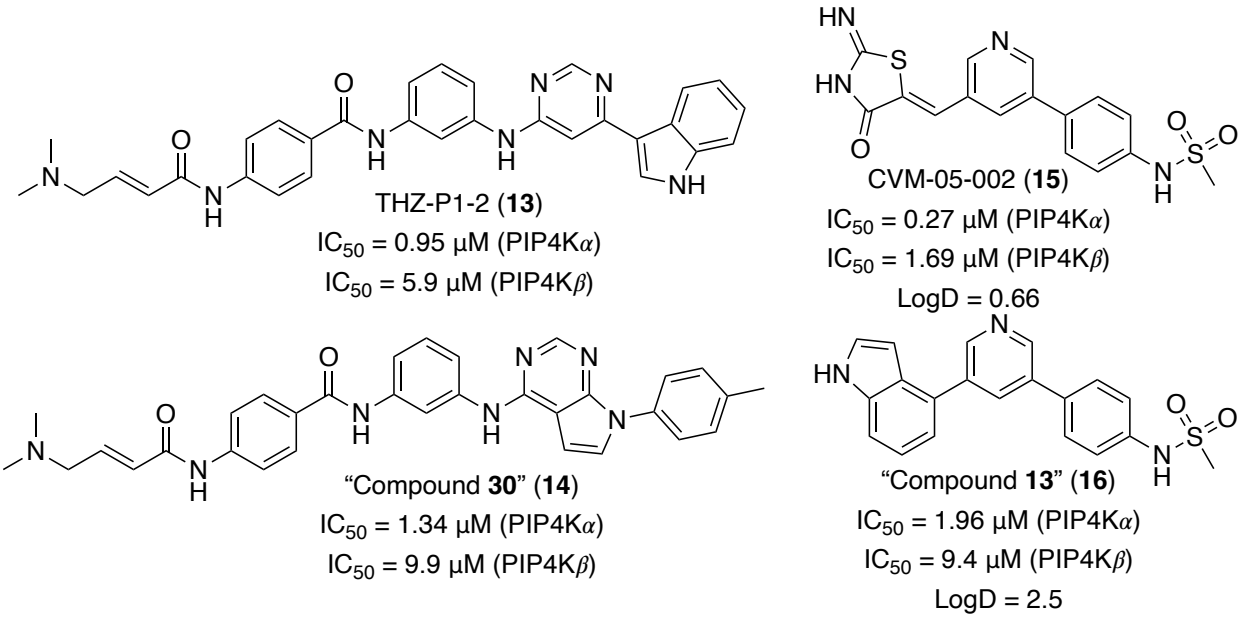

Scheme 1.4. Covalent PIP4K inhibitors and Pan-PIP4k inhibitors.

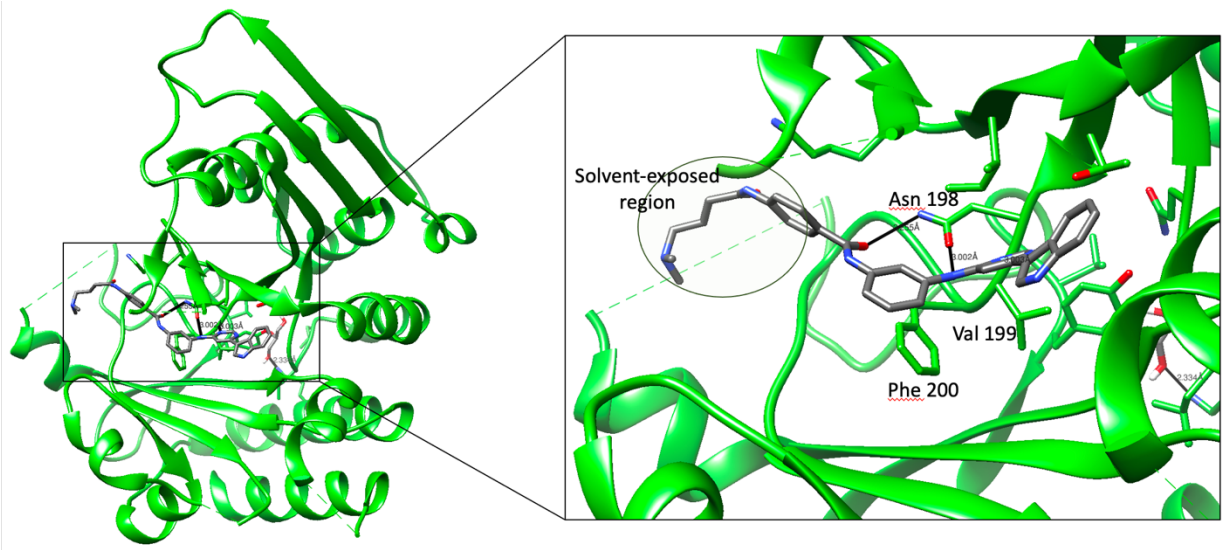

Figure 1.9. Crystal structure of PIP4K**α** bound with THZ-P1-2 (**13**) (dark gray). H-bonds are shown as black bonds[57, 59] (PDB: 6OSP).

In 2020, the same group identified another reversible PI5P4K inhibitor, CVM-05-002 (**15**) (**Scheme 1.4**), through a HTS of an in-house kinase inhibitor library[53]. Among all the derivatives, CVM-05-002 (**15**), contains a rhodanine-like (Z)-5-methylenethiazolidin-4-one moiety, which displayed the strongest inhibitory activity against PIP4Kα during the screen, with an IC_{50} of 0.27 μM[60]. Also, the kinome-wide profiling of CVM-05-002 (**15**) revealed that it is a pan-PIP4K inhibitor. In addition, the obtained crystal structure of CVM-05-002 (**15**) and PIP4Kα complex (1.7 Å) indicates a noncovalent binding, with mainly hydrogen bond interactions of CVM-05-002 (**15**) with the ATP-binding pocket (**Figure 1.10**). However, because of the high polarity (log D 0.66), the bioavailability of CVM-05-002 (**15**) might be problematic[60]. Thus, to balance the lipophilicity and potency, SAR of CVM-05-002 (**15**) was explored. The newly developed "compound **13**" (**16**) (**Scheme 1.4**), which lacks the thiazolidinone scaffold, exhibits a better cellular potency and selectivity.

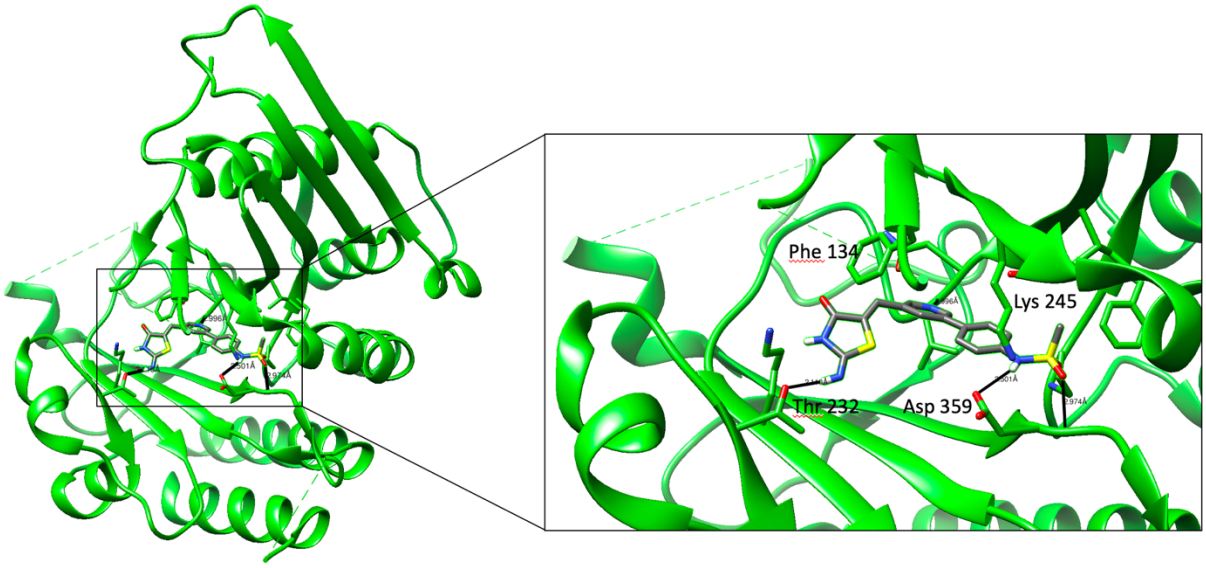

Figure 1.10. Crystal structure of PIP4K**α** bound with inhibitor CVM-002 (**15**) (dark gray). H-bonds are shown as black bonds[60] (PDB: 6UX9).

1.4. Type III PIPK – PIKfyve

Because of the presence of a characteristic N-terminal FYVE finger domain, the type III PIPK is also called PIKfyve. The FYVE finger domain is a PI3P-binding motifs, which can associate with membrane PI3P, and in turn, direct the localization of PIKfyve onto the cell membrane. In addition, PIKfyve also has a PIPK kinase domain, which is responsible for the synthesis of PI(3,5)P2 and PI5P[61-63]. $PI(3,5)P_2$ is a low-abundance phosphoinositide, only constituting about 0.05–0.1% of total phosphoinositide lipids, but is critical for lysosome biology[7, 61, 64].

The human PIKfyve complex structure was firstly elucidated by Reinisch et al. through cryo-electron microscopy (cryo-EM) studies[65]. This study revealed that the human PIKfyve complex comprises a star-shaped pentamer protein VAC14 homolog (Vac14, also known as ArPIKfyve, associated regulator of PIKfyve), a monomer phosphatidylinositol 3,5-bisphosphate 5-phosphatase (Fig4), and a monomer lipid kinase PIKfyve (**Figure 1.11**). Among the complex, the Vac14 acts as a scaffolding protein, the Fig4 functions as a lipid phosphatase and protein phosphatase, and the PIKfyve acts as a lipid kinase and protein kinase[65]. Thus, it is believed that the activity of PIKfyve is regulated by the protein complex, and the hypothetic mechanism can be summarized as follow: (1) PIKfyve works as a lipid kinase, converting PI5P into $PI(3,5)P_2$, and a protein kinase, possibly auto-phosphorylating itself to suppress the lipid kinase activity and stimulate the Fig4 lipid phosphatase activity. (2) Fig4 also acts as a lipid phosphatase, reversing $PI(3,5)P_2$ to PI5P, and a protein phosphatase, which stimulates the PIKfyve activity by dephosphorylating the auto-phosphorylated PIKfyve.

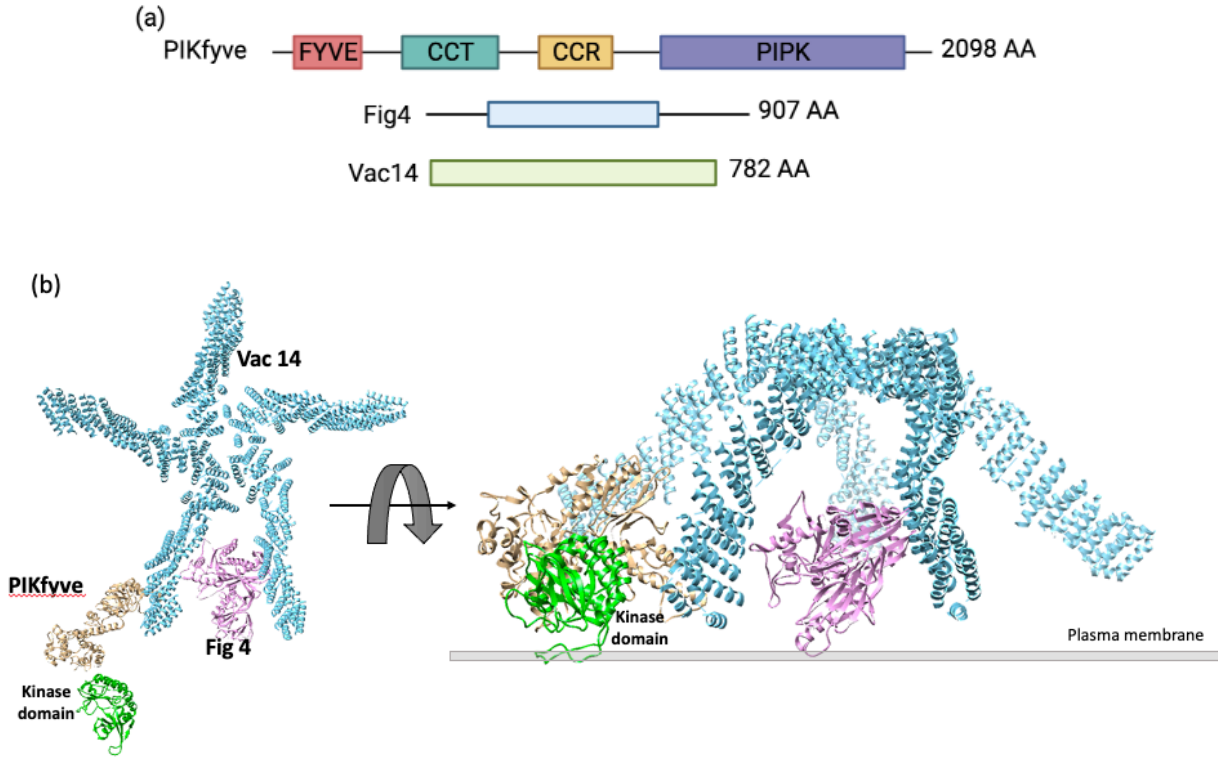

Figure 1.11. Reconstruction of the human PIKfyve complex[65]. (a) Domain organization of PIKfyve, Fig4, and Vac14. (b). The architecture of the reconstructed complex of PIKfyve, Fig4, and Vac14 (PDB: 7K1Y, 7K2V, and 7K1W). The model of PIKfyve complex interacting with plasma membrane.

Besides being regulated by the PIKfyve-Vac14-Fig4 complex, PIKfyve is also self-regulated. In addition to the *N*-terminal FYVE finger domain and the *C*-terminal kinase domain, other two domains, conserved cysteine-rich (CCT) domain and chaperone-containing TCP1 (CCR1) domain, are inserted in between. The CCT domain was believed essential for the interaction with Vac14, whereas the CCR domain was found involved in the self-regulation of the kinase activity[61]. To be more specific, the CCR domain reversibly inhibits the kinase activity by directly interacting with the kinase domain, whereas the inhibition can be relieved by posttranslational modifications and altered interactions with other proteins[61].

Many studies have shown that the PIKfyve, through the production of $PI(3,5)P_2$, played a critical role in regulation of endocytic pathways[66]. The cellular $PI(3,5)P_2$ is exclusively synthesized from PI3P by PIKfyve. PI3P is enriched on the early endosome[66]. With its PI3P-binding motif, the FYVE finger domain, PIKfyve is highly localized on the early endosome[67]. However, in contrast to PI3P, the enzymatic product, $PI(3,5)P_2$, is predominantly gathered in the late endosomes[67]. Kinase deficient point mutation, knockout, or pharmacological inhibition of PIKfyve, all resulted in fewer but enlarged endo/lysosomes[63, 68-70]. It is very likely due to the impaired ion homeostasis and pH within the endomembrane system, which leads to the disruption of endosomal membrane dynamics, an imbalance favoring fusion over fission[71-73].

In addition to swelling, the maturation of endosome and phagosome were blocked by the suppression of PIKfyve activity. Laporte et al. first found that, in *Caenorhabditis elegans*, losing the function PIKfyve led to the enlargement of vacuoles, and impaired acidification and terminal maturation of lysosomes[74]. A similar impairment of lysosome maturation in mammalian cells was demonstrated by Guillaume van Niel et al. Since the $P(3,5)P_2$ level is closely related to the membrane modeling by inhibition of PIKfyve activity, the lysosome reformation from endolysosomes were impaired, as well as the accumulation and enlargement of the endolysosomes[75]. Later, Botelho et al. found that, by pharmacological inhibition of PIKfyve, the localization of LAMP1, an endogenous late endosome and lysosome marker, on phagosomes was dramatically decreased, which strongly suggested a direct role PIKfyve played in phagosome maturation[71, 76].

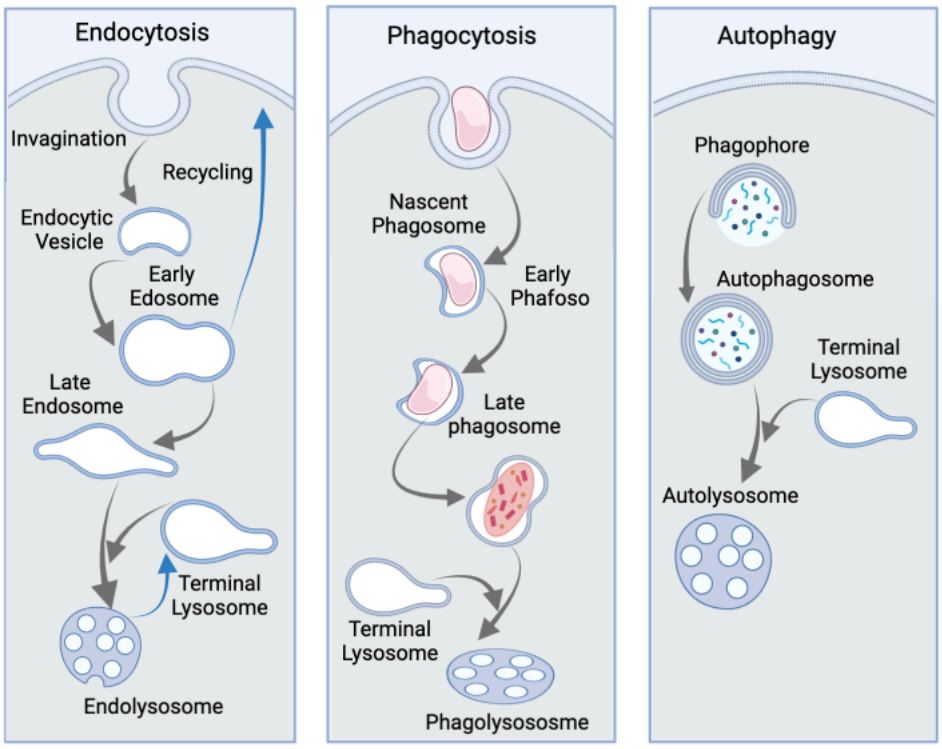

Figure 1.12. The diagram of the process of endocytosis, phagocytosis, and autophagy pathway[77].

In response to PIKfyve inhibition, a similar form of defects in autophagy system was also observed in neurons. Osborne et al. found that, inhibition of PIKfyve by YM-201636 (**17**) resulted in an accumulation of the autophagosome marker protein LC3-II, which directly indicated a defect in fusion of autophagosome with lysosome[78]. The fundamental explanation of the defectives in endocytosis and autophagy system, with the suppression of PIKfyve activity, is a result of the reduced production of $PI(3,5)P_2$, which is responsible for the fusion of endo/phagosome with lysosome, and is critical for the digestion activity of the engulfed proteins[63]. Because Ca^{2+} triggers membrane fusion, as the phosphoinositide-gated lysosomal Ca^{2+} channel[73], TRPML (transient receptor potential mucolipin channel 1) is the downstream affecter of PIKfyve and mediates the phagosome-lysosome fusion[79]. Thus, the blockage of TRPML1 mediated Ca^{2+} release from

lysosomal stores upon PIKfyve inhibition leads to the defectiveness of membrane retrieve, and finally the impairment of phagosome maturation[73, 79]. Moreover, Kaoru Hazeki and co-worker also found that, the phagosome acidification was also dependent on TRPML1[79].

Lastly, PIKfyve is required for the retrograde traffic of protein from endosomes to the trans-Golgi-network (TGN) and endocytic recycling[80]. The trafficking of proteins, including the cation-independent mannose-6-phosphate receptor (CI-MPR), sortilin, furin, and Shiga Toxin B, to the TGN was perturbed by inhibition of PIKfyve activity[80]. In terms of the endocytic recycling, suppression of PIKfyve activity promoted recycling of AMPA-type glutamate receptors (AMPARs) but decreased recycling of β1-intergrin[80].

1.4.1. PIKfyve in diseases and its therapeutic benefits

The production of $PI(3,5)P_2$ is regulated by the PIKfyve complex, as discussed before. Thus, the alternation of PIKfyve, Fig4 or Vac14 can lead to the perturbation of $PI(3,5)P_2$ level , and finally result in diseases. In yeast, the deletion of Fab1, the homologous protein of PIKfyve in yeast, leads to a defect in cell growth[81]. In mice, the global deletion of PIKfyve gene leads to the death of embryos[82], while partial loss of PIKfyve activity results in a viable but extensively neurodegenerated model[83]. PIKfyve knockout mouse models also demonstrated that PIKfyve is essential for specific tissue and cell growth, such as the intestine, muscles, and myeloid cells[84-87]. In humans, many diseases have been proven to be related to the defects in the PIKfyve complex, especially the neurodegeneration disease, including Charcot-Marie-Tooth syndrome (CMT4J)[88], amyotrophic lateral sclerosis (ALS)[89], primary lateral sclerosis (PLS)[90], and YuniseVaron syndrome[91, 92].

Recently, because of the discovery of PIKfyve inhibitors, such as Apilimod (**18**), YM-20636 (**17**), and Vacoline-1 (**20**), more and more interests have been dedicated to PIKfyve. By

pharmacological inhibition of PIKfyve with these inhibitors, many other diseases have also been found to be linked to PIKfyve, including cancer, viral infections, as well as regulation of the immune system. Apilimod (**18**), the most extensively characterized PIKfyve inhibitor, is currently undergoing clinic trials for the prevention of SARS-Cov-2 infection.

1.4.1.1. Neurodegeneration disease

The endo/lysosome system plays a critical role in the nervous system, since it regulates a variety of neuronal functions, including neurite outgrowth, retrograde transport, and synaptic plasticity[93-96]. As the crucial regulator of the endo/lysosome system, PIKfyve regulates the morphology, maturation, and intracellular trafficking of the endo/lysosome. Thus, disruption of PIKfyve activity has been linked to many human diseases, especially those in the nervous system.[93] Studies have shown that integration and acidification of vesicles and protease activity of the late endosomes and the lysosomes in neurons were impaired upon PIKfyve inhibition,. Also, the decreased production of $PI(3,5)P_2$ results in a vacuolar phenotype and defective autophagy in the central nervous system, which finally leads to the neuronal cell death and subsequent neurodegeneration in mice[78, 88, 95-97].

The enlargement of endosomes in neurons and peripheral cells is observed in early-stage Alzheimer's disease (AD) and Down syndrome (DS) patients, which indicated the involvement of endolysosomal abnormalities in the development of Alzheimer brain lesions[98-100]. Alzheimer's disease (AD), as the most prevalent form of dementia, is believed to be resulting from two major neuropathological lesions: amyloid plaques and neurofibrillary tangles (NFTs)[99]. Amyloid plaques are an aggregation of misfolded amyloid beta (Aß) protein cleaved from the Amyloid Precursor Protein (APP), which are enriched with the structure of ß-sheet and accumulated in the central nervous system (CNS)[98, 99]. NFTs are constituted of hyperphosphorylated and aggregated tau

proteins, which are packed into a protease-resistant and β-sheet-rich highly ordered structures[100-103]. Although they are two different pathogenesis, increasing evidence supports that dysregulation in autophagy and endolysosomal routes promoted the initiation and progression of both the amyloid plaques and NFTs.

To be more specific, after generation by brain neurons, the APP is subsequently cleaved by secretase to form Aß peptides, whose abnormal accumulation leads to neurotoxicity in the brain[98]. This abnormal accumulation results from the imbalance between the Aß peptides synthesis and clearance. Increased synthesis and/or attenuated clearance of Aß result in misfolding, aggregation and extracellular accumulation, and eventually lead to the formation of amyloid plaques[98]. In neurons, the major pathway of Aß aggregates and APP clearance is through the autophagy route. Thus, impairment of autophagy is closely related to the pathogenesis of AD, which was also confirmed with the observations of autophagy dysfunction in AD patients. In addition, Wassmer et al. reported a direct binding of APP and PIKfyve complex, through which, APP stimulates the activity of PIKfyve and the subsequent formation of $PI(3,5)P_2$ positive vesicle for its intracellular trafficking[104, 105]. This feedback loop between APP and PIKfyve indicates an alternative plausible pathogenesis of AD, where aberrant APP processing leads to the abnormal endosomal homeostasis through a lack of $PI(3,5)P_2$ production, which eventually results in the accumulation of Aß and neurodegeneration.

On the other hand, neurofibrillary tangles, another hallmark of AD pathology, are insoluble intraneuronal fibrillary aggregates consist of hyperphosphorylated tau proteins, which are linked to AD and other neurodegenerative tauopathies[101, 102]. Abnormal endolysosomal–autophagic system, by dysfunction of PIKfyve, may also contribute to the self-aggregation of tau. Firstly, endosomal membranes, as the signaling platforms, whose abnormality may impair various cellular

signaling cascades, including the kinases and phosphatases that regulate the phosphorylation of tau[106]. Thus, the defects in endolysosomal–autophagic system may contribute to the hyperphosphorylation of tau. Secondly, abnormal endolysosomal–autophagic system also reduce the clearance of tau[98, 107]. Both contribute to the aggregation of toxic tau species, and lead to the pathogenesis of AD. Soares et al. used fluorophore labeled preformed fibrils (PFFs) to confirm that the delivery of tau aggregated into lysosomes can be blocked by pharmacological inhibition of PIKfyve[106].

Besides the pathogenetic role of PIKfyve played in AD, PIKfyve inhibition can have beneficial effects in treatment of Amyotrophic Lateral Sclerosis (ALS)[108, 109]. Indeed, PIKfyve inhibitor Apilimod (**18**) is in the clinical trial for the treatment of ALS. ALS is a rare, rapidly progressive, and lethal neurodegenerative disease, whose pathogenesis is characterized as the loss of motor neurons in brain and spinal cord[108]. The hallmark of ALS is the abnormal accumulation of intracellular protein aggregates[108]. One of the protein aggregates is the poly-dipeptides encoded by pathogenic GGGGCC expansions in the *C9ORF72* gene. Inhibition of PIKfyve by Apilimod (18) controls endosomal trafficking of DPRs from early endosomes to late endosomes, which prohibits the endolysosomal escape of DPRs and the aggregate spreading[109].

1.4.1.2. Cancer

The PIKfyve dysfunction mediated endolysosomal homeostasis disruption may result in the neuronal cell death, leading to neurodegeneration diseases. However, PIKfyve dysfunction may not be always a catastrophe, as it can induce selective antiproliferation and cytotoxic effects in cancer cells for anticancer treatment[110, 111]. In 2014, Oppelt et al. have validated the role of PIKfyve in controlling tumor cell migration and invasion[112]. Then, Lichenstein et al. demonstrated the anticancer effect of PIKfyve dysfunction on B-cell non-Hodgkin lymphoma[113]. In this study,

selective antiproliferation and cytotoxic effects against B-NHL cells, via an endolysosomal homeostasis disruption, was induced by the inhibition of PIKfyve with Apilimod (**18**). Later in 2019, Xie et al. reported a similar antiproliferation effect on liver cancer, which was exhibited by inhibition of PIKfyve with YM201636 (**17**) and the following induced autophagy effect via upregulation of epidermal growth factor receptor (EGFR) expression[114]. In 2020, Stewart et al. further demonstrated that PIKfyve is an anticancer target in multiple myeloma[115].

Interestingly, recent studies also showed that, inhibition of PIKfyve can not only induce cancer cell death directly, but also enhance the therapeutic response of immune checkpoint therapy toward cancer cells[110, 111]. Qiao et al. found that, pharmacological inhibition of PIKfyve in castration-resistant prostate cancer (CRPC) cells resulted in autophagy inhibition and tumor growth blockage[116]. Besides, it also upregulated chemokine secretion, including CXCL10, and subsequently promoted T cell infiltration of the tumor tissue, which ultimately enhanced the therapeutic response to immune checkpoint therapy. Further studies demonstrated that genetic knockout of PIKfyve also led to accumulation of autophagosome and lysosome, which explained why the increasing secretion of chemokines resulted from the decreasing autophagic flux (**Figure 1.13**)[116]. This study revealed that, inhibition of PIKfyve can be a new therapeutic method for the treatment of CRPC and can also turn tumor from “cold” into “hot” to benefit immunotherapies.

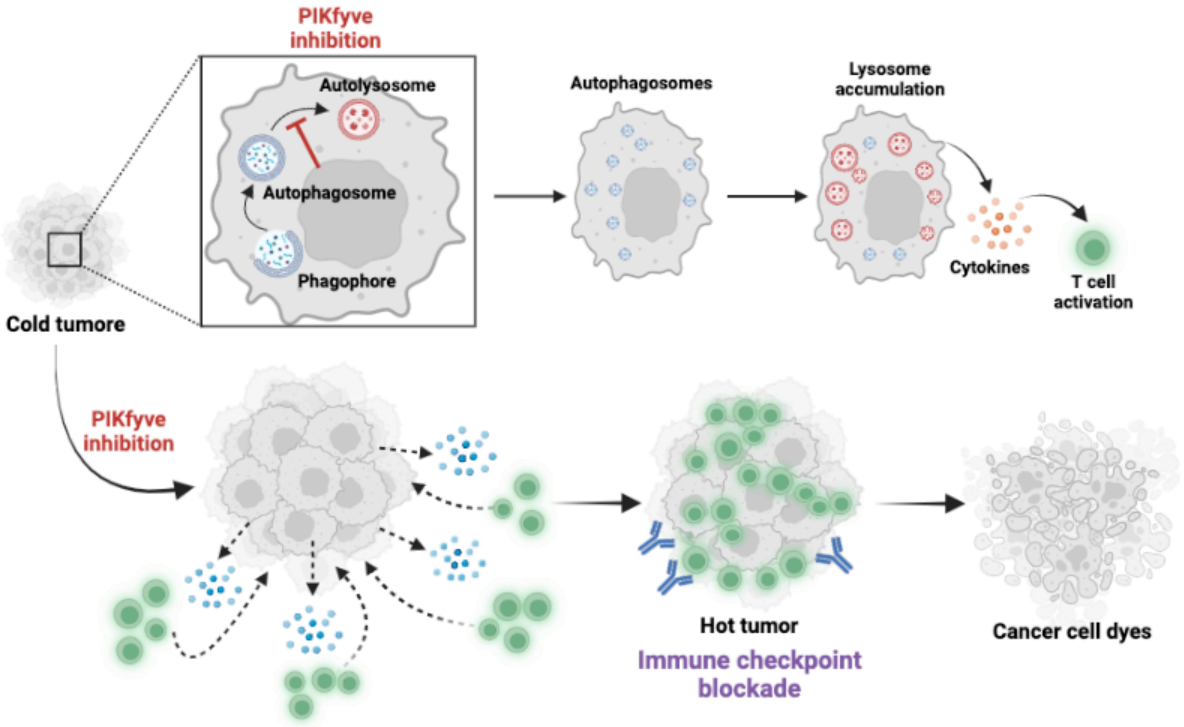

Figure 1.13. The mechanism of turning cold tumor into hot by inhibition of PIKfyve[116]. Where the inhibition of PIKfyve promotes accumulation of lysosomes, which facilitate the secretion of cytokines for T cells activation. Then, the activated T cells infiltrate the tumors turnover the cold tumor into hot, which enhanced the therapeutic effects of immune checkpoint blockage.

1.4.1.3. Viral infection

The blockage of endosome maturation and its fusion with lysosome via PIKfyve inhibition was used as the mechanism for antiviral infection, which depended on the fact that the infection and replication of some viruses rely on the endolysosome system of the host cells[117]. In 2008, Parker et al. reported that by inhibition of PIKfyve could block retroviral budding via disruption of endomembrane transport[118]. Later, many similar antiviral activities were discovered in PIKfyve inhibition studies. In 2010 and 2017, similar antiviral effects on Salmonella and Ebola virus infection by inhibition of PIKfyve were discovered by Teasdale et al. and White et al.,

respectively[119, 120]. In 2020, inhibition of PIKfyve with Apilimod (**18**) was found to prevent the severe acute respiratory syndrome coronavirus 2 (SARS-CoV-2) infection[121-126].

SARS-CoV-2, because of its highly transmissible ability, has spread fast all over the world and caused the global pandemic known as coronavirus disease 2019 (COVID-2019). The high infectious capacity and the 1-5% mortality rates associated with SARS-CoV-2 render it a great thread to the world[127]. Structurally, the coronavirus consists of four glycoproteins, including nucleocapsid (N), membrane (M), envelope (E) and spike (S) proteins (**Figure 1.14**)[121, 127, 128]. The S glycoprotein is predominantly responsible for binding to the host cell receptor, angiotensin-converting enzyme 2 (ACE2), and fusing the viral membrane with the host cell membrane. The M, E and N glycoproteins play roles in virus particle assembly, replication, and release, respectively[121, 127, 128]. During the studies of prevention and treatment of SARS-CoV-2, multiple therapeutic targets were discovered in its entry route. Upon binding of S protein to the host cell receptor ACE2, a subsequent cleavage of the S protein by host cell proteases followed, which is mediated by TMPRSS2 during the cell surface direct fusion pathway, as well as the cathepsins in the endocytosis pathway[121, 128, 129]. Indeed, there has been many agents identified for disrupting the interaction between the S protein and ACE2, such as the ACE2 mimetics, monoclonal antibodies, as well as the antibodies elicited by vaccine, all of them inhibiting the entry route[121, 130]. Besides, agents targeting the post-receptor-binding steps include camostat mesylate, a serine protease inhibitor, restricting the TMPRSS2- mediated entry pathway. Applied together with hydroxychloroquine and chloroquine, which block endosomal acidification necessary for cathepsin activity, they enhance the inhibition of the cathepsin- mediated entry pathway (**Figure 1.14**)[121, 129].

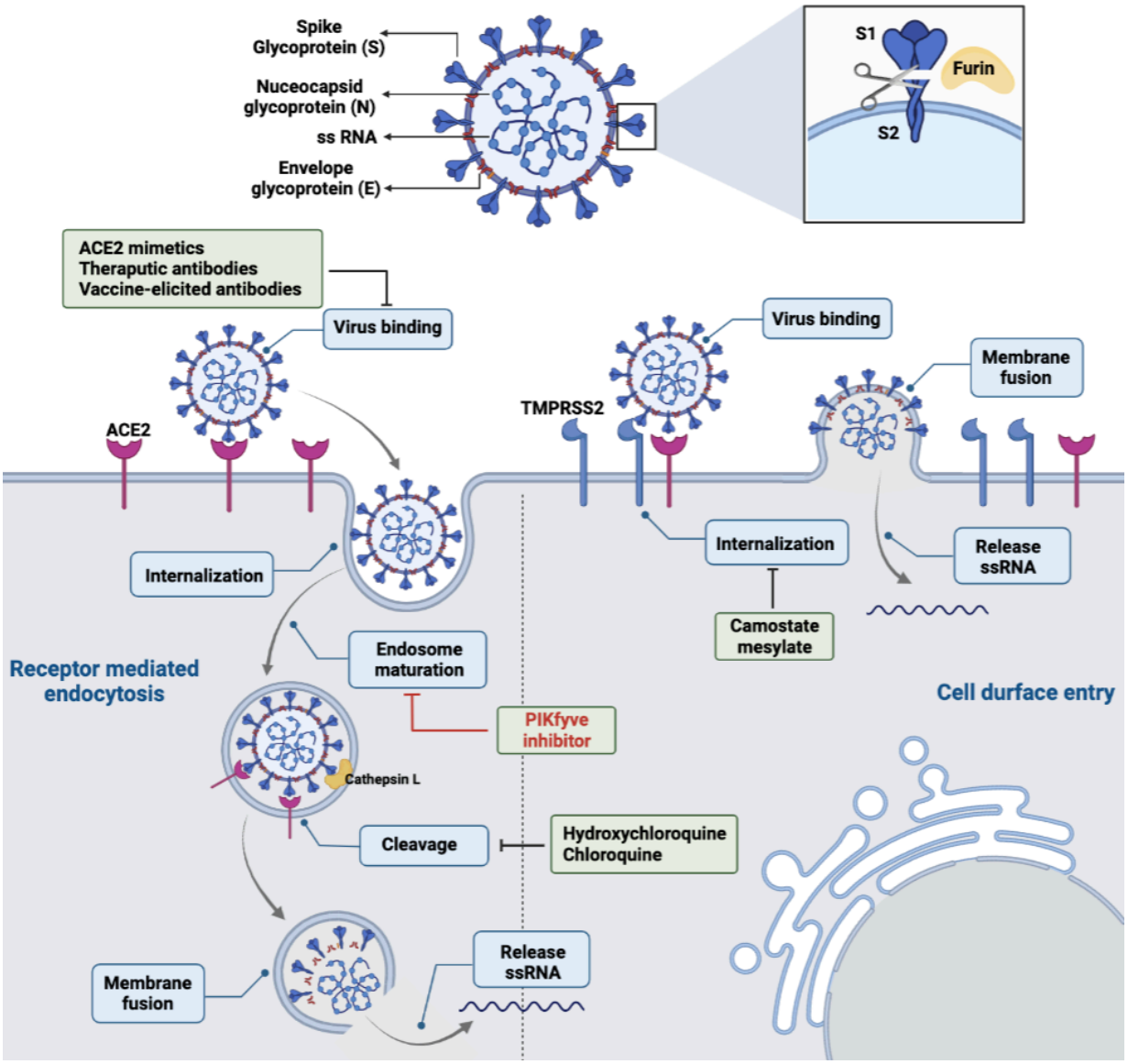

Figure 1.14. Two distinct SARS-Cov-2 entry pathway and the corresponding inhibiting method[128]. Inhibition of PIKfyve blocks maturation of viral containing early endosome, which not only attenuated the acidification of endosome for cathepsin L cleavage of spike protein, but also blocks the release of ssRNA for viral replication.

Interestingly, in terms of cathepsin mediated entry pathway, many studies have shown that, inhibition of PIKfyve kinase can cause a defect in viral trafficking, thus blocking SARS-CoV-2 infection (**Figure 1.14**). In 2020, Chanda and colleagues identified a serial of inhibitors, including Apilimod (18), can antagonize SARS-CoV-2 replication through repurposing of clinical-stage and

FDA -approved small molecules[122]. In the same year, Qu et al. demonstrated that, SARS-CoV-2 enters cells through endocytosis and PIKfyve played a role in this process[123]. Meanwhile, Kang et al. reported that inhibition of PIKfyve kinase with Apilimod (**18**) and Vacoulin-1 (**20**), perturbed the late endosomal trafficking of viral pathogens, and ultimately blocked the release of viral ssRNA into the cytoplasm for replication[124]. However, as mentioned before, there are two pathways of SARS-CoV-2 infection, mediated by the host cell protease cathepsin and TMPRSS2, alone or in combination. In fact, when TMPRSS2 is present, the entry pathway becomes cathepsin independent. Thus, in late 2021, the same group demonstrated that, by the combined usage of Apilimod (**18**) with the TMPRSS2 protease inhibitors, can synergistically prevent SARS-CoV-2 infection in different cell types[125]. In addition, recent studies have shown that the recent Omicron variant of SARS-CoV-2 may preferentially infect cells via the cathepsin-endosomal pathway, rather than through the plasma membrane entry route[126, 131]. Thus, PIKfyve might be a better therapeutic target for the prevention of Omicron infection.

1.4.1.4. Innate immune responses and autoimmune disease.

In 2013, Cai et al. demonstrated that the intracellular target of Apilimod (**18**) is PIKfyve, which plays a critical role in endosome maturation, acidification, and intracellular cargo trafficking. It is the first time that PIKfyve has been linked with the innate immune system[132]. Apilimod (**18**) was previously identified as an inhibitor of interleukin 12 (IL-12) and IL-23 production by Wada and colleagues in 2007[133]. Although Apilimod (**18**) has been evaluated in clinical trials for the treatment of Crohn's disease and rheumatoid arthritis, it was not until 2013 that the cellular target PIKfyve had been identified. The mechanism of PIKfyve effecting the production of IL-12 and IL-23 has been subsequently studied.

Pattern recognition receptors (PRRs) play critical roles in the innate immune system because they initiate the detection of invading pathogens by recognizing the pathogen-associated molecular patterns (PAMPs), and subsequently transmit the signals into cells and activate the innate immune responses via producing inflammatory cytokines[134, 135]. Toll-like receptors (TLRs), as the first identified PRRs, were found comprising 10 members (TLR1–TLR10) in human, and whose cellular localization was proven being important for regulating the signaling. Based on the localization, TLRs can be divided into two subfamilies, the cell surface TLRs and the intracellular TLRs. Cell surface TLRs include TLR1, TLR2, TLR4, TLR5, TLR6, and TLR10, whereas intracellular TLRs, which are localized in the intracellular compartments, such as endosomes, include TLR3, TLR7, TLR8, TLR9, TLR11, TLR12, and TLR13[135-137].

TLR9, one of the intracellular TLRs, is a receptor of unmethylated CpG motifs recognizing viral DNA and RNA within the endosomes[138]. TLR9 is originally expressed in endoplasmic reticulum (ER) and then transported to endolysosomes, where it is proteolytically cleaved by cathepsins at its ectodomain for activation[135-139]. Activated PLR9 meets its ligand CpG motifs in endolysosomes and then stimulate the expression of cytokines. Thus, the intracellular trafficking of both TLR9 and CpG is essential for TLR9 signaling (**Figure 1.15**)[135-139]. As discussed before, PIKfyve regulates the endosome trafficking through production of PI(3,5)P_2. To demonstrate the role PIKfyve played in TLR9 signaling, Hazeki et al. treated macrophages with a PIKfyve inhibitor YM201636 (**17**) and monitored the localization of CpG[138]. What they found was, with the inhibition of PIKfyve, the CpG was enriched in the early endosomes, whereas the TLR9 was localized in the late endosomes. CpG mediated expression of cytokine also decreased in the absence of PIKfyve. However, different from the effect of PIKfyve dysfunction in macrophage, in

plasmacytoid DCs, the localization of CpG in early endosomes promotes the type I IFN production, whereas CpG in lysosomes leads to nuclear factor (NF)-κB activation[138-140].

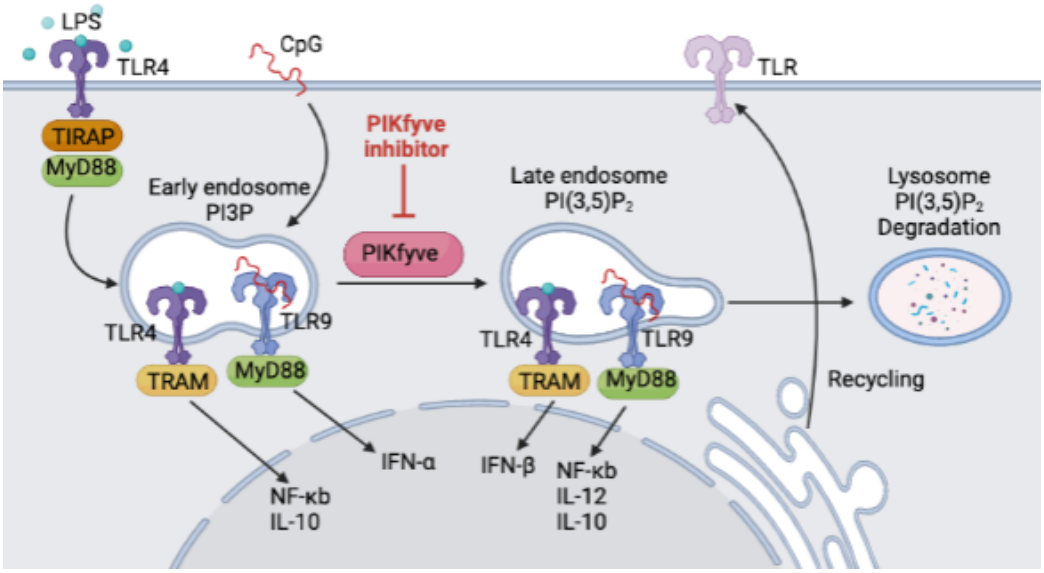

Figure 1.15. The role of PIKfyve in toll-like receptor (TLR)-mediated responses[138].

Another TLR affected by PIKfyve is TLR4, which is a well characterized cell surface TLR. Upon recognition of LPS on cell surface, the complex formed was internalized via endocytosis with the help of CD14[138, 141]. The IFN-γ/LPS induced IL-12 production requires the transport of the TLR4-LPS complex from the early endosome to the late endosome (**Figure 1.15**). Thus, the inhibition of PIKfyve with Apilimod (**18**) or the siRNA-mediated knockdown of PIKfyve resulted in a decreased production of IL-20. On the other hand, the MyD88-dependent TLR4 signaling pathway was strongly preferred in the absence of PIKfyve function, where the LPS-induced NF-κB activation was promoted[138].

Many studies have linked TLR2 and TLR4 with inflammatory autoimmune diseases[142, 143]. For example, in rheumatoid arthritis (RA) patients, a synovial hyperplasia and inflammatory cell infiltration caused tissue destruction and joint disability, with higher expression levels of TLR2

and TLR4 than healthy donors[142]. Correspondingly, the LPS stimulated IL-6 and TNFα production were dramatically increased in peripheral blood mononuclear cells from onset rheumatoid arthritis patients than in cells from healthy control subjects. Besides, TLR2 activation increase angiogenesis, cell adhesion, and invasion, which are all the key mechanisms involved in the pathogenesis of RA. Moreover, the elevation of TLR2 and TLR4 expression was also found in systemic lupus erythematosus (SLE) and Psoriasis[142]. As the critical regulator of TLR2 and TLR4 signaling through endocytosis, PIKfyve can have therapeutic effects on autoimmune diseases.

1.4.2. PIKfyve inhibitors

The history of discovering PIKfyve inhibitors can be traced back to the last decade. Most of the PIKfyve inhibitors are discovered through high HTS over small molecule libraries for inhibition of PIKfyve specifically or inhibiting a certain cellular function. For example, while originally synthesized by Hayakawa et al. as an inhibitor of PI3K[144], in 2008, Parker and collogues found that, YM201636 (**17**) (**Scheme 1.5**) has a potent inhibitory activity against PIKfyve *in vitro*, with an IC_{50} of 33 nM, as well as blocking the retroviral budding[118]. During the following 10 years, many other PIKfyve inhibitors were identified, including Apilimod (**18**) and vacuolin-1 (**20**) (**Scheme 1.5**), with most of them proven to have valuable therapeutic benefits. Meanwhile, PIKfyve inhibitors are also valuable biological probes for the studies of cellular functions of PIKfyve, in parallel with genetic knockout of PIKfyve. In addition, in 2020, by repurposing FDA approved small molecules, Apilimod (18) was identified as an effective antiviral agent against SARS-CoV-2 infection[122]. Because of these encouraging results, more attention has been devoted to PIKfyve inhibitors.

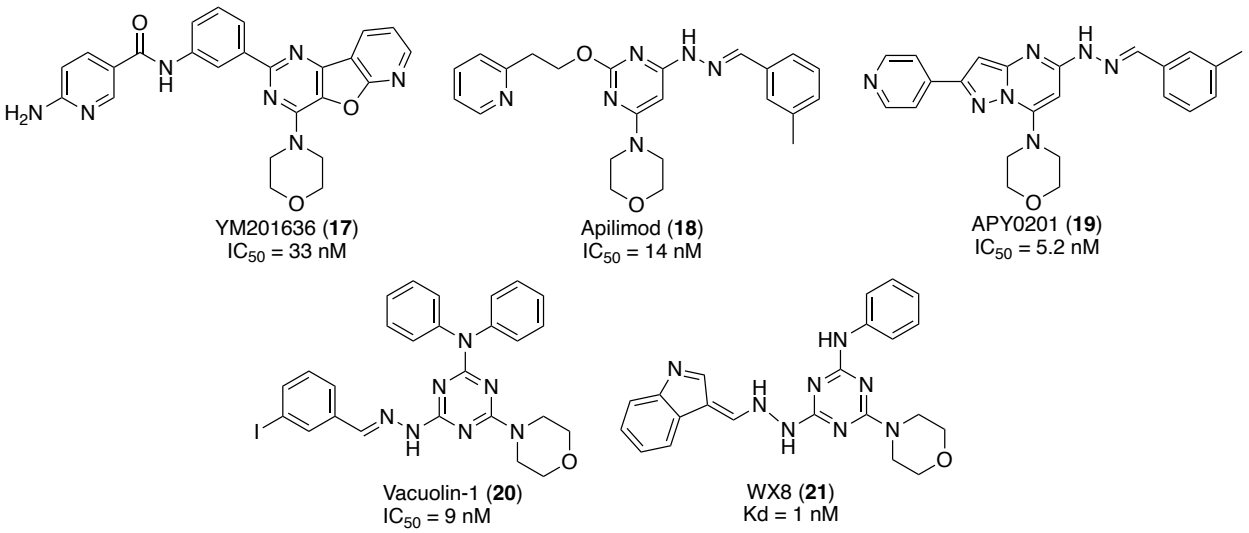

Scheme 1.5. PIKfyve inhibitors containing pyrimidine-morpholine or morpholino-triazine scaffold.

In 2007, Wada et al. discovered Apilimod (**18**) (**Scheme 1.5**) among an 80,000-compound library, as an inhibitor of interleukin-12 (IL-12) and IL-23 production via a cell base screen.[133]. The IL-12 is responsible for the differentiation of naive T cells into the type 1 T helper cell (Th1), whereas IL-23 is critical in generation of effector memory T cells and IL-17–producing T cells[133]. As a result, both IL-12 and IL-23 are important regulators of Th1 and Th7 mediated immune responses and are essential for the clearance of intracellular pathogens. However, excessive production of proinflammatory cytokines usually leads to serious autoimmune diseases, such as multiple sclerosis, rheumatoid arthritis, Crohn's disease, and psoriasis[133, 142]. Thus, suppression of IL-12 and IL-23 production was thought as an effective therapeutic strategy for treatment of autoimmune diseases. In this study, Wada et al. also demonstrated Apilimod (**18**) as a selective inhibitor suppressing Th1 mediated immune response but not Th2. The studies of Apilimod (**18**) on mouse inflammatory bowel disease model showed a markedly reduced inflammatory histopathologic change in the colon[133]. All the results indicated that Apilimod (**18**) is a potential

drug for the treatment of Th1-related autoimmune diseases. As a matter of fact, Apilimod (**18**) was in clinical trials for treatment of rheumatoid arthritis and Crohn's disease. However, at that time, the actual cellular target of Apilimod (**18**) was still unclear.

In 2013, Cai et al. demonstrated that PIKfyve is the target of Apilimod (**18**)[132]. By employing a quantitative chemical proteomics approach, they found that only 3 proteins, PIKfyve, Vac14, and Sac3, interacted with Apilimod (**18**). In a subsequent independent pulldown experiment, among the 3 candidates, only PIKfyve, competed with an inactive Apilimod (**18**) analog AP109. Thus, they concluded that PIKfyve is the actual target of Apilimod (**18**). The *in vitro* activity assay showed that Apilimod (18) inhibited PIKfyve activity with an IC_{50} of 14 nM[132]. Moreover, the lipid kinase inhibition profiling of Apilimod (**18**) indicated that it had no activity toward other kinases, including PIP4K, PIP5K, PI3K, PI4K and mTOR. To further confirm the inhibition activity of Apilimod (**18**) toward IL-12/IL-23 production and the correlation between PIKfyve and TLR-cytokine production, Cai et al. evaluated the cytokine production in BMDCs from Vac14(L156R) (PIKfyve knockout mice are embryonic lethal and the Vac14 L156R mutation blocks its interaction with PIKfyve) mice, where the production of IL12p40 but not CXCL2 was impaired upon treatment with IFNγ/LPS, which are consistent with the cytokine-profiling patterns observed in cells treated with Apilimod (**18**)[132]. In sum, all the results indicated that PIKfyve is a promising target and Apilimod (**18**) is a potent immunomodulatory agent for treatment of Th1- and Th17-mediated inflammatory diseases.

Apart from autoimmune diseases, Apilimod (**18**) was also identified as an anti-proliferative agent and antiviral infection agent. In 2017, Gayle et al. found that pharmacological inhibition of PIKfyve by Apilimod (**18**) induced a selective anti-proliferative and cytotoxic effects against B-cell non-Hodgkin lymphoma (B-NHL)[113]. Furthermore, genome wide CRISPR screen

demonstrated that lysosome dysfunction is a major factor contributing to the cytotoxicity of Apilimod (**18**) toward B-NHL. Accordingly, Apilimod (**18**) is in a phase I clinical trial study for evaluation of the safety and pharmacokinetics in patients with B-NHL.

In 2014, Hayakawa and collogues discovered another inhibitor of IL-12 production, APY0201 (**19**) (**Scheme 1.5**), through a phenotypic cell-based screening and directed medicinal chemistry campaigns[115]. APY0201 (**19**) strongly inhibited IL-12p70 production with an IC_{50} of 8.4 nM. Meanwhile, a significant reduction of IL-12p70 production was also confirmed in mouse orally administrated with APY0201 (**19**). Using a chemical proteomics approach, they also found that the target of APY0201 (**19**) is PIKfyve, with an IC_{50} of 5.2 nM. In addition, the native kinase profiling of APY0201 (**19**) revealed its excellent selectivity. Compared to Apilimod (**18**), APY0201 (**19**) showed an even better selectivity, which might be attributed to its unique pyrazolo[1,5-a] pyrimidine structure.

Comparing the above three inhibitors, i.e., YM201636 (**17**), Apilimod (**18**) and APY0201 (**19**), they share a morpholino-pyrimidine scaffold as their structural core. This unique structure feature may explain why these compounds have the same anti-cytokine production effect and the cellular targets are all PIKfyve. The varied inhibition ability toward PIKfyve might result from the different side groups and their interactions with the amino acids in binding pocket.

Apart from the pyrimidine-morpholine scaffold, morpholino-triazine scaffold is another type of structure core found in PIKfyve inhibitors. For example, Sano et al. identified that vasuolin-1 (**20**) (**Scheme 1.5**) is a potent PIKfyve inhibitor with an IC_{50} value of 9 nM, which is an ATP-competitive inhibitor bearing a distinct morpholino-triazine scaffold[145]. The inhibition effect of vacuolin-1 (**20**) in the late step of autophagy maturation is the same as YM201636 (**17**). Another PIKfyve inhibitor with the morpholino-triazine scaffold is WX8 (**21**) (**Scheme 1.5**), which was

discovered by Sharma et al. in 2019[146]. The WX8-family is a group of compounds that can induce cytoplasmic vacuoles accumulation, meanwhile sharing a morpholino-triazine scaffold core. The WX8-family was originally identified in a high throughput screen as compounds that induce DNA re-replication selectively in cancer cells[147]. Later examination revealed that cells treated with these 5 compounds resulted in rapid accumulation of vacuoles[146]. These observations intrigued scientists to study more about this WX8 (**21**) family. By tracking fluorescence labeled lysosome specific biomarkers in live cells that has been pre-treated with WX8 family members, the observed results indicated that the accumulated vacuoles were enlarged lysosomes, which resulted from the homotypic lysosome fusion, rather than heterotypic fusion of lysosomes with autophagosomes, or a reversible inhibition of lysosome fission[146]. Because of the presence of the distinct morpholino-triazine scaffold, which suggests a possibility of anti-phosphatidylinositol kinase activity, Sharma et al. screened WX8 (**21**) over a panel of 468 human kinases, and revealed that WX8 (**21**) bound specifically to PIKfyve, with a K_d value of 1nM[146]. Meanwhile, in this study, Sharma et al. also found that, WX8 (**21**) can selectively kill melanoma A375 cells, a type of autophagy-dependent cancer cell, and it was 100-times more lethal than the lysosomal inhibitors, hydroxychloroquine and chloroquine[146]. Thus, all these results provided a foundation that PIKfyve is a potential target for drug development that could selectively kill autophagy-dependent cancer cells, and inhibition of PIKfyve mediated dysregulation of autophagy may increase the effectiveness of established anti-cancer therapies through combinatorial treatments.

The morpholino-triazine or the triazine scaffold is not the only one in compounds with inhibitory activities against phosphatidylinositol kinases. For example, in 2016, Terajima et al. discovered AS2677131 (**22**) and AS2795440 (**23**) (**Scheme 1.6**) as novel inhibitors, which exhibited pharmacological inhibitory activities for the production of IL-12p40, IL-6 but not for

TNFα in activated macrophages and dendritic cells. Furthermore, they could block the expression of IgM-induced MHC class II on B cell[148]. Through a chemical biological method, these two inhibitors were found to be bound to PIKfyve specifically. In addition, oral administration of AS2677131 (**22**) suppressed adjuvant-induced arthritis in rats[148].

Other atypical PIKfyve inhibitors include MOMIPP (**24**)[149], ESK981 (**25**)[116, 150], and XMU-MP-7 (**26**)[126] (**Scheme 1.6**). MOMIPPP (**24**) was initially identified as a compound inducing methuosis[151]. Then, in 2018, Cho et al. found that MOMIPP is a PIKfyve inhibitor, with a K_d value of 5.3 nM[149]. ESK981 (**25**) is a phase I cleared (maximum tolerated dose was 97.4 mg m^{-2} daily) orally bioavailable multi-tyrosine kinase inhibitor (MTKI), which was originally identified as an angiogenesis inhibitor[116]. In 2021, Qiao and colleagues repurposed it for the treatment of advanced prostate cancer and found that it has an autophagy inhibitory property decreasing tumor growth and potentiating immunotherapeutic responses[116]. An affinity binding screening of ESK981 (**25**) over 22 phosphoinositide kinases found that ESK981 (**25**) exhibited 100% inhibition for PIKfyve, with a K_d value of 12nM. Mechanistically, treatment of ESK981 (**25**) enhances therapeutic response of immune checkpoint blockage by upregulating CXCL10 expression and promoting T cell infiltration in tumor. XMU-MP-7 (**26**), which was originally discovered as a cancer methuosis inducer, was repurposed as antiviral agent against SARS-CoV-2 and its various variants, especially the highly contagious Delta and the heaviest mutated Omicron, and the results showed that it was highly effective in comparison to Apilimod (**18**) and other FDA-approved small molecule drugs for COVID-19 treatment[126]. Likewise, affinity binding assay revealed that XUM-MP-7 (**26**) was a PIKfyve inhibitor, which dramatically induced vacuoles in cells as Apilimod (**18**). Thus, the mechanism that MUM-MP-7 (**26**) blocks SARS-CoV-2 is the same as Apilimod (**18**).

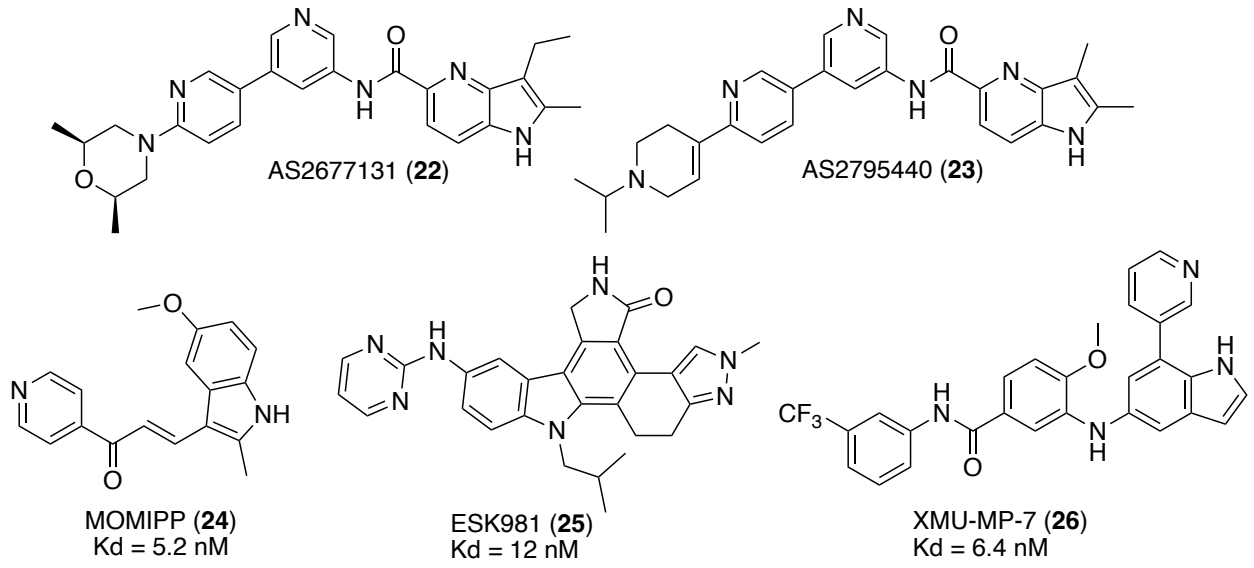

Scheme 1.6. Atypical PIKfyve inhibitors.

1.5. Discussion

Current research of PIPK function and dysfunction revealed novel roles of PIPKs in disease pathogenesis. Not only PIP5K, as an upstream effector of PI3K/Akt pathway, whose dysfunction has been linked to tumorigenesis, but also PIKfyve, as the major regulator of endolysosomal system, whose dysfunction was often related to neurodegenerative diseases, has substantial merits as novel targets for inhibitor design to prevent viral infection and enhancing tumor infiltrations by T cells. So far, there have been many PIPK inhibitors identified (Some of them are summarized in **Table 1.1**), most of which was discovered through HTS and empirical optimization on the basis of SAR. Some of the inhibitors showed fantastic outcomes in preclinical studies, and one of the PIKfyve inhibitors, Apilimod (**18**), is in clinical trials for its safety in NHL and ALS patients, as well as for the prevention of SARS-Cov-2 infection.

Table 1.1. PIPK inhibitors

Target	Inhibitor	Affinity	Inhibition Mechanism	Application
PIP5K	UNC2320 (**1**)	PIP5Kγ IC_{50} = 41 nM	ATP competitive	Chronic pain
	ISA-2011B (**2**)	/	/	Prostate cancer & breast cancers
	NCT504 (**3**)	PIP5K α/β/γ IC_{50} = 1.7 / 1.0 / 0.67 μM	ATP competitive	/
	"Compound **13**" (**4**)	PIP5Kα IC_{50} = 1.55 μM	Substrate competitive	/
PIP4K	I-OMe-AG-538 (**5**)	PIP4Kα IC_{50} = 1 uM	ATP competitive	/
	a131 (**6**)	PIP4Kα IC_{50} = 1.9 uM	ATP competitive	Cancer
	BAY-091 (**7**)	PIP4Kα IC_{50} = 3 nM	ATP competitive	/
	BAY-297 (**8**)	PIP4Kα IC_{50} = 69 nM	ATP competitive	/
	SAR088 (**9**)	PIP4Kβ IC_{50} = 3.8 uM	ATP competitive	Diabetes
	NIH-12848 (**10**)	PIP4Kγ IC_{50} = 1 uM	Substrate competitive	/
	NCT-504 (**11**)	PIP4Kγ IC_{50} = 15.8 uM	Allosteric	Neurodegenerative disorders
	"Compound **40**" (**12**)	PIP5Kγ Kd = 68 nM	ATP competitive & allosteric	/
	THZ-P1-2 (**13**)	PIP4K α/β IC_{50} = 0.95 / 5.9 uM	Covalent inhibitor	cancer
	"Compound **30**" (**14**)	PIP4K α/β IC_{50} = 1.34 / 9.9 uM	Covalent inhibitor	/
	CVM-05-002 (**15**)	PIP4K α/β IC_{50} = 0.27 / 1.69 uM	ATP competitive	/
	"Compound **13**" (**16**)	PIP4K α/β IC_{50} = 1.96 / 9.4 uM	ATP competitive	/

Table 1.2 (cont'd)

PIKfyve	YM201636 (**17**)	IC_{50} = 33 nM	ATP competitive	Viral infection
	Apilimod (**18**)	IC_{50} = 14 nM	ATP competitive	Viral infection & autoimmune diseases & cancers
	APY0201 (**19**)	IC_{50} = 5.2 nM	ATP competitive	/
	Vacuoline-1 (**20**)	Kd = 9 nM	ATP competitive	neurodegenerative disorders
	WX8 (**21**)	Kd = 1nM	ATP competitive	cancers
	AS2677131 (**22**)	/	ATP competitive	anti-inflammatory
	AS2795440 (**23**)	/	ATP competitive	anti-inflammatory
	MOMIPP (**24**)	Kd = 5.2 nM	ATP competitive	
	ESK981 (**25**)	Kd = 12nM	ATP competitive	Enhance immune check point therapy
	XMU-MP-7 (**26**)	Kd = 6.4 nM	ATP competitive	Viral infection (omicron)

There is still much to be learned about PIPKs. The study of PIPKs, especially the role PIPKs in diseases and PIPK inhibitors, has attracted increasing attention in the recent decade. Except for Apilimod (**18**), all the other PIPK inhibitors are currently only in preclinical studies, and no PIPK inhibitor has been approved for clinical usage.

After literature review, in my opinion, there are many challenges remaining in the development of PIPK targeting therapies. First, targeting PIPKs as therapeutic method exhibits potential safety risks. As the interconverting enzymes in the phosphoinositide signaling system, the way PIPKs affect physiological functions is mostly through the regulation of phosphoinositide interconversion. For example, PIKfyve dysfunction blocks endosome maturation, which is mediated via decreasing $PI(3,5)P_2$ production on endosomal membrane. However, the

phosphoinositide signaling system can be viewed as a network, that is, when one PPIn is altered, another one may also be affected. Moreover, as the second massager and the convergence point of many other signaling pathways, any alternations in PIP_2 level can be amplified and significantly affecting the following signaling routes. Thus, simply inhibiting one PIPK may result in unpredictable adverse effects. Second, each PIPK has different subcellular distributions and distinct local functions. For example, PIKfyve is essential for neuron growth, whose dysfunction results in neurodegenerative disease. In epithelial cells, PIKfyve is essential for endo-lysosome fusion, whose inhibition may prevent viral infection. Therefore, to develop PIPK inhibitors, the biodistribution *in vivo* or the targeted delivery to the desired organ must be considered.

Despite these concerns, there are many considerable merits for developing PIPK-targeting therapies. In the timeline of the 20-year of PI3K inhibitor discovery, many patients with advanced cancer emerge resistance to new PI3K targeting treatments due to PI3K mutations. Thus, it is necessary to identify new and complementary targets for development of novel therapies. One of such targets could be PIP5K, which is an upstream regulator of PI3K/Akt pathway. The inhibition of PI3K and PIP5K together may result in synergistic inhibitory effects, as well as ameliorating the resistance problem. On the other hand, for Omicron variant of SARS-Cov-2, the infection is preferentially through the cathepsin mediated endocytosis pathway, where the traditional serine protease inhibitors may not be able to block its entry. Thus, the study of PIKfyve inhibitor may provide additional treatment options.

In summary, it is imperative to investigate the PIPK functions and targeting therapies. But, during the study, it is more desirable to take the phosphoinositide signaling system as a whole and obtain a comprehensive picture of the roles PIPKs played in the physiological signaling network.

Chapter 2 Rational Design and Synthesis of D-galactosyl lysophospholipids as Selective Substrates and Non-ATP-Competitive Inhibitors of Phosphatidylinositol Phosphate Kinases

2.1. Introduction

A common strategy of developing kinase inhibitor is to target the ATP binding site, which is a deep cleft sandwiched by the *N*-terminal and the *C*-terminal lobes conserved in all eukaryotic kinases. Inhibitors targeting the ATP binding site have been reported for various PIPK family members [35, 37, 57, 60, 132, 152]. However, the fact that more than 500 human kinases share a similar ATP binding pocket imposes a challenge to develop highly selective ATP-competitive inhibitors. Other ATP-utilizing enzymes may also be affected by kinase inhibitors [153]. As the intracellular ATP concentration is in millimolar range [154] and the K_M values for ATP of a large majority of kinases fall within the range of low to medium micromolar [155], an effective ATP-competitive inhibitor must have a high affinity with a dissociation constant of low nanomolar or better to effectively compete with intracellular ATP. To circumvent the potential pitfalls associated with ATP competition, an alternative strategy is to target the substrate binding site, which can be unique in geometric and electrostatic properties among the kinases as they phosphorylate distinct substrates (**Scheme 2.1**). Targeting the substrate binding site has been demonstrated to be an effective approach to develop kinase inhibitors with high selectivity [156]. In addition, additive or synergistic effects among inhibitors with distinct working mechanisms would lead to better therapeutic effectiveness and lower adverse effects when they are applied together.

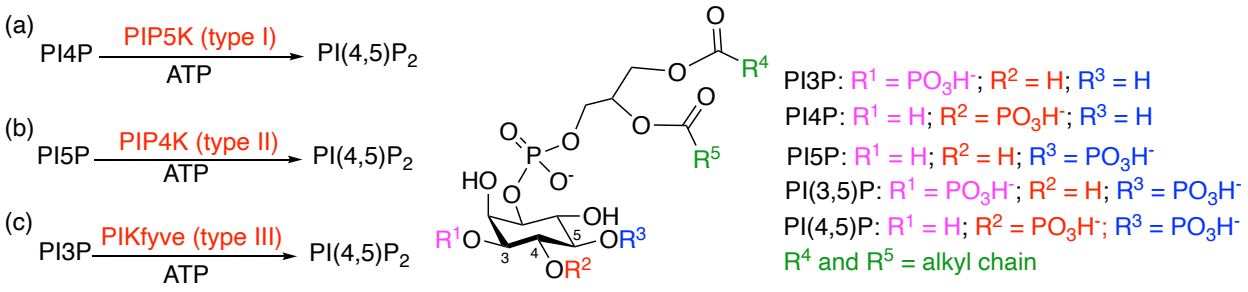

Scheme 2.1. Schematic representation of PIP (PI3P, PI4P and PI5P) phosphorylation by PIPKs. (a) Phosphorylation of PI4P by PIP5K (type I); (b) Phosphorylation of PI5P by PIP4K (type II); and (c) Phosphorylation of PI3P by PIKfyve (type III).

To date, there have been no inhibitors reported aimed at the substrate binding sites of lipid kinases. In this chapter, we designed and synthesized novel lipid substrate mimetics to target PIPK's substrate binding site by taking advantage of the nearly identical stereochemistry between *myo*-inositol and β-D-galactose (**Scheme 2.2a**). Specifically, we produced a panel of D-galactosyl lysophospholipids **1-6** (**Schemes 2.2b & c**) to mimic PI4P, the natural substrate of PIP5K, as a new strategy to develop PIPK inhibitors. Our data showed that (1) a PI4P mimetic was efficiently phosphorylated by PIP5Ks in the same manner as PI4P, but it could not be phosphorylated by PIP4Ks or PIKfyve, indicative of an artificial substrate with a higher selectivity than PI4P; and (2) derivatization of the PI4P mimetic led to the discovery of a non-ATP-competitive pan-PIPK inhibitor with a preference towards PIKfyve, which additively reduced the activity of PIKfyve with an ATP-competitive inhibitor, Apilimod. These findings open the door toward developing D-galactose-based phosphoinositide mimetics as selective inhibitors of PIPKs and other phosphoinositide-processing enzymes, many of which have been validated as drug targets [157-160].

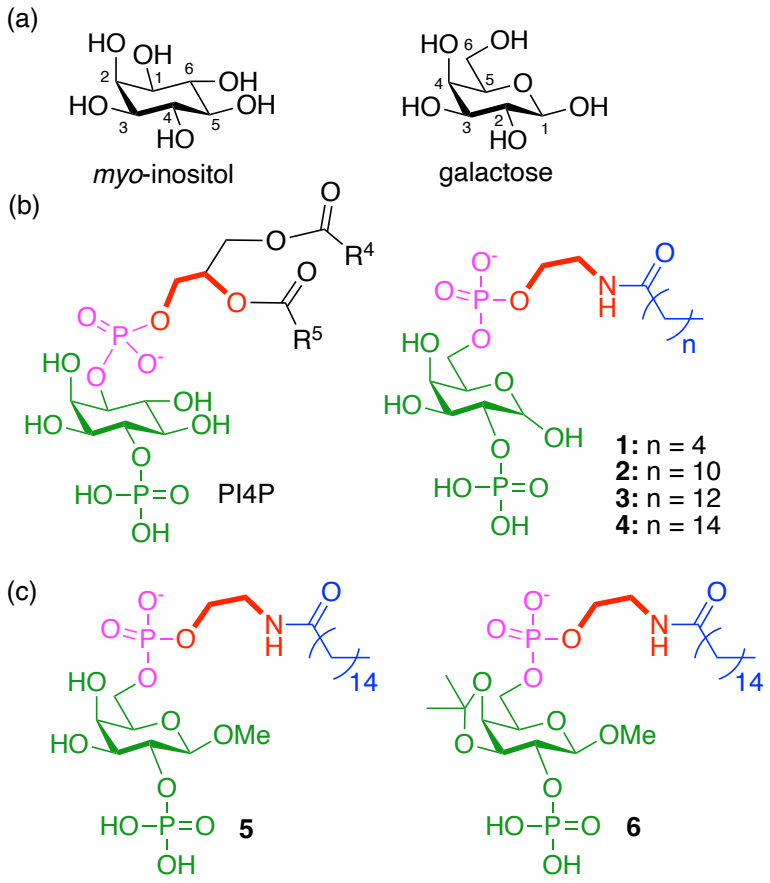

Scheme 2.2. PI4P mimetics synthesized in this work. (a) Comparison of stereochemistry between myo-inositol and D-galactose. (b) Comparison of PI4P with designed 2-phosphate D-galactosyl lysophospholipids (**1-4**). (c) Derivatives of **4** (i.e., compounds 5 and 6) designed as potential lipid substrate competitive inhibitors. The equivalent components are shown in the same color and the ethanolamine linker is bolded.

2.2. Results

2.2.1. Design and synthesis of D-galactosyl lysophospholipids 1-4

Our first designs were a series of the PI4P mimetics **1-4** (**Scheme 2.2b**) with varied length of the alkyl chain. To enhance the overall synthetic efficiency, we envisioned that the 2-*O* and 6-*O* positions of galactoside **7** can be functionalized sequentially with phosphoramidites **8** and **9** first (**Scheme 2.3**). Phosphoramidite **9** bears a t-butoxycarbonyl (BOC) protected ethanolamine linker. Upon formation of the phosphate esters, the Boc group could be removed to generate the free

amine, which could be amidated to divergently produce PI4P mimetics **1-4** with varying chain length.

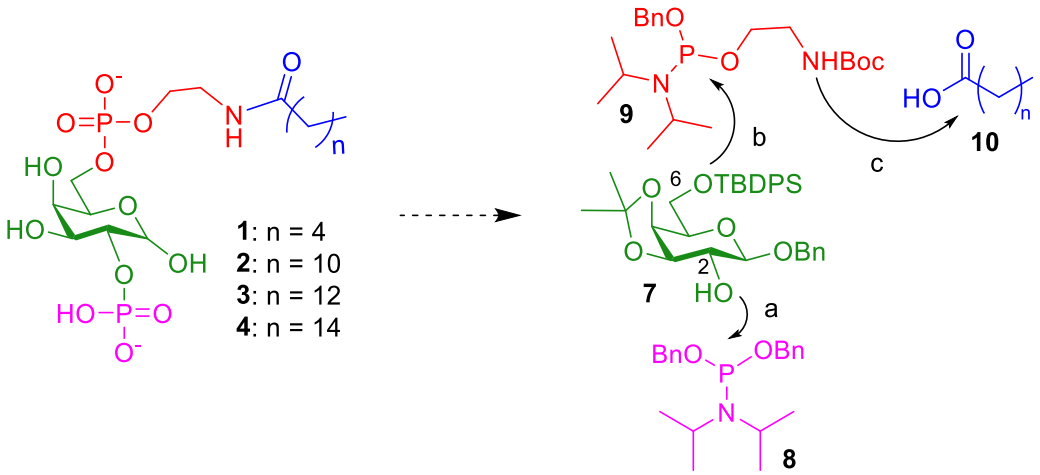

Scheme 2.3. Retrosynthetic design of D-galactosyl lysophospholipids **1-4**.

To synthesize the galactoside building block **7**, we started with the commercially available D-galactose pentaacetate (**Scheme 2.4a**). Glycosylation of D-galactose pentaacetate with benzyl alcohol promoted by boron trifluoride-diethyl ether complex ($BF_3{\cdot}OEt_2$) provided the corresponding β-benzyl glycoside **11** ($^3J_{H1\text{-}H2}$ = 7.9 Hz). The reaction should be quenched in 4 hours upon complete consumption of the starting material to obtain the β-glycoside as the major product, as prolonged treatment led to the formation of the corresponding α-glycoside as the major product presumably due to *in situ* anomerization of **11**. Global deacetylation of **11** under the Zemplén condition followed by selective protection of the primary OH with *tert*-butyldiphenylsilyl moiety (TBDPS), and protection of 3,4-diols with 2,2-dimethoxypropane gave the desired galactoside building block **7**.

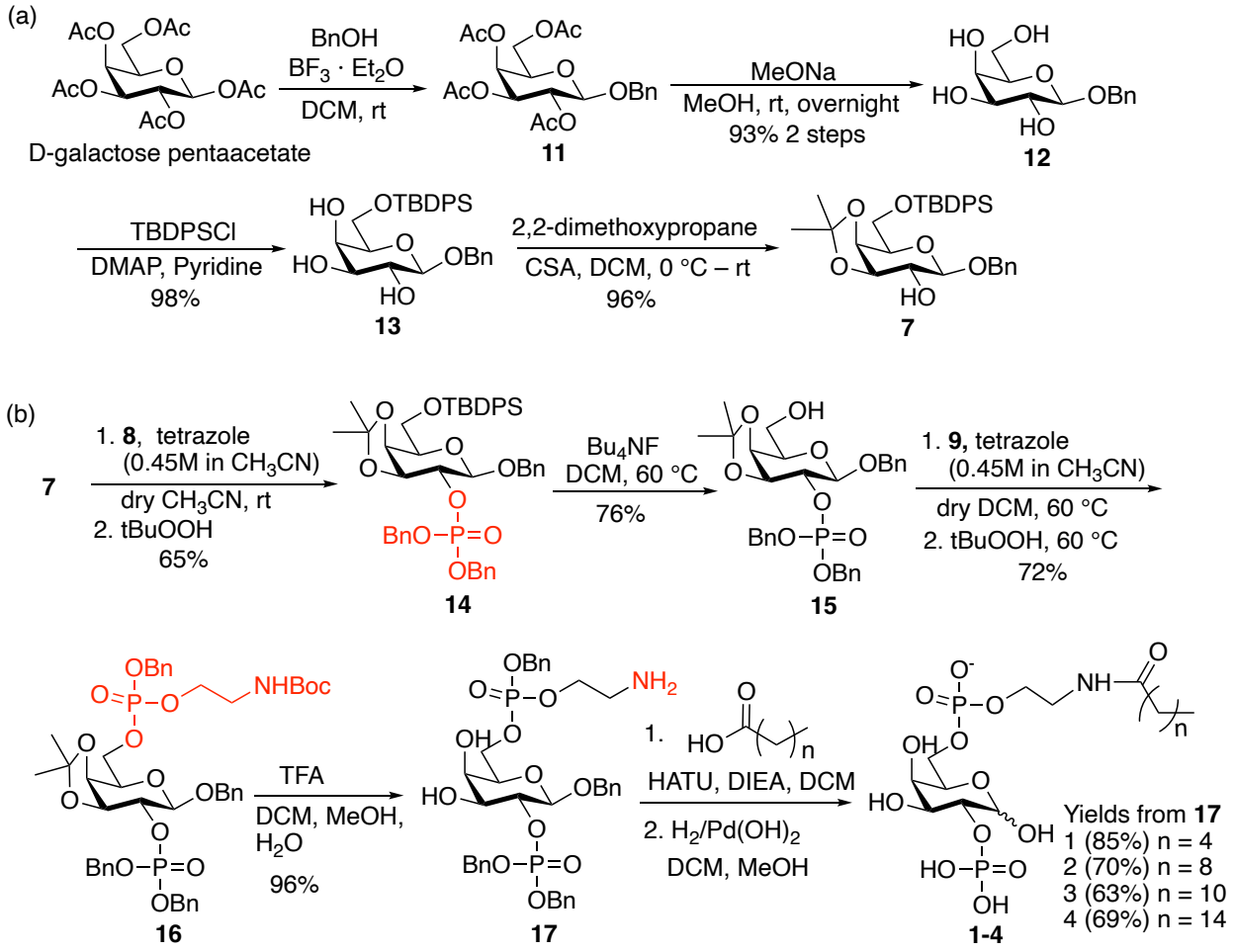

Scheme 2.4. (a) Synthesis of the D-galactoside building block **7**. (b) Synthesis of the D-galactosyl lysophospholipids **1-4**.

The phosphorylation of 2-OH of galactoside **7** was performed via a one-pot protocol, using dibenzyl phosphoramidite **8** and *t*BuO$_2$H as the phosphorylating and oxidizing reagents (**Scheme 2.4b**), respectively, to furnish the mono phosphorylated compound **14**. After removal of the 6-*O*-TBDPS from **14**, the second phosphate group was installed with the freshly made phosphoramidite **9** (**Scheme 2.4b**), followed by *in situ* oxidation to afford the diphosphorylated compound **16**. The BOC and isopropylidene groups of **16** were then deprotected by treatment with trifluoroacetic acid (TFA), and the resulting free amine was coupled with alkanoic acids followed by catalytic

hydrogenolysis with $Pd(OH)_2$ under H_2 producing the final compounds **1-4** with varied lengths of the fatty acid acyl chain.

2.2.2. Identification of a D-galactosyl PI4P mimetic as the selective substrate of PIP5Ks.

With compounds **1-4** in hand, their interactions with PIP5K were tested, as PIP5K utilizes PI4P as the natural substrate. The compounds were incubated with the purified PIP5Kα from zebrafish (zPIP5Kα) in the presence of radioactive γ-^{32}P-ATP and Mg^{2+}. The lipophilic substances were then extracted by organic solvent and subjected to thin-layer chromatography (TLC) analysis, followed by exposure to a storage phosphor screen and quantification by a phosphoimager. As shown in **Figure 2.1a**, significant amounts of phosphorylated species were detected only for **3** and **4**, with the phosphorylation of **4** much more prominent than that for **3**. The dose-dependent study indicated that **4** is phosphorylated by zPIP5Kα with the K_M of 10±1.3 μM (**Figure 2.1b**).

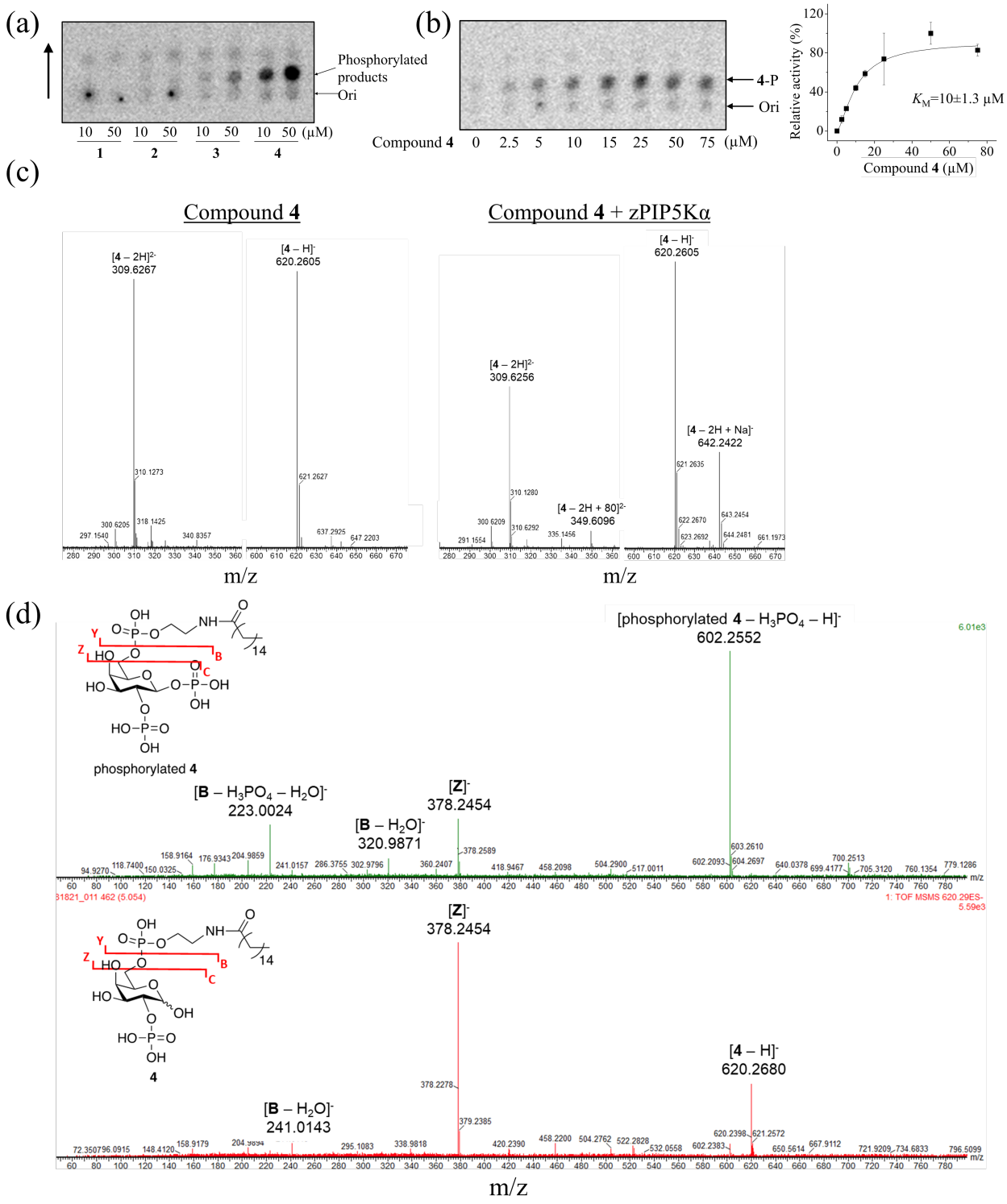

Figure 2.1. Phosphorylation of 2-phosphate D-galactosyl lysophospholids by zPIP5Kα. (a) TLC of the phosphorylation reactions of the PI4P mimetics (**1-4**) with varied length of fatty acyl chain as detected via radioactive ^{32}P. Ori stands for the origin of the reaction mixture spotted on the TLC. The direction of TLC is indicated by the arrow. (b) Dose-dependent phosphorylation of **4** by

Figure 2.1 (cont'd)
zPIP5Kα. 4-P stands for phosphorylated compound **4**. The K_M was estimated by curve fitting using the Hill model based on the intensities of ^{32}P radioactivities of product spots on TLC. The error bars indicate the S.D. (n=2). (c) Identification of mono-phosphorylated compound **4** by mass spectrometry. The MS spectra of **4** before (left) and after (right) reaction with zPIP5Kα. The double-charged species (349.6096 Da) corresponds to the phosphorylated compound **4**. (d) MS/MS fragmentation of phosphorylated **4** (upper) and **4** (lower) after separation by ion-pair liquid chromatography (Figure S1). The proposed fragmentation patterns of compound **4** and its phosphorylated product are depicted.

In order to characterize the product, mass spectrometry analysis was carried out. With compound **4** as the substrate (621.26 Da), a newly formed double-charged species with +80 Da molecular weight in the negative ion mode (349.61 Da) was detected in the reaction mixture after the treatment with zPIP5Kα, indicative of mono-phosphorylation on a hydroxyl group (**Figure 2.1c**). No double or multiple phosphorylated products were detected. MS/MS fragmentation of the phosphorylated product separated in an ion-pair liquid chromatography (**Figure S1**), together with MS/MS fragmentation of **4** conducted under the same condition, supported a fragmentation pattern where the glycosyl phosphate bond at the anomeric position and the phosphodiester bond at C6 are broken, whereas the phosphoester bond at C2 is preserved in both **4** and its phosphorylated product (**Figure 2.1d**). These results indicate that the anomeric OH of **4** likely adopts the equatorial configuration in the enzyme binding site similar to the *myo*-inositol 4-phosphate of PI4P so that **4** is phosphorylated by PIP5K in the same manner as PI4P. Given that these D-galactosyl lysophospholipids likely form micelles with different sizes, the dependence of reactivity of the PI4P mimetics on fatty acyl chain length, i.e., **4** has the highest reactivity compared to **1**-**3**, supports the notion that PIP5K's activity is membrane surface dependent and highly sensitive to membrane properties [161-163].

Next, we tested whether **4** could be phosphorylated by other members in the PIPK family, including mouse PIP5Kγ (mPIP5Kγ), zPIP5Kα, human PIP4Kα (hPIP4Kα), human PIP4Kγ

(hPIP4Kγ), and human PIKfyve (hPIKfyve). Except for hPIKfyve which was expressed in mammalian cells with an *N*-terminal FLAG tag, the other PIPKs were expressed in *E.coli* with an N-terminal His-tag (**Figure S2**). As shown in **Figures 2.2** and **2.11**, although PI4P was phosphorylated by all the tested PIPKs, **4** was only robustly processed by PIP5Ks, including the mPIP5Kγ from mouse and zPIP5Kα from zebrafish, but not by PIP4Ks or PIKfyve under the same conditions, indicating that **4** is a selective substrate exhibiting a greater preference for PIP5K over the other two types of PIPKs than PI4P.

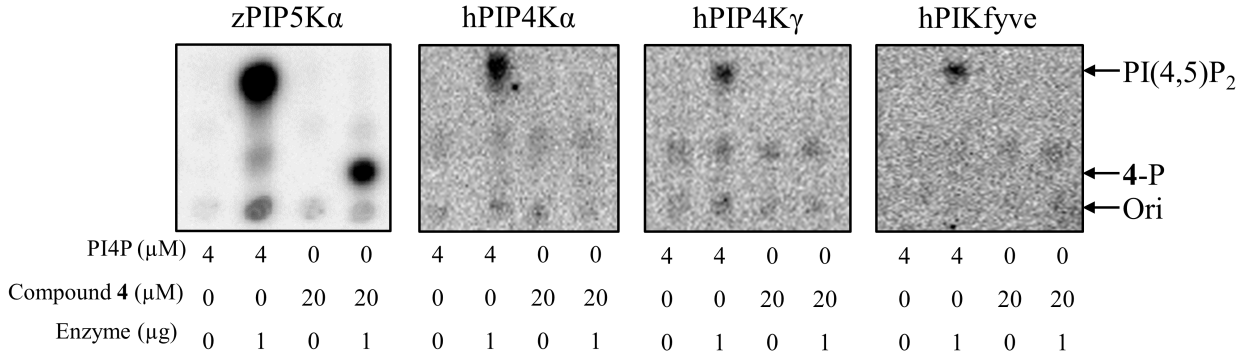

Figure 2.2. Comparison of PI4P and compound **4** phosphorylation by PIPKs. Phosphorylation of **4** by mPIP5Kγ is shown in Figure S3 zPIP5Kα exhibited a higher enzymatic activity towards PI4P than other PIPKs tested.

2.2.3. Identification of a D-galactosyl PI3P mimetic as the selective substrate of PIKfyve.

With the finding that compound **4** was a selective substrate of PIP5Ks, which can be phosphorylated at the anomeric position by PIP5K as proved by LC-MS/MS study, we wondered whether we could design and synthesis another D-galactosyl lysophospholipid as a selective substrate of PIKfyve by mimicking its natural substrate PI3P. The only difference in structure between PI3P and PI4P is the phosphorylation site on the inositol ring, where PI3P was phosphorylated on 3-position (**Scheme 2.5a**) while PI4P was phosphorylated on 4-position (**Scheme 2.2b**). Therefore, a plausible PI3P mimetic substrate of PIKfyve is the one that simply

shift the phosphate on 2-*O* position of compound **4** to its 3-*O* position, as compound **18** (**Scheme 2.5a**). Similarly, to synthesize compound **18**, the 3-*O* and 6-*O* positions of galactoside building block **19** could be functionalized with phosphoramidites **8** and **9** sequentially, and lastly linked with alkanoic acid to form compound **18 (Scheme 2.5b)**.

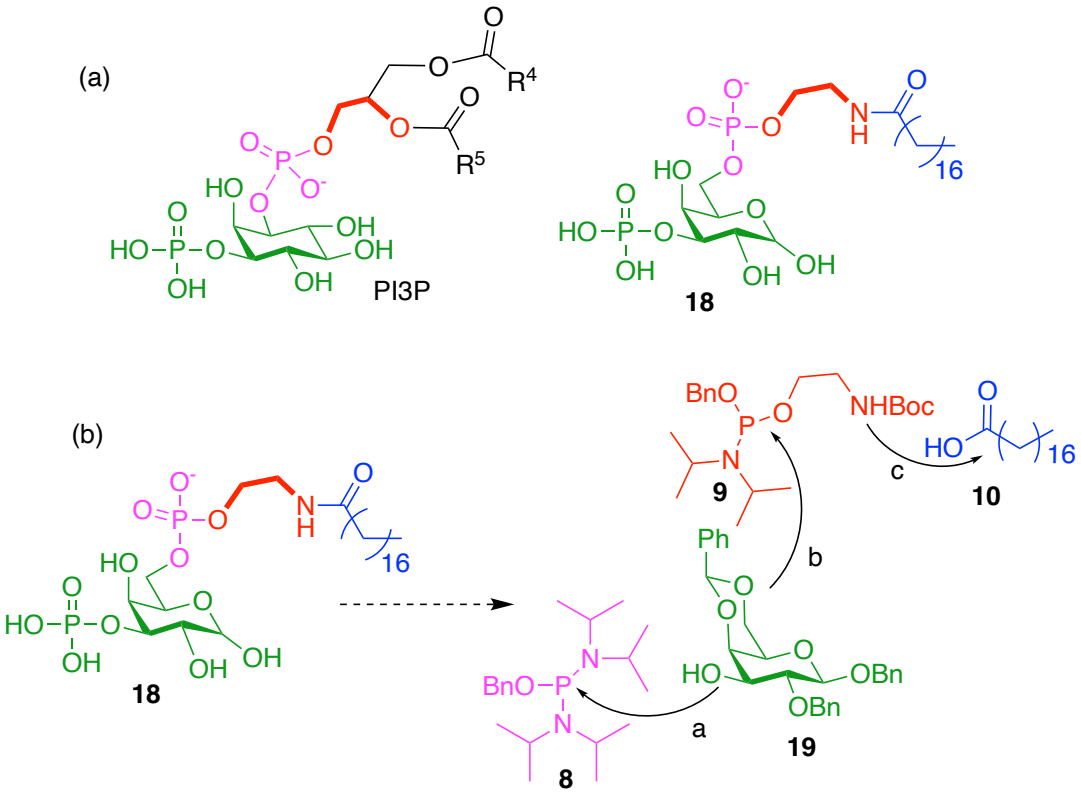

Scheme 2.5. Synthesis of the D-galactosyl lysophospholipid **18** as PI3P mimetics. (a) Comparison of PI3P with designed 3-phosphate D-galactosyl lysophospholipid **18**. (b) Retrosynthetic design of D-galactosyl lysophospholipids **18**.

The key consideration in synthesizing compound **18** is to differentiate 3-*O* and 6-*O* positions of galactose for sequential phosphorylation. Therefore, compound **19** was designed and synthesized with the anomeric and 2-*O* position protected with benzyl groups and 5-*O* and 6-*O* position protected with benzylidene group (**Scheme 2.9**). Then, the 3-OH of galactoside **19** was phosphorylated by phosphoramidite **8** via the same one-pot protocol (**Scheme 2.6**). The

benzylidene group of the generated mono phosphorylated compound **20** was selectively cleaved by triethylsilane (Et_3SiH) and phenylboron dichloride ($PhBCl_2$) to afford the compound **21** with a free 6-OH. The second phosphate group was then constituted with the freshly made phosphoramidite **9** (**Scheme 2.8**) and subsequently oxidized with *t*BuO_2H to form the diphosphorylated compound **22**. The subsequent BOC deprotection, palmitic acid coupling, and global hydrogenolysis of benzyl groups were all carried out following the protocols of preparation of **4**.

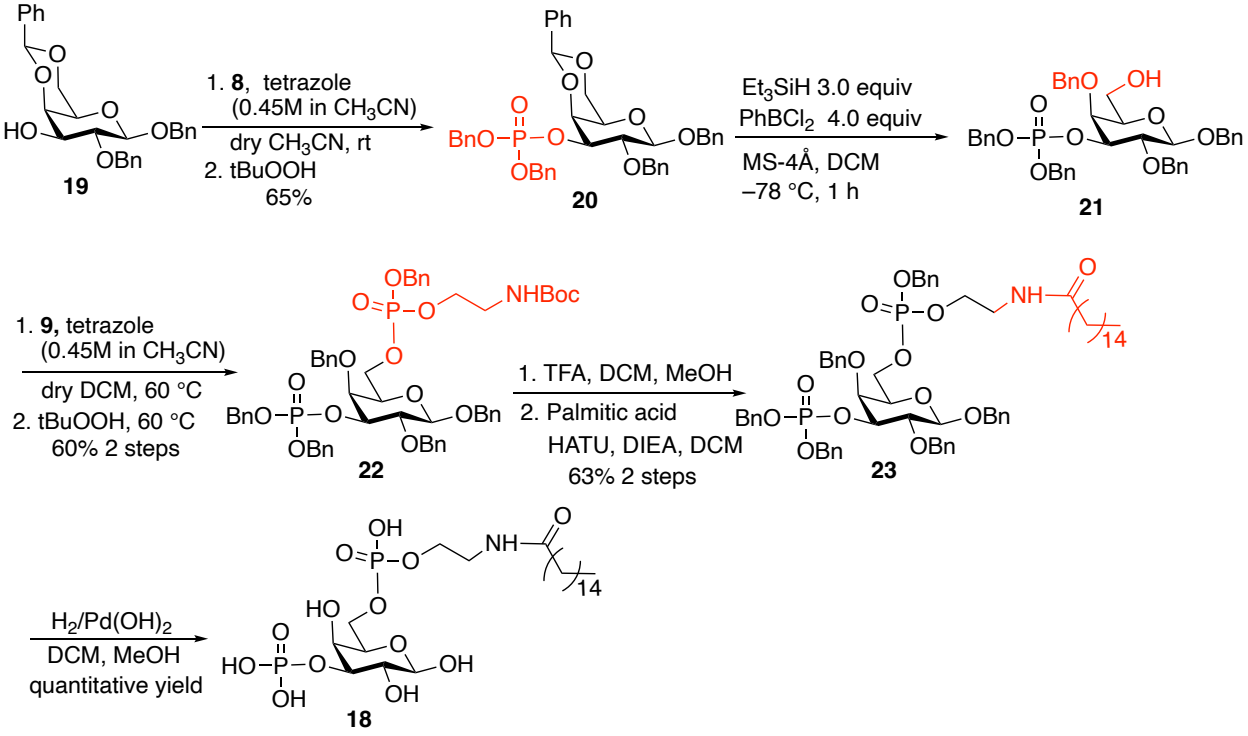

Scheme 2.6. Synthesis of the D-galactosyl lysophospholipid **18** as a selective substrate of PIKfyve.

With compound **18** in hand, we examined its interaction with PIKfyve and its selectivity over the other 2 lipid kinases, using the same radiometric TLC assay. Compound **18** was incubated with the purified hPIKfyve, zPIP4Kα, hPIP4Kα and hPIP4Kγ, in the presence of radioactive γ-^{32}P-ATP and Mg^{2+}. The generated phosphorylated products were extracted by organic solvent and

subjected to TLC analysis. As shown in **Figure 2.3**, compound **18** was significantly phosphorylated by hPIKfyve and zPIP5Kα in a dose dependent manner, but not by human PIP4Kα or PIP4Kγ. Different from compound **4**, which can only be phosphorylated by PIP5K but not the other lipid kinases, compound **18** can be phosphorylated by both hPIKfyve and zPIP5kα, but not PIP4Ks. Compound **18** exhibited a weaker selectivity than compound **4**.

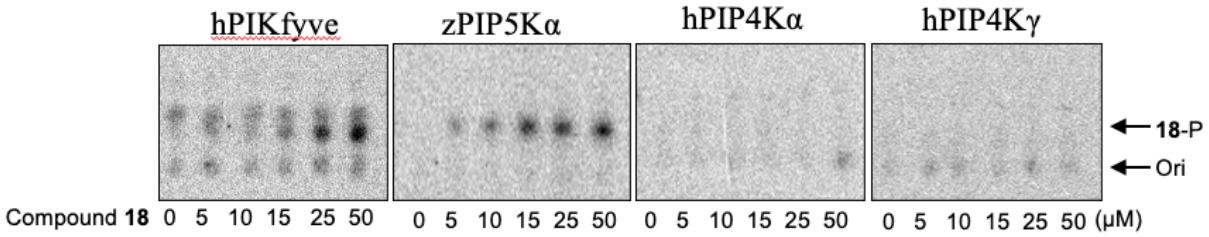

Figure 2.3. Dose-dependent phosphorylation of **18** by purified hPIKfyve, zPIP4Kα, hPIP4Kα and hPIP4Kγ, and comparison of the phosphorylation by PIPKs.

2.2.4. Discovery of a D-galactosyl lysophospholipid as a non-ATP competitive pan-PIPK inhibitor.

As compounds **3** and **4** can be phosphorylated by zPIP5Kα, we expected that they can compete for the enzyme's active site with the natural substrate PI4P. Indeed, as shown in **Figure 2.4**, **4** exhibited a dose-dependent inhibition against PI4P phosphorylation by zPIP5Kα with concomitantly increased phosphorylation of **4**. In contrast, inhibition of zPIP5Kα by **3** was fairly weak even at the high concentration and phosphorylation of **3** was also much less than that of **4**. The positive correlation between the compound reactivity and the inhibition potency is consistent with the notion that the PI4P mimetics **3** and **4** compete with PI4P for the kinase active site. These results also suggest that the observed inhibition of PIP5K is unlikely due to the membrane disruption caused by the lysolipid or detergent effect, because compound **3** would otherwise be a

more potent inhibitor than **4** as a lysophospholipid with a shorter fatty acyl chain perturbs membrane more than the one with a longer aliphatic chain [164].

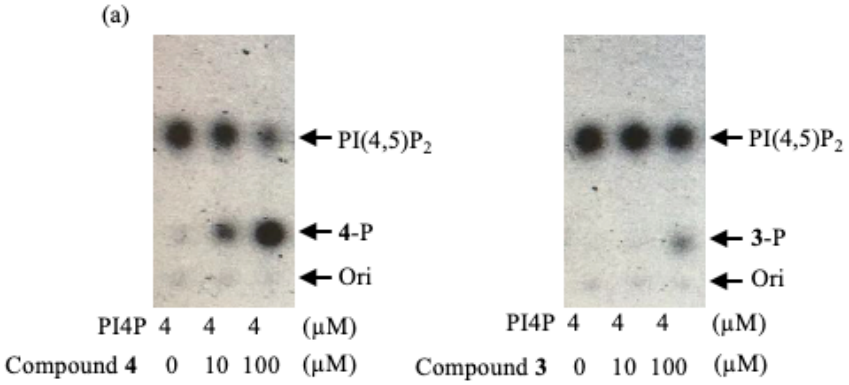

Figure 2.4. Inhibition of zPIP5Kα by **3** and **4**.

Next, we aimed to transform compound **4** into a competitive inhibitor of PIPKs. We first designed compound **5**, which was synthesized starting from methyl-β-D-galactopyranoside **24** following a similar synthetic strategy as that for the preparation of **4** leading to methyl-galactoside **25** (**Scheme 2.7a and Scheme 2.10**). Hydrogenolysis of the benzyl groups in **25** produced **5**, which contained a methoxy group at the anomeric position of the galactoside, thus could not be phosphorylated at the anomeric center. Incubation of **5** with zPIP5Kα and γ-^{32}P-ATP and Mg^{2+} under the same condition as in phosphorylation of **4** did not lead to any ^{32}P labeled products. The lack of phosphorylation of **5** supports the notion that 1-*O* of **4** is phosphorylated by zPIP5Kα. However, **5** did not exhibit significant inhibitory effects toward zPIP5Kα either (**Figure 2.6a**).

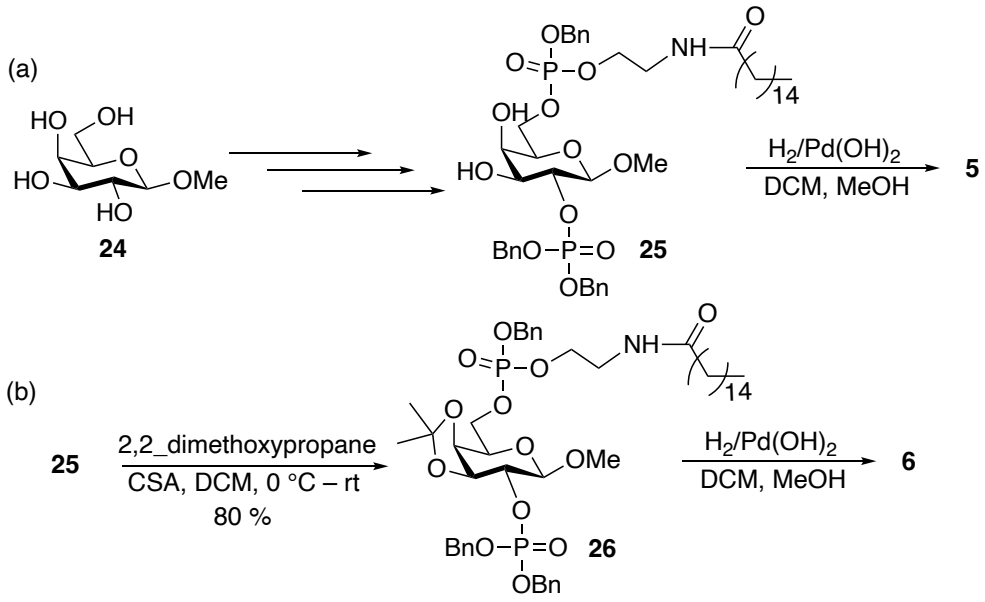

Scheme 2.7. Syntheses of (a) methyl galactoside **5** and (b) **6**.

By examining the structural model of PI4P-bound zPIP5Kα (**Figure 2.5**) [9, 165], we noticed that there is space between the loop containing the PIPK signature "DLKGS" motif near the active site and 2-OH/3-OH of *myo*-inositol of PI4P. We then designed compound **6**, which contains an isopropyl group linking 3-OH and 4-OH of D-galactose (corresponding to 2-OH and 3-OH of *myo*-inositol, **Scheme 2.2a**) potentially filling up this space for better interactions with the enzyme. For synthesis of **6**, the 3,4-diols of compound **25** were functionalized by the isopropylidene group (**Scheme 2.7b**), which was then followed by the hydrogenolysis of the benzyl groups to produce **6**.

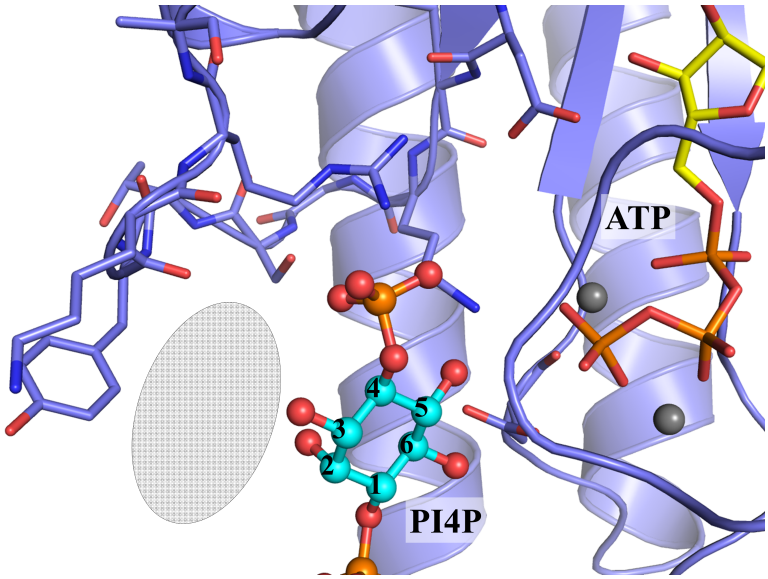

Figure 2.5. Structural model of zPIP5Kα with bound ATP and PI4P. The shaded area indicates a plausible cavity between PI4P and the loop containing the "DLKGS" motif conserved in the PIPK family. The model was built based on the crystal structure of the ATP-bound zPIP5Kα (PDB: 6CMW). PI4P was modeled based on previous mutagenesis studies and structural comparison with other eukaryotic kinases.

Remarkably, compound **6** was found to be a zPIP5Kα inhibitor with the apparent IC_{50} of ~15 μM (**Figures 2.6a** & **2.14**). mPIP5Kγ was also similarly inhibited by **6 (Figure 2.6a)**. As the inhibition by **6** can only be relieved by adding the excessive amount of PI4P, but not by adding ATP (**Figures 2.6b** & **c**), we concluded that **6** is a non-ATP-competitive inhibitor of zPIP5Kα. We next examined the activities of **6** against other PIPKs and it turned out that **6** inhibited all the tested PIPKs, including hPIP4Kα, hPIP4Kγ, and hPIKfyve (**Figure 2.6d**). hPIKfyve appeared to be most sensitive to **6** and the apparent IC_{50} is more than two times smaller than that for zPIP5Kα (6.2 vs 15 μM). Based on these results, we concluded that **6** is a pan-PIPK inhibitor with a preference toward PIKfyve.

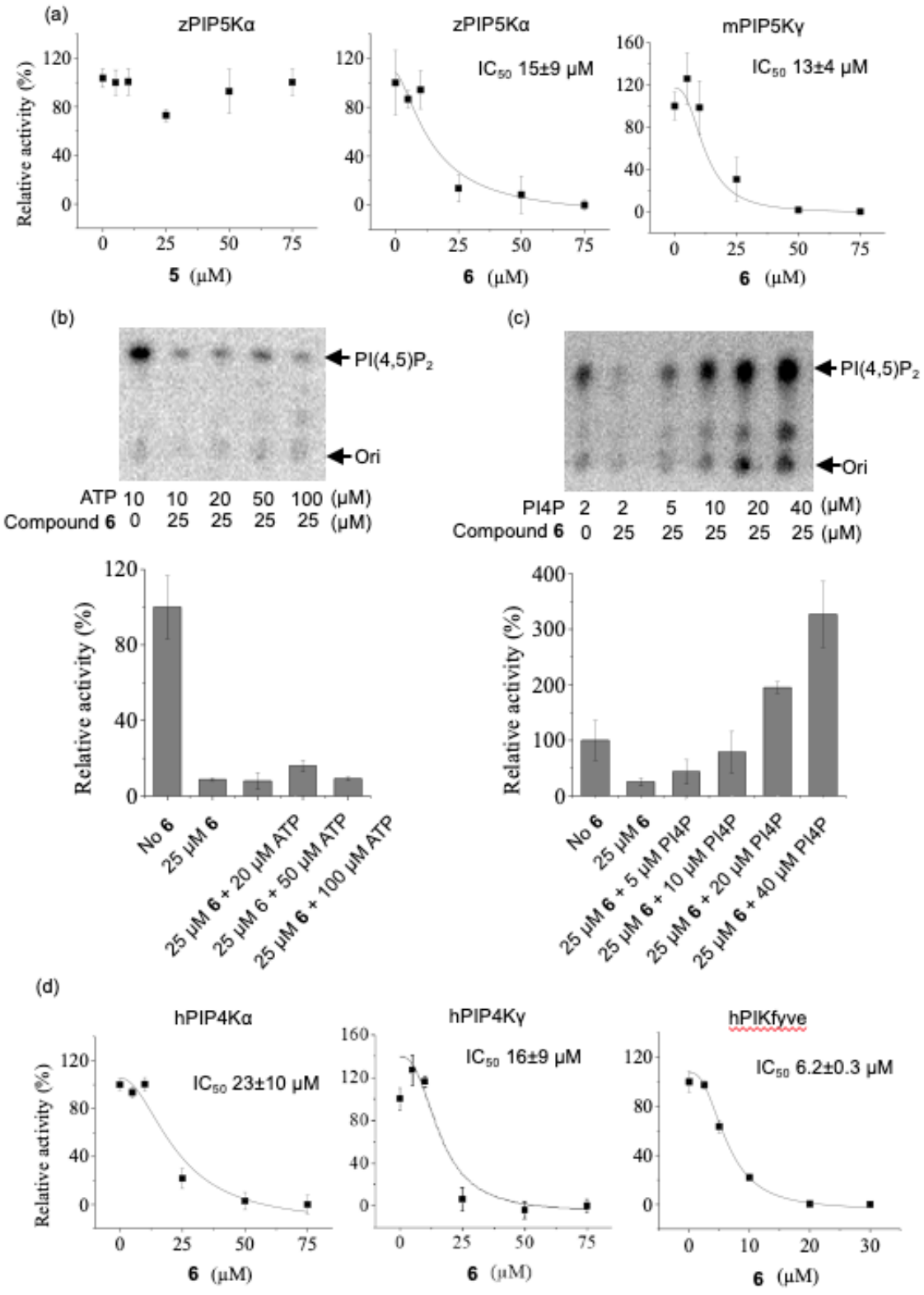

Figure 2.6. Discovery of a non-ATP-competitive pan-PIPK inhibitor with preference toward PIKfyve. (a) Comparison of compound **4** derivatives (compounds **5** and **6**) on inhibition of PIP5Ks.

Figure 2.6 (cont'd)
IC_{50} values were estimated by curve fitting using the Hill model. (b) Inability of ATP to relief inhibition of zPIP5Kα by **6**. (c) Restoration of zPIP5Kα's activity by addition of excessive amount of PI4P. (d) Inhibition of PIP4Ks and PIKfyve by **6**. The shown representative results are from one out of 3-4 independent experiments with three replicates for each data point. The error bars indicate the S.D. The representative TLC results of PIPK inhibition is shown in Figure S4.

PIKfyve is a drug target for a variety of diseases, in particular SARS-CoV-2 infection [122, 124, 166, 167]. Apilimod is a selective PIKfyve inhibitor under clinical evaluation against SARS-CoV-2 and ALS. As **6** targets the lipid substrate binding site, we next examined whether its inhibitory effect can be combined with Apilimod which is known to target the ATP binding site (**Figure S5**). As shown in **Figure 2.7**, when Apilimod at 1 nM was combined with **6** at 5 μM, an additive inhibitory effect was observed, indicating that **6** can significantly potentiate the effectiveness of Aplilimod as a PIKfyve inhibitor.

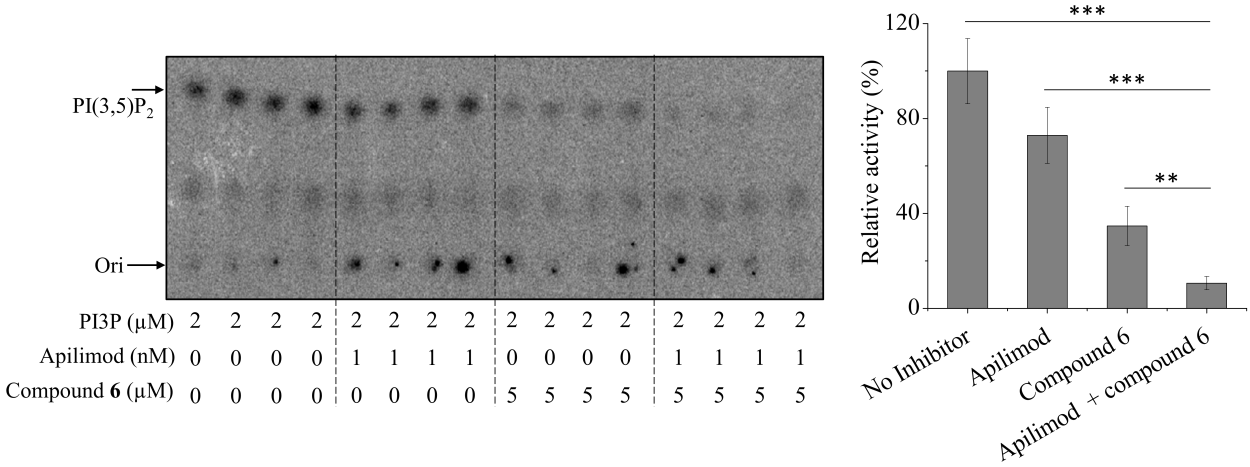

Figure 2.7. Inhibition of hPIKfyve by Apilimod and compound **6**. The shown representative results are from one out of two independent experiments with four replicates for each data point shown. The error bars indicate the S.D. **: P<0.01; ***: P<0.001.

2.2.5. Inhibition of PIP5K by compound 6 results in reduced transferrin endocytosis.

The clathrin-mediated endocytosis requires the production of $PI(4,5)P_2$ on plasma membrane for initiating assembly of CCP (clathrin-coated pits). Therefore, we hypothesis that

inhibition of PIP5K by compound **6** may block the clathrin-mediated endocytosis. To assess it, transferrin was selected as the subject, whose internalization was initiated by binding to the transferrin receptor on plasma membrane and then engulfed into cell via clathrin-mediated endocytosis. HEK293T cells were pretreated with compound **6** for 2 hours, then Alexa 488 conjugated transferrin was added and incubated for 12min. After washing and fixation, the cells were imaged under a confocal microscope for quantitation of internalized transferrin. As shown in **Figure 2.8**, for the cells treated with compound **6**, the intracellular transferrin level was significantly decreased when compared to the control group (DMSO). Quantification of the fluorescence images showed that 10 μM compound **6** inhibited ~ 40% transferrin internalization.

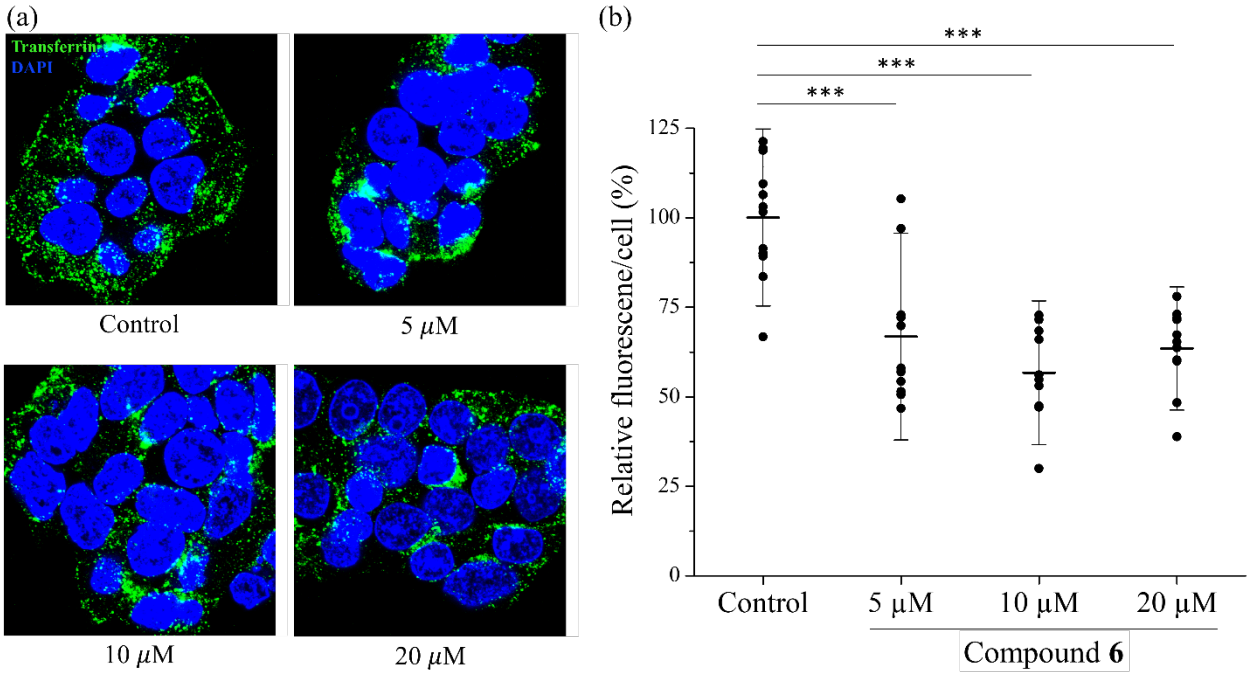

Figure 2.8. Inhibition of transferrin endocytosis by compound **6**. (a) Representative confocal images of HEK293T cells after incubation with Alexa 488 conjugated transferrin (green) in the absence or presence of indicated concentration of compound **6**. The nuclei were stained with DAPI (blue). (b) Quantification of transferrin endocytosis. The green fluorescence intensity per cell is expressed as the percentage of that of the cells in the control group. Each data point represents the average fluorescence intensity per cell in one image and 10-12 images (~200 cells in total) were analyzed for each condition. Statistical analysis was conducted using Student's *t*-test. ***: P<0.001 (Images collected by Dr. Chi Zhang).

2.3. Discussion

PIPKs are promising drug targets against a variety of human diseases, but most of the reported PIPK inhibitors fall into the category of ATP competitors [35, 37, 57, 60, 132, 152]. Targeting the non-ATP binding sites through kinase substrate analogs as non-ATP-competitive inhibitors is an attractive strategy to circumvent the concerns associated with ATP-competitive inhibitors. Two compounds identified in large scale screenings were reported to be the lipid substrate competitive inhibitors for PIP5Kα and PIP4Kγ, respectively [38, 54], but there is no similarity in chemistry between the headgroups of the natural phospholipid substrates and the reported compounds which contain three or four aromatic rings with extremely low aqueous solubility. To the best of our knowledge, the compounds discovered in this work are the first to target the lipid substrate binding sites of PIPKs through rational design.

Using D-galactose derivatives to mimic the *myo*-inositol moiety of phosphoinositides has two advantages over directly derivatizing *myo*-inositol. Firstly, as the phosphoinositides are critically involved in cell signaling, the cells are highly sensitive to the concentration changes of these low-abundance lipids. It is conceivable that a synthetic *myo*-inositol-based phosphoinositide analog and/or its metabolic products may interfere with cell signaling processes, causing unexpected adverse effects. As galactose is one of the major intracellular metabolites, the galactose derivative derived from the synthesized compound is less likely to severely disrupt cell functions when applied at a low micromolar concentration. Secondly, from the perspective of synthesis, differentiating the almost identical hydroxyl groups of *myo*-inositol is much more challenging than galactose functionalization. Indeed, synthesis of *myo*-inositol derivatives often takes more than 20 steps [168, 169], whereas producing D-galactosyl lysophospholipids in this work only took 10 or fewer steps from the commercially available compounds. D-Galactose based phosphonate analogs were

reported to suppress phosphatidylinositol biosynthesis in mycobacteria, but those compounds were shown not to be the substrates of the target enzymes even at millimolar concentration [170]. In contrast, in this work we show that the D-galactose-based PI4P mimetic **4** can be robustly phosphorylated by PIP5Ks with the K_M of 10 μM for zPIP5Kα (**Figure 2.1**). It is for the first time that a D-galactose derivative is shown to enter the active site and be processed by a phosphoinositide-processing enzyme.

It is interesting that, although PI4P was processed by all the PIPK family members in the *in vitro* kinase assay (**Figure 2.2**), which can be attributed to substrate promiscuity of PIPKs [171], compound **4** exhibited a strict selectivity toward PIP5K. The small but substantial structural differences between **4** and PI4P in their headgroups likely account for the high selectivity of the former, making it better distinguishing the substrate binding pockets of different PIPK family members. While **4** is a selective substrate of PIP5K, it is unexpected that **6**, which is a derivative of **4**, turned out to be a pan-PIPK inhibitor (**Figures 2.6a** & **d**). A non-specific detergent effect on kinase activity can be excluded because the structurally similar compound **5** showed no effects on the kinase activity up to 75 μM (**Figure 2.6a**). The ATP and PI4P competition assays further indicated that **6** is a non-ATP-competitive inhibitor, which targets the lipid substrate binding site (**Figures 2.6b** & **c**). Given that the lipid-facing substrate binding pocket of PIPKs is highly dynamic, partially due to the lipid sensing function of the activation loop [162, 163], we postulate that the substrate binding pockets of different PIPKs may be flexible enough to accommodate **6**, but only when bound with PIP5Ks can **4** adopt a productive orientation to allow phosphorylation to occur.

In summary, we demonstrate that the rationally designed D-galactosyl lysophospholipids are promising candidates for developing potent and selective non-ATP-competitive inhibitors of

PIPKs. The strategy of design and synthesis of D-galactose-based phosphoinositide mimetics presented in this work is likely applicable to the study of other phosphoinositide-processing enzymes associated with many diseases.

2.4. Experimental methods

2.4.1. Materials and methods

Chemicals used were reagent grade as supplied. Analytical thin-layer chromatography was performed using silica gel 60 F254 glass plates. Compound spots were visualized by UV light (254 nm) and by staining with a yellow solution containing $Ce(NH_4)_2(NO_3)_6$ and $(NH_4)_6Mo_7O_{24}\cdot 4H_2O$ in 6% H_2SO_4. Flash column chromatography was performed on silica gel 60 (230–400 Mesh). NMR spectra were recorded on Agilent 500MHz DDR2 NMR spectrometer and referenced using Me_4Si (0 ppm), residual $CHCl_3$ (d ^{1}H-NMR 7.26 ppm, ^{13}C-NMR 77.0 ppm). All optical rotations were measured at 25 °C using the sodium D line. High resolution mass spectra were recorded on a Waters Xevo G2-XS QTof quadropole mass spectrometer.

2.4.2. Mass spectrometry

The kinase reactions were carried out in a 1.5 mL microcentrifuge tube with 50 μM **4**, 50 μM ATP, 0.1 μM zPIP5Kα and reaction buffer (100 mM Tris-HCl pH 8.0, 5 mM EGTA, 10 mM $MgCl_2$). After incubated at room temperature for 4 h or overnight, the protein was precipitated out by adding acetonitrile. Then, the acetonitrile was evaporated under N_2 stream, and water was removed by a lyophilizer. The reversed phase ion-pairing UPLC/ESI/MS/MS analysis of kinase reactions were performed on a waters Xevo G2-XS QTof quadrupole mass spectrometer with an ESI probe. Mass spectrometry was operated in the negative ion mode with capillary voltage of 4000 V and at a source temperature of 600 °C. The UHPLC system consisted of an Agilent 1290 binary pump, with an autosampler at 10 °C. The injection volume was 5 μL for all kinase reaction.

The kinase reactions were chromatographically resolved in an ACQUITY UPLC BEH C18 column, 1.7 μm, 2.1 x 150 mm (Waters, part# 186002353). Mobile phase A was 8.0mM DMHA (dimethylhexylamine) and 2.2 mM acetic acid in water, pH 9.0. Mobile phase B was methanol. The gradient gradually increased from 0% to 40% of mobile phase B for 10 min and then decreased to 0% of mobile phase B for additional 5 min. For all steps the solvent flow rate was 0.3 mL/min and column temperature were kept at 40 °C.

2.4.3. Genes and constructs

The synthesized gene of zebrafish PIP5Kα with optimized codon was inserted in a pET41b vector with a C-terminal His-tag. The cDNAs for human PIP4Kα, human PIP4Kγ, mouse PIP5Kγ isoform 1, and human PIKfyve were purchased from Horizon Discovery with the catalog numbers of MHS6278-202806784 (GenBank: BC018034.1), MHS1010-202807181 (GenBank: BC028596.2), MMM1013-202768039 (GenBank: BC019138.1), and OHS5893-202503964 (GenBank: BC172527.1), respectively. The genes encoding hPIP4Kα, hPIP4Kγ, and mPIP5Kγ were cloned in a modified pET17 vector with an *N*-terminal His-tag for expression in *E.coli*. The gene of hPIKfyve was cloned in the pcDNA3.1 vector with an *N*-terminal FLAG tag for expression in mammalian cells.

2.4.4. Protein expression and purification

hPIP4Kα and mPIP4Kγ were expressed in Rosetta-2 (DE3) cells (Millipore). After the OD_{600} reached around 0.5, the cells growing in Luria-Bertani (LB) medium were induced with 0.1 mM isopropyl-β-D-thiogalactoside (IPTG). The cells were left to grow overnight at room temperature, harvested and re-suspended in the lysis buffer containing 20 mM Tris pH 8.0, 300 mM NaCl, 5% glycerol, and EDTA-free protease inhibitor cocktail. After lysis by sonication, the cell lysate was applied to centrifugation (20,000× *g* at 4 °C) for 40 minutes. The supernatant was

collected and loaded on a Ni-NTA column (Qiagen) for binding at 4 °C for 4 hours. After washing with the washing buffer (20 mM Tris pH 8.0, 300 mM NaCl, 5% glycerol, and 10 mM imidazole) for four times, the protein was eluted by the elution buffer (washing buffer plus 200 mM imidazole). The protein was further purified using a Superdex 200 Increase 10/300 GL column (GE healthcare) equilibrated with the running buffer containing 10 mM HEPES pH 7.3, 300 mM NaCl, and 5% glycerol. zPIP5Kα was overexpressed in BL21-CodonPlus®(DE3)-RIL cells (Stratagene) in LB medium. After the OD_{600} reached 0.3, the cells were induced with 0.1 mM IPTG and left to grow overnight at room temperature. The purification procedure was the same as that for PIP4Ks, except that 0.5% Triton X-100 (American Bioanalytical) was added to the cell lysate and Talon metal affinity column (Clontech) was used for purification. 0.01% Triton X-100 was included in the running buffer for size-exclusion chromatography.

hPIKfyve was expressed in Expi293F cells (Thermo Fisher) transiently transfected with the pcDNA3.1 vector harboring the DNA encoding the full length human PIKfyve with an N-terminal FLAG tag. The cells were cultured in EXPi293 Expression Medium at 8% CO_2 and 37 °C with shaking at 130 rpm. When the cells reached a density of 3-5 x 10^6 cells/mL (100 mL culture in 500 mL flask), the cells were split to a density of 1.5 x 10^6 cells/mL and cultured overnight. On the next day, 100 μg of PIKfyve plasmid was added to 6 mL of Opti-MEM I reduced serum medium and mixed by swirling, while 320 μL of EXPifectamine 293 was mixed with 5.6 mL of Opti-MEM I reduced serum medium. After incubated at room temperature for 5 min, the two solutions were combined, incubated at room temperature for 20 min, and slowly transferred to cell culture. One day after the transfection (18-22 h), 0.6 mL of ExpiFectamine 293 transfection enhancer 1 and 6 mL of ExpiFectamine 293 transfection enhancer 2 were added to the cell culture flask. The cells were harvested four days after transfection and re-suspended in lysis buffer

containing 50 mM Tris, 300 mM NaCl, pH 7.4, and 5% glycerol. Then, the cell suspension was applied to sonication for 15 min on ice. The anti-flag M2 affinity gel (MilliporeSigma, Cat#A2220) was balanced with the TBS buffer (50 mM Tris, 150 mM NaCl, pH 7.4) after washing with 0.1 M glycine buffer, pH 3.5 for three times. The cell lysate after sonication was applied to centrifugation (11,000 rpm at 4°C) for 15 min and the resulting supernatant was mixed with the prepared anti-flag M2 beads. After incubated at 4 °C for 2 h with gentle shaking, the beads were washed with purification buffer (50mM Tris, 300mM NaCl, pH7.4, 5% glycerol) for five times. Then, the protein was slowly eluted with three column volumes of elution buffer containing the purification buffer supplemented with 100 μg/ml Flag peptide (MedChemExpress, Cat#HY-P0223).

Kinase assay

The following components were included in one reaction (50 μL): 0.25-1 μg of purified kinase, 100 mM Tris-HCl (pH 8.0), 5 mM EGTA, 10 mM $MgCl_2$, 50 μM ATP with 1 μCi [γ-^{32}P] ATP (PerkinElmer), and 2 μM diC16-PI4P (Echelon Biosciences Inc.). The reaction was performed at room temperature for 1 h and then quenched by the addition of lipid extraction solution containing chloroform, methanol, and HCl with a volume ratio of 3.3:3.7:0.1, as well as bovine follicular fluid (10 mg/ml). After vortexing for 20 s, the sample was centrifuged at 6000 rpm for 2 min. The aqueous layer was removed, and the lower organic layer was spotted on TLC plate (6 μl) and separated by a developing solvent (water, acetic acid, methanol, acetone, chloroform with a volume ratio 1:1.3:1.7:2.1:4.5). The product of the reaction was quantified by a Storm 820 PhosphorImager (GE). For the inhibition assay, the inhibitors were added to the reaction mixture at the indicated concentrations.

2.4.5. Immunoblotting

All the samples were heated in SDS sample loading buffer at 96 °C for 6 min, and then applied to SDS-PAGE and Western blot. hPIP4Kα, hPIP4Kγ, zPIP5Kα and mPIP5Kγ proteins

were detected by using anti-His Tag antibody at 1:6000 (Invitrogen, Cat#37-2900) and horseradish peroxidase (HRP)-conjugated anti-mouse IgG at 1:7000 (Cell Signaling Technology, Cat# 7076S). FLAG-hPIKfyve was detected by using rat anti-FLAG antibody at 1:4000 (Stratagene, Cat#200474-21) and HRP-conjugated anti-rat IgG at 1:7000 (Cell Signaling Technology, Cat# 7077S). After reacting with the detection reagent (Cytiva, RPN2232), the images were taken using a Bio-Rad ChemiDoc Imaging System.

2.4.6. Transferrin endocytosis assay using immunofluorescence microscopy

HEK 293T cells were seeded on poly-D-lysine (Corning, Cat# 354210) coated sterile glass coverslipd in 24-wells trays for 16 hours in the basal medium. After preincubation with different concentrations of inhibitor at 37 °C for 2 hours, Alexa 488 conjugated transferrin (Thermo Fisher Scientific, Cat# T13342) was added into each well and incubated at 37 °C for 12 min. Then, the cells were washed 6 times with ice-cold acidic buffer (100 mM glycine, 20 mM magnesium acetate, 50 mM potassium chloride, pH 2.2) and fixed for 15 min at room temperature using 4% formaldehyde. After three washes with DPBS (Sigma-Aldrich, Cat# D8537-500ML), coverslips were mounted on slides with fluoroshield mounting medium with DAPI (Abcam, Cat# ab104139). Samples were viewed using a Spectral-based Olympus FluoView 1000 CLSM.

2.4.7. General procedures

2.4.7.1. General procedure for global deacetylation

To a solution of acetyl (Ac)-containing compound (1.0 equiv) in MeOH/DCM (2:1), 3.0 equivalents of NaOMe (25 wt. % in methanol) were added. The reaction mixture was stirred at room temperature for 6 hours, after which amberlite H^+ resin was added to obtain pH~7. Then, the resin was filtered, and the filtrate was evaporated under vacuum. The obtained residue was purified by silica gel chromatography to give the deacylated compound.

2.4.7.2. General procedure for the one-pot phosphorylation

The solution of starting material (1.0 equiv) and tetrazole (0.45 M in acetonitrile) (1.5-2.0 equiv) in dry acetonitrile was cooled to 0 °C, followed by dropwise addition of phosphoramidite (1.2 equiv) in CH_3CN. The reaction was warmed to room temperature or further heated to reflux. After the consumption of the starting material (indicated by TLC), 3.0 equivalents of *t*-BuOOH (5M in decane) were added. The reaction was stirred for another 6 hours and monitored by TLC. After the completion of reaction, the reaction mixture was poured to aqueous $NaHCO_3$ solution and extracted with DMC 3 times. The organic layer was collected and dried over anhydrous Na_2SO_4. After concentrated under vacuum, the crude product was purified on silica gel column to afford the designed product.

2.4.7.3. General procedure for TBDPS protection

The starting material (1.0 equiv) was dissolved in anhydrous pyridine and the mixture was cooled to 0 °C. After the addition of 1.2 equivalents of TBDPSCl and 1.0 equivalents of DMAP, the reaction mixture was warmed to room temperature and stirred for overnight. Then, pyridine was evaporated on a high vacuum pump and the residue was dissolved in ethyl acetate. The mixture was washed with 10% aqueous HCl solution to remove the remaining pyridine and the organic layer was dried over anhydrous Na_2SO_4. The volatiles were evaporated, and the residue was purified on a silica column to afford desired compound.

2.4.7.4.General Procedure for TBDPS removal

To the solution of starting material (1.0 equiv) in THF, 3.0 equivalents of tetrabutylammonium fluoride (1.0 M in THF) was added. The reaction was heated to 60 °C and stirred for 6 hours. After completion, the reaction was diluted with DCM and washed with saturated aqueous $NaHCO_3$ solution and water successively. After dried over anhydrous Na_2SO_4

and concentrated under vacuum, the organic layer was applied to silica gel chromatography for purification and afforded the desired product.

2.4.7.5. General procedure for Boc removal

TFA was added to the solution of starting material in DCM: MeOH: H_2O (2:1:1). The reaction was stirred at room temperature for overnight. After completion, the solvent was removed under vacuum and the crude product were applied to silica gel chromatography.

2.4.7.6. General procedure for amidation reaction

The crude product from Boc removal reaction was redissolved in dry DCM. Then, 1.2 equivalent of 1-[bis(dimethylamino)methylene]-1H-1,2,3-triazolo[4,5-b] pyridinium 3-oxid hexafluorophosphate (HATU) and 1.5 equivalent of alkanoic acid was added. After stirred at room temperature for 10 min, 1.5 equivalent of *N*,*N*-diisopropylethylamine (DIEA) was added. The reaction was stirred for another 3 hours and monitored by TLC. The reaction mixture was poured into HCl solution after completion and extracted with DCM 3 times. The combined organic layer was washed with aqueous $NaHCO_3$ solution and brine, respectively. After dried over anhydrous Na_2SO_4, the organic layer was concentrated under vacuum, and further purified by silica gel chromatography to afford the desired compound.

2.4.7.7. General procedure for global debenzylation

To a solution of starting material (50 mg) in DCM/MeOH (1/1), $Pd(OH)_2/C$ (100 mg) was added. The resulting mixture was stirred under H_2 atmosphere and monitored by TLC. After the completion of the reaction, the mixture was filtered and concentrated under vacuum, and the residue was further purified by a LH-20 column to afford the desired product in quantitative yield.

2.4.8. Product preparation and characterization data

To prepare phosphoramidite **9**, the commercially available bis(diisopropylamino)chlorophosphine was treated with benzyl alcohol first (**Scheme 2.8**), which was followed by the coupling with 2-(Boc-amino) ethanol, promoted by tetrazolide diisopropylamino, to afford the phosphoramidite **9**.

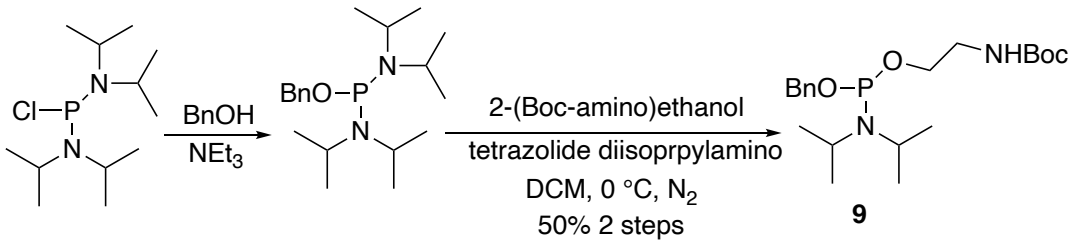

Scheme 2.8. Synthesis of phosphoramidite **9**.

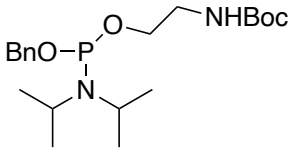

Benzyl-(2-(tert-butoxycarbonylamido)ethyl)-N,N-diisopropylphosphoramidite (9)

The mixture of benzyl alcohol (168 μL, 1.6 mmol) and triethylamine (700 μL ,4.8 mmol) in Et_2O was added dropwise to the solution of bis(dimethylamino)chlorophosphine (250 mg, 1.6 mmol) in Et_2O under N_2 at 0 °C. After stirred for 2 hours, the reaction mixture was filtered, and the filtration was concentrated under vacuum to obtain bis(dimethylamino)benzyloxyl phosphine. To a solution of 2-(Boc-amino)ethanol (541.56 mg, 1.6 mmol) and diisopropylammonium tetrazolide (172.55 mg, 1.92 mmol) in DCM/CH_3CN (2:1), 1.0 equivalent of bis(dimethylamino)benzyloxyl phosphine (257.77 mg, 1.6 mmol) was added. The reaction was stirred at room temperature under N_2 for 4 hours, after which the reaction mixture was poured into saturated aqueous $NaHCO_3$ solution, and the aqueous layer was extracted by DCM 3 times. The

organic layer was combined and dried over Na_2SO_4. DCM was removed under vacuum and the resulting residue was purified by silica gel chromatography (prewashed with 3% triethylamine in Hexane to give the phosphoramidite **9** in 50% yield.

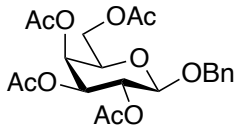

Benzyl 2,3,4,6-tetra-O-acetyl-β-D-galactopyranoside (11)

Benzyl alcohol (3.0 ml, 30.8 mmol) and boron trifluoride etherate (4.0 ml, 31.0 mmol) were mixed in dry DCM and cooled to 0 °C. After stirred at 0 °C for 1 hour, β-D-galactose pentaacetate (10.0 g, 25.60 mmol) was added slowly to the reaction mixture. The reaction was maintained at 0 °C and stirred for another 4 hours as monitored by TLC. After completion, the reaction was quenched by adding triethylamine. Then, the reaction mixture was diluted with DCM, and washed with saturated aqueous $NaHCO_3$ solution and water successively. The organic layer was collected and dried over anhydrous Na_2SO_4. The volatiles were evaporated, and the resulting residue was purified by column chromatography to afford compound **11**. $[\alpha]^{25}_D$ 27.96 (c = 1, CH_2Cl_2); ^{1}H NMR (500 MHz, $CDCl_3$) δ 7.39 – 7.24 (m, 5H), 5.38 (dd, *J* = 3.5, 1.2 Hz, 1H, H-4), 5.28 (dd, *J* = 10.4, 7.9 Hz, 1H, H-2), 4.98 (dd, *J* = 10.4, 3.5 Hz, 1H, H-3), 4.91 (d, *J* = 12.3 Hz, 1H, Bn), 4.63 (d, *J* = 12.3 Hz, 1H, Bn), 4.51 (d, *J* = 7.9 Hz, 1H, H-1), 4.21 (dd, *J* = 11.3, 6.5 Hz, 1H, H-6), 4.18 (dd, *J* = 11.3, 6.5 Hz, 1H, H-6), 3.88 (td, *J* = 6.8, 1.2 Hz, 1H, H-5), 2.16 (s, 3H), 2.07 (s, 3H), 2.01 (s, 3H), 1.97 (s, 3H). ^{13}C NMR (125 MHz, $CDCl_3$) δ 170.57, 170.44, 170.31, 169.58, 136.83, 128.71, 128.60, 128.15, 127.89, 127.12, 99.91, 89.84, 71.05, 70.87, 70.82, 68.97, 67.18, 61.45, 20.89, 20.85, 20.83, 20.73. HRMS: $[M+H]^+$ $C_{21}H_{27}O_{10}$ calcd 439.1526, obsd 439.1552.

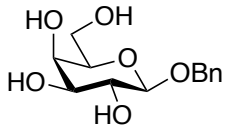

Benzyl 2,3,4,6-*tetra*-hydroxyl-*β*-D-galactopyranoside (12)

Compound **12** was prepared from compound **11** (4.5 g, 10.27mmol) by following the general procedure for global deacetylation, providing the product in 93% yield. $[\alpha]^{25}_{D}$ 153.75 (c = 0.1, CH_2Cl_2); ^{1}H NMR (500 MHz, CD_3OD) δ 7.44 – 7.39 (m, 2H), 7.34 – 7.30 (m, 2H), 7.29 – 7.22 (m, 1H), 4.93 (d, *J* = 11.9 Hz, 1H, Bn), 4.66 (d, *J* = 11.9 Hz, 1H, Bn), 4.31 (d, *J* = 7.7 Hz, 1H, H-1), 3.84 (d, *J* = 3.42 Hz, 1H, H-4), 3.79 (dd, *J* = 11.4, 6.8 Hz, 1H, H-6), 3.74 (dd, *J* = 11.4, 6.8 Hz, 1H, H-6), 3.58 (dd, *J* = 9.7, 7.7 Hz, 1H, H-2), 3.50 (ddd, *J* = 6.6, 5.3, 1.2 Hz, 1H, H-5), 3.46 (dd, *J* = 9.7, 3.42 Hz, 1H, H-3). ^{13}C NMR (125 MHz, CD_3OD) δ 137.75, 127.92, 127.84, 127.79, 127.28, 127.24, 102.48, 75.31, 73.55, 71.15, 70.26, 68.95, 61.14. HRMS: $[M+Na]^+$ $C_{13}H_{18}NaO_6$ calcd 293.1001, obsd 293.1050.

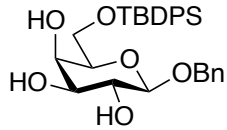

Benzyl 6-*O*-(*tert*-butyldiphenylsilyl)-2,3,4-*tri*-hydroxyl-*β*-D-galactopyranoside (13)

Compound **13** was prepared from compound **12** (2.58 g, 9.55 mmol) by following the general procedure for TBDPS protection, providing the product in 98% yield. $[\alpha]^{25}_{D}$ -30.53 (c = 2, CH_2Cl_2); ^{1}H NMR (500 MHz, $CDCl_3$) δ 7.75 – 7.67 (m, 6H), 7.48 – 7.29 (m, 9H), 4.92 (d, *J* = 11.6 Hz, 1H, Bn), 4.59 (d, *J* = 11.6 Hz, 1H, Bn), 4.32 (d, *J* = 7.7 Hz, 1H, H-1), 4.09 (dd, *J* = 3.5, 1.1 Hz, 1H, H-4), 4.02 – 3.92 (m, 2H, H-6), 3.72 (dd, *J* = 9.5, 7.7 Hz, 1H, H-2), 3.58 (dd, *J* = 9.5, 3.5 Hz, 1H, H-5), 3.56 – 3.53 (1H, H-3), 1.08 (s, 9H). ^{13}C m, NMR (125 MHz, $CDCl_3$) δ 149.67, 136.97, 136.15, 135.66, 135.56, 134.81, 133.07, 132.86, 129.92, 129.91, 129.64, 128.51, 128.23, 128.03, 127.84,

127.82, 127.72, 123.85, 101.67, 77.23, 74.45, 73.62, 72.25, 70.72, 68.87, 63.11, 26.80, 26.56, 19.20. HRMS: $[M+Na]^+$ $C_{29}H_{36}NaO_6Si$ calcd 531.2179, obsd 531.2310.

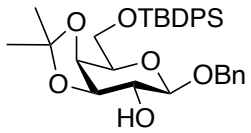

Benzyl 6-*O*-(*tert*-butyldiphenylsilyl)-3,4-*O*-isopropylidene-*β*-D-galactopyranoside (7)

Compound **13** (4.75 g, 9.36 mmol) was dissolved in acetone, then 2,2-dimethoxy propane (1.72 mL, 14.05 mmol) and camphorsulfonic acid (0.42 g, 1.87 mmol) were added. After stirred at room temperature overnight, Et_3N was added to neutralize the excess CSA and bring the pH around 7. The reaction mixture was concentrated under vacuum, and the residue was diluted with DCM and washed with aqueous $NaHCO_3$ solution and saturated NaCl solution successively. The organic layer was collected and dried over anhydrous Na_2SO_4. The volatiles were removed under vacuum and the resulted residue was purified by silica gel column chromatography to afford the designed product **7** in 96% yield. $[\alpha]^{25}_D$ 0.72 (c = 0.7, CH_2Cl_2); ^{1}H NMR (500 MHz, $CDCl_3$) δ 7.75 – 7.68 (m, 6H), 7.47 – 7.28 (m, 9H), 4.90 (d, *J* = 11.6 Hz, 1H, Bn), 4.58 (d, *J* = 11.6 Hz, 1H, Bn), 4.26 – 4.24 (m, 1H, H-4), 4.23 (d, *J* = 8.4 Hz, 1H, H-1), 4.05 (dd, *J* = 7.4, 5.4 Hz, 1H, H-3), 4.02 – 3.95 (m, 2H, H-6), 3.88 – 3.84 (m, 1H, H-5), 3.64 – 3.59 (m, 1H, H-2), 1.51 (s, 3H), 1.34 (s, 3H), 1.07 (s, 9H). ^{13}C NMR (125 MHz, $CDCl_3$) δ 137.00, 135.65, 135.63, 133.49, 133.41, 129.68, 128.52, 128.09, 128.03, 127.67, 127.62, 109.45, 96.46, 76.18, 72.85, 69.70, 69.38, 68.95, 63.02, 27.76, 26.78, 25.91, 19.22, 14.20, 1.02. HRMS: $[M+Na]^+$ $C_{32}H_{40}NaO_6Si$ calcd 571.2492, obsd 571.2604.

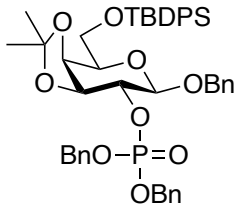

Benzyl 2-*O*-(dibenzylphosphono)-6-*O*-(*tert*-butyldiphenylsilyl)-3,4-*O*-isopropylidene-*β*-D-galactopyranoside (14)

Compound **14** was prepared from compound **7** (414.5 mg, 0.755 mmol) and phosphoramidite **8** by following the general procedure for one-pot phosphorylation, providing the product in 65% yield. $[\alpha]^{25}_{D}$ -5.09 (c = 0.6, CH_2Cl_2); ^{1}H NMR (500 MHz, $CDCl_3$) δ 7.74 – 7.66 (m, 5H), 7.46 – 7.21 (m, 20H), 5.06 – 4.99 (m, 3H, Bn), 4.96 (dd, *J* = 11.9, 7.5 Hz, 1H, Bn), 4.88 (d, *J* = 11.7 Hz, 1H, Bn), 4.58 (d, *J* = 11.7 Hz, 1H, Bn), 4.46 – 4.38 (m, 2H, H-1, H-2), 4.26 (dd, *J* = 5.3, 2.0 Hz, 1H, H-4), 4.21 (t, *J* = 6.0 Hz, 1H, H-3), 3.97 (dd, *J* = 6.7, 1.5 Hz, 2H, H-6), 3.87 (dt, *J* = 8.0, 4.0 Hz, 1H, H-5), 1.49 (s, 3H), 1.32 (s, 3H), 1.07 (s, 9H). ^{13}C NMR (125 MHz, $CDCl_3$) δ 136.74, 135.62, 135.58, 133.33, 133.25, 129.76, 128.57, 128.41, 128.36, 128.34, 128.28, 128.17, 128.14, 127.81, 127.75, 127.69, 127.68, 127.43, 110.49, 99.02, 98.97, 80.83, 79.15, 79.09, 78.07, 78.05, 73.68, 73.52, 70.24, 69.09, 69.05, 68.99, 68.95, 62.64, 27.86, 26.98, 26.75, 26.39, 25.76, 19.22, 14.21. HRMS: $[M+Na]^+$ $C_{46}H_{53}NaO_9PSi$ calcd 831.3094, obsd 831.3122.

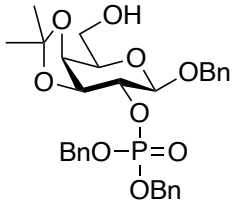

Benzyl 2-*O*-(dibenzylphosphono)-3,4-*O*-isopropylidene-*β*-D-galactopyranoside (15)

Compound **15** was prepared from compound **14** (505 mg, 0.62 mmol) by following the general procedure for TBDPS removal reaction, providing the product in 76% yield. $[\alpha]^{25}_{D}$ -6.4 (c = 1, CH_2Cl_2); ^{1}H NMR (500 MHz, $CDCl_3$) δ 7.38 – 7.22 (m, 15H), 5.07 – 4.95 (m, 4H, Bn), 4.88 (d, *J*

= 11.8 Hz, 1H, Bn), 4.66 (d, *J* = 11.8 Hz, 1H, Bn), 4.50 (d, *J* = 8.1 Hz, 1H, H-1), 4.43 (m, 1H, H-2), 4.25 (dd, *J* = 7.1, 5.5 Hz, 1H, H-3), 4.17 – 4.16 (m, 1H, H-4), 4.01 – 3.95 (m, 1H, H-5), 3.83 (qt, *J* = 7.1, 2.8 Hz, 2H, H-6), 1.51 (s, 3H), 1.33 (s, 3H). ^{13}C NMR (125 MHz, $CDCl_3$) δ 171.19, 136.84, 136.09, 128.40, 128.38, 128.24, 128.21, 128.20, 127.94, 127.82, 127.71, 110.91, 99.53, 99.49, 78.80, 78.75, 78.19, 78.16, 74.22, 73.32, 71.03, 69.15, 69.11, 69.06, 69.02, 62.34, 60.42, 27.77, 26.42, 21.08, 14.21. HRMS: $[M+Na]^+$ $C_{30}H_{35}NaO_9P$ calcd 593.1917 obsd 593.1935.

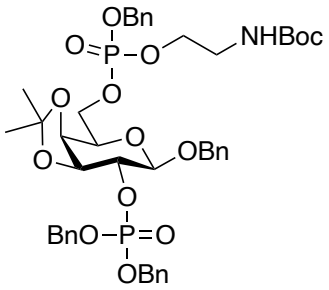

Benzyl 2-*O*-(dibenzylphosphono)-6-*O*-((benzyl)-(2-(*tert*-butoxycarbonylamido)-ethyl)-phospono)-3,4-*O*-isopropylidene-*β*-D-galactopyranoside (16)

Compound **16** was prepared from compound **15** (243mg, 0.43 mmol) and the freshly prepared phosphoramidite **9** (206mg, 0.52 mmol) by following the general procedure for the one-pot phosphorylation reaction, which providing the product in 72% yield. $[\alpha]^{25}_D$ -2.86 (c = 0.7, CH_2Cl_2); ^{1}H NMR (500 MHz, $CDCl_3$) δ 7.43 – 7.20 (m, 20H, Bn), 5.12 (dd, *J* = 8.9, 2.4 Hz, 2H, Bn), 5.06 – 4.92 (m, 4H, Bn), 4.87 (dd, *J* = 11.8, 3.0 Hz, 1H, Bn), 4.56 (dd, *J* = 11.8, 6.6 Hz, 1H, Bn), 4.43 (d, *J* = 6.9 Hz, 1H, H-1), 4.41 – 4.36 (m, 1H, H-2), 4.31 – 4.23 (m, 2H, H-6), 4.20 (q, *J* = 5.8 Hz, 1H, H-3), 4.13 – 4.09 (m, 1H, H-4), 4.08 – 4.03 (m, 2H, OCH_2), 3.93 (m, 1H, H-5), 3.36 (q, *J* = 4.9 Hz, 2H, CH_2N),1.46 (s, 3H), 1.42 (s, 9H), 1.29 (s, 3H). ^{13}C NMR (125 MHz, $CDCl_3$) δ 136.43, 135.83, 135.76, 135.49, 128.88, 128.74, 128.44, 128.42, 128.35, 128.33, 128.15, 127.98, 127.82, 127.70, 110.99, 110.97, 98.97, 98.92, 78.74, 78.69, 77.84, 73.30, 71.56, 71.50, 70.63,

69.78, 69.32, 69.23, 67.27, 66.26, 40.85, 28.36, 27.68, 26.35, 14.20. HRMS: $[M+Na]^+$ $C_{44}H_{55}NaNO_{14}P_2$ calcd 906.2996, obsd 906.3072.

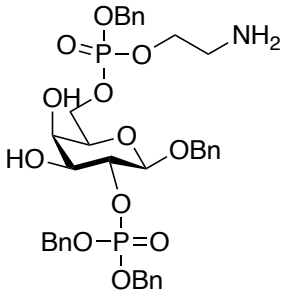

Benzyl 2-*O*-(dibenzylphosphono)-6-*O*-((benzyl)-(2-aminoethyl)-phospono)-*β*-D-galactopyranoside (17)

Compound **17** was prepared from compound **16** (216 mg, 0.25 mmol) by following the general procedure for Boc deprotection. $[\alpha]^{25}_D$ -25.0 (c = 0.1, CH_2Cl_2); ^{1}H NMR (500 MHz, CD_3OD) δ 7.52 – 7.05 (m, 20H, 4Bn), 5.19 (t, *J* = 8.2 Hz, 2H, CH_2Ph), 5.08 (d, *J* = 7.4 Hz, 2H, CH_2Ph), 4.94 (m, 2H, CH_2Ph), 4.91 – 4.83 (m, 1H, CH_2Ph), 4.62 (dd, *J* = 7.9, 1.8 Hz, 1H, H-1), 4.59 – 4.50 (m, 1H, CH_2Ph), 4.46 (m, 1H, H-2), 4.40 – 4.17 (m, 4H, H-6, $POCH_2$, H-4), 3.88 (dt, *J* = 8.6, 3.9 Hz, 1H, H-6), 3.86 – 3.72 (m, 2H, H-3, H-5), 3.25 – 3.17 (m, 2H, CH_2N). ^{13}C NMR (125 MHz, CD_3OD) δ 137.04, 135.56, 128.63, 128.61, 128.44, 128.16, 128.14, 128.11, 128.10, 128.07, 128.03, 128.01, 127.76, 127.72, 127.59, 127.58, 127.47, 127.40, 100.24, 78.54, 78.49, 73.24, 73.18, 71.97, 70.59, 69.98, 69.93, 69.38, 69.34, 69.16, 69.11, 67.16, 64.01, 39.44, 39.38. HRMS: $[M+H]^+$ $C_{36}H_{44}NO_{12}P_2$ calcd 744.2260, obsd 744.2365.

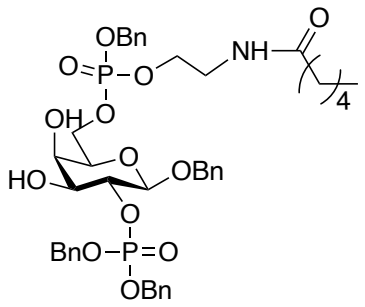

Benzyl 2-*O*-(dibenzylphosphono)-6-*O*-((benzyl)-(2-hexanamidoethyl)-phospono)-β-D-galactopyranoside (17-1)

Compound **17-1** was prepared from the crude product **17** and hexanoic acid (19.74 mg, 0.17 mmol) by following the general procedure for amidation reaction, affording the compound **in** 85% yield in two steps. $[\alpha]^{25}_{D}$ -6.80 (c = 0.25, CH_2Cl_2); ^{1}H NMR (500 MHz, $CDCl_3$) δ 7.42 – 7.14 (m, 20H, 4Bn), 5.11 (dd, *J* = 9.0, 4.0 Hz, 2H, CH_2Ph), 5.04 (m, 2H, CH_2Ph), 4.97 (d, *J* = 81.9 Hz, 2H, CH_2Ph), 4.91 (d, *J* = 15.9 Hz, 1H, CHPh), 4.58 (dd, *J* = 11.7, 8.0 Hz, 1H, CHPh), 4.46 (dd, *J* = 7.7, 3.9 Hz, 1H, H-1), 4.40 – 4.32 (m, 1H, H-2), 4.32 – 4.23 (m, 2H, H-6), 4.10 (dq, *J* = 11.4, 5.7 Hz, 2H, $POCH_2$), 3.92 (dd, *J* = 18.0, 3.5 Hz, 1H, H-4), 3.71 (m, 1H, H-3), 3.66 (q, *J* = 6.1 Hz, 1H, H-5), 3.57 – 3.42 (m, 2H, CH_2N), 2.18 – 2.09 (m, 2H, $C(O)CH_2$), 1.60 (dt, *J* = 8.0, 3.7 Hz, 2H, $C(O)CH_2CH_2$), 1.36 – 1.21 (m, 4H), 0.88 (td, *J* = 7.0, 2.4 Hz, 3H, CH_3). ^{13}C NMR (125 MHz, $CDCl_3$) δ174.80, 128.91, 128.76, 128.69, 128.59, 128.49, 128.42, 128.19, 128.16, 128.07, 127.97, 127.78, 99.69, 78.40, 78.36, 77.29, 77.03, 76.78, 72.71, 71.05, 69.98, 69.87, 69.82, 67.87, 67.20, 39.72, 36.53, 31.43, 29.71, 25.28, 22.40, 13.96. HRMS: $[M+H]^+$ $C_{42}H_{54}NO_{13}P_2$ calcd 842.2992, obsd 842.3062.

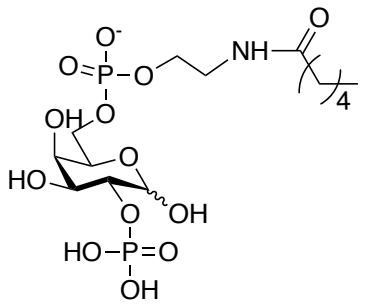

2-*O*-Phosphono-6-*O*-((2-hexanamidoethyl)-phospono)-α/β-D-galactopyranoside (1)

Compound **1** was prepared from compound **17-1** (68.65 mg, 0.08 mmol) by following the general procedure for global debenzylation, leading to the formation of product in a quantitative yield. $[\alpha]^{25}_{D}$ -3.58 (c = 0.32, CH_2Cl_2); ^{1}H NMR (500 MHz, CD_3OD : $CDCl_3$: D_2O = 4:2:1) δ 5.35 (dd, *J* = 7.0, 2.6 Hz, 1H, H-1a), 4.35 (td, *J* = 9.0, 3.6 Hz, 1H, H-2a), 4.25 (dd, *J* = 7.3, 4.9 Hz, 1H, H-6a), 4.21 – 4.05 (m, 4H, H-6a, H-4a, $POCH_2$), 3.97 (d, *J* = 2.36 Hz, 1H, H-3a), 3.86 – 3.79 (m, 1H, H-5a), 3.53 – 3.46 (m, 2H, CH_2N), 2.30 (td, *J* = 7.7, 3.8 Hz, 2H, $C(O)CH_2$), 1.64 (m, 2H, $C(O)CH_2CH_2$), 1.42 – 1.27 (m, 4H), 0.93 (t, *J* = 6.9 Hz, 3H, CH_3). ^{13}C NMR (125 MHz, CD_3OD : $CDCl_3$: D_2O = 4:2:1) δ 176.78, 118.43, 92.27, 75.70, 70.47, 69.71, 66.29, 55.11, 49.51, 49.34, 49.17, 49.00, 48.83, 48.66, 48.49, 36.42, 32.15, 26.44, 23.16, 18.33, 14.21. HRMS: $[M-H]^-$ $C_{14}H_{28}NO_{13}P_2$ calcd 480.1114, obsd 480.1038.

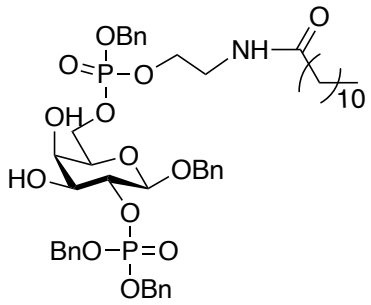

Benzyl 2-*O*-(dibenzylphosphono)-6-*O*-((benzyl)-(2-dodecanamidoethyl)-phospono)-3,4-*di*-hydroxyl-β-D-galactopyranoside (17-2)

Compound **17-2** was synthesized from compound **17** and lauric acid by following the general procedure for amidation reaction, affording the compound in 70% yield in two steps. $[\alpha]^{25}_{D}$ -6.0 (c = 0.3, CH_2Cl_2); ^{1}H NMR (500 MHz, $CDCl_3$) δ 7.51 – 7.09 (m, 20H), 5.11 (m, 2H, CH_2Ph), 5.05 (d, *J* = 7.9 Hz, 2H, CH_2Ph), 5.02 – 4.93 (m, 2H, CH_2Ph), 4.90 (dt, *J* = 11.6, 2.4 Hz, 1H, CH_2Ph), 4.58 (m, 1H, CH_2Ph), 4.46 (m, 1H, H-1), 4.38 (m, 1H, H-2), 4.27 (m, 2H, H-6), 4.10 (m, 2H, $POCH_2$), 3.93 (dt, *J* = 17.4, 2.4 Hz, 1H, H-4), 3.71 (dt, *J* = 8.9, 3.5 Hz, 1H, H-3), 3.65 (q, *J* = 6.3 Hz, 1H, H-5), 3.49 (q, *J* = 4.8 Hz, 2H, CH_2NCO), 2.13 (t, *J* = 7.7 Hz, 2H, $C(O)CH_2$), 1.60 (dt, *J* = 15.4, 7.8 Hz, 2H, $C(O)CH_2CH_2$), 1.33 – 1.23 (m, 16H), 0.88 (t, *J* = 6.9, 3H). ^{13}C NMR (125 MHz, $CDCl_3$) δ 173.79, 136.74, 129.01, 128.86, 128.76, 128.69, 128.59, 128.57, 128.53, 128.30, 128.27, 128.18, 128.09, 128.07, 127.88, 99.75, 78.50, 78.46, 77.42, 77.16, 76.91, 72.84, 71.12, 71.03, 70.02, 70.02, 68.11, 67.30, 66.01, 39.80, 36.69, 32.03, 29.76, 29.74, 29.64, 29.61, 29.52, 29.47, 29.45, 25.75, 22.81, 14.26. HRMS: $[M+H]^+$ $C_{48}H_{66}NO_{13}P_2$ calcd 926.3931, obsd 926.3961.

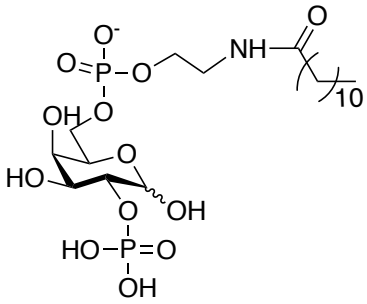

2-*O*-Phosphono-6-*O*-((2-dodecanamidoethyl)-phospono)-*α*/*β*-D-galactopyranoside (2)

Compound **2** was synthesized from **17-2** in quantitative yield following the general procedure of global debenzylation reaction. $[\alpha]^{25}_{D}$ -0.8 (c = 0.88, CH_2Cl_2); ^{1}H NMR (500 MHz, CD_3OD : $CDCl_3$: D_2O = 4:2:1) δ 5.36 (d, *J* = 3.5 Hz, 2H, H-1a), 4.64 (d, *J* = 7.6 Hz, 1H, H-1b), 4.39 – 4.33 (m, 2H, H-2a), 4.29 – 4.22 (m, 1H, H-5), 4.20 – 4.10 (m, 2H, H-6), 4.06 (dt, *J* = 7.1, 5.4 Hz, 3H, $POCH_2$), 3.96 (t, *J* = 3.6 Hz, 1H, H-3), 3.88 (d, *J* = 3.2 Hz, 1H, H-4), 3.47 (q, *J* = 5.3 Hz, 3H, CH_2NCO), 2.01 (t, *J* = 2.5 Hz, 2H, $C(O)CH_2$), 1.61 (m, 2H, $C(O)\ CH_2CH_2$), 1.31 (m,

24H), 0.91 (t, J = 6.9 Hz, 5H). ^{13}C NMR (125 MHz, CD_3OD : $CDCl_3$: D_2O = 4:2:1) δ 176.70, 92.40, 75.67, 70.57, 69.79, 69.17, 66.52, 40.71, 36.86, 34.70, 32.90, 30.59, 30.57, 30.46, 30.31, 30.29, 30.14, 26.79, 23.59, 14.40. HRMS: $[M-H]^-$ $C_{20}H_{40}NO_{13}P_2$ calcd 564.2053, obsd 564,1978.

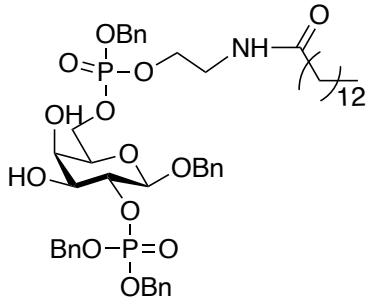

Benzyl 2-*O*-(dibenzylphosphono)-6-*O*-((benzyl)-(2-tetradecanamidoethyl)-phospono)-*β*-D-galactopyranoside (17-3)

Compound **17-3** was synthesized from compound **17** and myristic acid by following the general procedure for amidation reaction, affording the compound in 63% yield in two steps. $[\alpha]^{25}_D$ -6.67 (c = 0.03, CH_2Cl_2); ^{1}H NMR (500 MHz, $CDCl_3$) δ 7.45 – 7.11 (m, 20H), 6.15 (dd, J = 14.2, 8.5 Hz, 1H, NH), 5.12 (dd, J = 9.0, 4.1 Hz, 2H, CH_2Ph), 5.07 – 5.02 (m, 2H, CH_2Ph), 5.01 – 4.94 (m, 2H, CH_2Ph), 4.91 (dd, J = 11.9, 3.3 Hz, 1H, CH_2Ph), 4.58 (dd, J = 11.7, 8.1 Hz, 1H, CH_2Ph), 4.46 (dd, J = 7.7, 3.7 Hz, 1H, H-1), 4.38 – 4.31 (m, 1H, H-2), 4.27 (m, 2H, H-6), 4.11 (dq, J = 9.0, 4.6 Hz, 2H, $POCH_2$), 3.96 – 3.88 (m, 1H, H-4), 3.72 (m, 1H, H-3), 3.70 – 3.63 (m, 1H, H-5), 3.50 (t, J = 4.7 Hz, 2H, CH_2N), 2.16 – 2.10 (m, 2H, $C(O)CH_2$), 1.61 (m, 2H, $C(O)$ CH_2CH_2), 1.25 (m, 20H), 0.89 (t, J = 7.0, 3H, CH_3). ^{13}C NMR (125 MHz, $CDCl_3$) δ172.98, 129.86, 129.78, 129.51, 129.48, 129.44, 129.37, 129.30, 129.29, 129.26, 128.98, 128.81, 101.54, 80.03, 73.53, 73.50, 71.88, 70.48, 61.53, 49.51, 49.34, 49.29, 49.17, 49.00, 48.83, 48.66, 48.49, 38.88, 37.06, 34.95, 33.08, 30.81, 30.79, 30.77, 30.65, 30.62, 30.49, 30.44, 30.33, 30.25, 26.97, 26.10, 23.75, 20.86, 14.47. HRMS: $[M+Na]^+$ $C_{50}H_{69}NNaO_{13}P_2$ calcd 976.4136, obsd 976.4095.

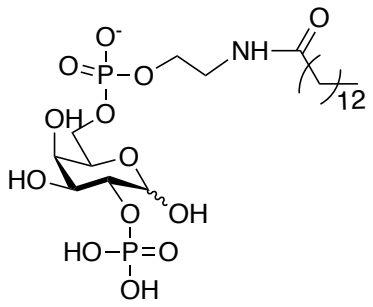

2-*O*-Phosphono-6-*O*-((2-tetradecanamidoethyl)-phospono)-α/β-D-galactopyranoside (3)

Compound **3** was synthesized from **17-3** in quantitative yield following the general procedure of global debenzylation reaction. $[\alpha]^{25}_{D}$ -5.2 (c = 0.15, CH_2Cl_2); ^{1}H NMR (500 MHz, CD_3OD : $CDCl_3$: D_2O = 4:2:1) δ 5.43-5.29 (m, 1H, H-1a), 4.31 (m, 1H, H-2), 4.19 (d, *J* = 6.7 Hz, 1H, H-5), 4.01-3.91 (m, 5H, H-6, H-4, $POCH_2$), 3.66 (d, *J* = 3.7 Hz, 1H, H-3), 3.40 (t, *J* = 5.1 Hz, 2H, CH_2N), 2.23-2.15 (m, 2H, $C(O)CH_2$), 1.58 (m, 2H, $C(O)CH_2CH_2$), 1.26 (m, *J* = 7.39 Hz, 20H), 0.85 (t, *J* = 6.69 Hz, 3H).^{13}C NMR (125 MHz, CD_3OD : $CDCl_3$: D_2O = 4:2:1) δ 176.85, 92.55, 75.82, 70.72, 69.94, 69.32, 66.67, 40.86, 37.01, 34.85, 33.05, 30.74, 30.72, 30.61, 30.46, 30.44, 30.29, 30.14, 26.94, 26.03, 23.74, 14.55. HRMS: $[M-H]^-$ $C_{22}H_{44}NO_{13}P_2$ calcd 592.2366, obsd 592.2292.

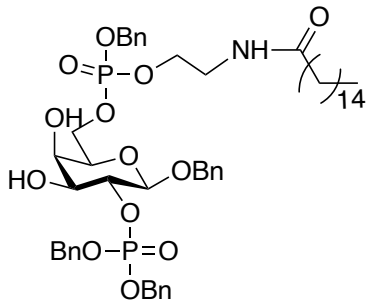

Benzyl 2-*O*-(dibenzylphosphono)-6-*O*-((benzyl)-(2-palmitamidoethyl)-phospono)-β-D-galactopyranoside (17-4)

Compound **17-4** was synthesized from compound **17** and palmitic acid by following the general procedure for amidation reaction, affording the compound in 69% yield in two steps. $[\alpha]^{25}_{D}$

-6.67 (c = 0.15, CH_2Cl_2); ^{1}H NMR (500 MHz, $CDCl_3$) δ 7.49 – 7.06 (m, 20H), 5.10 (dd, *J* = 9.0, 3.9 Hz, 2H), 5.03 (dd, *J* = 8.0, 1.5 Hz, 2H), 4.99 – 4.92 (m, 2H), 4.89 (dd, *J* = 12.0, 3.5 Hz, 1H, CHPh), 4.57 (dd, *J* = 11.7, 7.7 Hz, 1H, CHPh), 4.45 (dd, *J* = 7.7, 3.9 Hz, 1H, H-1), 4.37 (m 1H, H-2), 4.32 – 4.20 (m, 2H, H-6), 4.09 (dq, *J* = 10.0, 5.1 Hz, 2H, $POCH_2$), 3.92 (dd, *J* = 17.4, 3.5 Hz, 1H, H-4), 3.70 (dt, *J* = 8.8, 4.3 Hz, 1H, H-3), 3.64 (q, *J* = 6.1 Hz, 1H, H-5), 3.47 (t, *J* = 4.6 Hz, 2H, CH_2N), 2.12 (t, *J* = 7.7 Hz, 2H, $C(O)CH_2$), 1.57 (m, 2H, $C(O)CH_2CH_2$), 1.32 – 1.18 (m, 24H), 0.88 (t, *J* = 6.8 Hz, 3H). ^{13}C NMR (125 MHz, $CDCl_3$) δ 173.76, 136.76, 135.59, 129.01, 128.86, 128.77, 128.69, 128.59, 128.57, 128.53, 128.52, 128.30, 128.27, 128.18, 128.09, 128.07, 127.88, 99.75, 78.52, 78.48, 72.85, 71.12, 71.03, 70.05, 69.97, 69.92, 68.08, 67.30, 39.80, 36.69, 32.05, 29.83, 29.80, 29.78, 29.65, 29.52, 29.49, 29.46, 25.75, 22.82, 14.26. HRMS: $[M+H]^+$ $C_{52}H_{74}NO_{13}P_2$ calcd 982.4557, obsd 982.4592.

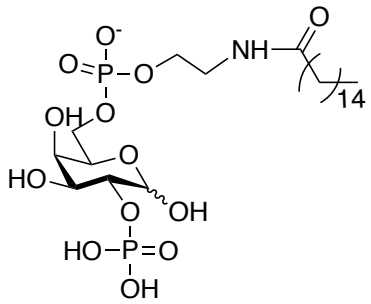

2-*O*-Phosphono-6-*O*-((2-palmitamidoethyl)-phospono)-*α*/*β*-D-galactopyranoside (4)

Compound **4** was synthesized from **17-4** in quantitative yield following the general procedure of global debenzylation reaction. $[\alpha]^{25}_D$ -3.2 (c = 0.8, CH_2Cl_2); ^{1}H NMR (500 MHz, CD_3OD : $CDCl_3$: D_2O = 4:2:1) δ 5.33 (dd, *J* = 6.7, 2.5 Hz, 1H, H-1a), 4.63 (d, *J* = 7.5 Hz, 0.5H, H-1b), 4.39 – 4.33 (m, 1H, H-2a), 4.24 (t, *J* = 6.2 Hz, 1H, H-5a), 4.19 – 4.12 (m, 2H, H-6a),), 4.12 – 4.09 (m, 1H, H-6b), 4.06 (q, *J* = 6.1 Hz, 4H, POCH2), 4.00 – 3.94 (m, 1H, H-3a), 3.88 (d, *J* = 3.2 Hz, 1H, H-4a), 3.46 (t, *J* = 5.4 Hz, 2H, CH_2N), 2.24 (td, *J* = 7.6, 2.6 Hz, 2H, $C(O)CH_2$), 1.60 (m, 2H, $C(O)CH_2CH_2$), 1.39 – 1.23 (m, 24H), 0.91 (t, *J* = 6.7 Hz, 3H). ^{13}C NMR (125 MHz,

CD_3OD : $CDCl_3$: D_2O = 4:2:1) δ 177.25, 92.47, 75.76, 74.63, 70.63, 69.85, 66.65, 49.66, 49.49, 49.32, 49.15, 48.98, 48.81, 48.64, 40.78, 36.92, 32.99, 30.73, 30.71, 30.69, 30.56, 30.40, 30.39, 30.23, 26.89, 23.69, 14.54. HRMS: $[M-H]^-$ $C_{24}H_{48}NO_{13}P_2$ calcd 620.2679, obsd 620.2609.

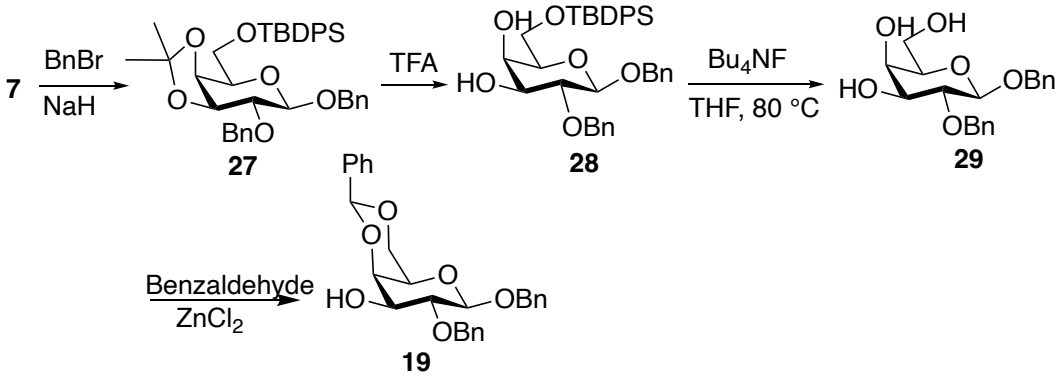

Scheme 2.9. Synthesis of dibenzyl protected building block **19**.

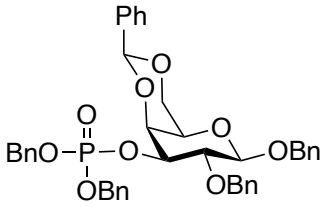

1,2-Di-*O*-benzyl 3-*O*-(dibenzylphosphono)-5,6-*O*-benzylidene-*β*-D-galactopyranoside (20)

Compound **20** was prepared from compound **19** (500 mg, 1.115 mmol) and phosphoramidite **8** by following the general procedure for one-pot phosphorylation, providing the product in 80% yield. $[\alpha]^{25}_D$ 16.05 (c = 0.38, CH_2Cl_2); ^{1}H NMR (500 MHz, cdcl$_3$) δ 7.59 – 7.10 (m, 25H), 5.60 – 5.49 (m, 1H), 5.16 – 4.87 (m, 6H, Bn), 4.67 (m, 2H, Bn), 4.56 (dd, *J* = 7.8, 1.7 Hz, 1H, H-1), 4.54 – 4.44 (m, 2H, H-3, H-4), 4.40 – 4.34 (m, 1H, H-6), 4.06 (dd, *J* = 12.4, 2.0 Hz, 1H, H-6), 3.94 (td, *J* = 8.4, 1.8 Hz, 1H, H-2), 3.46 (d, *J* = 15.6 Hz, 1H, H-5). ^{13}C NMR (125 MHz, cdcl$_3$) δ 171.18, 138.29, 137.56, 137.22, 129.18, 129.02, 128.70, 128.41, 128.39, 128.34, 128.29, 128.25, 128.21, 128.18, 128.14, 128.02, 127.98, 127.94, 127.80, 127.78, 127.75, 127.67, 127.59, 127.58, 127.47, 126.47, 126.35, 102.36, 102.22, 101.44, 101.07, 79.28, 77.64, 77.59, 76.94, 75.49,

74.99, 74.64, 72.48, 71.07, 70.96, 69.26, 69.22, 69.17, 68.97, 66.53, 65.93, 60.41, 21.07, 14.20. HRMS: $[M+Na]^+$ $C_{41}H_{41}NaO_9P$ calcd 731.2386, obsd 731.2463.

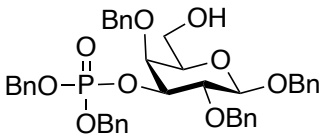

1,2,4-Tri-*O*-benzyl-3-*O*-(dibenzylphosphono) -*β*-D-galactopyranoside (21)

A suspension of compound **20** (200 mg, 0.28 mmol) and MS-4Å (1.0 g) in dry DCM (20 mL) was stirred for 1 h at room temperature under N_2. Then, the reaction mixture was cooled to -78 °C, and followed by addition of Et_3SiH (133 µL, 0.84 mmol). After that, $PhBCl_2$ (145 µL, 1.12 mmol) in DCM was added to the reaction over 1h via a syringe. The temperature was kept at -78 °C and stirred for 1 h. The reaction was quenched with Et_3N and MeOH and then filtered through celite. The filtrate was washed with saturated $NaHCO_3$ solution and brine. The organic layer was collected and dried over anhydrate Na_2SO_4. After concentrated under vacuum, the residue was purified on silica gel chromatography to afford compound **21** in 76% yield. $[\alpha]^{25}_D$ 7.31 (c = 1.67, CH_2Cl_2); ^{1}H NMR (500 MHz, $CDCl_3$) δ 7.48 – 7.04 (m, 25H), 5.04 – 4.89 (m, 7H, Bn), 4.86 (dd, *J* = 11.7, 1.9 Hz, 1H, Bn), 4.68 (m, 2H, Bn), 4.58 (dd, *J* = 11.8, 1.9 Hz, 1H, Bn), 4.47 (dd, *J* = 7.7, 1.8 Hz, 1H, H-1), 4.41 – 4.33 (m, 1H, H-3), 3.94 (d, *J* = 3.1 Hz, 1H, H-4), 3.88 (m, 1H, H-2), 3.69 (m, 1H, H-6), 3.43 – 3.28 (m, 2H, H-5, H-6). ^{13}C NMR (125 MHz, $CDCl_3$) δ 138.26, 137.73, 137.21, 137.19, 135.67, 128.68, 128.66, 128.56, 128.54, 128.52, 128.50, 128.47, 128.45, 128.43, 128.39, 128.37, 128.22, 128.20, 128.03, 128.01, 127.96, 127.94, 127.88, 127.86, 127.83, 127.54, 127.51, 102.63, 79.88, 79.84, 79.82, 77.75, 77.71, 77.69, 74.95, 74.93, 74.56, 74.54, 74.10, 74.08, 73.73, 71.34, 71.32, 69.51, 69.47, 69.46, 69.41, 61.61, 61.59. HRMS: $[M+Na]^+$ $C_{41}H_{43}NaO_9P$ calcd 733.2543, obsd 733.2675.

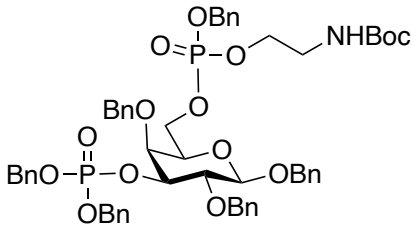

1,2,4-Tri-*O*-benzyl 2-*O*-(dibenzylphosphono)-6-*O*-((benzyl)-(2-(*tert*-butoxycarbonylamido)-ethyl)-phospono)-*β*-D-galactopyranoside (22)

Compound **21** (150 mg, 0.21 mmol) was used for the synthesis of compound **22** by following the general procedure of the one-pot phosphorylation reaction, in the presence of freshly made phosphoramidite **9**, providing the desired compound in 72% yield. $[\alpha]^{25}_{D}$ 3.21 (c = 0.53, CH_2Cl_2); ^{1}H NMR (500 MHz, $CDCl_3$) δ 7.49 – 7.07 (m, 30H), 5.15 – 4.81 (m, 9H, Bn), 4.66 (d, *J* = 11.1 Hz, 1H, Bn), 4.63 – 4.58 (m, 1H, Bn), 4.53 (dd, *J* = 11.6, 1.7 Hz, 1H, Bn), 4.42 (dd, *J* = 7.6, 1.9 Hz, 1H, H-1), 4.39 – 4.30 (m, 1H, H-3), 4.06 (m, 2H, H-6), 4.00 (dd, *J* = 12.6, 5.7 Hz, 2H, $POCH_2$), 3.93 (d, *J* = 3.3 Hz, 1H, H-4), 3.84 (m, 1H, H-2), 3.53 – 3.42 (m, 1H, H-5), 3.37 – 3.29 (m, 2H, CH_2N), 1.41 (s, 9H, BOC). ^{13}C NMR (125 MHz, $CDCl_3$) δ 171.18, 138.19, 137.01, 128.83, 128.79, 128.72, 128.69, 128.55, 128.50, 128.44, 128.40, 128.30, 128.28, 128.19, 128.15, 128.12, 128.11, 128.03, 127.98, 127.95, 127.88, 127.83, 127.53, 102.27, 79.44, 74.88, 71.10, 69.68, 69.64, 69.51, 69.46, 67.57, 60.40, 40.80, 28.37, 28.35, 21.07, 14.20. HRMS: $[M+Na]^+$ $C_{55}H_{63}NNaO_{14}P_2$ calcd 1046.3622, obsd 1046.3745.

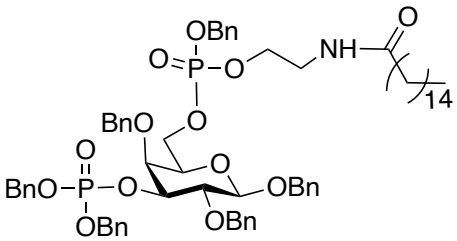

1,2,4-Tri-*O*-benzyl 3-*O*-(dibenzylphosphono)-6-*O*-((benzyl)-(2-palmitamidoethyl)-phospono)-*β*-D-galactopyranoside (23)

Compound **22** (150 mg, 0.15 mmol) was applied to the general procedure of Boc removal, followed by the general procedure of amidation reaction with palmitic acid (45 mg, 0.165 mmol), affording the desired compound in 65% yield in two steps. $[\alpha]^{25}_{D}$ 4.48 (c = 0.58, CH_2Cl_2); ^{1}H NMR (500 MHz, $CDCl_3$) δ 7.38 – 7.18 (m, 30H), 5.04 (dq, *J* = 9.1, 2.9 Hz, 2H, Bn), 4.98 – 4.85 (m, 7H, Bn), 4.66 (d, *J* = 11.3 Hz, 1H, Bn), 4.63 – 4.59 (m, 1H, Bn), 4.54 (m, 1H, Bn), 4.44 (dt, *J* = 7.5, 2.8 Hz, 1H, H-1), 4.33 (s, 1H, H-3), 4.20 – 4.07 (m, 1H, H-6), 4.04 – 4.00 (m, 2H, $POCH_2$), 3.94 (m, 1H, H-4), 3.91 – 3.77 (m, 2H, H-2, H-6), 3.49 – 3.41 (m, 3H, H-5, CH_2N), 2.14 – 2.06 (m, 2H, $C(O)CH_2$), 1.56 (m, 2H, $C(O)CH_2CH_2$), 1.24 (m, 26H), 0.88 (t, *J* = 6.8 Hz, 3H, Me). ^{13}C NMR (125 MHz, $CDCl_3$) δ 173.58, 138.48, 138.10, 128.90, 128.75, 128.57, 128.51, 128.47, 128.43, 128.32, 128.30, 128.22, 128.16, 128.13, 128.09, 127.94, 127.91, 127.87, 127.83, 127.78, 127.58, 102.36, 74.93, 71.28, 69.55, 67.09, 39.71, 36.52, 31.92, 29.70, 29.69, 29.66, 29.54, 29.42, 29.37, 25.66, 25.62, 22.70, 14.14. HRMS: $[M+Na]^+$ $C_{66}H_{85}NNaO_{13}P_2$ calcd 1184.5394, obsd 1184.5815.

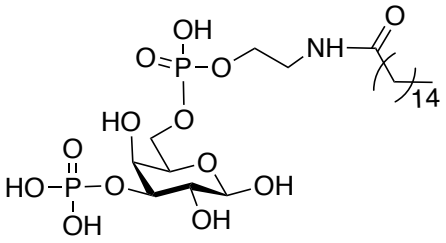

3-*O*-Phosphono-6-*O*-((2-palmitamidoethyl)-phospono)-α/β-D-galactopyranoside (18)

Compound **18** was synthesized from **23** in quantitative yield following the general procedure of global debenzylation reaction. The product was further purified with an LH-20 column. $[\alpha]^{25}_{D}$ 10.71 (c = 0.14, CH_2Cl_2);^{1}H NMR (500 MHz, CD_3OD : $CDCl_3$: D_2O = 4:2:1) δ 5.19 (d, *J* = 3.9 Hz, 1H, H-1a), 4.52 (d, *J* = 7.8 Hz, 1H, H-1b), 4.39 (m, H-3a), 4.29 – 4.23 (m, 1H, H-4), 4.19 (t, *J* = 6.4 Hz, 1H, H-5a), 4.15 (d, *J* = 3.1 Hz, 1H, H-4), 4.14 – 4.09 (m, 1H, H-3b), 4.09 – 4.03 (m, 2H, H-6), 4.00 – 3.92 (m, 6H, H-6, $OPCH_2$), 3.90 (dd, *J* = 10.0, 3.8 Hz, 1H, H-2a), 3.76

(t, J = 6.2 Hz, 1H, H-5), 3.65 – 3.58 (m, 1H, H-2b), 3.39 (t, J = 5.5 Hz, 4H, CH_2N), 2.17 (t, J = 7.7 Hz, 4H, $C(O)CH_2$), 1.55 (m, 4H, $C(O)CH_2CH_2$), 1.34 – 1.10 (m, 52H), 0.83 (t, J = 6.9 Hz, 6H, Me). ^{13}C NMR (125 MHz, CD_3OD : $CDCl_3$: D_2O = 4:2:1) δ 175.77, 128.23, 102.04, 96.70, 92.66, 80.62, 78.68, 77.87, 77.61, 77.36, 76.04, 75.99, 72.91, 72.85, 70.81, 70.76, 68.56, 68.49, 67.84, 67.38, 67.33, 67.22, 65.34, 65.29, 65.02, 60.37, 53.51, 41.55, 39.65, 39.59, 38.07, 36.09, 35.99, 31.75, 29.54, 29.51, 29.50, 29.45, 29.41, 29.39, 29.28, 29.25, 29.17, 29.13, 28.99, 25.74, 25.72, 24.51, 22.48, 13.65, 13.62. HRMS: $[M-H]^-$ $C_{24}H_{48}NO_{13}P_2$ calcd 620.2679, obsd 620.2602.

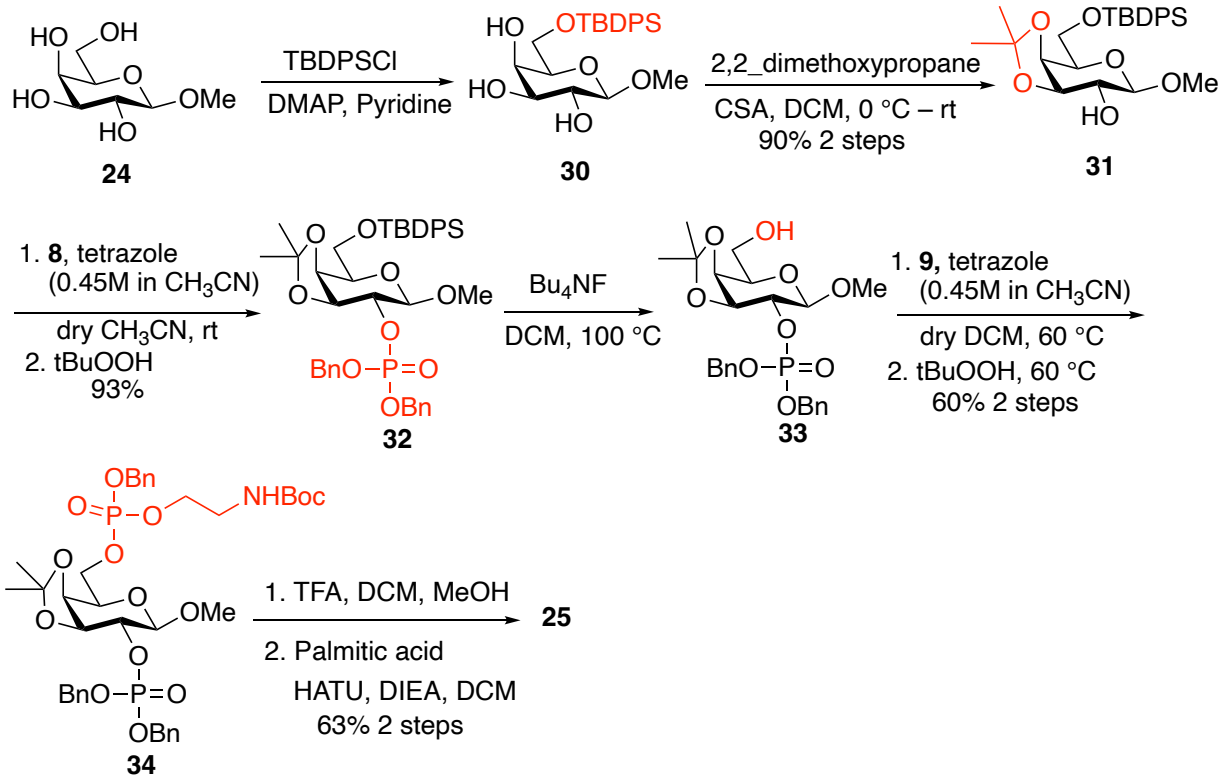

Scheme 2.10. Synthesis of methyl-galactoside **25**.

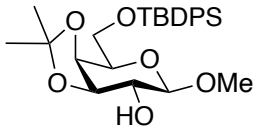

Methyl 6-*O*-(*tert*-butyldiphenylsilyl)-2-hydroxyl-3,4-*O*-isopropylidene-*β*-D-galactopyranoside (31)

The 6-OH of methyl-β-D-galactopyranoside (2 g, 10.3 mmol) was protected by TBDPSCl with the general procedure for TBDPS protection. Then, the crude compound was dissolved in acetone, and 2,2-dimethoxy propane (1.8 mL, 12.36 mmol) and camphorsulfonic acid (0.12 g, 0.52 mmol) were added. After stirred at room temperature overnight, Et_3N was added to neutralize the excess CSA and bring the pH around 7. The reaction mixture was concentrated under vacuum, and the residue was diluted with DCM and washed with aqueous $NaHCO_3$ solution and saturated NaCl solution successively. The organic layer was collected and dried over anhydrous Na_2SO_4. The volatiles were removed under vacuum and the resulted residue was purified by silica gel column chromatography to afford the designed product **31** in 90% yield in two steps. $[\alpha]^{25}_D$ -2.9 (c = 3, CH_2Cl_2); ^{1}H NMR (500 MHz, $CDCl_3$) δ 7.74 – 7.69 (m, 4H), 7.47 – 7.35 (m, 6H), 4.29 (dd, *J* = 5.4, 2.2 Hz, 1H, H-4), 4.10 – 4.07 (m, 2H, H-1, H-3), 4.02 – 3.92 (m, 2H, H-6), 3.88 (m, 1H, H-5), 3.55 (d, *J* = 7.9 Hz, 1H, H-2), 3.53 (s, 3H, Me), 1.52 (s, 3H), 1.36 (s, 3H), 1.07 (s, 9H). ^{13}C NMR (125 MHz, $CDCl_3$) δ 135.63, 135.58, 133.42, 133.31, 129.73, 127.71, 127.64, 110.06, 103.26, 78.62, 74.00, 73.59, 73.20, 62.60, 60.42, 56.90, 28.22, 26.73, 26.31, 19.22, 14.21. HRMS: $[M+Na]^+$ $C_{26}H_{36}NaO_6Si$ calcd 495.2179, obsd 495.2314.

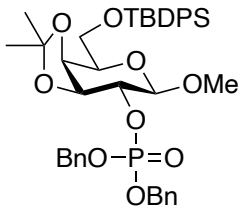

Methyl 6-*O*-(*tert*-butyldiphenylsilyl)-2-*O*-(dibenzylphosphono)-3,4-*O*-isopropylidene-*β*-D-galactopyranoside (32)

Compound **32** was prepared from compound **31** (4.86 g, 10.2 mmol) and phosphoramidite **8** (3.6 ml, 10.3 mmol) following the general procedure for one-pot phosphorylation, providing the product in 93% yield. $[\alpha]^{25}_{D}$ 7.71 (c = 1, CH_2Cl_2); ^{1}H NMR (500 MHz, $CDCl_3$) δ 7.74 – 7.66 (m, 4H), 7.48 – 7.24 (m, 16H), 5.11 (dd, *J* = 9.7, 7.2 Hz, 4H, Bn), 4.37 – 4.21 (m, 4H, H-1, H-2, H-3, H-4), 3.99 – 3.91 (m, 2H, H-6), 3.88 (m, 1H, H-5), 3.44 (s, 3H, Me), 1.49 (s, 3H), 1.33 (s, 3H), 1.06 (s, 9H). ^{13}C NMR (125 MHz, $CDCl_3$) δ 136.20, 136.14, 135.61, 135.57, 133.33, 133.26, 129.74, 128.56, 128.43, 128.41, 128.27, 128.23, 127.95, 127.92, 127.78, 127.72, 127.65, 110.43, 101.54, 101.50, 79.22, 79.17, 77.94, 77.91, 73.56, 73.34, 69.09, 69.05, 69.03, 68.99, 62.52, 60.41, 56.52, 27.85, 26.71, 26.37, 25.76, 21.08, 19.20, 14.21. HRMS: $[M+Na]^+$ $C_{40}H_{49}NaO_9PSi$ calcd 755.2781, obsd 755.2812.

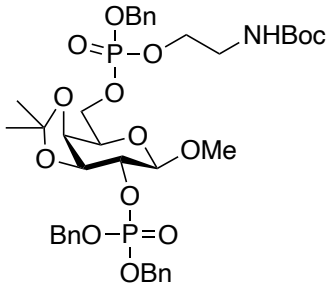

Methyl 2-*O*-(dibenzylphosphono)-6-*O*-((benzyl)-(2-(*tert*-butoxycarbonylamido)ethyl)-phospono)-3,4-*O*-isopropylidene-*β*-D-galactopyranoside (34)

Compound **3** (7 g, 9.55 mmol) was first applied the general reaction for TBDPS removal. The formed crude product was directly used as the starting material for the synthesis of compound

34 following the general procedure of the one-pot phosphorylation reaction, in the presence of freshly made phosphoramidite **9**, providing the desired compound in 60% yield in 2 steps. $[\alpha]^{25}_{D}$ 14.95 (c = 1, CH_2Cl_2); ^{1}H NMR (500 MHz, $CDCl_3$) δ 7.46 – 7.29 (m, 15H), 5.14 – 5.07 (m, 6H), 4.96 (s, 1H, NH), 4.36 – 4.18 (m, 5H, H-1, H-2, H-3, H-6), 4.08 (m, 3H, H-4, OCH_2), 3.95 (ddt, *J* = 6.3, 4.6, 2.8 Hz, 1H, H-5), 3.44 (s, 3H, Me), 3.37 (q, *J* = 5.5 Hz, 2H, CH_2N), 1.48 (s, 3H), 1.44 (s, 9H), 1.30 (t, *J* = 2.5 Hz, 3H). ^{13}C NMR (125 MHz, $CDCl_3$) δ 136.02, 128.83, 128.71, 128.44, 128.33, 128.31, 128.14, 127.91, 127.78, 110.89, 101.35, 78.48, 77.69, 73.21, 71.43, 69.65, 69.15, 69.11, 66.21, 56.73, 56.70, 28.36, 27.65, 26.35. HRMS: $[M+Na]^+$ $C_{38}H_{51}NNaO_{14}P_2$ calcd 830.2785, obsd 830.2796.

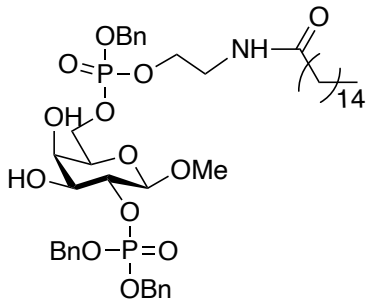

Methyl 2-*O*-(dibenzylphosphono)-6-*O*-((benzyl)-(2-palmitamidoethyl)-phospono)-*β*-D-galactopyranoside (25)

Compound **25** (4.6 g, 5.73 mmol) was applied the general procedure of Boc removal, followed by the general procedure of amidation reaction with palmitic acid (1.6 g, 6.3 mmol), affording the desired compound in 63% yield in two steps. $[\alpha]^{25}_{D}$ -19.09 (c = 0.1, CH_2Cl_2); ^{1}H NMR (500 MHz, CD_3OD) δ 7.54 – 7.29 (m, 15H), 5.17 – 5.08 (m, 6H, Bn), 4.40 – 4.31 (m, 1H, H-1), 4.26 – 4.16 (m, 2H, H-6), 4.10 (q, *J* = 7.2 Hz, 2H, OCH_2), 3.83 (t, *J* = 4.1 Hz, 1H, H-5), 3.81 – 3.68 (m, 3H, H-4, H-3, H-2), 3.47 – 3.40 (m, 5H, CH_2N, Me), 2.18 (t, *J* = 7.6 Hz, 2H, $C(O)CH_2$), 1.63 – 1.55 (m, 2H, $C(O)CH_2CH_2$), 1.34 – 1.25 (m, 24H), 0.96 – 0.80 (t, 3H, CH_3). ^{13}C NMR (125 MHz, CD_3OD) δ 175.27, 136.05, 128.46, 128.36, 128.16, 128.14, 128.07, 128.05, 127.89, 127.61, 127.43,

102.09, 78.65, 73.17, 71.99, 69.54, 69.25, 69.13, 69.08, 68.95, 66.30, 55.80, 39.19, 37.46, 35.64, 31.67, 29.39, 29.37, 29.36, 29.24, 29.08, 28.92, 27.33, 25.56, 22.34, 13.05. HRMS: $[M+H]^+$ $C_{46}H_{70}NO_{13}P_2$ calcd 906.4644, obsd 906.4788.

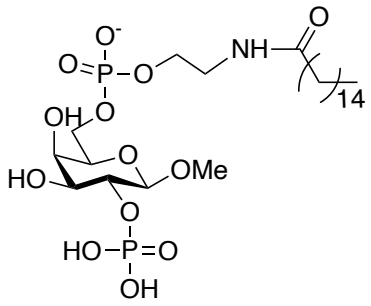

Methyl 2-*O*-phosphono-6-*O*-((2-palmitamidoethyl)-phospono)-*β*-D-galactopyranoside (5)

Compound **5** was synthesized from **19** in quantitative yield following the general procedure of global debenzylation reaction. $[\alpha]^{25}_D$ -2.35 (c = 1, CH_2Cl_2); ^1H NMR (500 MHz, CD_3OD : $CDCl_3$: D_2O = 4:2:1) δ 4.35 (d, *J* = 7.6 Hz, 1H, H-1), 4.17 – 4.02 (m, 3H, H-2, H-3, H-4), 3.97 (m, 3H, H-5, $POCH_2$), 3.80 – 3.63 (m, 2H, H-6),), 3.52 (s, 3H, OCH_3), 3.42 (t, *J* = 5.4 Hz, 2H, CH_2N), 2.24 – 2.18 (m, 2H, $C(O)CH_2$), 1.58 (m, 2H, $C(O)CH_2CH_2$), 1.26 (d, *J* = 5.1 Hz, 24H), 0.87 (t, *J* = 6.9 Hz, 3H, CH_3). ^{13}C NMR (125 MHz, CD_3OD : $CDCl_3$: D_2O = 4:2:1) δ 176.66, 103.57, 103.54, 77.83, 74.28, 73.23, 69.19, 65.79, 65.48, 63.72, 57.82, 49.51, 49.34, 49.17, 49.00, 48.83, 48.66, 48.49, 40.67, 39.04, 39.02, 37.00, 32.76, 30.54, 30.53, 30.48, 30.45, 30.32, 30.19, 28.76, 26.72, 23.49, 14.69, 14.67. HRMS: $[M-H]^-$ $C_{25}H_{50}NO_{13}P_2$ calcd 634.2836, obsd 634.2779.

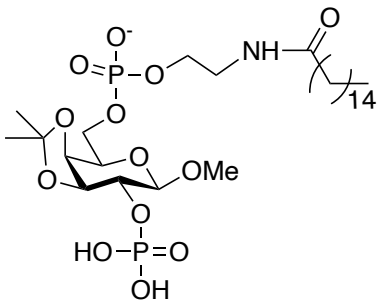

Methyl 2-*O*-phosphono-6-*O*-((2-palmitamidoethyl)-phospono)-3,4-*O*-isopropylidene-*β*-D-galactopyranoside (6)

Compound **19** (500 mg, 0.56 mmol) was dissolved in acetone, then 2,2-dimethoxy propane (0.08 mL, 0.67 mmol) and camphorsulfonic acid (20 mg, 0.12 mmol) were added. After stirred at room temperature overnight, Et_3N was added to neutralize the pH around 7. The reaction mixture was concentrated under vacuum, and the residue was diluted with DCM and washed with aqueous $NaHCO_3$ solution and saturated NaCl solution successively. The organic layer was collected and dried over anhydrous Na_2SO_4. The volatiles were removed under vacuum and the resulted residue was purified by silica gel column chromatography to afford isopropylidene protected intermediate, which was applied the general procedure of global debenzylation, and provided the desired product in 58% yield in two steps. $[\alpha]^{25}_D$ 0.19 (c = 3, CH_2Cl_2); ^{1}H NMR (500 MHz, CD_3OD : $CDCl_3$: D_2O = 4:2:1) δ4.74 (m, 1H, H-4) 4.58 (dd, *J* = 7.2, 4.0 Hz, 1H, H-2), 4.35 (dd, *J* = 7.1, 1.9 Hz, 1H, H-1), 4.13 (m, 2H, H-3, H-5), 4.06 – 3.96 (m, 2H, H-6), 3.92 (dt, *J* = 7.0, 5.3 Hz, 2H, $POCH_2$), 3.46 (s, 3H, Me), 3.41 (t, *J* = 5.3 Hz, 2H, CH_2N), 2.23 – 2.18 (m, 2H, $C(O)CH_2$), 1.58 (m, 2H, $C(O)CH_2CH_2$), 1.25 (d, *J* = 3.6 Hz, 24H), 0.87 (t, *J* = 6.9 Hz, 3H). ^{13}C NMR (125 MHz, CD_3OD : $CDCl_3$: D_2O = 4:2:1) δ 173.07, 105.93, 103.25, 68.82, 68.10, 59.29, 49.51, 49.34, 49.17, 49.00, 48.83, 48.79, 48.66, 48.49, 47.73, 43.47, 43.42, 32.63, 30.36, 30.32, 27.49, 26.64, 25.24, 23.35, 20.15, 20.09, 19.18, 14.52, 5.57. HRMS: $[M-H]^-$ $C_{28}H_{54}NO_{13}P_2$ calcd 674.3149, obsd 674.3087.

Chapter 3 Immobilization of PIP5Kα on Nanodiscs Through Conjugation with PE for Structural Characterization

3.1 Introduction

The crystal structures of PIP5Ks and PIP4Ks have revealed the presence of a flattened basic surface, which is not only essential for their binding to the phospholipid membrane, but also critical for their substrate phosphorylation[172-174]. This flattened basic surface associate with the phospholipid membrane by electrostatic interactions[173]. Further mutagenesis and functional studies of PIP5K also showed that the activity of PIP5K can be modulated by the membrane phospholipid composition, and phosphatidic acid, unsaturated phosphoserine, and sterols can stimulate PIP5K activity[161, 163, 175], suggesting a membrane recognition mechanism associated with PIP5K. Besides, the activation loop, which is a short segment in the close proximity of the conserved catalytic site of PIP5K, is also a part of this membrane binding surface. This activation loop differs in amino acid sequence between PIP5Ks and PIP4Ks, which largely determines substrate specificity[9-11]. By swapping the activation loops of PIP5K and PIP4K, not only the substrate specificities were switched[11], but also their subcellular distribution was altered. These observations indicate a direct interaction of this activation loop with membrane, and it may also confer the membrane sensing capacity of PIP5K. However, so far, this activation loop is disordered in all the available crystal structures of PIPKs (**Figure 3.1).** To study this activation loop, Hu lab has carried out an NMR study using a short peptide commensurate with the activating loop of zPIP5Kα and revealed that this unstructured peptide folds into an amphipathic helix upon association with the 1,2-dihexanoyl-sn-glycero-3-phosphocholine (DHPC) micellar surface (**Figure 3.1**)[162]. The hydrophobic side of this amphipathic helix can be imbedded into the lipid bilayer, whereas the hydrophilic side, bearing positive charges, can interact with the negative

charged lipid head groups, all of which enhanced the membrane sensing function of zPIP5Kα. Meanwhile, the mutagenesis and activity assays indicated that this amphipathic helix is also crucial for the kinase activity. Therefore, it is valuable to elucidate the structure of PIP5K with membrane bound activation loop to establish the structural basis of the membrane sensing mechanism of PIP5K. It is also important to solve the structure of the intact substrate binding pocket to clarify how the lipid substrate and competitive inhibitor interact with the enzyme to better understand the catalytic mechanism and optimize the lead compounds for improved potency and selectivity.

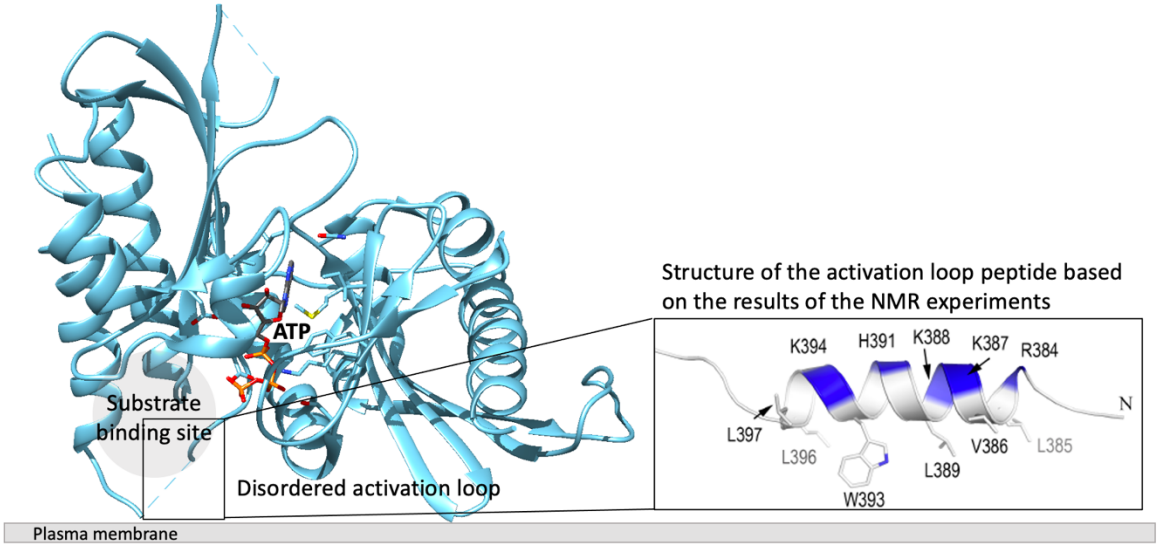

Figure 3.1. The activation loop of PIP5Kα. Left: the membrane-binding model of zPIP5Kα with the severely disordered activation loop shown as the dash line (PDB: 4TZ7). Right: the amphipathic helix of the activation loop peptide derived from NMR study[162].

Since the activation loop is folded only when it is associated with membrane surface, it is necessary to include membrane bilayer or membrane mimetics in structural study. One of the best membrane mimetic systems is nanodiscs, which have been shown to be excellent in membrane protein studies[176-180]. Nanodiscs are discoidal lipid bilayers, whose typical diameter is 8-16 nm[176, 177]. Nanodiscs are obtained by wrapping lipid bilayers with two copies of membrane scaffold

protein (MSP) (**Figure 3.2a**). Because of the encircling amphipathic helix feature of MSP, the hydrophobic tails of lipid bilayer are covered by MSP and makes nanodiscs stable in aqueous solutions. Meanwhile, by incorporate membrane proteins into the lipid bilayer, these insoluble membrane proteins become stable, and preserve their structures and activities in aqueous buffers[177]. Although there have been numerous applications of nanodiscs for study of integral membrane proteins, it is rare to use nanodiscs to study peripheral membrane proteins, partially because the association of peripheral membrane proteins, including, PIPKs, is weak and transient. Consistently, the previous trials in Hu lab have shown that zPIP5Kα failed to form a stable complex with nanodiscs, preventing further structural characterization.

To ensure the formation of zPIP5Kα-nanodisc complex, an alternative solution is through covalent binding, which is much more stable than the reversible electrostatic interaction. One such covalent bond can be obtained through the cysteine-maleimide chemistry, whose high chemoselectivity, fast reaction kinetic as well as the mild reaction condition, have made it widely used in protein conjugations. There is only one cysteine present on the flattened surface of zPIP5Kα while other cysteines are buried (**Figure 3.2b**). Meantime, the lipid composition of nanodiscs can be varied from dimyristoylphosphatidylcholine (DMPC) only to different ratios of DMPC and dimyristoylphosphatidylethanolamine (DMPE) mixture, where the MDPE bears a free amine and therefore can be functionalized. Thus, through incorporation of a hetero-bifunctional crosslinker sulfosuccinimidyl-4-(*N*-maleimidomethyl) cyclohexane-1-carboxylate (sulfo-SMCC), which containing an *N*-hydroxysuccinimide (NHS) ester and a maleimide group, the zPIP5Kα-nanodisc complex can be formed via a covalent conjugation (**Figure 3.2c**). Once it is achieved, the complex will be evaluated, and the structure will be solved using cryogenic electron microscopy (Cryo-EM) with the activation loop associated with the lipid surface of the nanodiscs.

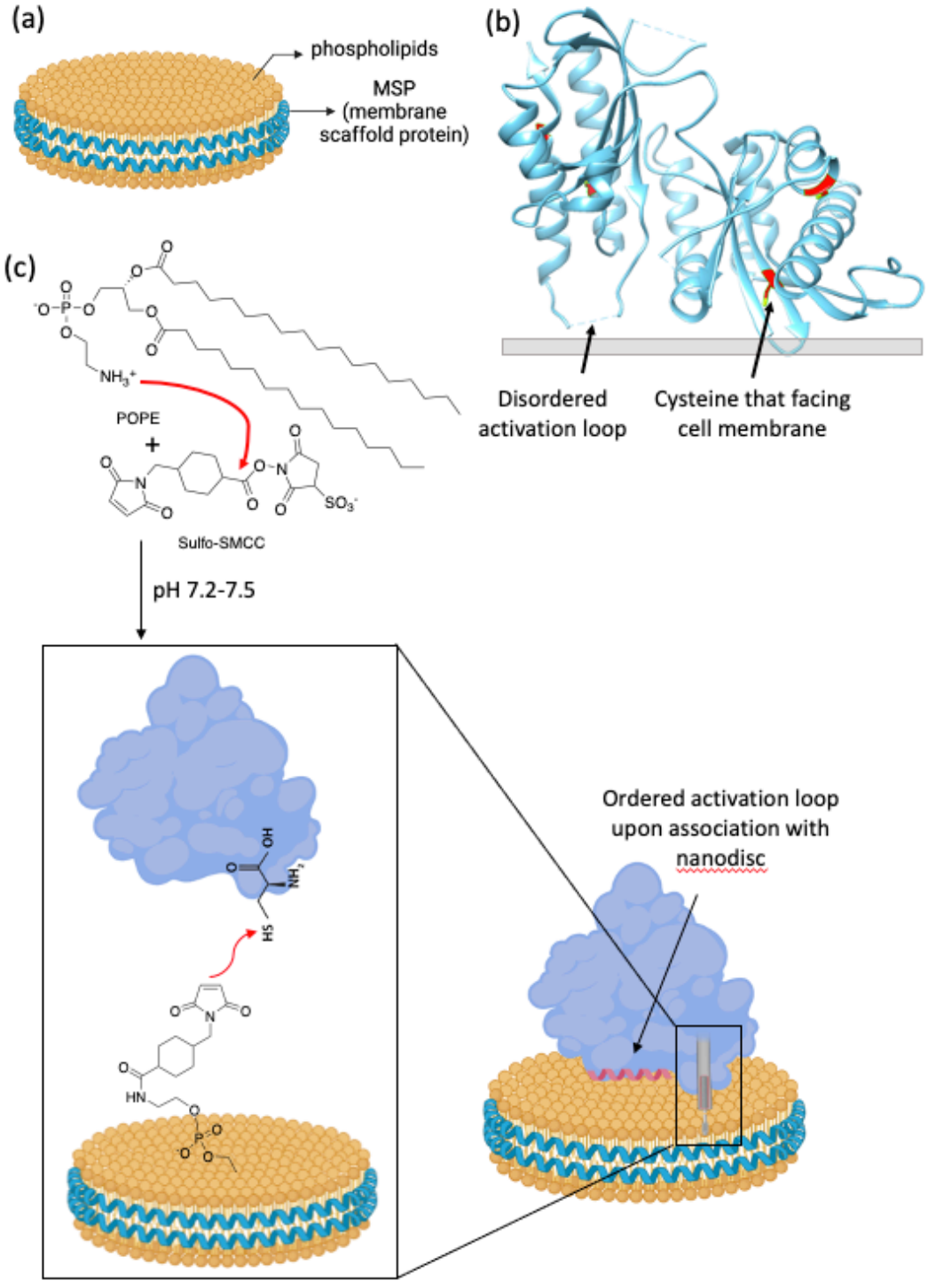

Figure 3.2. Model of zPIP5Kα-nanodisc complex. (a) Model of nanodisc. (b) The membrane-binding model of zPIP5Kα (PDB: 4TZ7). The cysteine residues are marked in red, and only one cysteine is in the flattened surface facing the cell membrane. (c) Schematic of construction of zPIP5Kα-nanodisc complex. DMPE Lipids couple with hetero-bifunctional crosslinker sulfo-SMCC to form the maleimide lipids, which then assemble with DMPC and MSP to form nanodisc.

Figure 3.2 (cont'd)
Then the maleimide exposed on nanodisc couples with the solo exposed cysteine residue of zPIP5Kα to form the zPIP5Kα-nanodisc complex via a covalent bond.

3.2 Results

To construct the zPIP5Kα -nanodisc complex, firstly, the sulfo-SMCC modified DMPE was generated. Simply mixing DMPE and sulfo-SMCC in DCM in the presence of triethylamine with stirring overnight, led to the formation of maleimide-DMPE (**Figure 3.3a**). The ^{31}P-NMR analysis indicated an approximately 50% conversion (**Figure 3.3b**).

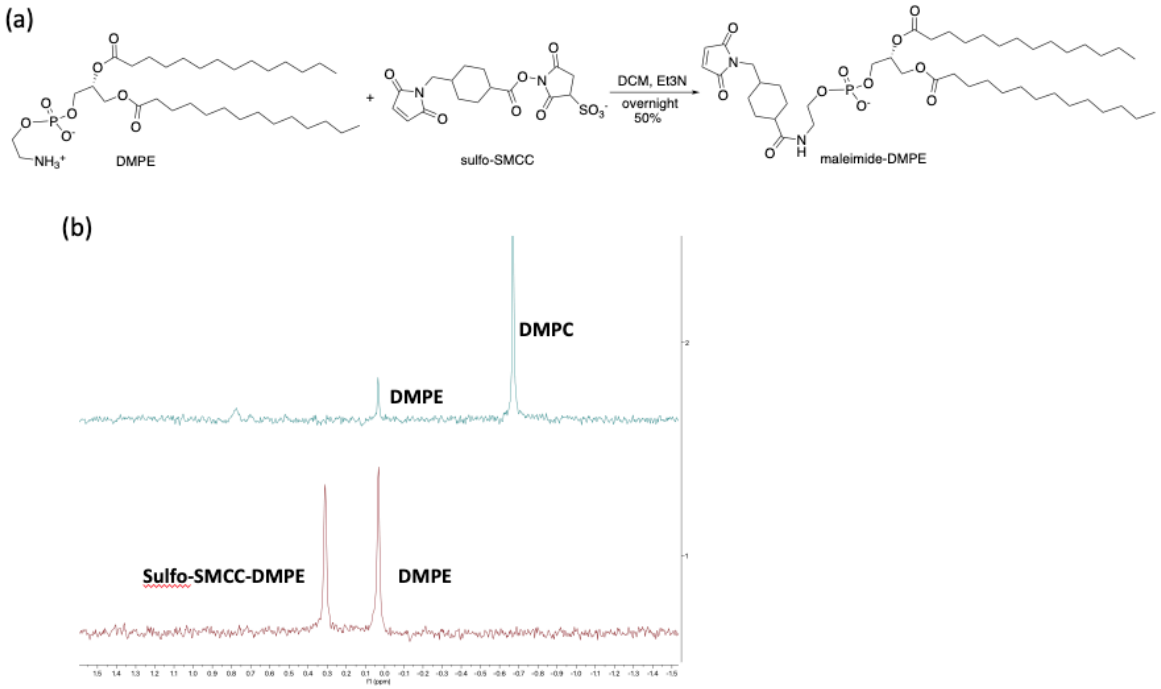

Figure 3.3. Schematic of DMPE and sulfo-SMCC coupling. (a) Synthesis of maleimide functionalized lipid for nanodisc construction. (b) Quantitation of DMPE and sulfo-SMCC coupling efficiency by ^{31}P-NMR. Upper panel shows the ^{31}P-NMR spectrum of a phospholipid mixture DMPE/ DMPC 1:8.5, and the integration ratio of the two peaks corresponding to the molar ratio of these two lipids. Lower panel shows the ^{31}P-NMR spectrum of the reaction mixture of DMPE and sulfo-SMCC coupling, and the integration ratio indicated a 50% conversion.

The modified DMPE and DMPC were used to generate the nanodiscs. Different molar ratios of modified DMPE to DMPC (1:3, 1:4, 1:5, 1:6), as well as different molar ratios of lipids

to MSP (50:1, 60:1, 70:1) were used to generate the nanodiscs. After multiple tries, the best performance was obtained with modified DMPE/ DMPC 1:3 and lipid/MSP 70:1 (**Figure 3.4a**). With the generated nanodiscs in hand, the protein-nanodisc conjugation reaction was carried out. Purified zPIP5Kα (**Figure 3.4b**) was incubated with maleimide-decorated nanodiscs at pH 7.3, and the generated protein-nanodisc complexes were purified with FPLC (**Figures 3.4c & d**).

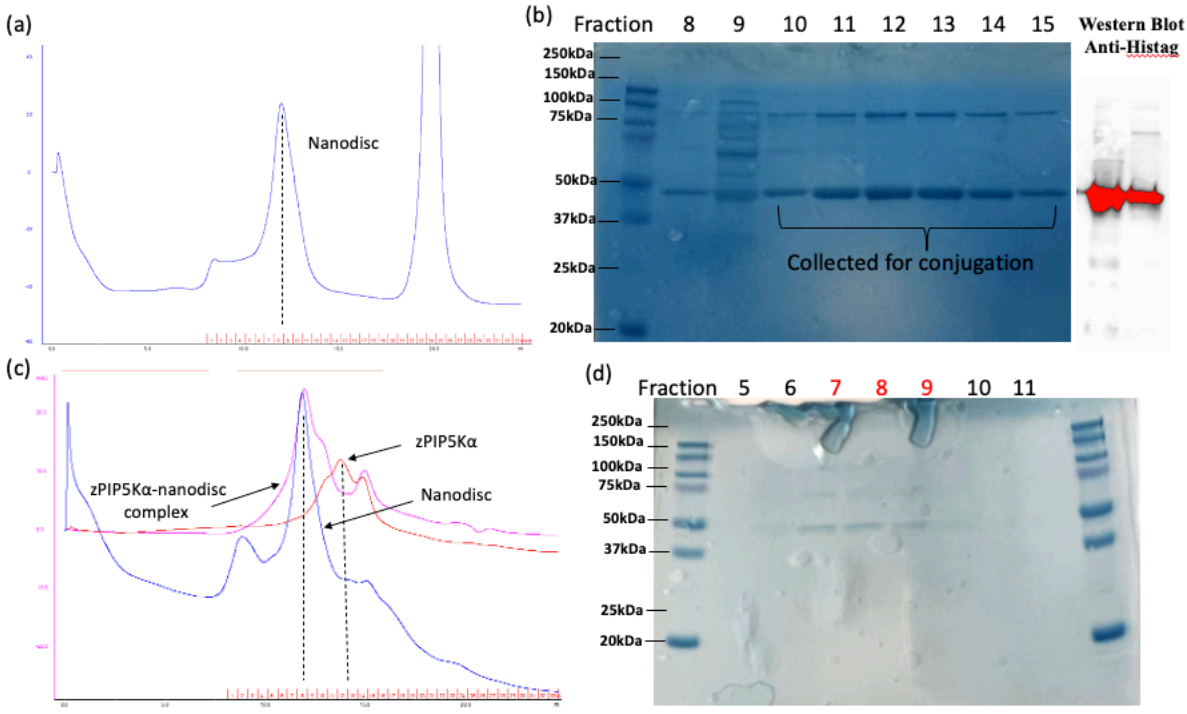

Figure 3.4. Generation of zPIP5Kα-nanodisc complex. (a) The FPLC analysis of generated nanodiscs. Maleimide DMPE/ DMPC = 1:3 and lipid/MSP = 70:1 (X axis: elution volume; Y axis: UV absorption). (b) FPLC purified zPIP5Kα and Western blot. The proteins were concentrated in fractions from 10 to 14. (c) FPLC analysis of protein-nanodiscs conjugation. The pure nanodisc was presented in blue curve. The elution profile of zPIP5Kα was shown as the red curve. The zPIP5Kα-nanodiscs complex was presented in pink curve. Comparing with the zPIP5Kα alone, the pink curve presenting the zPIP5Kα-nanodisc complex showed no peak at the elution volume corresponding to zPIP5Kα, indicative of a change of molecular weight of the protein. (d) SDS-page analysis of FPLC purified zPIP5Kα-nanodisc complex exhibited a shift of zPIP5Kα peak (fraction 7-9) from fraction 11-14 for zPIP5Kα alone. This result suggests the successful conjugation of zPIP5Kα with nanodiscs.

To confirm the formation of the zPIP5Kα-nanodisc complex, the purified zPIP5Kα-nanodisc complexes were then applied to cryo-EM analysis. By which, the binary architecture of the zPIP5Kα-nanodisc complex was elucidated (**Figure 3.5**). The 2D-classification images clearly show the association of the nanodisc (oval circle) and the zPIP5Kα (blurred particle), which demonstrates the feasibility of protein immobilization on nanodiscs as a potential approach to study the interactions of peripheral membrane proteins with lipid bilayer.

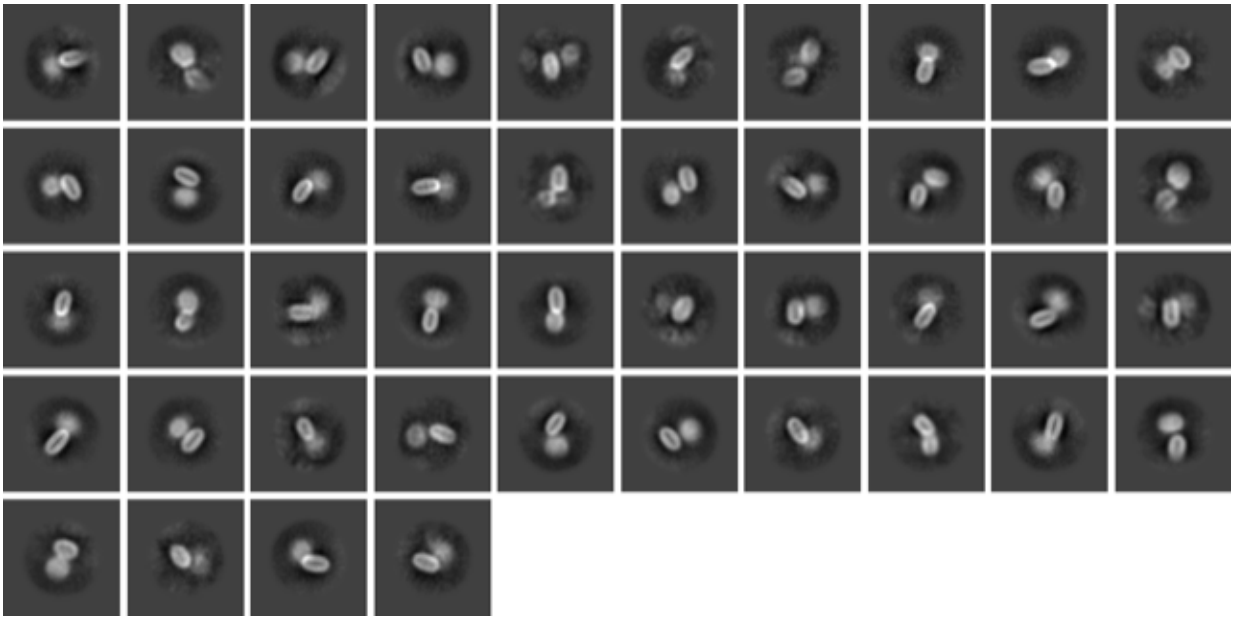

Figure 3.5. Cyro-EM analysis of the zPIP5Kα-nanodisc complexes. 2D-classification (selected views) of the zPIP5Kα-nanodisc complexes indicates a binary architecture, where the nanodisc (oval circle) and the zPIP5Kα (blurred particle) directly associated together (Images generated by Dr. Min Su in University of Michigan).

3.3 Discussion

Here I presented the initial study of generating zPIP5Kα-nanodisc complex through maleimide modified nanodisc to conjugate with the lipid-facing cysteine residue on zPIP5Kα. The Cyro-EM analysis indicated a direct association of the nanodisc and the zPIP5Kα (**Figure 3.5**) and proved the feasibility of constructing peripheral membrane proteins-nanodisc complex through protein-

lipid conjugation. As far as I know, it is the first time that protein-nanodiscs complex was formed via a covalent bond. However, although we've observed the binary complex structure in cryo-EM analysis, more studies are needed, including proteomic studies by mass spectrometry to confirm maleimide modification of the lipid-facing cysteine residue in zPIP5Kα. The ultimate goal of this study is to elucidate the intact structure of zPIP5Kα in the membrane bound state using cryo-EM. For this purpose, the sample heterogeneity issue must be solved.

3.4 Experimental method

3.4.1. DMPE modification

DMPE (20 mg, 0.03 mmol) and sulfo-SMCC (12.39 mg, 0.03 mmol) were dissolved in anhydrous DCM. After the addition of a drop of triethylamine, the reaction was stirred at room temperature overnight. Next day, the solvent was removed under vacuum, and the resulted product was analyzed by ^{31}P-NMR.

3.4.2. zPIP5Kα

zPIP5Kα was overexpressed in BL21-CodonPlus®(DE3)-RIL cells (Stratagene) in LB medium. After the OD_{600} reached 0.3, the cells were induced with 0.1 mM IPTG and left to grow overnight at room temperaturm. Next day, the cells were harvested and re-suspended in the lysis buffer containing 20 mM Tris pH 8.0, 300 mM NaCl, 5% glycerol, 1 mM TCEP and EDTA-free protease inhibitor cocktail. After lysis by sonication, the cell lysate was applied to centrifugation (20,000× *g* at 4 °C) for 50 minutes. The supernatant was collected and loaded on a Ni-NTA column (Qiagen) for binding at 4 °C for 2 hours. After washing with the washing buffer (20 mM Tris pH 8.0, 300 mM NaCl, 5% glycerol, 1 mM TCEP and 10 mM imidazole) for four times, the protein was eluted by the elution buffer (washing buffer plus 200 mM imidazole). The protein was further

purified using a Superdex 200 Increase 10/300 GL column (GE healthcare) equilibrated with the running buffer containing 10 mM HEPES pH 7.3, 300 mM NaCl, and 1% glycerol.

3.4.3. Nanodisc generation

The maleimide functionalized DMPE and DMPC (1:3) were dissolved in chloroform, and dried under a mild stream of N_2 to form a thin layer at the bottom of test tube. This lipid film was further dried under vacuum overnight. Then, the lipid film was rehydrated in rehydration buffer (20 mM tris, pH 7.3, 150 mM NaCl). During the vertex and sonication, the detergent DDM was gradually added, until the solution became clear. Then corresponding amount of MSP (lipid : MSP = 70 : 1) was added to the lipid/DDM mixture, and incubated at 4 °C for 1 hour. After that, the Biobeads were added, and incubated at 4 °C overnight. The generated PC/PE(modi)-containing nanodisc was further purified by gel filtration.

3.4.4. PIP5k and nanodisc conjugation

Freshly purified zPIP5Kα protein was mixed with freshly made nanodiscs in a proper ratio (one zPIP5Kα dimmer per nanodiscs, the molar ration of MSP : zPIP5Kα =1 : 1). The reaction was incubated at 4 °C for 2 hours or overnight. And the reaction mixture was directly applied to gel filtration for purification.

REFERENCES

1. Folch, J., Complete fractionation of brain cephalin: isolation from it of phosphatidyl serine, phosphatidyl ethanolamine, and diphosphoinositide. *J.Bio.Chem.* **1949,** *177*, 497-504.

2. Hokin, L. E.; Hokin, M. R., Metabolism of phospholipids in vitro. *Biochem. Cell Biol.* **1956,** *34*, 349-360.

3. Hokin, L. E.; Hokin, M. R., Effects of acetylcholine on the turnover of phosphoryl units in individual phospholipids of pancreas slices and brain cortex slices. *Biochim. Biophys. Acta.* **1955,** *18*, 102-110.

4. Redman, C. M.; Hokin, L. E., Phospholipide turnover in microsomal membranes of the pancreas during enzyme secretion. *J. Biophys. Biochem. Cytol.* **1959,** *6*, 207-214.

5. Hokin, L. E.; Hokin, M. R., Acetylcholine and the exchange of inositol and phosphate in brain phosphoinositide. *J. Biol. Chem.* **1958,** *233*, 818-821.

6. Berridge, M. J.; Ivrine, R. F., Inositol phosphates and cell signaling. *Nature* **1989,** *341*, 197-205.

7. Di Paolo, G.; De Camilli, P., Phosphoinositides in cell regulation and membrane dynamics. *Nature* **2006,** *443*, 651-657.

8. Balla, T., Phosphoinositides: tiny lipids with giant impact on cell regulation. *Physiol Rev* **2013,** *93* (3), 1019-137.

9. Muftuoglu, Y.; Xue, Y.; Gao, X.; Wu, D.; Ha, Y., Mechanism of substrate specificity of phosphatidylinositol phosphate kinases. *PNAS* **2016,** *113*, 8711-8716.

10. van den Bout, I.; Divecha, N., PIP5K-driven PtdIns(4,5)P2 synthesis: regulation and cellular functions. *J. Cell Sci.* **2009,** *122*, 3837-3850.

11. Kunz, J.; Fuelling, A.; Kolbe, L.; Anderson, R. A., Stereo-specific substrate recognition by phosphatidylinositol phosphate kinases is swapped by changing a single amino acid residue. *J. Biol. Chem.* **2002,** *277*, 5611-5619.

12. Thapa, N.; Choi, S.; Tan, X.; Wise, T.; Anderson, R. A., Phosphatidylinositol phosphate 5-kinase Igamma and phosphoinositide 3-kinase/Akt signaling couple to promote oncogenic growth. *J. Biol. Chem.* **2015,** *290*, 18843-18854.

13. Kamalesh, K.; Trivedi, D.; Toscano, S.; Sharma, S.; Kolay, S.; Raghu, P., Phosphatidylinositol 5-phosphate 4-kinase regulates early endosomal dynamics during clathrin-mediated endocytosis. *J. Cell Sci.* **2017,** *130*, 2119-2133.

14. Vazquez-Calvo, A.; Sobrino, F.; Martin-Acebes, M. A., Plasma membrane phosphatidylinositol 4,5 bisphosphate is required for internalization of foot-and-mouth disease virus and vesicular stomatitis virus. *PLoS One* **2012,** *7*, e45172.

15. Semenas, J.; Hedblom, A.; Miftakhova, R. R.; Sarwar, M.; Larsson, R.; Shcherbina, L.; Johansson, M. E.; Harkonen, P.; Sterner, O.; Persson, J. L., The role of PI3K/AKT-related PIP5K1alpha and the discovery of its selective inhibitor for treatment of advanced prostate cancer. *PNAS* **2014,** *111*, 3689-3698.

16. Sarwar, M.; Semenas, J.; Miftakhova, R. R.; Simoulis, A.; Robinson, B.; Wingren, A. G.; Mongan, N. P.; Heery, D. M.; Johnsson, H.; Abrahamsson, P.; Dizeyi, N.; Luo, J.; Persson, J. L., Targeted suppression of AR-V7 using PIP5K1α inhibitor overcomes enzalutamide resistance in prostate cancer cells. *Oncotarget* **2016,** *7*, 63065-63081.

17. Yamaguchi, H.; Yoshida, S.; Muroi, E.; Kawamura, M.; Kouchi, Z.; Nakamura, Y.; Sakai, R.; Fukami, K., Phosphatidylinositol 4,5-bisphosphate and PIP5-kinase Ialpha are required for invadopodia formation in human breast cancer cells. *Cancer Sci.* **2010,** *101*, 1632-1638.

18. Chen, C.; Wang, X.; Xiong, X.; Liu, Q.; Huang, Y.; Xu, Q.; Hu, J.; Ge, G.; Ling, K., Targeting type Igamma phosphatidylinositol phosphate kinase inhibits breast cancer metastasis. *Oncogene* **2015,** *34*, 4635-4646.

19. Sun, Y.; Turbin, D. A.; Ling, K.; Thapa, N.; Leung, S.; Huntsman, D. G.; Anderson, R. A., Type I gamma phosphatidylinositol phosphate kinase modulates invasion and proliferation and its expression correlates with poor prognosis in breast cancer. *Breast Cancer Research* **2010,** *12*.

20. Sarwar, M.; Syed Khaja, A. S.; Aleskandarany, M.; Karlsson, R.; Althobiti, M.; Odum, N.; Mongan, N. P.; Dizeyi, N.; Johnson, H.; Green, A. R.; Ellis, I. O.; Rakha, E. A.; Persson, J. L., The role of PIP5K1alpha/pAKT and targeted inhibition of growth of subtypes of breast cancer using PIP5K1alpha inhibitor. *Oncogene* **2019,** *38*, 375-389.

21. Vander Heiden, M. G.; Cantley, L. C.; Thompson, C. B., Understanding the Warburg effect: The metabolic requirements of cell proliferation. *Science* **2009,** *324*, 1029-1033.

22. Peng, W.; Huang, W.; Ge, X.; Xue, L.; Zhao, W.; Xue, J., Type Igamma phosphatidylinositol phosphate kinase promotes tumor growth by facilitating Warburg effect in colorectal cancer. *EBioMedicine* **2019,** *44*, 375-386.

23. Porciello, N.; Kunkl, M.; Viola, A.; Tuosto, L., Phosphatidylinositol 4-phosphate 5-kinases in the regulation of T cell activation. *Front. Immunol.* **2016,** *7*, 186.

24. Xue, J.; Chen, C.; Qi, M.; Huang, Y.; Wang, L.; Gao, Y.; Dong, H.; Ling, K., Type Iγ phosphatidylinositol phosphate kinase regulates PD-L1 expression by activating NF-κB. *Oncotarget* **2017,** *8*, 42414-42427.

25. Zoncu, R.; Perera, R. m.; Sebastian, R.; Nakatsu, F.; Chen, H., Loss of endocytic clathrin-coated pits upon acute depletion of phosphatidylinositol 4,5-bisphosphate. *PNAS* **2007,** *104*, 3793–3798.

26. Antonescu, C. N.; Aguet, F.; Danuser, G.; Schmid, S., L,, Phosphatidylinositol-(4,5)-bisphosphate regulates clathrin-coated pit initiation, stabilization, and size. *Mol. Biol. Cell.* **2011,** *22*, 2588–2600.

27. Shi, Y.; Berking, A.; Baade, T.; Legate, K. R.; Fassler, R.; Hauck, C. R., PIP5KIgamma90-generated phosphatidylinositol-4,5-bisphosphate promotes the uptake of Staphylococcus aureus by host cells. *Mol. Microbiol.* **2021,** *116*, 1249-1267.

28. Buser, J. R.; Maire, J.; Riddle, A.; Gong, X.; Nguyen, T.; Nelson, K.; Luo, N. L.; Ren, J.; Struve, J.; Sherman, L. S., Arrested preoligodendrocyte maturation contributes to myelination failure in premature infants. *Ann. Neurol.* **2012,** *71*, 93-109.

29. Tawk, M.; Makoukji, J.; Belle, M.; Fonte, C.; Trousson, A.; Hawkins, T.; Li, H.; Ghandour, S.; Schumacher, M.; Massaad, C., Wnt/beta-catenin signaling is an essential and direct driver of myelin gene expression and myelinogenesis. *J. Neurosci.* **2011,** *31*, 3729–3742.

30. Emery, B., Regulation of oligodendrocyte differentiation and myelination. *Science* **2010,** *330*, 779-782.

31. Fancy, S. P.; Baranzini, S. E.; Zhao, C.; Yuk, D. I.; Irvine, K. A.; Kaing, S.; Sanai, N.; Franklin, R. J.; Rowitch, D. H., Dysregulation of the Wnt pathway inhibits timely myelination and remyelination in the mammalian CNS. *Genes Dev.* **2009,** *23*, 1571–1585.

32. Lee, H.-K.; Chaboub, L. S.; Zhu, W.; Zollinger, D.; Rasband, M. N.; Fancy, S. P. J.; Deneen, B., Daam2-PIP5K Is a regulatory pathway for Wnt signaling and therapeutic target for remyelination in the CNS. *Neuron* **2015,** *85*, 1227-1243.

33. Gold, M. S.; Gebhart, G. F., Nociceptor sensitization in pain pathogenesis. *Nat. Med.* **2010,** *16*, 1248-1257.

34. Hucho, T. B.; Dina, O. A.; Levine, J. D., Epac mediates a cAMP-to-PKC signaling in inflammatory pain: an isolectin B4(+) neuron-specific mechanism. *J. Neurosci.* **2005,** *25*, 6119-6126.

35. Wright, B. D.; Loo, L.; Street, S. E.; Ma, A.; Taylor-Blake, B.; Stashko, M. A.; Jin, J.; Janzen, W. P.; Frye, S. V.; Zylka, M. J., The lipid kinase PIP5K1C regulates pain signaling and sensitization. *Neuron* **2014,** *82*, 836-847.

36. Larsson, R.; Blanco, N.; Johansson, M. E.; Sterner, O., Synthesis of C-1 indol-3-yl substituted tetrahydroisoquinoline derivatives via a Pictet–Spengler approach. *Tetrahedron Letters* **2012,** *53*, 4966-4970.

37. Andrews, D. M.; Cartic, S.; Cosulich, S.; Divecha, N.; Faulder, P.; Flemington, V.; Kern, O.; Kettle, J. G.; MacDonald, E.; McKelvie, J.; Pike, K. G.; Roberts, B.; Rowlinson, R.; Smith, J. M.; Stockley, M.; Swarbrick, M. E.; Treinies, I.; Waring, M. J., Identification and optimization of a novel series of selective PIP5K inhibitors. *Bioorg. Med. Chem.* **2022,** *54*, 116557.

38. Stratker, K.; Haidar, S.; Amesty, A.; El-Awaad, E.; Gotz, C.; Estevez-Braun, A.; Jose, J., Development of an in vitro screening assay for PIP5K1alpha lipid kinase and identification of potent inhibitors. *FEBS J.* **2020,** *287*, 3042-3064.

39. Carricaburu, V.; Lamia, K. A.; Lo, E.; Favereaux, L.; Payrastre, b.; Cantley, L. C.; Rameh, L. E., The phosphatidylinositol (PI)-5-phosphate 4-kinase type II enzyme controls insulin signaling by regulating PI-3,4,5-trisphosphate degradation. *PNAS* **2003,** *100*, 9867-9872.

40. Raghu, P., Emerging cell biological functions of phosphatidylinositol 5 phosphate 4 kinase. *Curr. Opin. Cell Biol.* **2021,** *71*, 15-20.

41. Fiume, R.; Stijf-Bultsma, Y.; Shah, Z. H.; Keune, W. J.; Jones, D. R.; Jude, J. G.; Divecha, N., PIP4K and the role of nuclear phosphoinositides in tumour suppression. *Biochim. Biophys. Acta.* **2015,** *1851*, 898-910.

42. Lamia, K. A.; Peroni, O. D.; Kim, Y. B.; Rameh, L. E.; Kahn, B. B.; Cantley, L. C., Increased insulin sensitivity and reduced adiposity in phosphatidylinositol 5-phosphate 4-kinase beta-/-mice. *Mol. Cell Biol.* **2004,** *24*, 5080-5087.

43. Sharma, S.; Mathre, S.; Ramya, V.; Shinde, D.; Raghu, P., Phosphatidylinositol 5 phosphate 4-kinase regulates plasma-membrane PIP3 turnover and insulin signaling. *Cell Rep.* **2019,** *27*, 1979-1990.

44. Keune, W. J.; Sims, A. H.; Jones, D. R.; Bultsma, Y.; Lynch, J. T.; Jirstrom, K.; Landberg, G.; Divecha, N., Low PIP4K2B expression in human breast tumors correlates with reduced patient survival: A role for PIP4K2B in the regulation of E-cadherin expression. *Cancer Res.* **2013,** *73*, 6913-6925.

45. Jude, J. G.; Spencer, G. J.; Huang, X.; Somerville, T. D. D.; Jones, D. R.; Divecha, N.; Somervaille, T. C. P., A targeted knockdown screen of genes coding for phosphoinositide modulators identifies PIP4K2A as required for acute myeloid leukemia cell proliferation and survival. *Oncogene* **2015,** *34*, 1253-1262.

46. Lima, K.; Coelho-Silva, J. L.; Kinker, G. S.; Pereira-Martins, D. A.; Traina, F.; Fernandes, P.; Markus, R. P.; Lucena-Araujo, A. R.; Machado-Neto, J. A., PIP4K2A and PIP4K2C transcript levels are associated with cytogenetic risk and survival outcomes in acute myeloid leukemia. *Cancer Genet.* **2019,** *233*, 56-66.

47. Luoh, S.-W.; Venkatesan, N.; Tripathi, R., Overexpression of the amplified PIP4K2B gene from 17q11–12 in breast cancer cells confers proliferation advantage. *Oncogene* **2004,** *23*, 1354-1363.

48. Emerling, B. M.; Hurov, J. B.; Poulogiannis, G.; Tsukazawa, K. S.; Choo-Wing, R.; Wulf, G. M.; Bell, E. L.; Shim, H. S.; Lamia, K. A.; Rameh, L. E.; Bellinger, G.; Sasaki, A. T.; Asara, J. M.; Yuan, X.; Bullock, A.; Denicola, G. M.; Song, J.; Brown, V.; Signoretti, S.; Cantley, L. C., Depletion of a putatively druggable class of phosphatidylinositol kinases inhibits growth of p53-null tumors. *Cell* **2013,** *155*, 844-857.

49. Voss, M. D.; Czechtizky, W.; Li, Z.; Rudolph, C.; Petry, S.; Brummerhop, H.; Langer, T.; Schiffer, A.; Schaefer, H. L., Discovery and pharmacological characterization of a novel small molecule inhibitor of phosphatidylinositol-5-phosphate 4-kinase, type II, beta. *Biochem. Biophys. Res. Commun.* **2014,** *449*, 327-331.

50. Wang, D. G.; Paddock, M. N.; Lundquist, M. R.; Sun, J. Y.; Mashadova, O.; Amadiume, S.; Bumpus, T. W.; Hodakoski, C.; Hopkins, B. D.; Fine, M.; Hill, A.; Yang, T. J.; Baskin, J. M.; Dow, L. E.; Cantley, L. C., PIP4Ks suppress insulin signaling through a catalytic-independent mechanism. *Cell Rep.* **2019,** *27*, 1991-2001.

51. Davis, M. I.; Sasaki, A. T.; Shen, M.; Emerling, B. M.; Thorne, N.; Michael, S.; Pragani, R.; Boxer, M.; Sumita, K.; Takeuchi, K.; Auld, D. S.; Li, Z.; Cantley, L. C.; Simeonov, A., A homogeneous, high-throughput assay for phosphatidylinositol 5-phosphate 4-kinase with a novel, rapid substrate preparation. *PLoS One* **2013,** *8*, e54127.

52. Kitagawa, M.; Liao, P. J.; Lee, K. H.; Wong, J.; Shang, S. C.; Minami, N.; Sampetrean, O.; Saya, H.; Lingyun, D.; Prabhu, N.; Diam, G. K.; Sobota, R.; Larsson, A.; Nordlund, P.; McCormick, F.; Ghosh, S.; Epstein, D. M.; Dymock, B. W.; Lee, S. H., Dual blockade of the lipid kinase PIP4Ks and mitotic pathways leads to cancer-selective lethality. *Nat. Commun.* **2017,** *8*, 2200.

53. Wortmann, L.; Brauer, N.; Holton, S. J.; Irlbacher, H.; Weiske, J.; Lechner, C.; Meier, R.; Karen, J.; Sioberg, C. B.; Putter, V.; Christ, C. D.; Ter Laak, A.; Lienau, P.; Lesche, R.; Nicke, B.; Cheung, S. H.; Bauser, M.; Haegebarth, A.; von Nussbaum, F.; Mumberg, D.; Lemos, C., Discovery and characterization of the potent and highly selective 1,7-naphthyridine-based inhibitors BAY-091 and BAY-297 of the kinase PIP4K2A. *J. Med. Chem.* **2021,** *64*, 15883-15911.

54. Clarke, J. H.; Giudici, M. L.; Burke, J. E.; Williams, R. L.; Maloney, D. J.; Marugan, J.; Irvine, R. F., The function of phosphatidylinositol 5-phosphate 4-kinase gamma (PI5P4Kgamma) explored using a specific inhibitor that targets the PI5P-binding site. *Biochem. J.* **2015,** *466*, 359-367.

55. Al-Ramahi, I.; Giridharan, S. S. P.; Chen, Y. C.; Patnaik, S.; Safren, N.; Hasegawa, J.; de Haro, M.; Wagner Gee, A. K.; Titus, S. A.; Jeong, H.; Clarke, J.; Krainc, D.; Zheng, W.; Irvine, R. F.; Barmada, S.; Ferrer, M.; Southall, N.; Weisman, L. S.; Botas, J.; Marugan, J. J., Inhibition of PIP4Kgamma ameliorates the pathological effects of mutant huntingtin protein. *Elife* **2017,** *6*, e29123.

56. Boffey, H. K.; Rooney, T. P. C.; Willems, H. M. G.; Edwards, S.; Green, C.; Howard, T.; Ogg, D.; Romero, T.; Scott, D. E.; Winpenny, D.; Duce, J.; Skidmore, J.; Clarke, J. H.; Andrews, S. P., Development of selective phosphatidylinositol 5-phosphate 4-kinase gamma inhibitors with a non-ATP-competitive, allosteric binding mode. *J. Med. Chem.* **2022,** *65*, 3359-3370.

57. Sivakumaren, S. C.; Shim, H.; Zhang, T.; Ferguson, F. M.; Lundquist, M. R.; Browne, C. M.; Seo, H. S.; Paddock, M. N.; Manz, T. D.; Jiang, B.; Hao, M. F.; Krishnan, P.; Wang, D. G.; Yang, T. J.; Kwiatkowski, N. P.; Ficarro, S. B.; Cunningham, J. M.; Marto, J. A.; Dhe-

Paganon, S.; Cantley, L. C.; Gray, N. S., Targeting the PI5P4K lipid kinase family in cancer using covalent inhibitors. *Cell Chem. Biol.* **2020,** *27*, 525-537.

58. Zhang, T.; Inesta-Vaquera, F.; Niepel, M.; Zhang, J.; Ficarro, S. B.; Machleidt, T.; Xie, T.; Marto, J. A.; Kim, N.; Sim, T., Discovery of potent and selective covalent inhibitors of JNK. *Chem. Biol.* **2012,** *19*, 140-154.

59. Manz, T. D.; Sivakumaren, S. C.; Yasgar, A.; Hall, M. D.; Davis, M. I.; Seo, H. S.; Card, J. D.; Ficarro, S. B.; Shim, H.; Marto, J. A.; Dhe-Paganon, S.; Sasaki, A. T.; Boxer, M. B.; Simeonov, A.; Cantley, L. C.; Shen, M.; Zhang, T.; Ferguson, F. M.; Gray, N. S., Structure-activity relationship dtudy of covalent pan-phosphatidylinositol 5-phosphate 4-kinase inhibitors. *ACS Med. Chem. Lett.* **2020,** *11*, 346-352.

60. Manz, T. D.; Sivakumaren, S. C.; Ferguson, F. M.; Zhang, T.; Yasgar, A.; Seo, H. S.; Ficarro, S. B.; Card, J. D.; Shim, H.; Miduturu, C. V.; Simeonov, A.; Shen, M.; Marto, J. A.; Dhe-Paganon, S.; Hall, M. D.; Cantley, L. C.; Gray, N. S., Discovery and structure-activity relationship study of (Z)-5-methylenethiazolidin-4-one derivatives as potent and selective pan-phosphatidylinositol 5-phosphate 4-kinase inhibitors. *J. Med. Chem.* **2020,** *63*, 4880-4895.

61. Lang, M. J.; Strunk, B. S.; Azad, N.; Petersen, J. L.; Weisman, L. S., An intramolecular interaction within the lipid kinase Fab1 regulates cellular phosphatidylinositol 3,5-bisphosphate lipid levels. *Mol. Biol. Cell* **2017,** *28*, 858-864.

62. Shisheva, A., PIKfyve: Partners, significance, debates and paradoxes. *Cell Biol. Int.* **2008,** *32*, 591-604.

63. Lartigue, J. D.; Polson, H.; Feldman, M.; Shokat, K.; Tooze, S. A.; Urbe, S.; Clague, M. J., PIKfyve regulation of endosome-linked pathways. *Traffic* **2009,** *10*, 883-893.

64. Wallroth, A.; Haucke, V., Phosphoinositide conversion in endocytosis and the endolysosomal system. *J. Biol. Chem.* **2018,** *293*, 1526-1535.

65. Lees, J. A.; Li, P.; Kumar, N.; Weisman, L. S.; Reinisch, K. M., Insights into lysosomal PI(3,5)P2 homeostasis from a structural-biochemical analysis of the PIKfyve lipid kinase complex. *Mol. Cell* **2020,** *80*, 736-743.

66. McCartney, A. J.; Zhang, Y.; Weisman, L. S., Phosphatidylinositol 3,5-bisphosphate: low abundance, high significance. *Bioessays* **2014,** *36*, 52-64.

67. Sbrissa, D.; Ikonomov, O. C.; Fu, Z.; Ijuin, T.; Gruenberg, J.; Takenawa, T.; Shisheva, A., Core protein machinery for mammalian phosphatidylinositol 3,5-bisphosphate synthesis and turnover that regulates the progression of endosomal transport. *J. Biol. Chem.* **2007,** *282*, 23878-23891.

68. Yamamoto, A.; DeWald, D. B.; Boronenkov, I. V.; Anderson, R. A.; Emr, S. D.; Koshland, D., Novel PI(4)P 5-kinase homologue, Fablp, essential for normal vacuole function and morphology in yeast. *Mol. Biol. Cell* **1995,** *6*, 525-539.

69. Rusten, T. E.; Rodahl, L. M. W.; Pattni, K.; Englund, C.; Samakovlis, C.; Dove, S.; Brech, A.; Stenmark, H., Fab1 phosphatidylinositol 3-phosphate 5-kinase controls trafficking but not silencing of endocytosed receptors. *Mol. Biol. Cell* **2006,** *17*, 3989-4001.

70. Ikonomov, O. C.; Sbrissa, D.; Shisheva, A., Mammalian cell morphology and endocytic membrane homeostasis require enzymatically active phosphoinositide 5-kinase PIKfyve. *J. Biol. Chem.* **2001,** *276*, 26141-26147.

71. Choy, C. H.; Saffi, G.; Gray, M. A.; Wallace, C.; Dayam, R. M.; Ou, Z. A.; Lenk, G.; Puertollano, R.; Watkins, S. C.; Botelho, R. J., Lysosome enlargement during inhibition of the lipid kinase PIKfyve proceeds through lysosome coalescence. *J. Cell. Sci.* **2018,** *131*, jcs213587.

72. Dong, X. P.; Shen, D.; Wang, X.; Dawson, T.; Li, X.; Zhang, Q.; Cheng, X.; Zhang, Y.; Weisman, L. S.; Delling, M.; Xu, H., PI(3,5)P(2) controls membrane trafficking by direct activation of mucolipin Ca(2+) release channels in the endolysosome. *Nat. Commun.* **2010,** *1*, 1-38.

73. Dayam, R. M.; Saric, A.; Shilliday, R. E.; Botelho, R. J., The phosphoinositide-gated lysosomal Ca(2+) channel, TRPML1, Is required for phagosome maturation. *Traffic* **2015,** *16*, 1010-1026.

74. Nicot, A. S.; Fares, H.; Payrastre, B.; Chisholm, A. D.; Labouesse, M.; Laporte, J., The phosphoinositide kinase PIKfyve/Fab1p regulates terminal lysosome maturation in Caenorhabditis elegans. *Mol. Biol. Cell* **2006,** *17*, 3062-3074.

75. Bissig, C.; Hurbain, I.; Raposo, G.; van Niel, G., PIKfyve activity regulates reformation of terminal storage lysosomes from endolysosomes. *Traffic* **2017,** *18*, 747-757.

76. Kim, G. H.; Dayam, R. M.; Prashar, A.; Terebiznik, M.; Botelho, R. J., PIKfyve inhibition interferes with phagosome and endosome maturation in macrophages. *Traffic* **2014,** *15*, 1143-1163.

77. Inpanathan, S.; Botelho, R. J., The Lysosome Signaling Platform: Adapting With the Times. *Front Cell Dev Biol* **2019,** *7*, 113.

78. Martin, S.; Harper, C. B.; May, L. M.; Coulson, E. J.; Meunier, F. A.; Osborne, S. L., Inhibition of PIKfyve by YM-201636 dysregulates autophagy and leads to apoptosis-independent neuronal cell death. *PLoS One* **2013,** *8*, e60152.

79. Isobe, Y.; Nigorikawa, K.; Tsurumi, G.; Takemasu, S.; Takasuga, S.; Kofuji, S.; Hazeki, K., PIKfyve accelerates phagosome acidification through activation of TRPML1 while arrests aberrant vacuolation independent of the Ca2+ channel. *J. Biochem.* **2019,** *165*, 75-84.

80. Rutherford, A. C.; Traer, C.; Wassmer, T.; Pattni, K.; Bujny, M. V.; Carlton, J. G.; Stenmark, H.; Cullen, P. J., The mammalian phosphatidylinositol 3-phosphate 5-kinase (PIKfyve) regulates endosome-to-TGN retrograde transport. *J. Cell Sci.* **2006,** *119*, 3944-3957.

81. Gary, J. D.; Sato, T. k.; Stefan, C. J.; Bonangelino, C. J.; Weisman, L. S.; Emr, S. D., Regulation of Fab1 phosphatidylinositol 3-phosphate 5-kinase pathway by Vac7 protein and Fig4, a polyphosphoinositide phosphatase family member. *Mol. Biol. Cell* **2002,** *13*, 1238-1251.

82. Ikonomov, O. C.; Sbrissa, D.; Delvecchio, K.; Xie, Y.; Jin, J.; Rappolee, D.; Shisheva, A., The phosphoinositide kinase pIKfyve Is vital in early embryonic development. *J. Biol. Chem.* **2011,** *286*, 13404-13413.

83. Zolov, S. N.; Bridges, D.; Zhang, Y.; Lee, W. W.; Riehle, E.; Verma, R.; Lenk, G. M.; Converso-Baran, K.; Weide, T.; Albin, R. L.; Saltiel, A. R.; Meisler, M. H.; Russell, M. W.; Weisman, L. S., In vivo, Pikfyve generates PI(3,5)P2, which serves as both a signaling lipid and the major precursor for PI5P. *PNAS* **2012,** *109*, 17472-17477.

84. Ikonomov, O. C.; Sbrissa, D.; Delvecchio, K.; Feng, H. Z.; Cartee, G. D.; Jin, J. P.; Shisheva, A., Muscle-specific Pikfyve gene disruption causes glucose intolerance, insulin resistance, adiposity, and hyperinsulinemia but not muscle fiber-type switching. *Am. J. Physiol. Endocrinol. Metab.* **2013,** *305*, 119-931.

85. Mironova, Y. A.; Lenk, G. M.; Lin, J.; Lee, S.-J.; Twiss, J. L.; Vaccari, I.; Bolino, A.; Havton, L. A.; Min, S.-H.; Abrams, C. S.; Shrager, P.; Meisler, M. H., PI(3,5)P2 biosynthesis regulates oligodendrocyte differentiation by intrinsic and extrinsic mechanisms. *eLife* **2016,** *5*, e13023.

86. Takasuga, S.; Horie, Y.; Sasaki, J.; Sun-Wada, G. H.; Kawamura, N.; Iizuka, R.; Mizuno, K.; Eguchi, S.; Kofuji, S.; Kimura, H.; Yamazaki, M.; Horie, C.; Odanaga, E.; Sato, Y.; Chida, S.; Kontani, K.; Harada, A.; Katada, T.; Suzuki, A.; Wada, Y.; Ohnishi, H.; Sasaki, T., Critical roles of type III phosphatidylinositol phosphate kinase in murine embryonic visceral endoderm and adult intestine. *PNAS* **2013,** *110*, 1726-1731.

87. Min, S. H.; Suzuki, A.; Weaver, L.; Guzman, J.; Chung, Y.; Jin, H.; Gonzalez, F.; Trasorras, C.; Zhao, L.; Spruce, L. A.; Seeholzer, S. H.; Behrens, E. M.; Abrams, C. S., PIKfyve deficiency in myeloid cells impairs lysosomal homeostasis in macrophages and promotes systemic inflammation in mice. *Mol. Cell Biol.* **2019,** *39*, e00158-19.

88. Chow, C. Y.; Zhang, Y.; Dowling, J. J.; Jin, N.; Adamska, M.; Shiga, K.; Szigeti, K.; Shy, M. E.; Li, J.; Zhang, X.; Lupski, J. R.; Weisman, L. S.; Meisler, M. H., Mutation of FIG4 causes neurodegeneration in the pale tremor mouse and patients with CMT4J. *Nature* **2007,** *448*, 68-72.

89. Chow, C. Y.; Landers, J. E.; Bergren, S. K.; Sapp, P. C.; Grant, A. E.; Jones, J. M.; Everett, L.; Lenk, G. M.; McKenna-Yasek, D. M.; Weisman, L. S.; Figlewicz, D.; Brown, R. H.; Meisler, M. H., Deleterious variants of FIG4, a phosphoinositide phosphatase, in patients with ALS. *Am. J. Hum. Genet.* **2009,** *84*, 85-88.

90. Zhang, Y.; Zolov, S. N.; Chow, C. Y.; Slutsky, S. G.; Richardson, S. C.; Piper, R. C.; Yang, B.; Nau, J. J.; Westrick, R. J.; Morrison, S. J.; Meisler, M. H.; Weisman, L. S., Loss of Vac14, a regulator of the signaling lipid phosphatidylinositol 3,5-bisphosphate, results in neurodegeneration in mice. *PNAS* **2007,** *104*, 17518-17523.

91. Campeau, P. M.; Lenk, G. M.; Lu, J. T.; Bae, Y.; Burrage, L.; Turnpenny, P.; Roman Corona-Rivera, J.; Morandi, L.; Mora, M.; Reutter, H.; Vulto-van Silfhout, A. T.; Faivre, L.; Haan, E.; Gibbs, R. A.; Meisler, M. H.; Lee, B. H., Yunis-Varon syndrome is caused by mutations in FIG4, encoding a phosphoinositide phosphatase. *Am. J. Hum. Genet.* **2013,** *92*, 781-791.

92. Rivero-Rios, P.; Weisman, L. S., Roles of PIKfyve in multiple cellular pathways. *Curr. Opin. Cell Biol.* **2022,** *76*, 102086.

93. Raghu, P.; Joseph, A.; Krishnan, H.; Singh, P.; Saha, S., Phosphoinositides: Regulators of nervous system function in health and disease. *Front. Mol. Neurosci.* **2019,** *12*, 208.

94. Dickson, E. J., Recent advances in understanding phosphoinositide signaling in the nervous system. *F1000Res* **2019,** *8*.

95. Ferguson, C. J.; Lenk, G. M.; Meisler, M. H., Defective autophagy in neurons and astrocytes from mice deficient in PI(3,5)P2. *Hum. Mol. Genet.* **2009,** *18*, 4868-4878.

96. Tsuruta, F.; Dolmetsch, R. E., PIKfyve mediates the motility of late endosomes and lysosomes in neuronal dendrites. *Neurosci. Lett.* **2015,** *605*, 18-23.

97. Komatsu, M.; Waguri, S.; Chiba, T.; Murata, S.; Iwata, J.; Tanida, I.; Ueno, T.; Koike, M.; Uchiyama, Y.; Kominami, E.; Tanaka, K., Loss of autophagy in the central nervous system causes neurodegeneration in mice. *Nature* **2006,** *441*, 880-884.

98. Peric, A.; Annaert, W., Early etiology of Alzheimer's disease: tipping the balance toward autophagy or endosomal dysfunction? *Acta. Neuropathol* **2015,** *129*, 363-381.

99. Ando, K.; Houben, S.; Homa, M.; de Fisenne, M. A.; Potier, M. C.; Erneux, C.; Brion, J. P.; Leroy, K., Alzheimer's disease: Tau pathology and dysfunction of endocytosis. *Front. Mol. Neurosci.* **2020,** *13*, 583755.

100. Annadurai, N.; De Sanctis, J. B.; Hajduch, M.; Das, V., Tau secretion and propagation: Perspectives for potential preventive interventions in Alzheimer's disease and other tauopathies. *Exp. Neurol.* **2021,** *343*, 113756.

101. Goedert, M.; Eisenberg, D. S.; Crowther, R. A., Propagation of tau aggregates and neurodegeneration. *Annu. Rev. Neurosci.* **2017,** *40*, 189-210.

102. Wei, Y.; Liu, M.; Wang, D., The propagation mechanisms of extracellular tau in Alzheimer's disease. *J. Neurol.* **2022,** *269*, 1164-1181.

103. Zhao, J.; Wu, H.; Tang, X. Q., Tau internalization: A complex step in tau propagation. *Ageing Res. Rev.* **2021,** *67*, 101272.

104. Balklava, Z.; Niehage, C.; Currinn, H.; Mellor, L.; Guscott, B.; Poulin, G.; Hoflack, B.; Wassmer, T., The amyloid precursor protein controls PIKfyve function. *PLoS One* **2015,** *10*, e0130485.

105. Currinn, H.; Guscott, B.; Balklava, Z.; Rothnie, A.; Wassmer, T., APP controls the formation of PI(3,5)P(2) vesicles through its binding of the PIKfyve complex. *Cell Mol. Life. Sci.* **2016,** *73*, 393-408.

106. Soares, A. C.; Ferreira, A.; Marien, J.; Delay, C.; Lee, E.; Trojanowski, J. Q.; Moechars, D.; Annaert, W.; De Muynck, L., PIKfyve activity is required for lysosomal trafficking of tau aggregates and tau seeding. *J. Biol. Chem.* **2021,** *296*, 100636.

107. Cooper, J. M.; Lathuiliere, A.; Migliorini, M.; Arai, A. L.; Wani, M. M.; Dujardin, S.; Muratoglu, S. C.; Hyman, B. T.; Strickland, D. K., Regulation of tau internalization, degradation, and seeding by LRP1 reveals multiple pathways for tau catabolism. *J. Biol. Chem.* **2021,** *296*, 100715.

108. Guo, W.; Vandoorne, T.; Steyaert, J.; Staats, K. A.; Van Den Bosch, L., The multifaceted role of kinases in amyotrophic lateral sclerosis: genetic, pathological and therapeutic implications. *Brain* **2020,** *143*, 1651-1673.

109. Pampalakis, G.; Angelis, G.; Zingkou, E.; Vekrellis, K.; Sotiropoulou, G., A chemogenomic approach is required for effective treatment of amyotrophic lateral sclerosis. *Clin. Transl. Med.* **2022,** *12*, e657.

110. Galluzzi, L.; Bravo-San Pedro, J. M.; Levine, B.; Green, D. R.; Kroemer, G., Pharmacological modulation of autophagy: therapeutic potential and persisting obstacles. *Nat. Rev. Drug Discov.* **2017,** *16*, 487-511.

111. Levy, J. M. M.; Towers, C. G.; Thorburn, A., Targeting autophagy in cancer. *Nat. Rev. Cancer* **2017,** *17*, 528-542.

112. Oppelt, A.; Haugsten, E. M.; Zech, T.; Danielsen, H. E.; Sveen, A.; Lobert, V. H.; Skotheim, R. I.; Wesche, J., PIKfyve, MTMR3 and their product PtdIns5P regulate cancer cell migration and invasion through activation of Rac1. *Biochem. J.* **2014,** *461*, 382-390.

113. Gayle, S.; Landrette, S.; Beeharry, N.; Conrad, C.; Hernandez, M.; Beckett, P.; Ferguson, S. M.; Mandelkern, T.; Zheng, M.; Xu, T.; Rothberg, J.; Lichenstein, H., Identification of apilimod as a first-in-class PIKfyve kinase inhibitor for treatment of B-cell non-Hodgkin lymphoma. *Blood* **2017,** *129*, 1768-1778.

114. Hou, J. Z.; Xi, Z. Q.; Niu, J.; Li, W.; Wang, X.; Liang, C.; Sun, H.; Fang, D.; Xie, S. Q., Inhibition of PIKfyve using YM201636 suppresses the growth of liver cancer via the induction of autophagy. *Oncol. Rep.* **2019,** *41*, 1971-1979.

115. de Campos, C. B.; Zhu, Y. X.; Sepetov, N.; Romanov, S.; Bruins, L. A.; Shi, C. X.; Stein, C. K.; Petit, J. L.; Polito, A. N.; Sharik, M. E.; Meermeier, E. W.; Ahmann, G. J.; Armenta, I. D. L.; Kruse, J.; Bergsagel, P. L.; Chesi, M.; Meurice, N.; Braggio, E.; Stewart, A. K., Identification of PIKfyve kinase as a target in multiple myeloma. *Haematologica* **2020,** *105*, 1641-1649.

116. Qiao, Y.; Choi, J.-E.; Tien, J. C.; Simko, S. A.; Rajendiran, T.; Vo, J. N.; Delekta, A. D.; Wang, L.; Xiao, L.; Hodge, N. B.; Desai, P.; Mendoza, S.; Juckette, K.; Xu, A.; Soni, T.; Su, F.; Wang, R.; Cao, X.; Yu, J.; Kryczek, I.; WanG, X.-M.; Wang, X.; Siddiqui, J.; Wang, Z.; Bernard, A.; Fernandez-SalaS, E.; Navone, N. M.; Ellison, S. J.; Ding, K.; Eskelinen, E.-L.; Heath, E. I.; Klionsky, D. J.; Zou, W.; Chinnaiyan, A. M., Autophagy inhibition by targeting PIKfyve potentiates response to immune checkpoint blockade in prostate cancer. *nature cancer* **2021,** *2*, 978-993.

117. Pedrioli, G.; Paganetti, P., Hijacking endocytosis and autophagy in extracellular vesicle communication: Where the inside meets the outside. *Front. Cell Dev. Biol.* **2020,** *8*, 595515.

118. Jefferies, H. B.; Cooke, F. T.; Jat, P.; Boucheron, C.; Koizumi, T.; Hayakawa, M.; Kaizawa, H.; Ohishi, T.; Workman, P.; Waterfield, M. D.; Parker, P. J., A selective PIKfyve inhibitor blocks PtdIns(3,5)P(2) production and disrupts endomembrane transport and retroviral budding. *EMBO Rep.* **2008,** *9*, 164-170.

119. Kerr, M. C.; Wang, J. T.; Castro, N. A.; Hamilton, N. A.; Town, L.; Brown, D. L.; Meunier, F. A.; Brown, N. F.; Stow, J. L.; Teasdale, R. D., Inhibition of the PtdIns(5) kinase PIKfyve disrupts intracellular replication of Salmonella. *EMBO J.* **2010,** *29*, 1331-1347.

120. Nelson, E. A.; Dyall, J.; Hoenen, T.; Barnes, A. B.; Zhou, H.; Liang, J. Y.; Michelotti, J.; Dewey, W. H.; DeWald, L. E.; Bennett, R. S.; Morris, P. J.; Guha, R.; Klumpp-Thomas, C.; McKnight, C.; Chen, Y. C.; Xu, X.; Wang, A.; Hughes, E.; Martin, S.; Thomas, C.; Jahrling, P. B.; Hensley, L. E.; Olinger, G. G., Jr.; White, J. M., The phosphatidylinositol-3-phosphate 5-kinase inhibitor apilimod blocks filoviral entry and infection. *PLoS Negl. Trop. Dis.* **2017,** *11*, e0005540.

121. Mahmoud, I. S.; Jarrar, Y. B.; Alshaer, W.; Ismail, S., SARS-CoV-2 entry in host cells-multiple targets for treatment and prevention. *Biochimie.* **2020,** *175*, 93-98.

122. Riva, L.; Yuan, S.; Yin, X.; Martin-Sancho, L.; Matsunaga, N.; Pache, L.; Burgstaller-Muehlbacher, S.; De Jesus, P. D.; Teriete, P.; Hull, M. V.; Chang, M. W.; Chan, J. F.; Cao, J.; Poon, V. K.; Herbert, K. M.; Cheng, K.; Nguyen, T. H.; Rubanov, A.; Pu, Y.; Nguyen, C.; Choi, A.; Rathnasinghe, R.; Schotsaert, M.; Miorin, L.; Dejosez, M.; Zwaka, T. P.; Sit, K. Y.; Martinez-Sobrido, L.; Liu, W. C.; White, K. M.; Chapman, M. E.; Lendy, E. K.; Glynne, R. J.; Albrecht, R.; Ruppin, E.; Mesecar, A. D.; Johnson, J. R.; Benner, C.; Sun, R.; Schultz, P. G.; Su, A. I.; Garcia-Sastre, A.; Chatterjee, A. K.; Yuen, K. Y.; Chanda, S. K., Discovery of SARS-CoV-2 antiviral drugs through large-scale compound repurposing. *Nature* **2020,** *586*, 113-119.

123. Ou, X.; Liu, Y.; Lei, X.; Li, P.; Mi, D.; Ren, L.; Guo, L.; Guo, R.; Chen, T.; Hu, J.; Xiang, Z.; Mu, Z.; Chen, X.; Chen, J.; Hu, K.; Jin, Q.; Wang, J.; Qian, Z., Characterization of spike glycoprotein of SARS-CoV-2 on virus entry and its immune cross-reactivity with SARS-CoV. *Nat. Commun.* **2020,** *11*, 1620.

124. Kang, Y. L.; Chou, Y. Y.; Rothlauf, P. W.; Liu, Z.; Soh, T. K.; Cureton, D.; Case, J. B.; Chen, R. E.; Diamond, M. S.; Whelan, S. P. J.; Kirchhausen, T., Inhibition of PIKfyve kinase prevents infection by Zaire ebolavirus and SARS-CoV-2. *PNAS* **2020,** *117*, 20803-20813.

125. Kreutzberger, A. J. B.; Sanyal, A.; Ojha, R.; Pyle, J. D.; Vapalahti, O.; Balistreri, G.; Kirchhausena, T., Synergistic block of SARS-CoV-2 infection by combined drug inhibition of the host entry factors PIKfyve kinase and TMPRSS2 protease. *J. Virol.* **2021,** *95*, e00975-21.

126. Su, J.; Zheng, J.; Huang, W.; Zhang, Y.; Lv, C.; Zhang, B.; Jiang, L.; Cheng, T.; Yuan, Q.; Xia, N.; Zhang, J.; Li, L.; Li, L.; Deng, X., PIKfyve inhibitors against SARS-CoV-2 and its variants including Omicron. *Signal Transduct Target Ther.* **2022,** *7*, 167.

127. Hu, B.; Guo, H.; Zhou, P.; Shi, Z. L., Characteristics of SARS-CoV-2 and COVID-19. *Nat. Rev. Microbiol.* **2021,** *19*, 141-154.

128. Jackson, C. B.; Farzan, M.; Chen, B.; Choe, H., Mechanisms of SARS-CoV-2 entry into cells. *Nat. Rev. Mol. Cell Biol.* **2022,** *23*, 3-20.

129. Li, H.; Zhou, Y.; Zhang, M.; Wang, H.; Zhao, Q.; Liu, J., Updated approaches against SARS-CoV-2. *Antimicrob. Agents Chemother.* **2020,** *64*, e00483-20.

130. Krammer, F., SARS-CoV-2 vaccines in development. *Nature* **2020,** *586*, 516-527.

131. Fan, Y.; Li, X.; Zhang, L.; Wan, S.; Zhang, L.; Zhou, F., SARS-CoV-2 Omicron variant: recent progress and future perspectives. *Signal Transduct. Target. Ther.* **2022,** *7*, 141.

132. Cai, X.; Xu, Y.; Cheung, A. K.; Tomlinson, R. C.; Alcazar-Roman, A.; Murphy, L.; Billich, A.; Zhang, B.; Feng, Y.; Klumpp, M.; Rondeau, J. M.; Fazal, A. N.; Wilson, C. J.; Myer, V.; Joberty, G.; Bouwmeester, T.; Labow, M. A.; Finan, P. M.; Porter, J. A.; Ploegh, H. L.; Baird, D.; De Camilli, P.; Tallarico, J. A.; Huang, Q., PIKfyve, a class III PI kinase, is the target of the small molecular IL-12/IL-23 inhibitor apilimod and a player in Toll-like receptor signaling. *Chem. Biol.* **2013,** *20*, 912-921.

133. Wada, Y.; Lu, R.; Zhou, D.; Chu, J.; Przewloka, T.; Zhang, S.; Li, L.; Wu, Y.; Qin, J.; Balasubramanyam, V.; Barsoum, J.; Ono, M., Selective abrogation of Th1 response by STA-5326, a potent IL-12/IL-23 inhibitor. *Blood* **2007,** *109*, 1156-1164.

134. Turvey, S. E.; Broide, D. H., Innate immunity. *J. Allergy Clin. Immunol.* **2010,** *125*, 24-32.

135. Kawasaki, T.; Kawai, T., Toll-like receptor signaling pathways. *Front. Immunol.* **2014,** *5*, 461.

136. Tan, Y.; Kagan, J. C., Microbe-inducible trafficking pathways that control Toll-like receptor signaling. *Traffic* **2017,** *18*, 6-17.

137. Leifer, C. A.; Medvedev, A. E., Molecular mechanisms of regulation of Toll-like receptor signaling. *J. Leukoc. Biol.* **2016,** *100*, 927-941.

138. Hazeki, K.; Nigorikawa, K.; Hazeki, O., The role of PIKfyve in toll-like receptor-mediated responses. In *Inflammation and Immunity in Cancer*, Springer Japan: 2015.

139. Hazeki, K.; Uehara, M.; Nigorikawa, K.; Hazeki, O., PIKfyve regulates the endosomal localization of CpG oligodeoxynucleotides to elicit TLR9-dependent cellular responses. *PLoS One* **2013,** *8*, e73894.

140. Hayashi, K.; Sasai, M.; Iwasaki, A., Toll-like receptor 9 trafficking and signaling for type I interferons requires PIKfyve activity. *Int. Immunol.* **2015,** *27*, 435-445.

141. Zanoni, I.; Ostuni, R.; Marek, L. R.; Barresi, S.; Barbalat, R.; Barton, G. M.; Granucci, F.; Kagan, J. C., CD14 controls the LPS-induced endocytosis of Toll-like receptor 4. *Cell* **2011,** *147*, 868-680.

142. Liu, Y.; Yin, H.; Zhao, M.; Lu, Q., TLR2 and TLR4 in autoimmune diseases: a comprehensive review. *Clin. Rev. Allergy Immunol.* **2014,** *47*, 136-147.

143. Marongiu, L.; Gornati, L.; Artuso, I.; Zanoni, I.; Granucci, F., Below the surface: The inner lives of TLR4 and TLR9. *J. Leukoc. Biol.* **2019,** *106*, 147-160.

144. Hayakawa, M.; Kaizawa, H.; Moritomo, H.; Koizumi, T.; Ohishi, T.; Okada, M.; Ohta, M.; Tsukamoto, S.; Parker, P. J.; Workman, P.; M., W., Synthesis and biological evaluation of 4-morpholino-2-phenylquinazolines and related derivatives as novel PI3 kinase p110alpha inhibitors. *Bioorg. Med. Chem.* **2006,** *14*, 6847-6858.

145. Sano, O.; Kazetani, K.; Funata, M.; Fukuda, Y.; Matsui, J.; Iwata, H., Vacuolin-1 inhibits autophagy by impairing lysosomal maturation via PIKfyve inhibition. *FEBS Lett* **2016,** *590*, 1576-1585.

146. Sharma, G.; Guardia, C. M.; Roy, A.; Vassilev, A.; Saric, A.; Griner, L. N.; Marugan, J.; Ferrer, M.; Bonifacino, J. S.; DePamphilis, M. L., A family of PIKFYVE inhibitors with therapeutic potential against autophagy-dependent cancer cells disrupt multiple events in lysosome homeostasis. *Autophagy* **2019,** *15*, 1694-1718.

147. Lee, C. Y.; Johnson, R. L.; Wichterman-Kouznetsova, J.; Guha, R.; Ferrer, M.; Tuzmen, P.; Martin, S. E.; Zhu, W.; DePamphilis, M. L., High-throughput screening for genes that prevent excess DNA replication in human cells and for molecules that inhibit them. *Methods* **2012,** *57*, 234-248.

148. Terajima, M.; Kaneko-Kobayashi, Y.; Nakamura, N.; Yuri, M.; Hiramoto, M.; Naitou, M.; Hattori, K.; Yokota, H.; Mizuhara, H.; Higashi, Y., Inhibition of c-Rel DNA binding is critical for the anti-inflammatory effects of novel PIKfyve inhibitor. *Eur. J. Pharmacol.* **2016,** *780*, 93-105.

149. Cho, H.; Geno, E.; Patoor, M.; Reid, A.; McDonald, R.; Hild, M.; Jenkins, J. L., Indolyl-pyridinyl-propenone-induced methuosis through the inhibition of PIKFYVE. *ACS Omega* **2018,** *3*, 6097-6103.

150. Hudkins, R. L.; Becknell, N. C.; Zulli, A. L.; Underiner, T.; Angeles, T. S.; Aimone, L. D.; Albom, M. S.; Chang, H.; Miknyoczki, S. J.; Hunter, K.; Jones-Bolin, S.; Zhao, H.; Bacon, E. R.; Mallamo, J. P.; Ator, M. A.; Ruggeri, B. A., Synthesis and Biological Profile of the pan-

Vascular Endothelial Growth Factor Receptor/Tyrosine Kinase with Immunoglobulin and Epidermal Growth Factor-Like Homology Domains 2 (VEGF-R/TIE-2) Inhibitor 11-(2-Methylpropyl)-12,13-dihydro-2-methyl-8-(pyrimidin-2-ylamino)-4H indazolo[5,4-a]pyrrolo[3,4-c]carbazol-4-one (CEP-11981): A Novel Oncology Therapeutic Agent. *J. Med. Chem.* **2012,** *55*, 903-913.

151. Robinson, M. W.; Overmeyer, J. H.; Young, A. M.; Erhardt, P. W.; Maltese, W. A., Synthesis and evaluation of indole-based chalcones as inducers of methuosis, a novel type of nonapoptotic cell death. *J. Med. Chem.* **2012,** *55*, 1940-1956.

152. Chen, S.; Chandra Tjin, C.; Gao, X.; Xue, Y.; Jiao, H.; Zhang, R.; Wu, M.; He, Z.; Ellman, J.; Ha, Y., Pharmacological inhibition of PI5P4Kalpha/beta disrupts cell energy metabolism and selectively kills p53-null tumor cells. *Proc Natl Acad Sci U S A* **2021,** *118* (21).

153. Fawaz, M. V.; Topper, M. E.; Firestine, S. M., The ATP-grasp enzymes. *Bioorg Chem* **2011,** *39* (5-6), 185-91.

154. Gribble, F. M.; Loussouarn, G.; Tucker, S. J.; Zhao, C.; Nichols, C. G.; Ashcroft, F. M., A novel method for measurement of submembrane ATP concentration. *J Biol Chem* **2000,** *275* (39), 30046-9.

155. Knight, Z. A.; Shokat, K. M., Features of selective kinase inhibitors. *Chem Biol* **2005,** *12* (6), 621-37.

156. Breen, M. E.; Soellner, M. B., Small molecule substrate phosphorylation site inhibitors of protein kinases: approaches and challenges. *ACS Chem Biol* **2015,** *10* (1), 175-89.

157. McNamara, C. W.; Lee, M. C.; Lim, C. S.; Lim, S. H.; Roland, J.; Simon, O.; Yeung, B. K.; Chatterjee, A. K.; McCormack, S. L.; Manary, M. J.; Zeeman, A. M.; Dechering, K. J.; Kumar, T. S.; Henrich, P. P.; Gagaring, K.; Ibanez, M.; Kato, N.; Kuhen, K. L.; Fischli, C.; Nagle, A.; Rottmann, M.; Plouffe, D. M.; Bursulaya, B.; Meister, S.; Rameh, L.; Trappe, J.; Haasen, D.; Timmerman, M.; Sauerwein, R. W.; Suwanarusk, R.; Russell, B.; Renia, L.; Nosten, F.; Tully, D. C.; Kocken, C. H.; Glynne, R. J.; Bodenreider, C.; Fidock, D. A.; Diagana, T. T.; Winzeler, E. A., Targeting Plasmodium PI(4)K to eliminate malaria. *Nature* **2013,** *504* (7479), 248-253.

158. Bojjireddy, N.; Botyanszki, J.; Hammond, G.; Creech, D.; Peterson, R.; Kemp, D. C.; Snead, M.; Brown, R.; Morrison, A.; Wilson, S.; Harrison, S.; Moore, C.; Balla, T., Pharmacological and genetic targeting of the PI4KA enzyme reveals its important role in maintaining plasma membrane phosphatidylinositol 4-phosphate and phosphatidylinositol 4,5-bisphosphate levels. *J Biol Chem* **2014,** *289* (9), 6120-32.

159. Manjunatha, U. H.; Vinayak, S.; Zambriski, J. A.; Chao, A. T.; Sy, T.; Noble, C. G.; Bonamy, G. M. C.; Kondreddi, R. R.; Zou, B.; Gedeck, P.; Brooks, C. F.; Herbert, G. T.; Sateriale, A.; Tandel, J.; Noh, S.; Lakshminarayana, S. B.; Lim, S. H.; Goodman, L. B.; Bodenreider, C.; Feng, G.; Zhang, L.; Blasco, F.; Wagner, J.; Leong, F. J.; Striepen, B.; Diagana, T. T., A Cryptosporidium PI(4)K inhibitor is a drug candidate for cryptosporidiosis. *Nature* **2017,** *546* (7658), 376-380.

160. Yang, J.; Nie, J.; Ma, X.; Wei, Y.; Peng, Y.; Wei, X., Targeting PI3K in cancer: mechanisms and advances in clinical trials. *Mol Cancer* **2019,** *18* (1), 26.

161. Shulga, Y. V.; Anderson, R. A.; Topham, M. K.; Epand, R. M., Phosphatidylinositol-4-phosphate 5-kinase isoforms exhibit acyl chain selectivity for both substrate and lipid activator. *J Biol Chem* **2012,** *287* (43), 35953-63.

162. Liu, A., Sui, D., Wu, D., Hu, J., The activation loop of PIP5K functions as a membrane sensor essential for lipid substrate processing. *Sci Adv* **2016,** *2*, e1600925.

163. Amos, S. T. A.; Kalli, A. C.; Shi, J.; Sansom, M. S. P., Membrane recognition and binding by the phosphatidylinositol phosphate kinase PIP5K1A: a multiscale simulation study. *Structure* **2019,** *27*, 1336-1346.

164. Arouri, A.; Mouritsen, O. G., Membrane-perturbing effect of fatty acids and lysolipids. *Prog Lipid Res* **2013,** *52* (1), 130-40.

165. Zeng, X.; Uyar, A.; Sui, D.; Donyapour, N.; Wu, D.; Dickson, A.; Hu, J., Structural insights into lethal contractural syndrome type 3 (LCCS3) caused by a missense mutation of PIP5Kgamma. *Biochem. J.* **2018,** *475*, 2257-2269.

166. Galindo, I.; Garaigorta, U.; Lasala, F.; Cuesta-Geijo, M. A.; Bueno, P.; Gil, C.; Delgado, R.; Gastaminza, P.; Alonso, C., Antiviral drugs targeting endosomal membrane proteins inhibit distant animal and human pathogenic viruses. *Antiviral Res* **2021,** *186*, 104990.

167. Kreutzberger, A. J. B.; Sanyal, A.; Ojha, R.; Pyle, J. D.; Vapalahti, O.; Balistreri, G.; Kirchhausen, T., Synergistic Block of SARS-CoV-2 Infection by Combined Drug Inhibition of the Host Entry Factors PIKfyve Kinase and TMPRSS2 Protease. *J Virol* **2021,** *95* (21), e0097521.

168. Kubiak, R. J.; Bruzik, K. S., Comprehensive and uniform synthesis of all naturally occurring phosphorylated phosphatidylinositols. *J Org Chem* **2003,** *68* (3), 960-8.

169. Conway, S. J.; Gardiner, J.; Grove, S. J.; Johns, M. K.; Lim, Z. Y.; Painter, G. F.; Robinson, D. E.; Schieber, C.; Thuring, J. W.; Wong, L. S.; Yin, M. X.; Burgess, A. W.; Catimel, B.; Hawkins, P. T.; Ktistakis, N. T.; Stephens, L. R.; Holmes, A. B., Synthesis and biological evaluation of phosphatidylinositol phosphate affinity probes. *Org Biomol Chem* **2010,** *8* (1), 66-76.

170. Dinev, Z.; Gannon, C. T.; Egan, C.; Watt, J. A.; McConville, M. J.; Williams, S. J., Galactose-derived phosphonate analogues as potential inhibitors of phosphatidylinositol biosynthesis in mycobacteria. *Org Biomol Chem* **2007,** *5* (6), 952-9.

171. Anderson, R. A.; Boronenkov, I. V.; Doughman, S. D.; Kunz, J.; Loijens, J. C., Phosphatidylinositol phosphate kinases, a multifaceted family of signaling enzymes. *J Biol Chem* **1999,** *274* (15), 9907-10.

172. Rao, V. D.; Misra, S.; Boronenkov, I. V.; Anderson, R. A.; Hurley, J. H., Structure of type IIb phosphatidylinositol phosphate kinase: A protein kinase fold flattened for interfacial phosphorylation. *Cell Press* **1998** *94* (829-839).

173. Burden, L. M.; Rao, V. D.; Murray, D.; Ghirlando, R.; Doughman, S. D.; Anderson, R. A.; Hurley, J. H., The flattened face of type IIa phosphatidylinositol phosphate kinase binds acidic phospholipid membranes. *Biochemistry* **1999** *38*, 15141-15149.

174. Hu, J.; Yuan, Q.; Kang, X.; Qin, Y.; Li, L.; Ha, Y.; Wu, D., Resolution of structure of PIP5K1A reveals molecular mechanism for its regulation by dimerization and dishevelled. *Nat. Commun.* **2015,** *6*, 8205.

175. Nishimura, T.; Gecht, M.; Covino, R.; Hummer, G.; Surma, M. A.; Klose, C.; Arai, H.; Kono, N.; Stefan, C. J., Osh proteins control nanoscale lipid organization necessary for PI(4,5)P2 synthesis. *Mol. Cell* **2019,** *75*, 1043-1057.

176. Denisov, I. G.; Sligar, S. G., Nanodiscs for structural and functional studies of membrane proteins. *Nat. Struct. Mol. Biol.* **2016,** *23*, 481-486.

177. Denisov, I. G.; Sligar, S. G., Nanodiscs in membrane biochemistry and biophysics. *Chem. Rev.* **2017,** *117*, 4669-4713.

178. Sligar, S. G.; Denisov, I. G., Nanodiscs: A toolkit for membrane protein science. *Protein Sci.* **2021,** *30*, 297-315.

179. Notti, R. Q.; Walz, T., Native-like environments afford novel mechanistic insights into membrane proteins. *Trends Biochem. Sci.* **2022,** *47*, 561-569.

180. Padmanabha Das, K. M.; Shih, W. M.; Wagner, G.; Nasr, M. L., Large nanodiscs: A potential game changer in structural biology of membrane protein complexes and virus entry. *Front. Bioeng. Biotechnol.* **2020,** *8*, 539.

APPENDIX A: Supplementary Figures

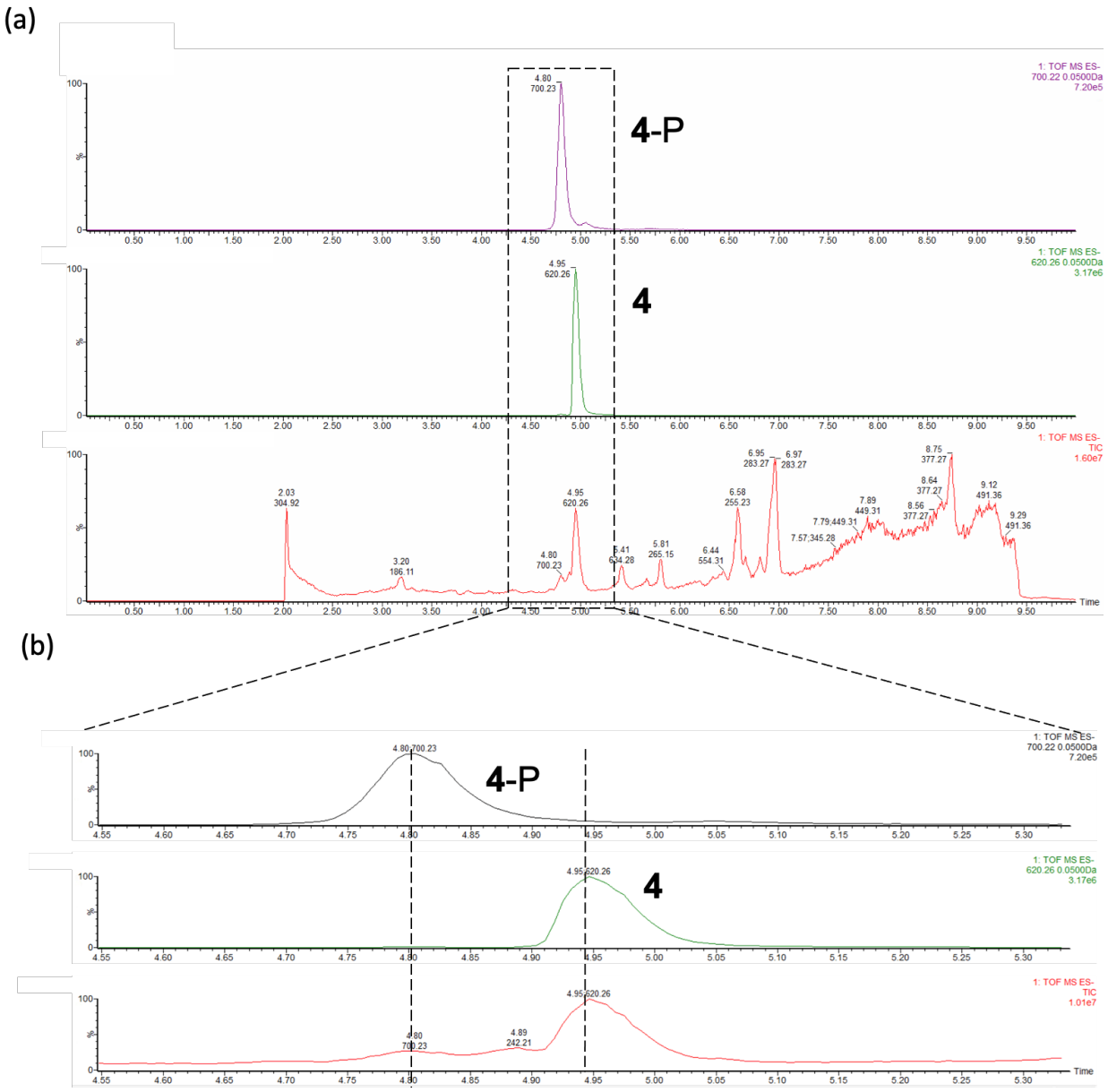

Figure S1. Separation of 4 phosphorylation product using ion-pair liquid chromatography. (a) Chromatography profiles of reaction mixture (*bottom*), the compound 4 with the MW of 620.26 Da (*middle*), and the mono-phosphorylated 4 with the MW of 700.23 Da *(top*). (b) Zoomed-in view of the regions framed in (a).

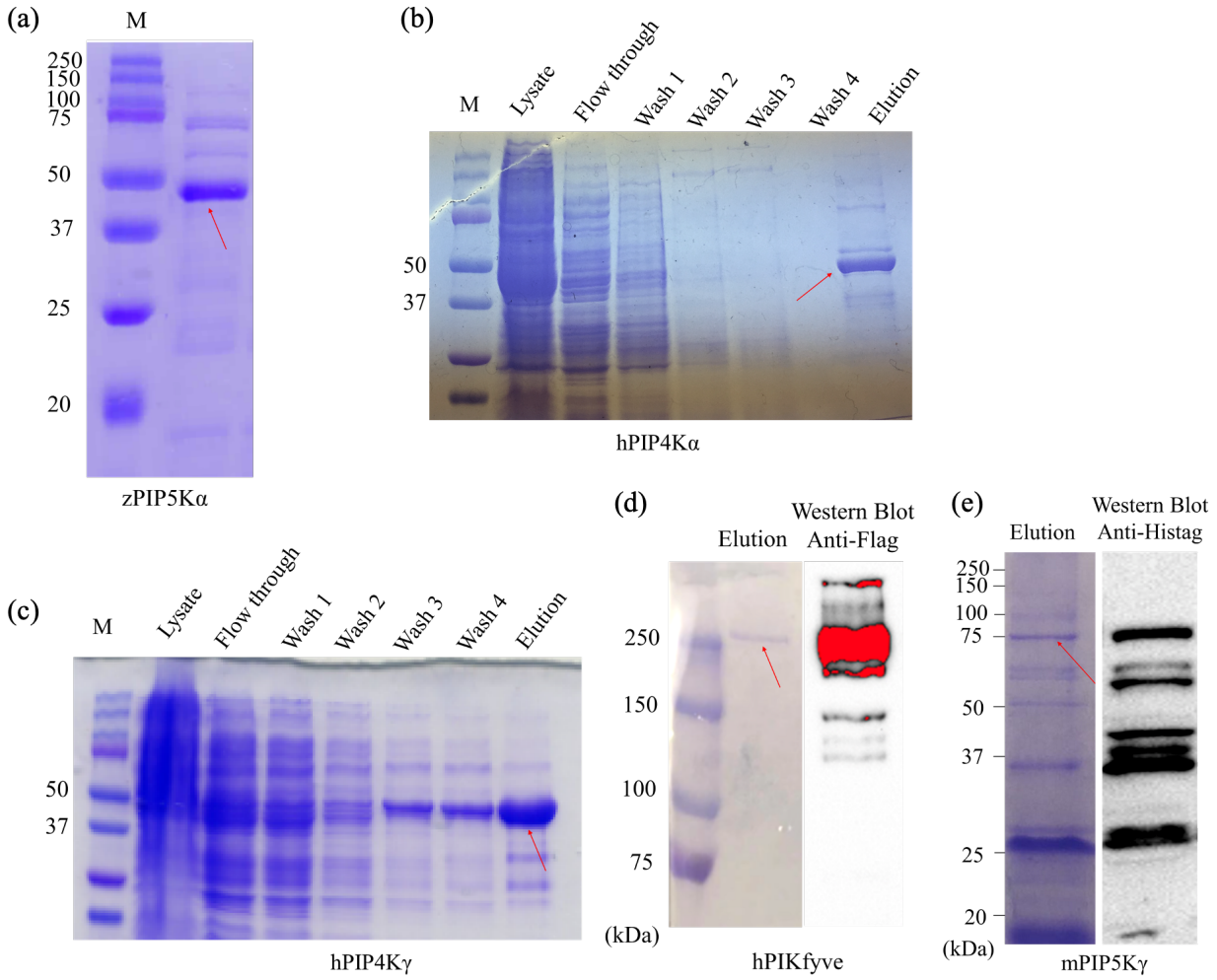

Figure S2. Purification of PIPKs. (a) zPIP5Kα. (b) hPIP4Kα. (c) hPIPK4Kγ. (d) hPIKfyve. (e) mPIP5Kγ. Except for N-flag-hPIKfyve expressed in HEK293F cells, the other histagged PIPKs were expressed in *E. coli*. hPIKfyve is confirmed by Western blot using an anti-Flag antibody. mPIP5Kγ is confirmed by Western blot using an anti-histag antibody with severe degradation due to instability of the purified protein.

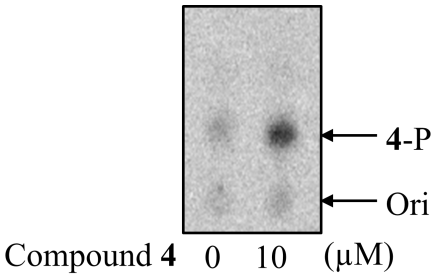

Figure S3. Phosphorylation of 4 by mPIP5Kγ. Purified mouse PIP5Kγ and compound 4 at the indicated concentration were mixed in the reaction buffer (100 mM Tris-HCl, pH 8.0, 5 mM EGTA, 10 mM $MgCl_2$, and 2 μM diC16-PI4P). The reaction was initiated by adding 50 μM ATP plus 1 μCi [γ-^{32}P] ATP (prepared in the reaction buffer). See more details in Experimental Section.

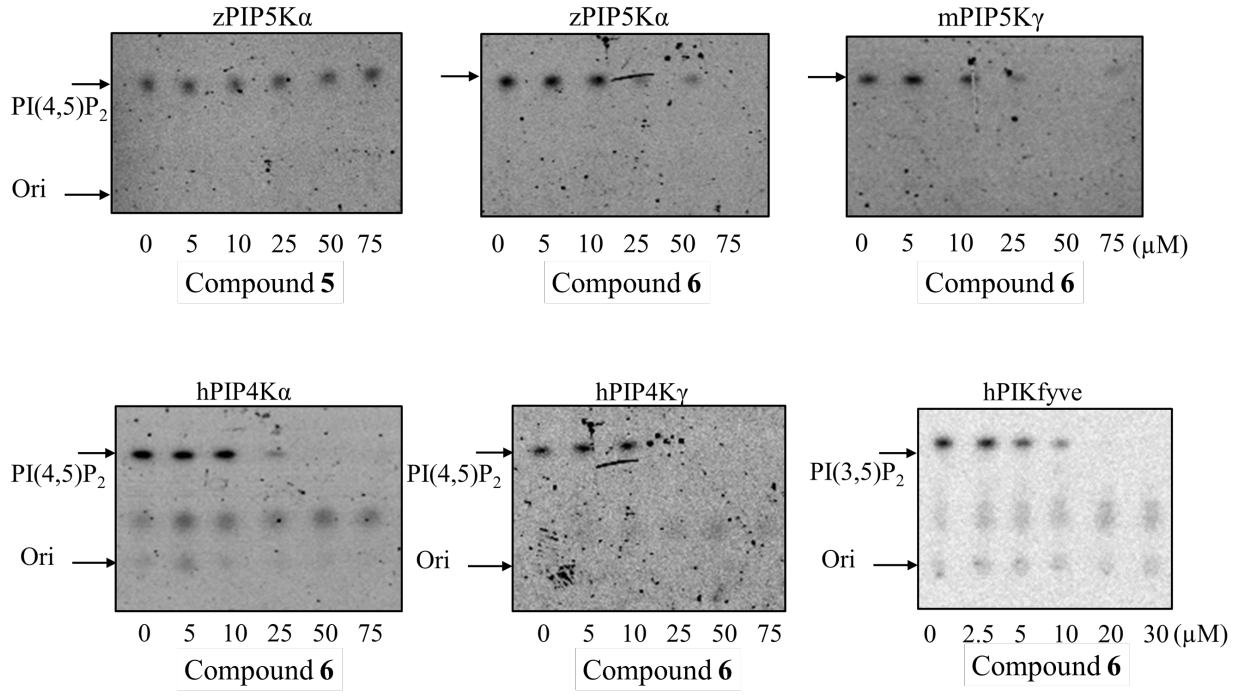

Figure S4. Representative TLC results of PIPK inhibition by compound 5 and compound 6.

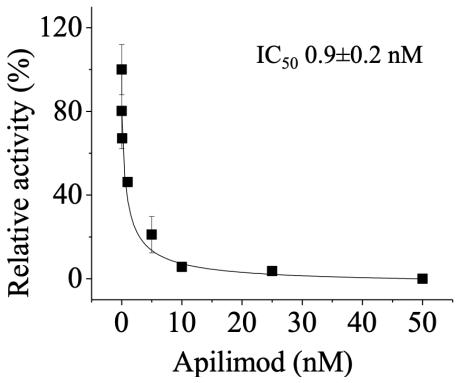

Figure S5. Inhibition of hPIKfyve by Apilimod. Purified hPIKfyve and Apilimod at the indicated concentrations were mixed in the reaction buffer (100 mM Tris-HCl, pH 8.0, 5 mM EGTA, 10 mM $MgCl_2$, and 2 μM diC16-PI4P). The reaction was initiated by adding 50 μM ATP plus 1 μCi [γ-^{32}P] ATP (prepared in the reaction buffer). See more details in Experimental Section.

APPENDIX B: NMR Spectra

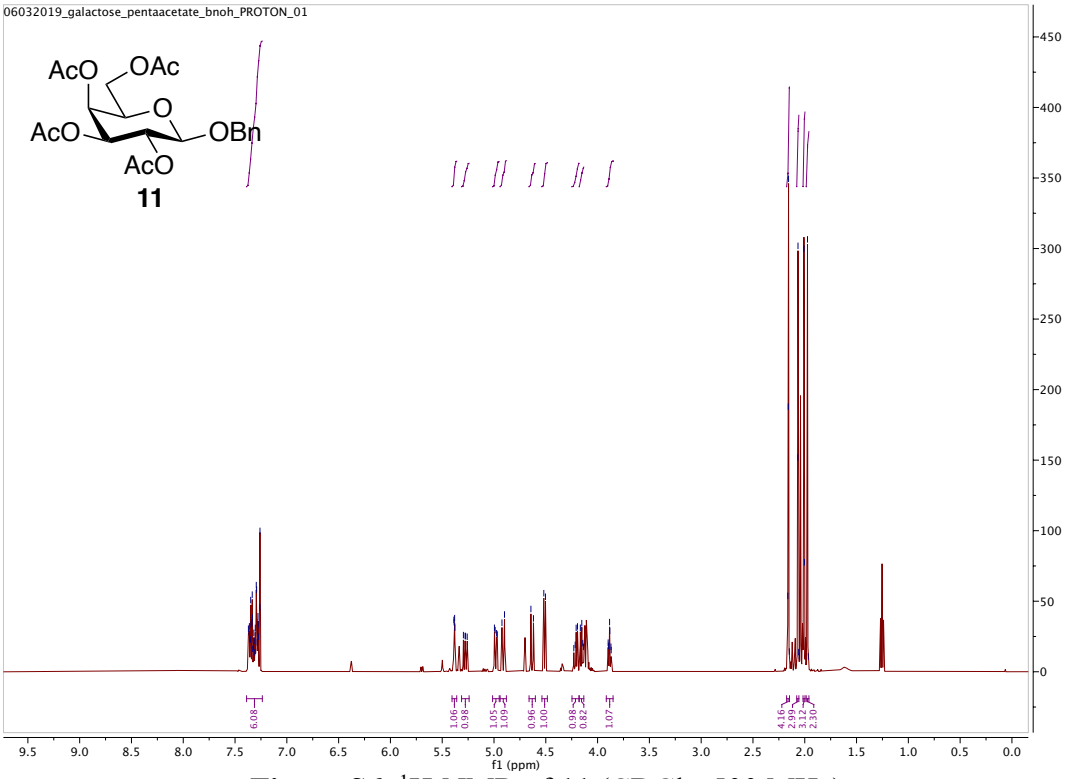

Figure S6. ^{1}H-NMR of **11** ($CDCl_3$, 500 MHz).

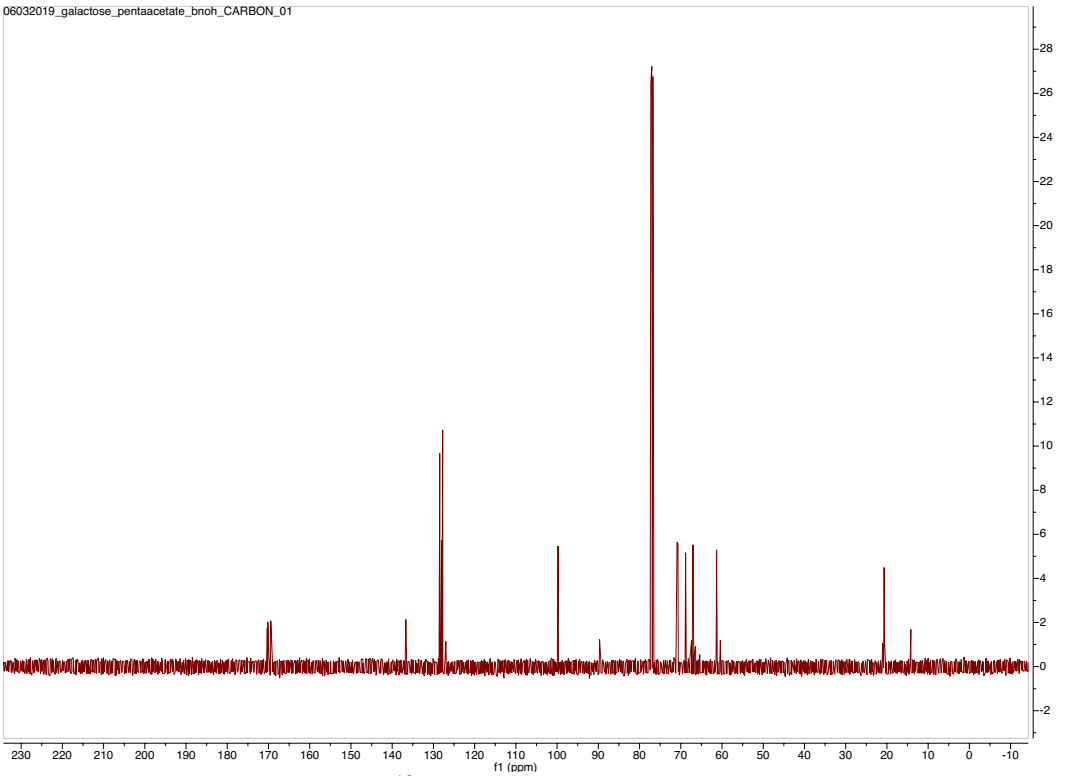

Figure S7. ^{13}C-NMR of **11** ($CDCl_3$, 125 MHz).

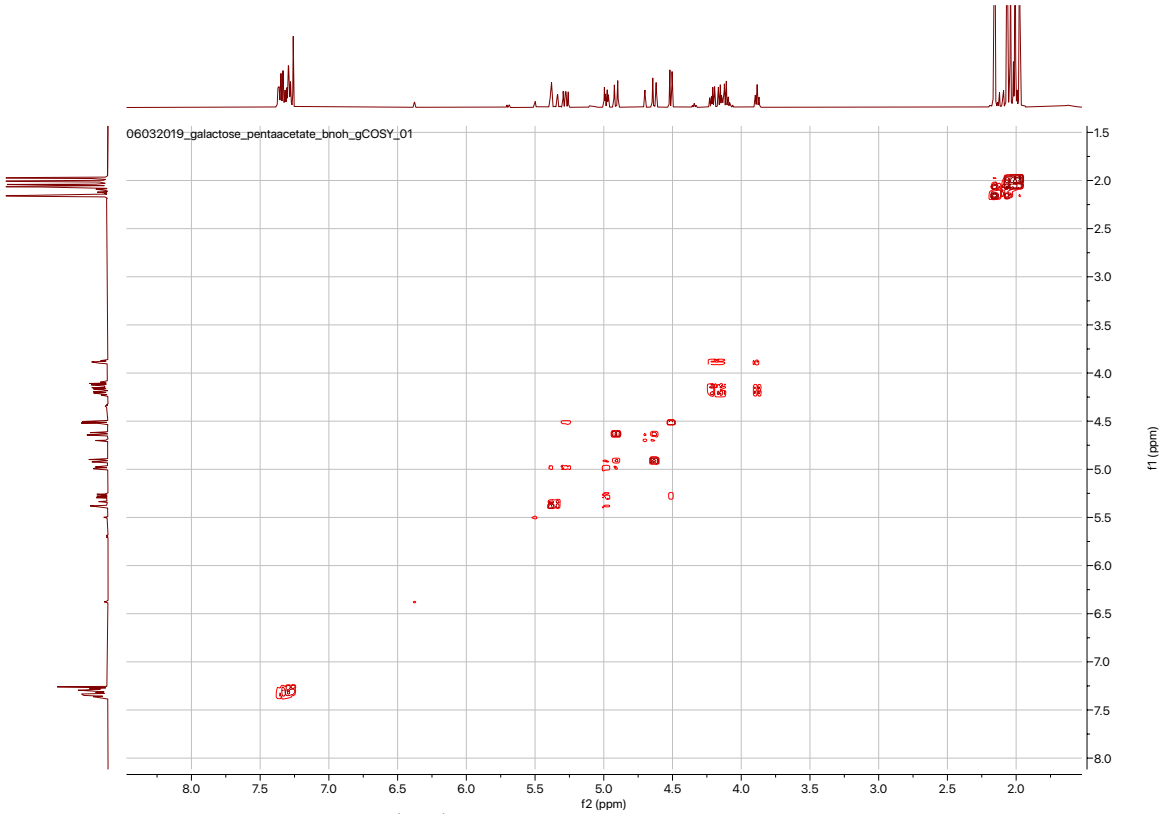

Figure S8. ^{1}H-^{1}H gCOSY of **11** ($CDCl_3$, 500 MHz).

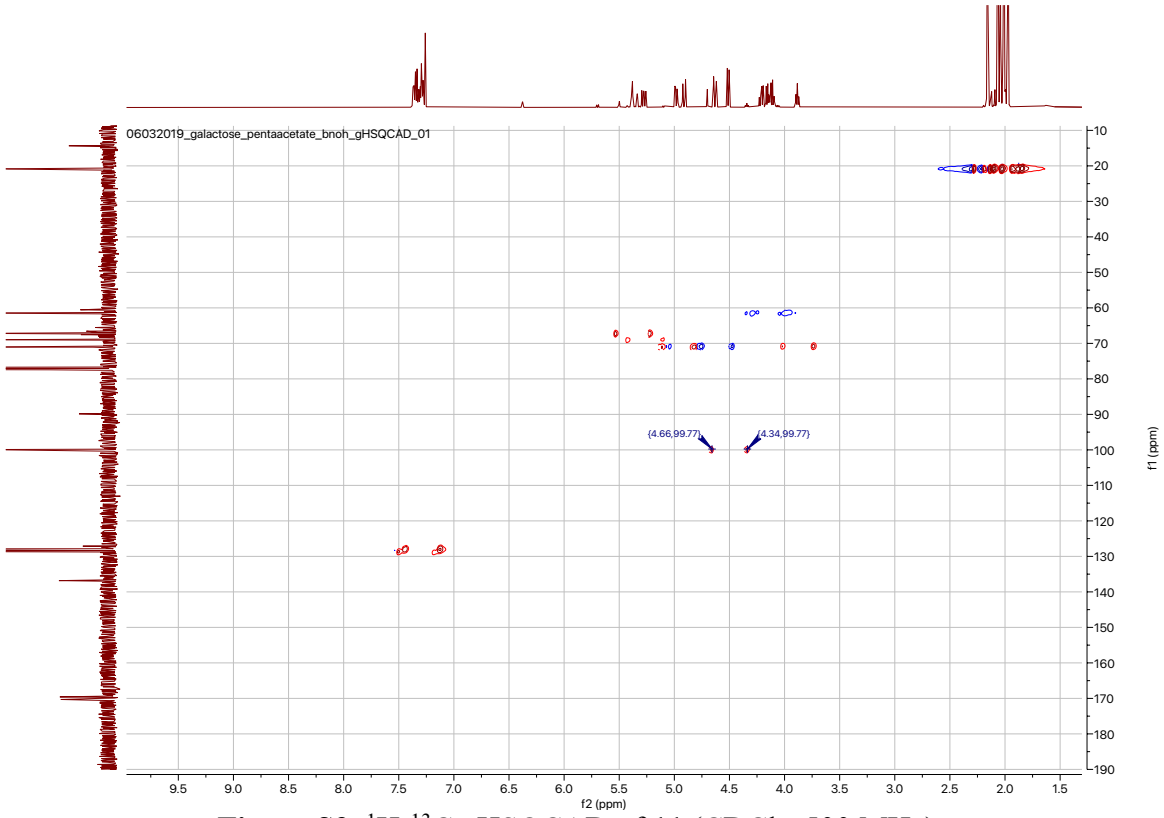

Figure S9. ^{1}H-^{13}C gHSQCAD of **11** ($CDCl_3$, 500 MHz).

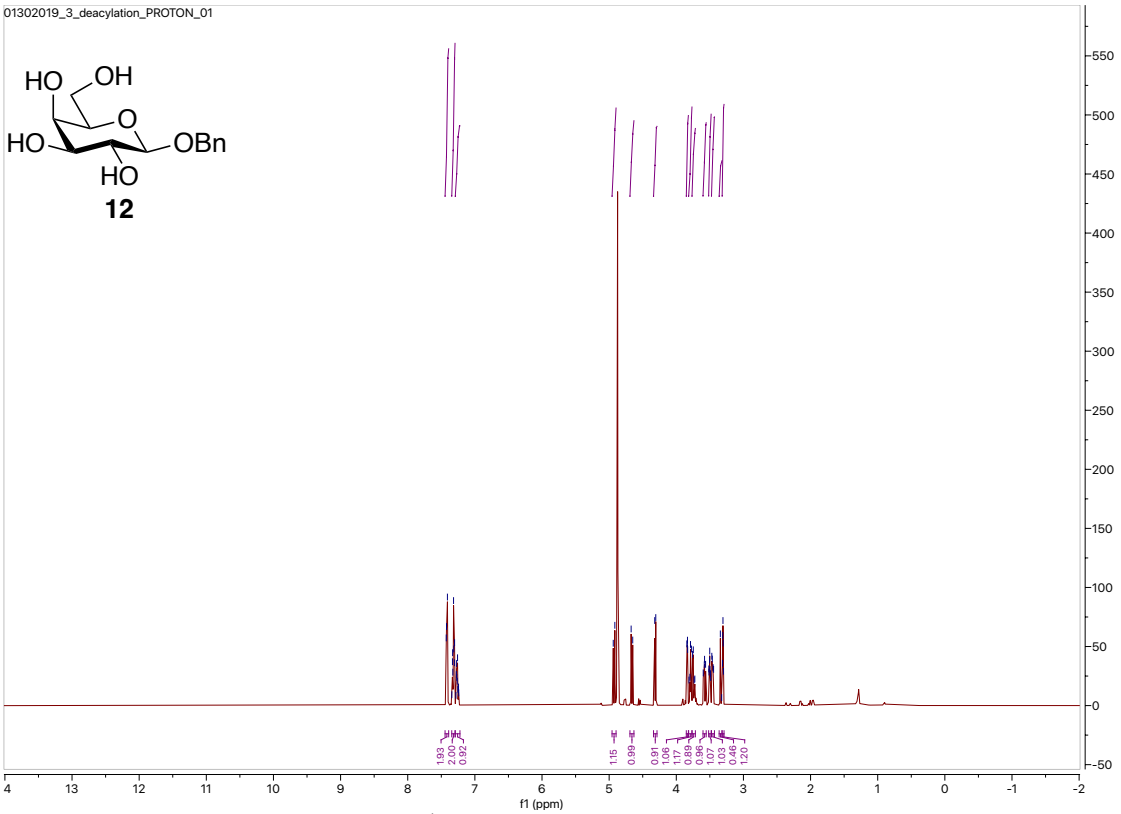

Figure S10. ^{1}H-NMR of **12** (CD_3OD, 500 MHz).

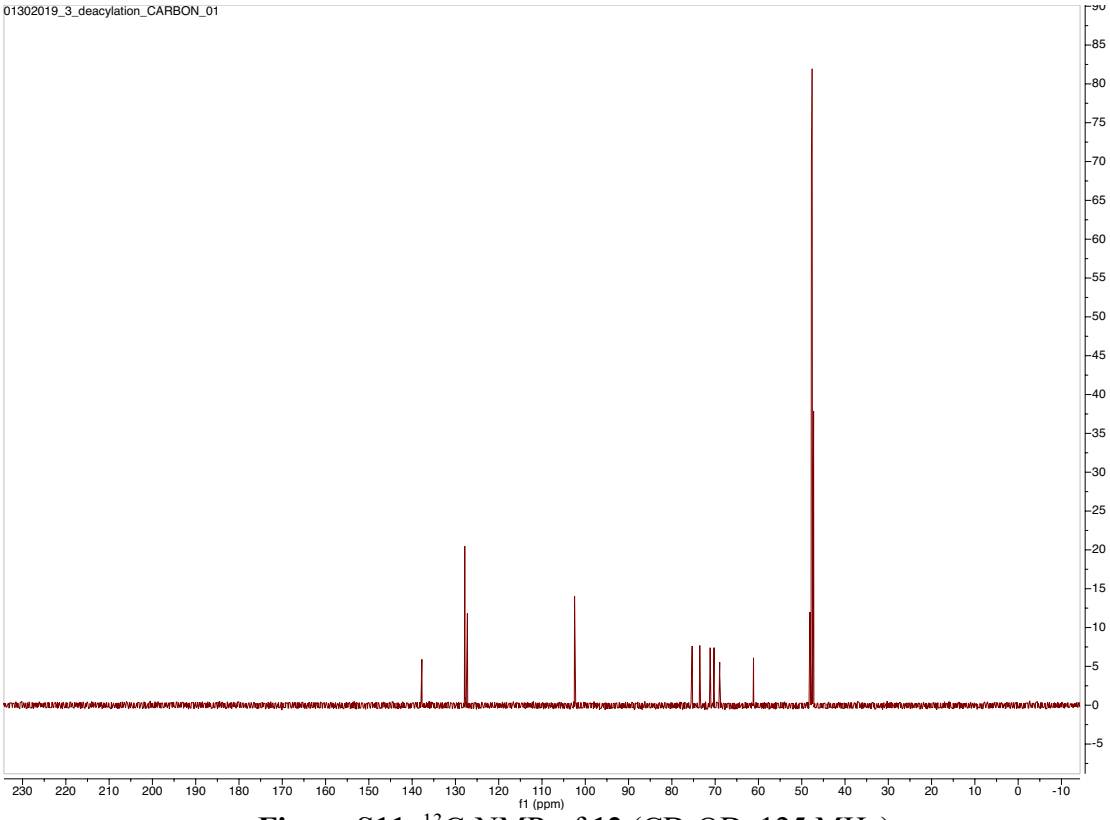

Figure S11. ^{13}C-NMR of **12** (CD_3OD, 125 MHz).

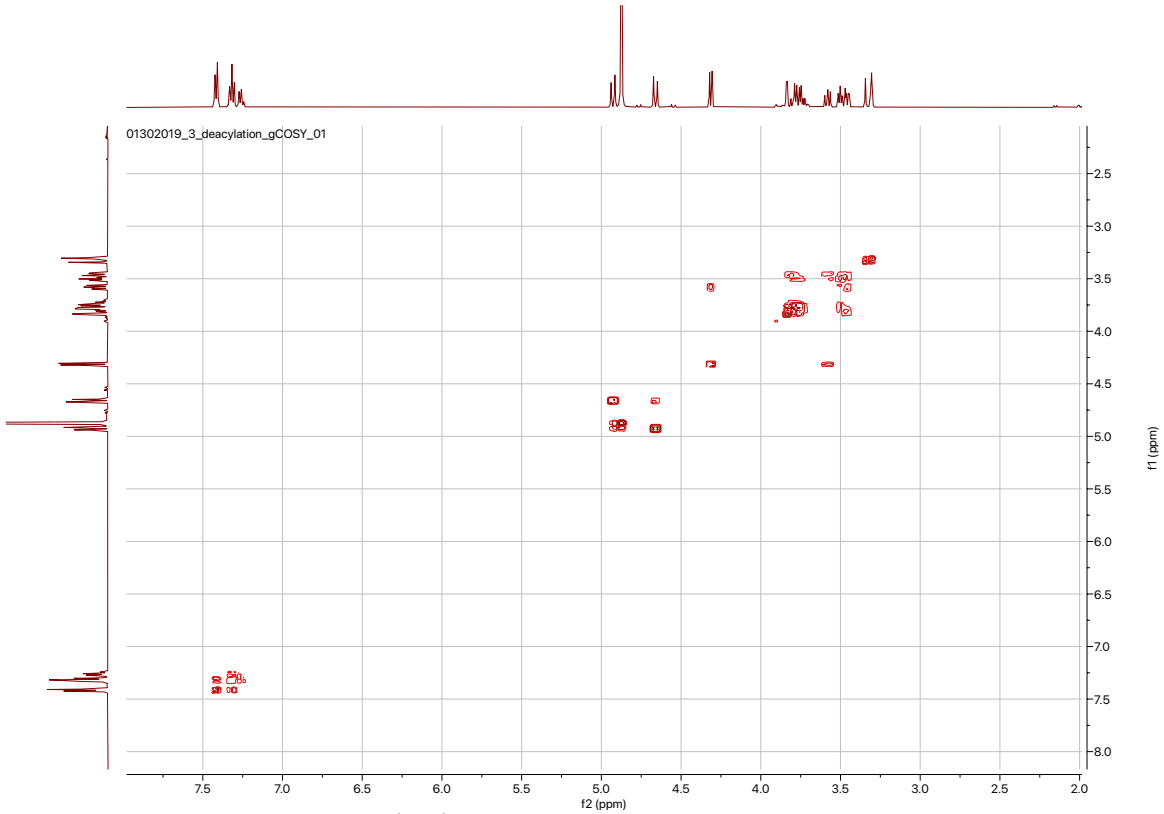

Figure S12. ^{1}H-^{1}H gCOSY of **12** (CD_3OD, 500 MHz).

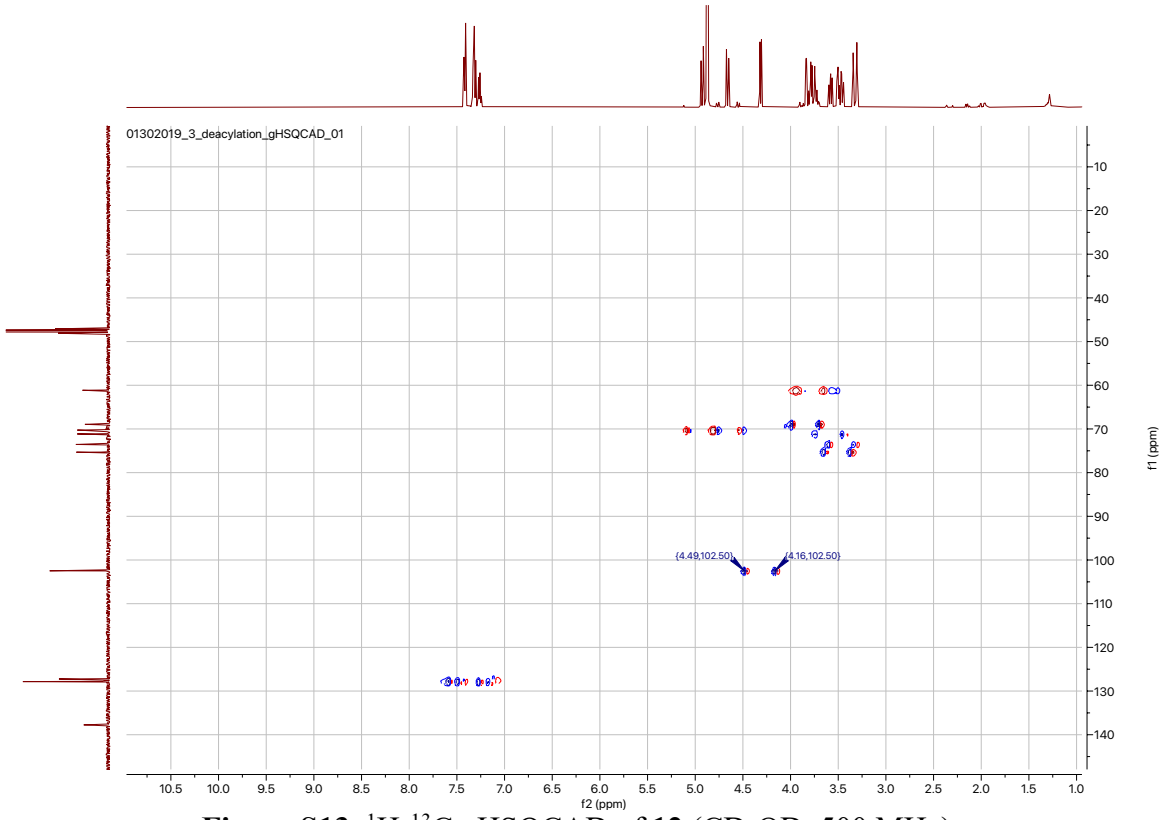

Figure S13. ^{1}H-^{13}C gHSQCAD of **12** (CD_3OD, 500 MHz).

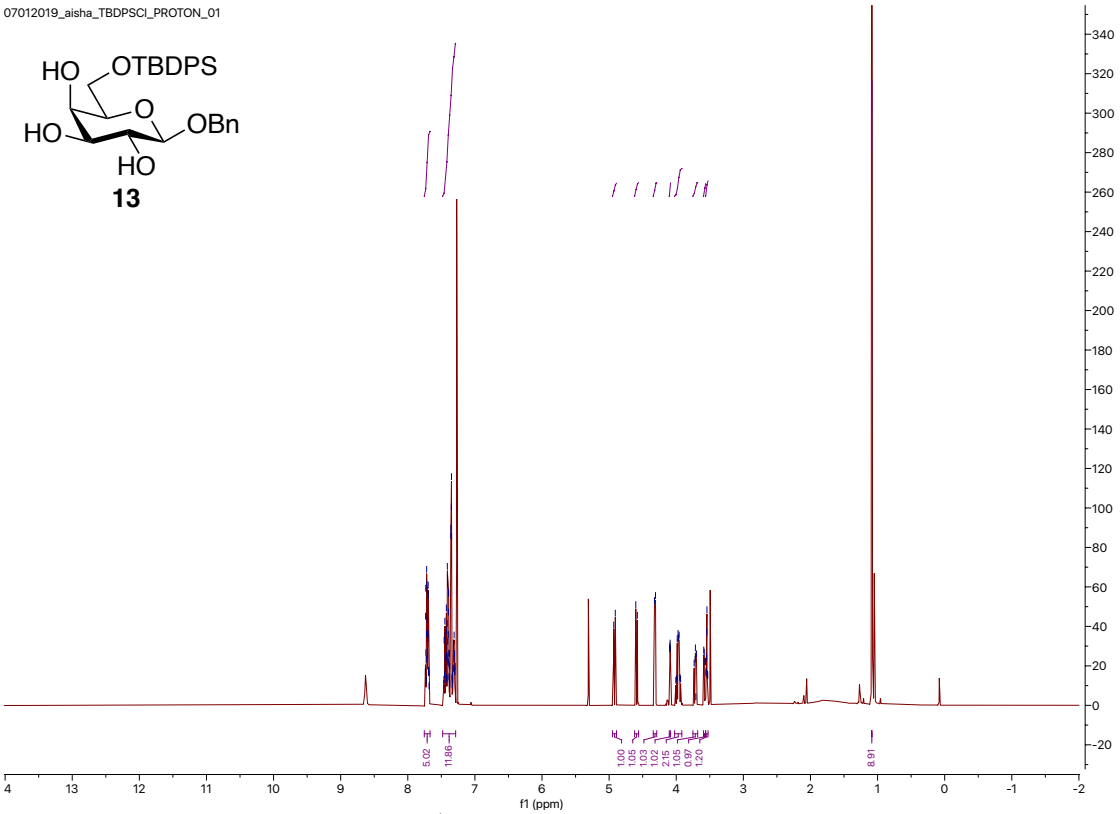

Figure S14. ^{1}H-NMR of **13** ($CDCl_3$, 500 MHz).

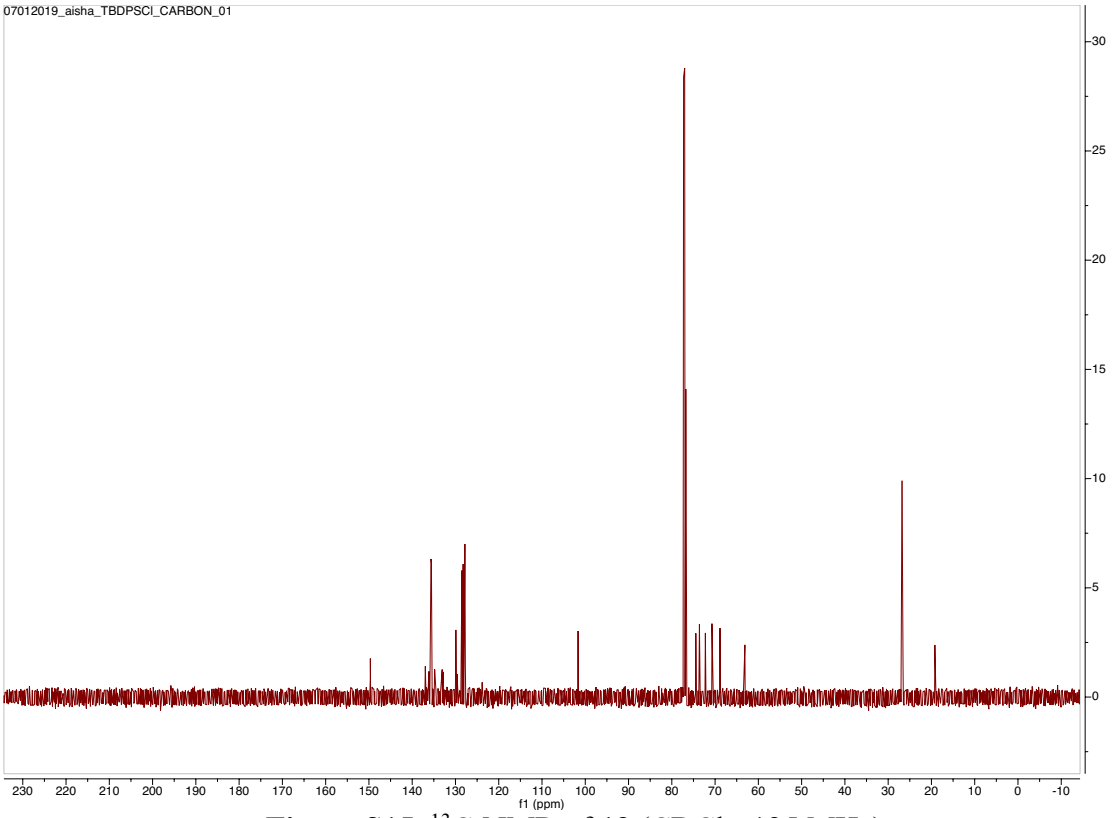

Figure S15. ^{13}C-NMR of **13** ($CDCl_3$, 125 MHz).

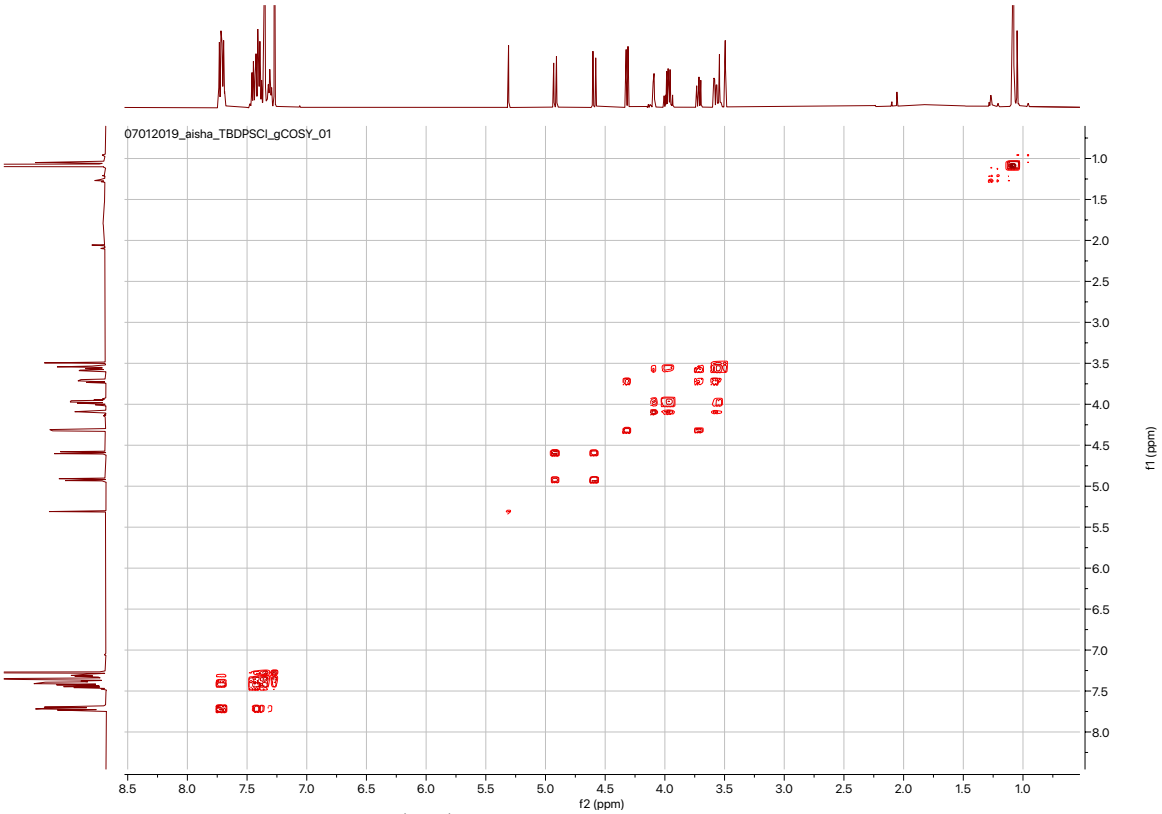

Figure S16. ^{1}H-^{1}H gCOSY of **13** ($CDCl_3$, 500 MHz).

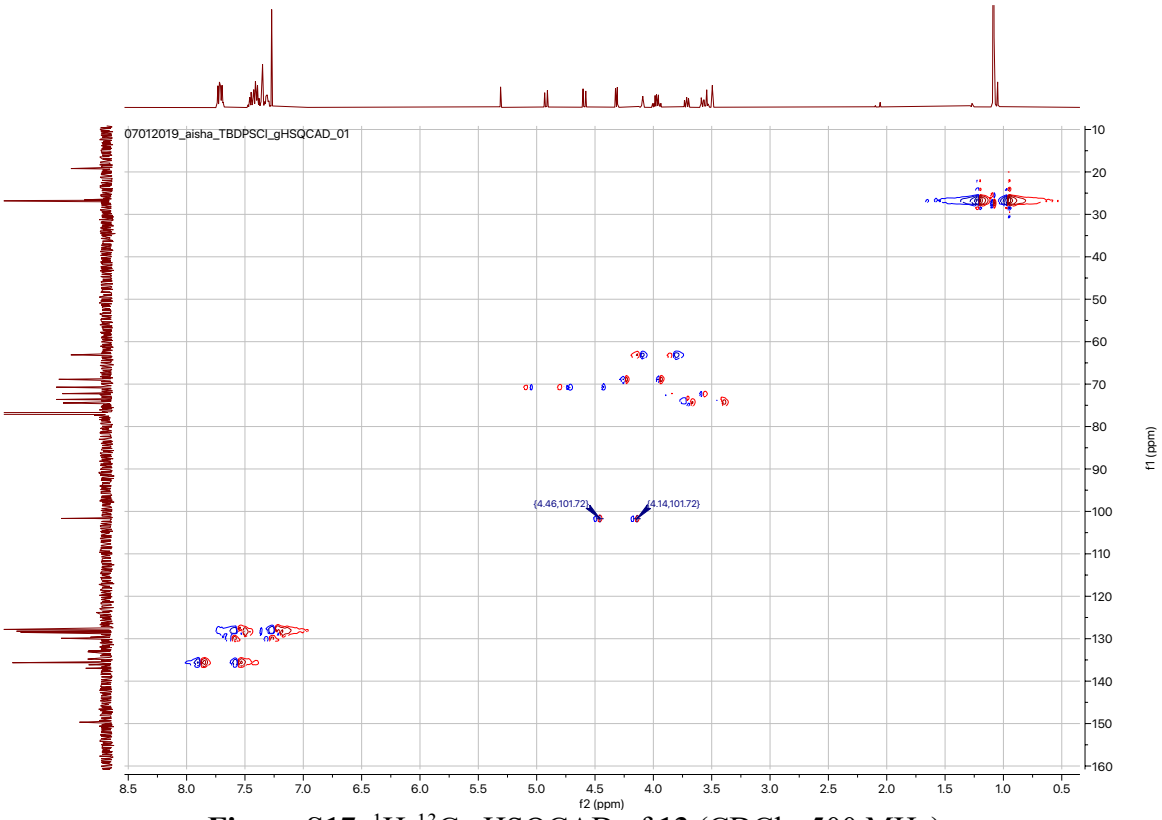

Figure S17. ^{1}H-^{13}C gHSQCAD of **13** ($CDCl_3$, 500 MHz).

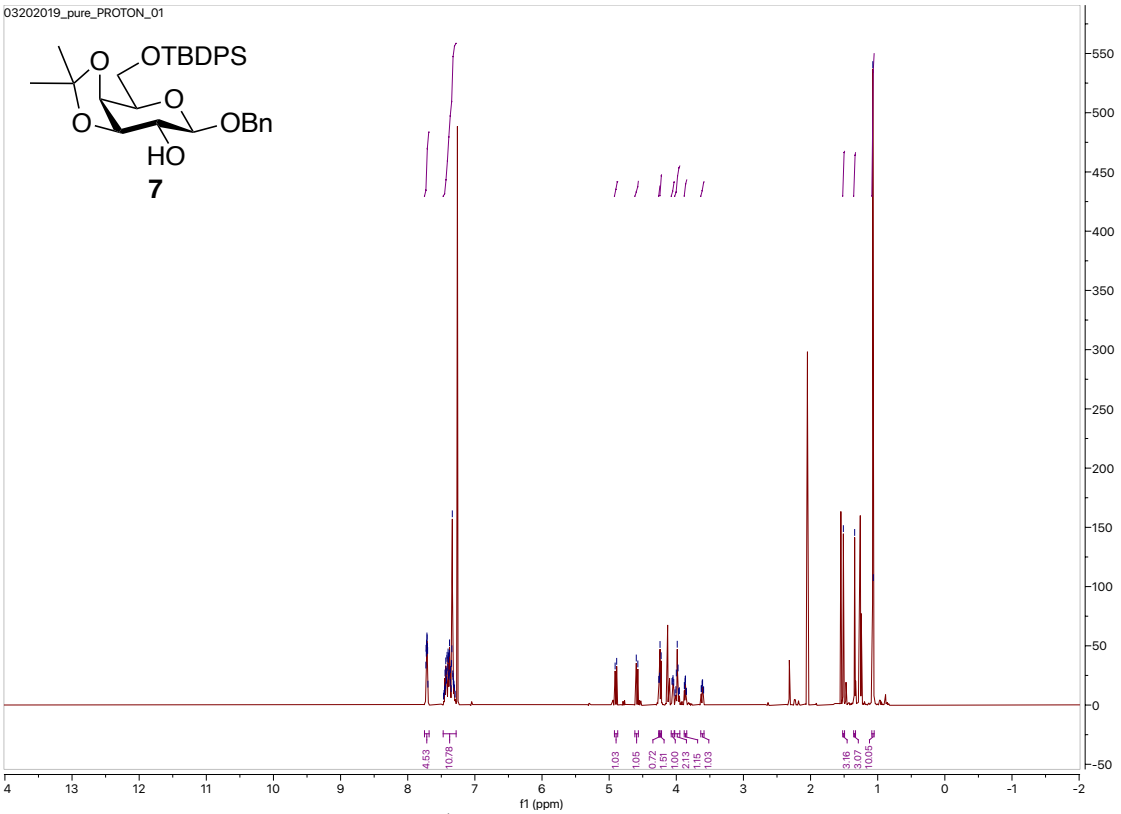

Figure S18. ^{1}H-NMR of **7** ($CDCl_3$, 500 MHz).

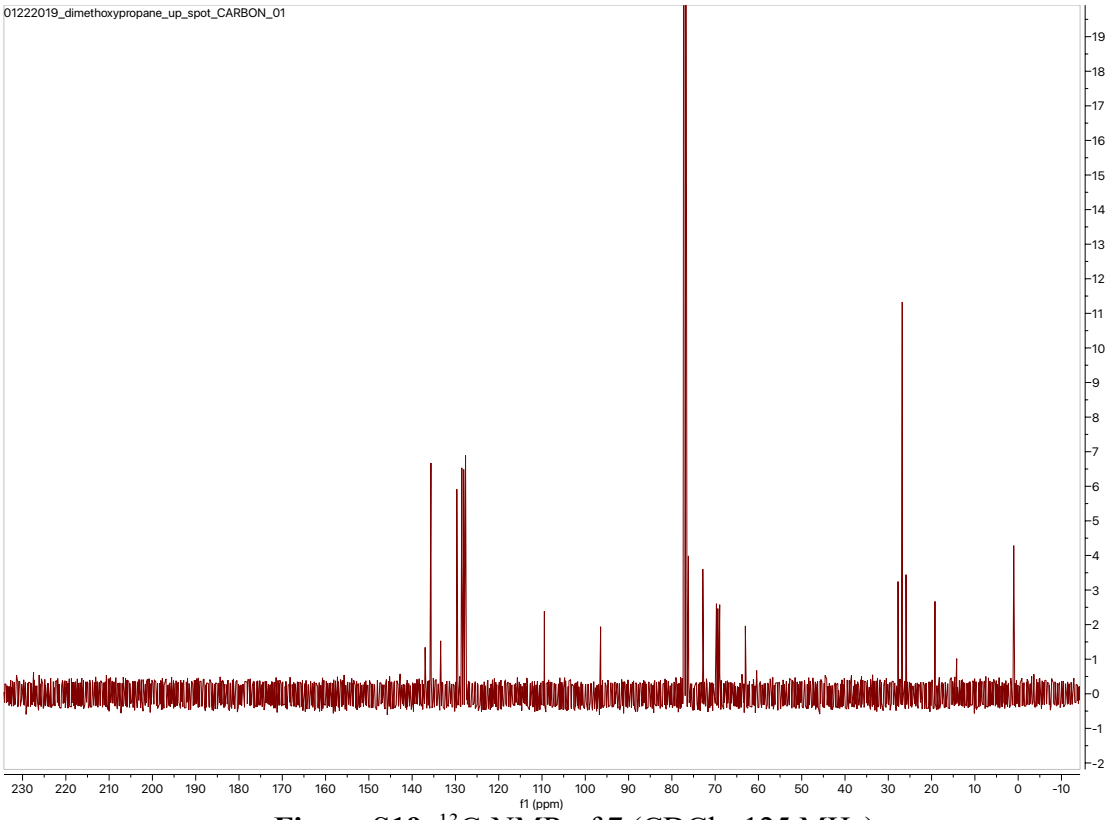

Figure S19. ^{13}C-NMR of **7** ($CDCl_3$, 125 MHz).

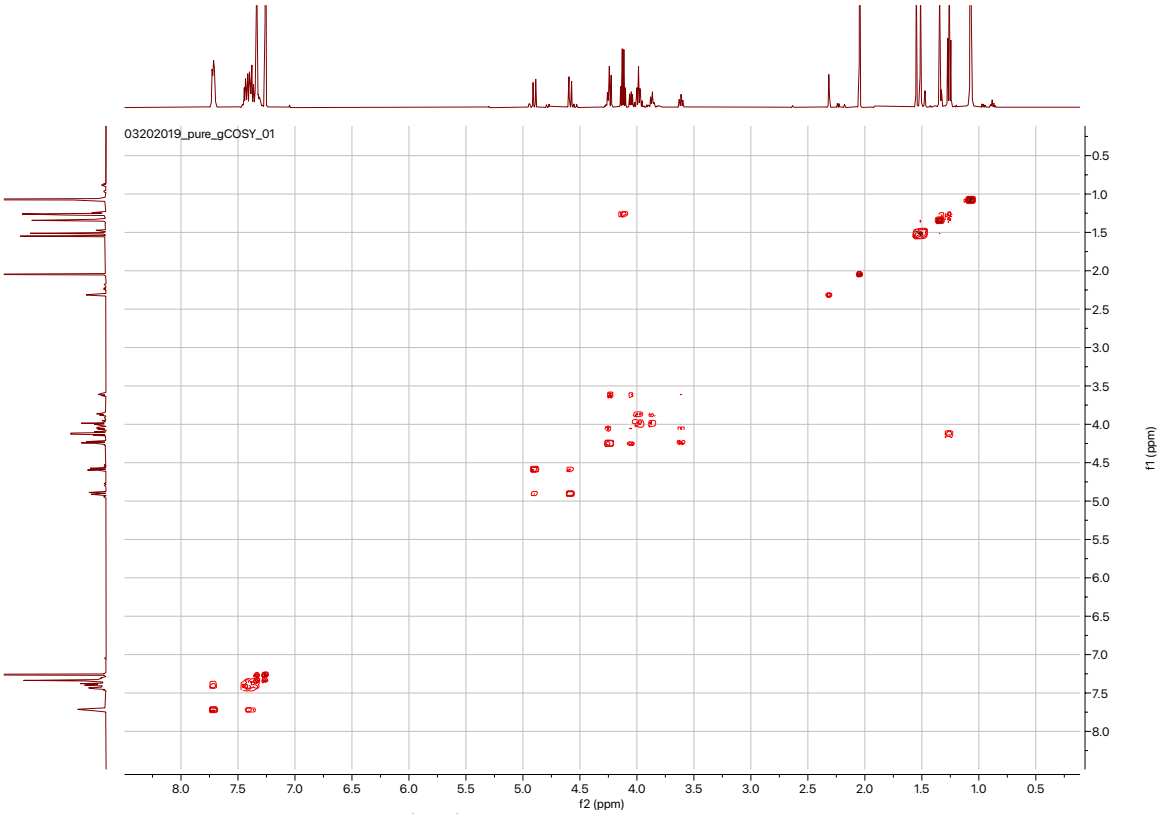

Figure S20. ^{1}H-^{1}H gCOSY of **7** ($CDCl_3$, 500 MHz).

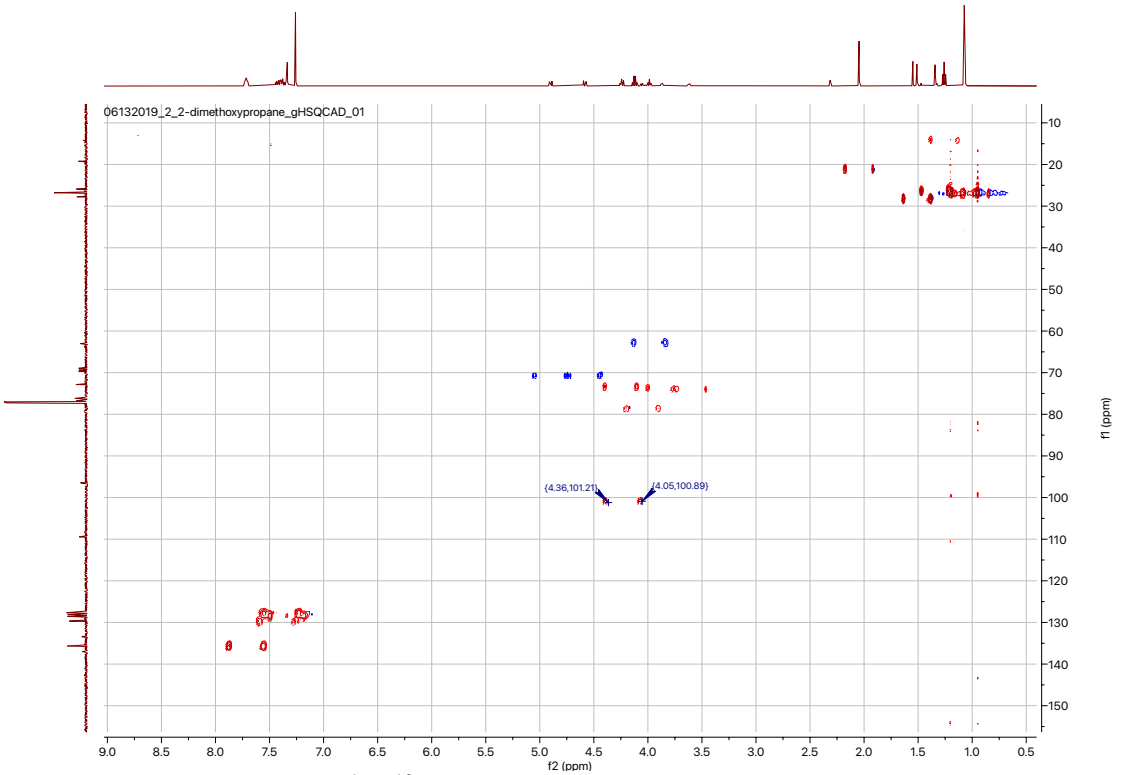

Figure S21. ^{1}H-^{13}C gHSQCAD of **7** ($CDCl_3$, 500 MHz).

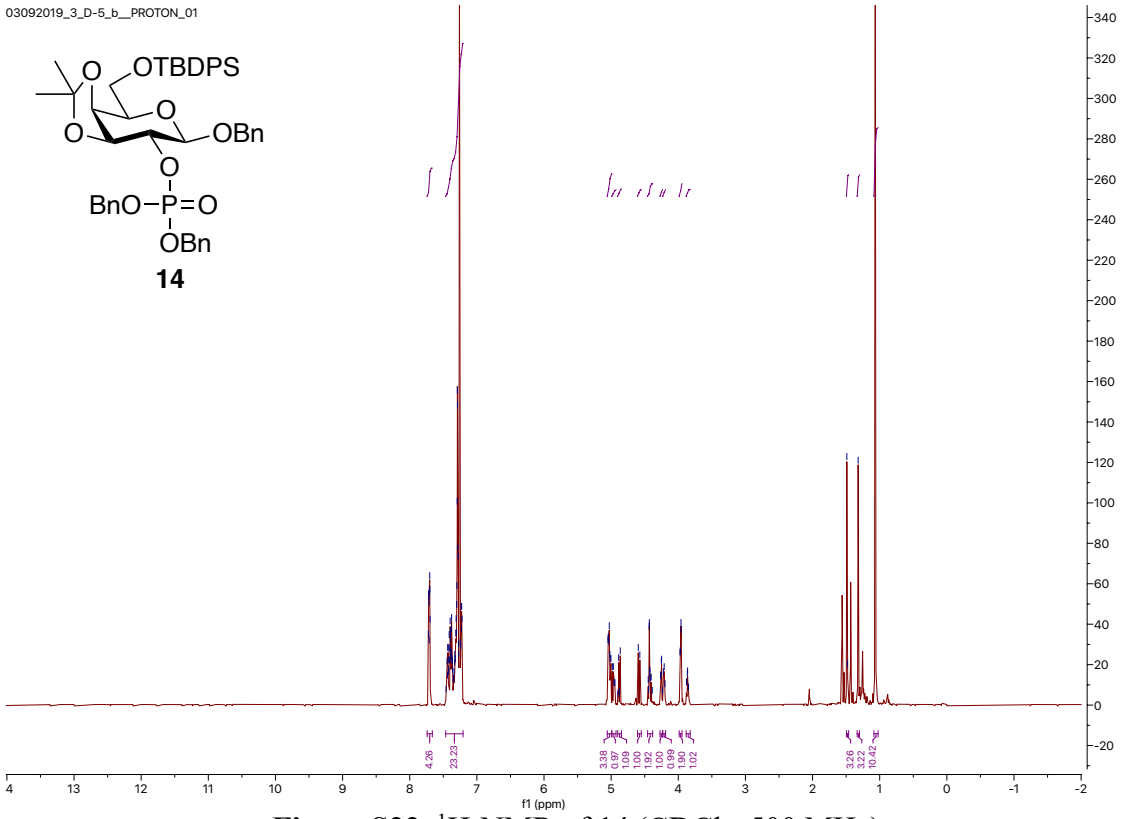

Figure S22. ^{1}H-NMR of **14** ($CDCl_3$, 500 MHz).

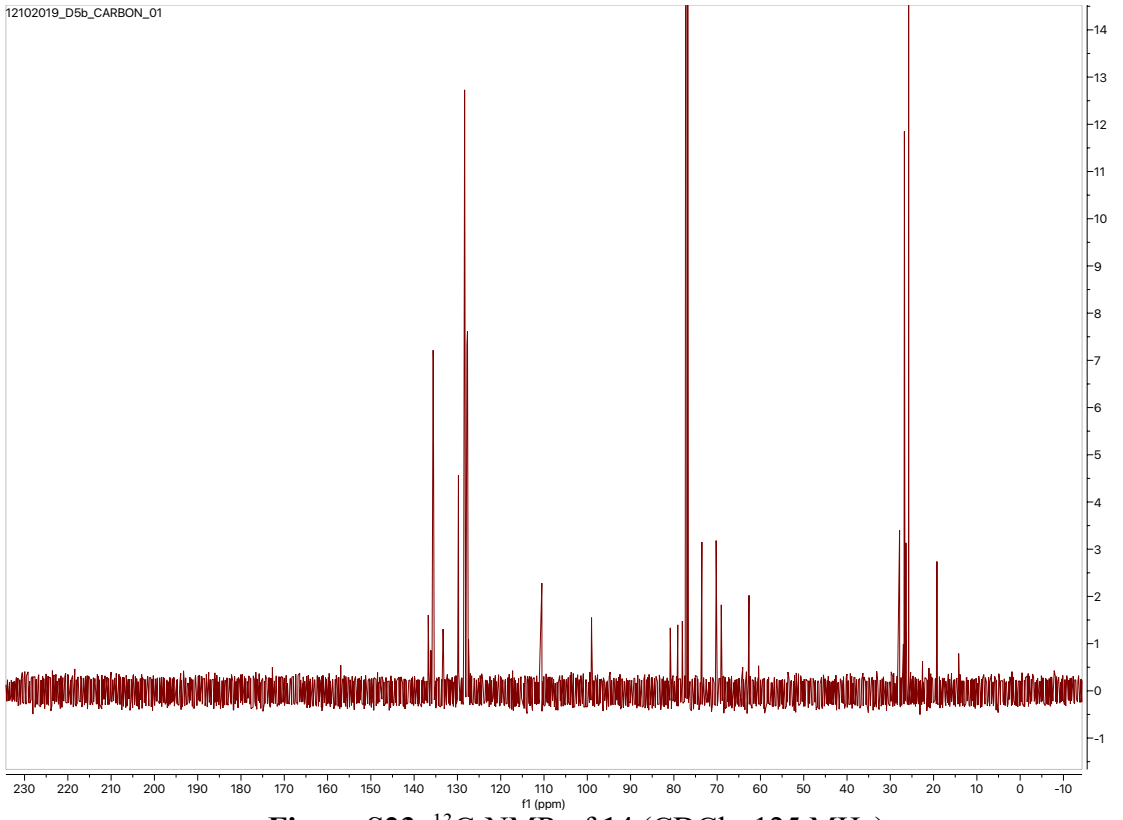

Figure S23. ^{13}C-NMR of **14** ($CDCl_3$, 125 MHz).

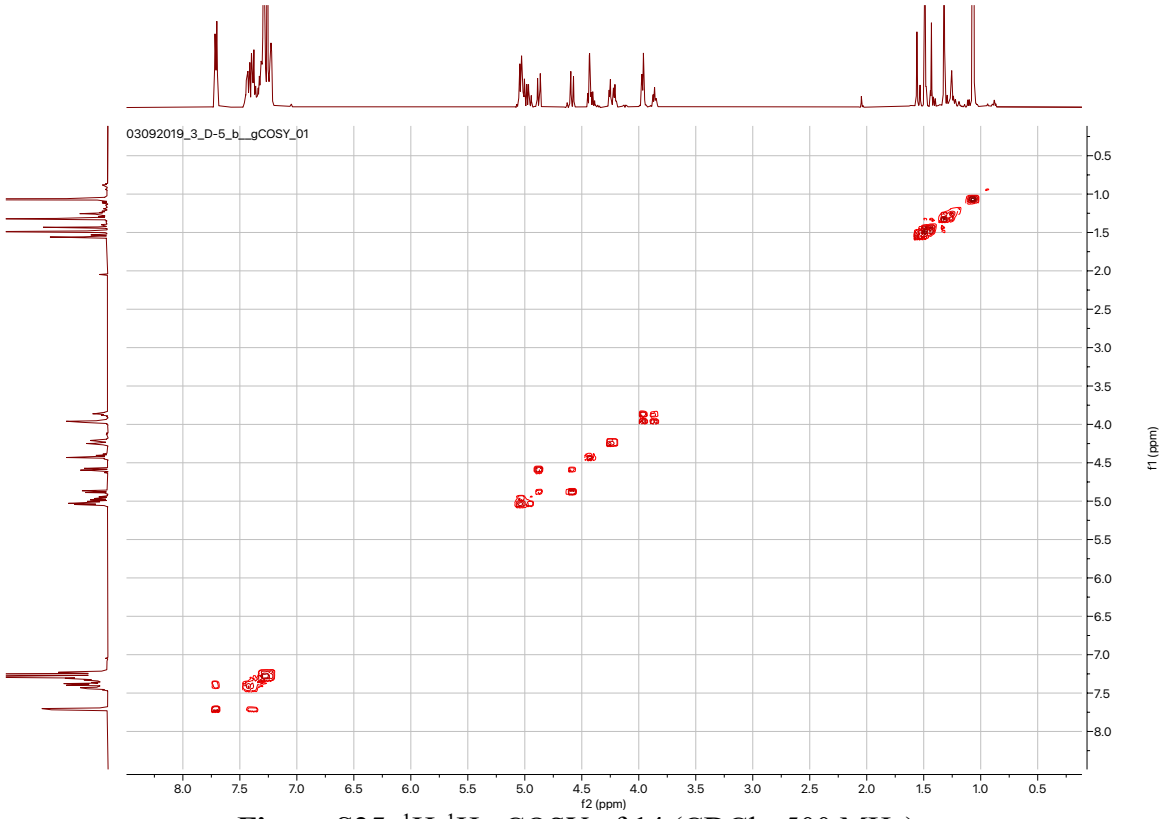

Figure S25. ^{1}H-^{1}H gCOSY of **14** ($CDCl_3$, 500 MHz).

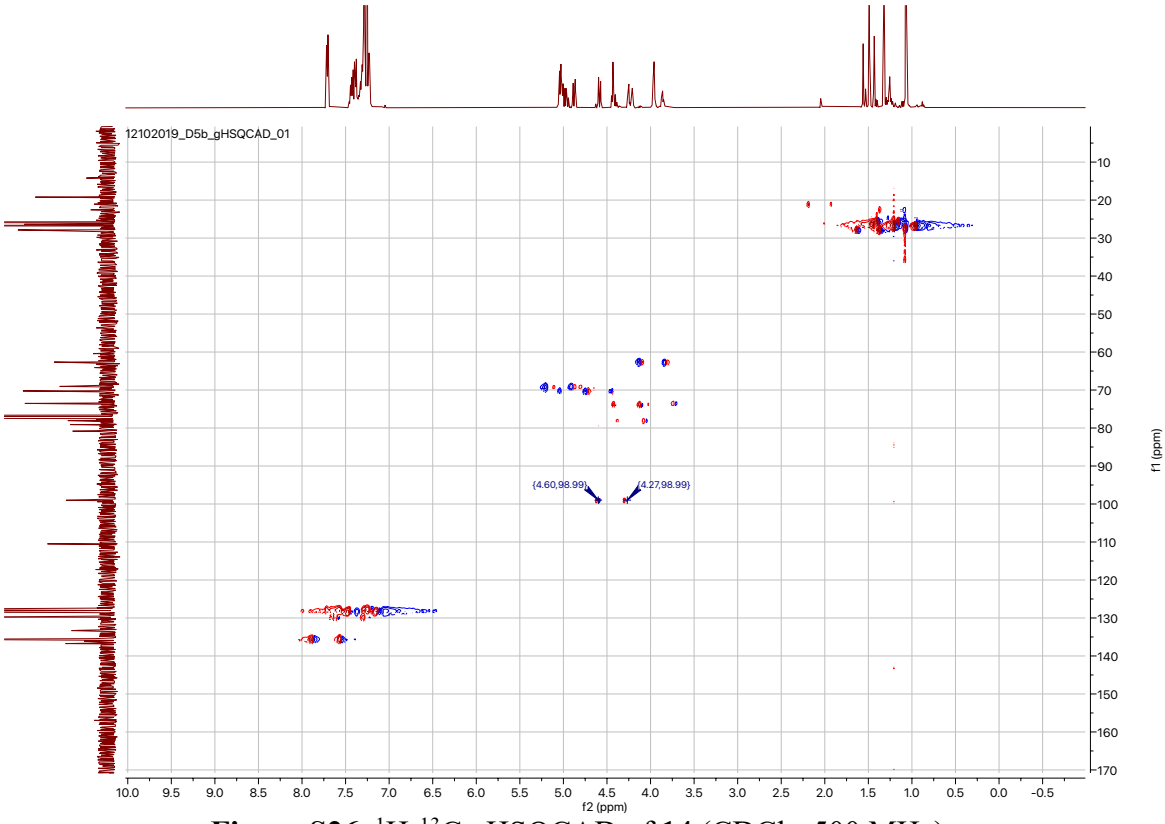

Figure S26. ^{1}H-^{13}C gHSQCAD of **14** ($CDCl_3$, 500 MHz).

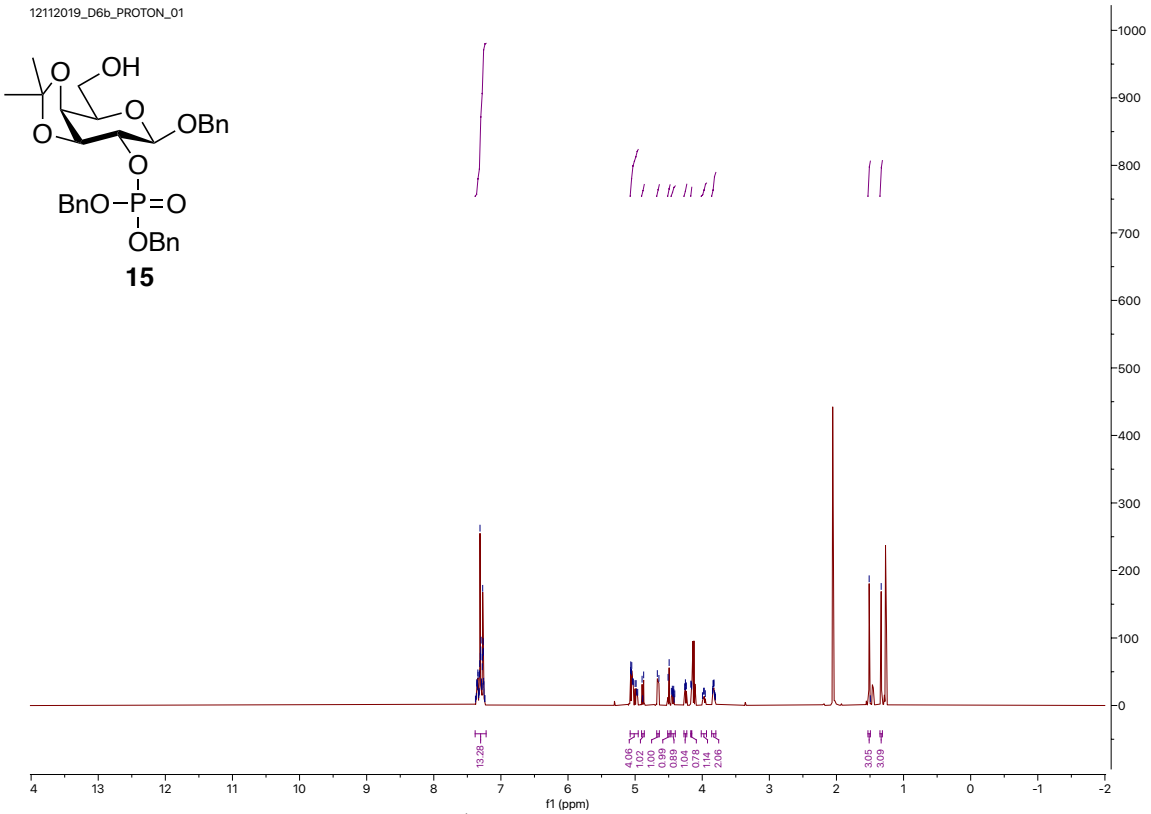

Figure S27. ^{1}H-NMR of **15** ($CDCl_3$, 500 MHz).

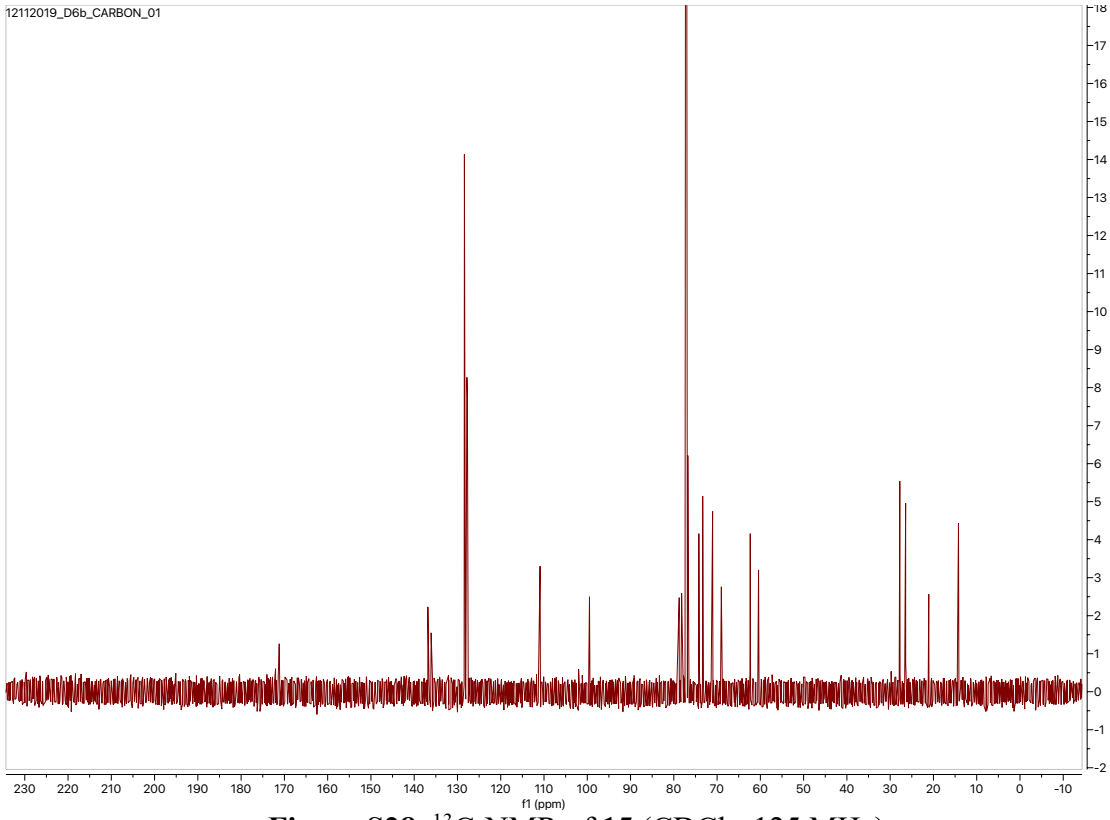

Figure S28. ^{13}C-NMR of **15** ($CDCl_3$, 125 MHz).

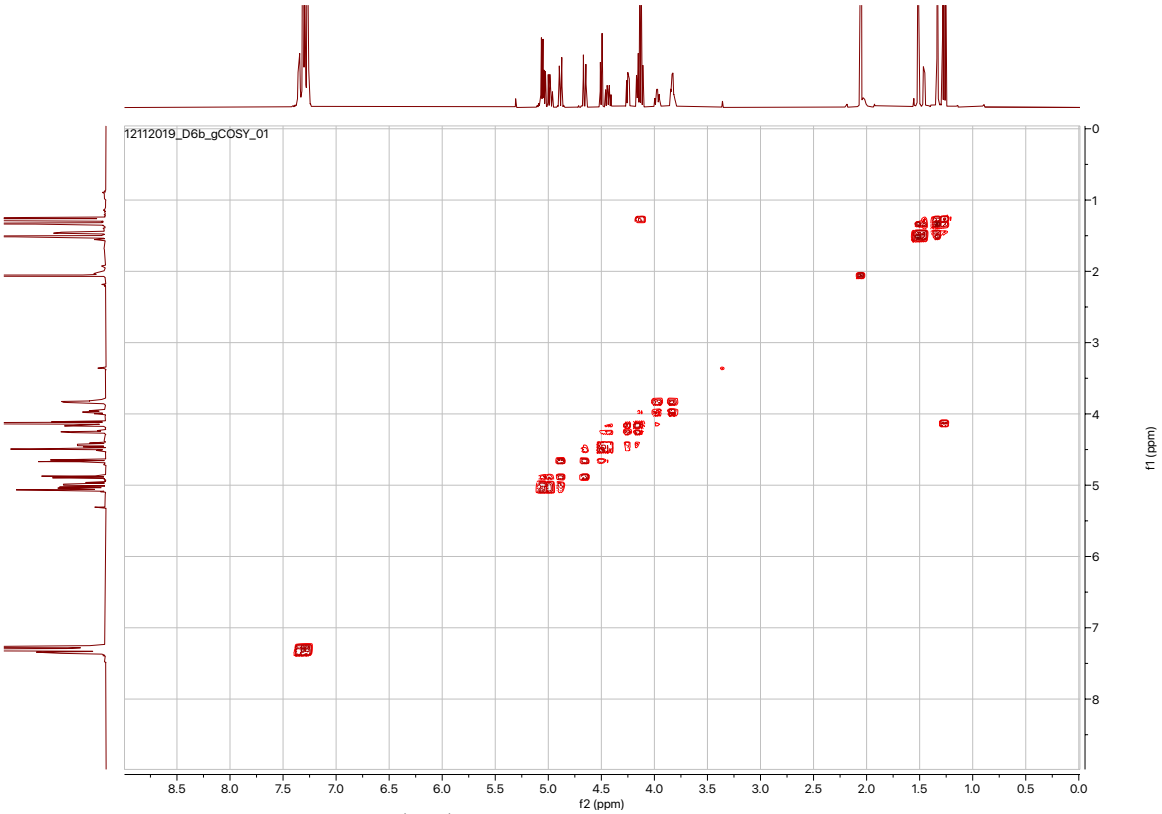

Figure S29. ^{1}H-^{1}H gCOSY of **15** ($CDCl_3$, 500 MHz).

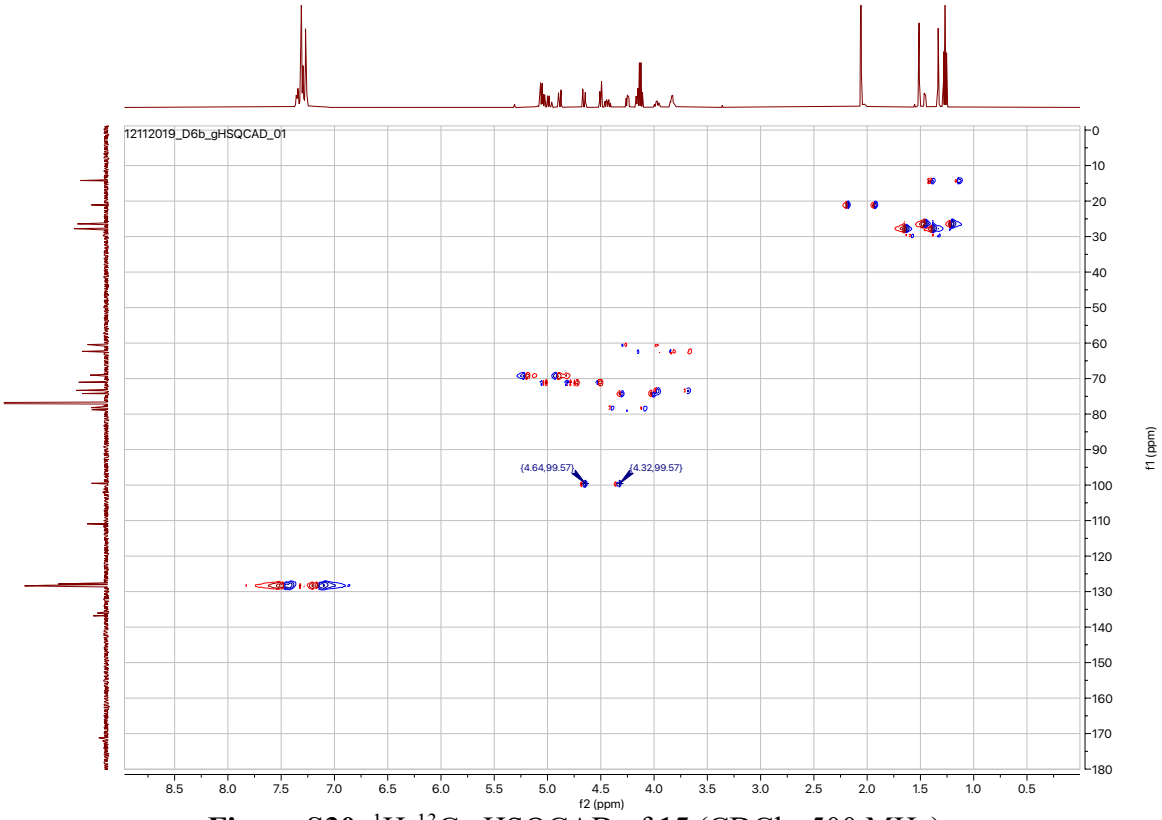

Figure S30. ^{1}H-^{13}C gHSQCAD of **15** ($CDCl_3$, 500 MHz).

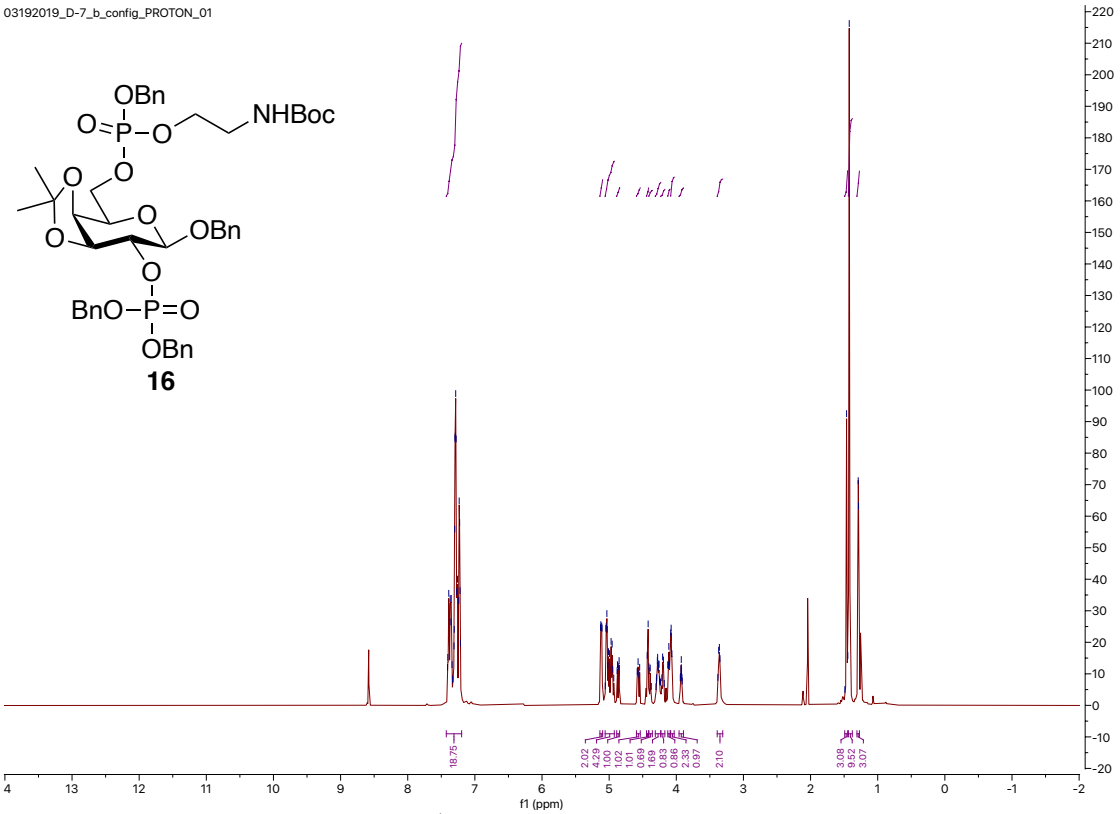

Figure S31. ^{1}H-NMR of **16** ($CDCl_3$, 500 MHz).

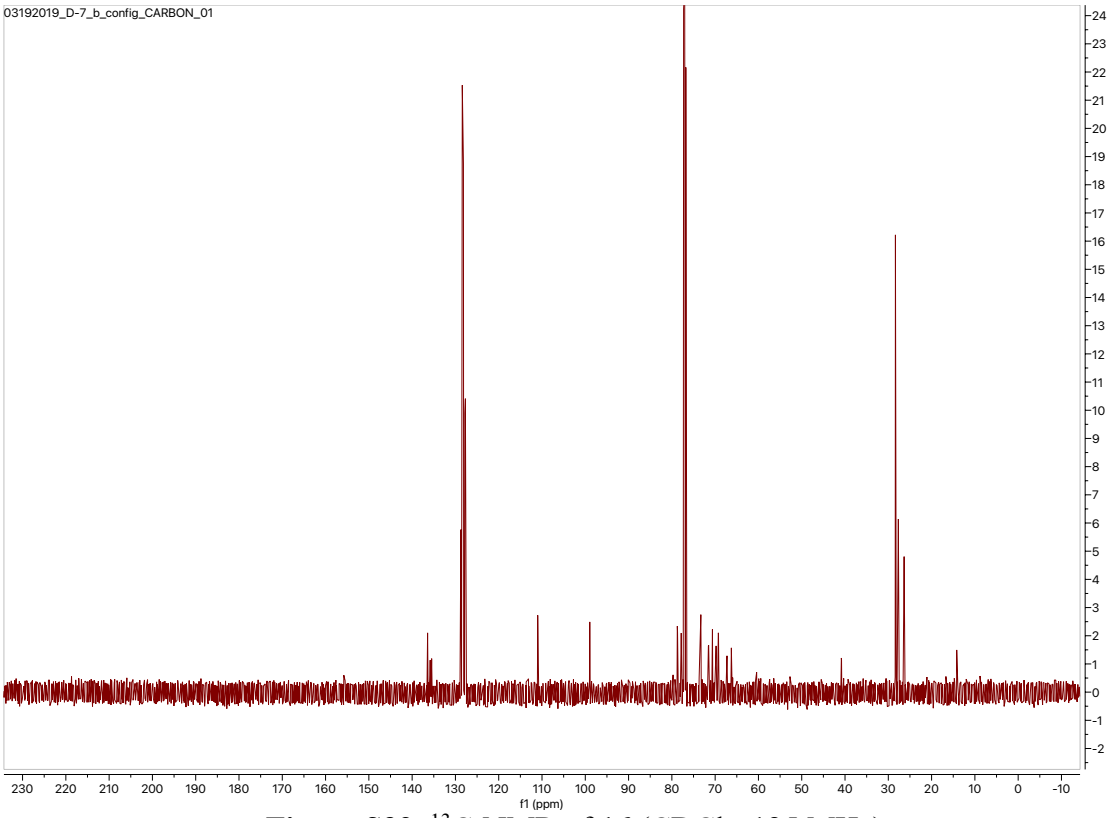

Figure S32. ^{13}C-NMR of **16** ($CDCl_3$, 125 MHz).

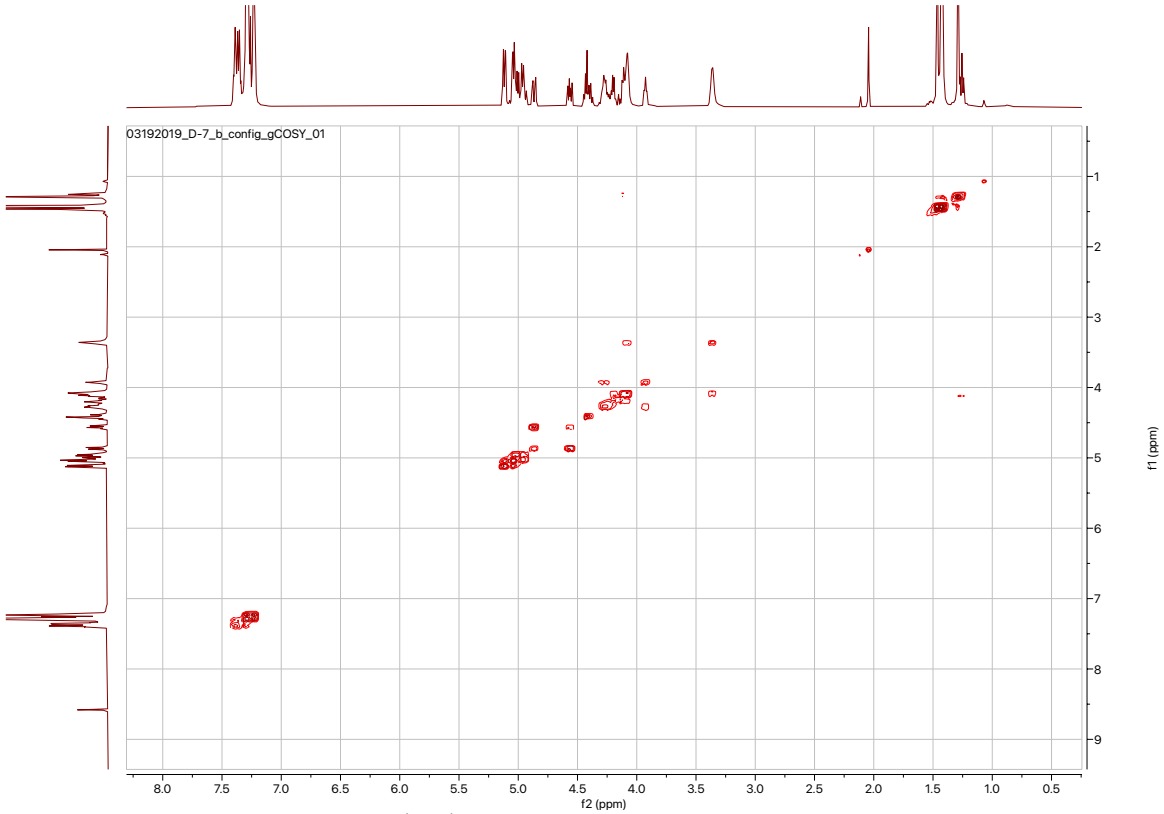

Figure S33. ^{1}H-^{1}H gCOSY of **16** ($CDCl_3$, 500 MHz).

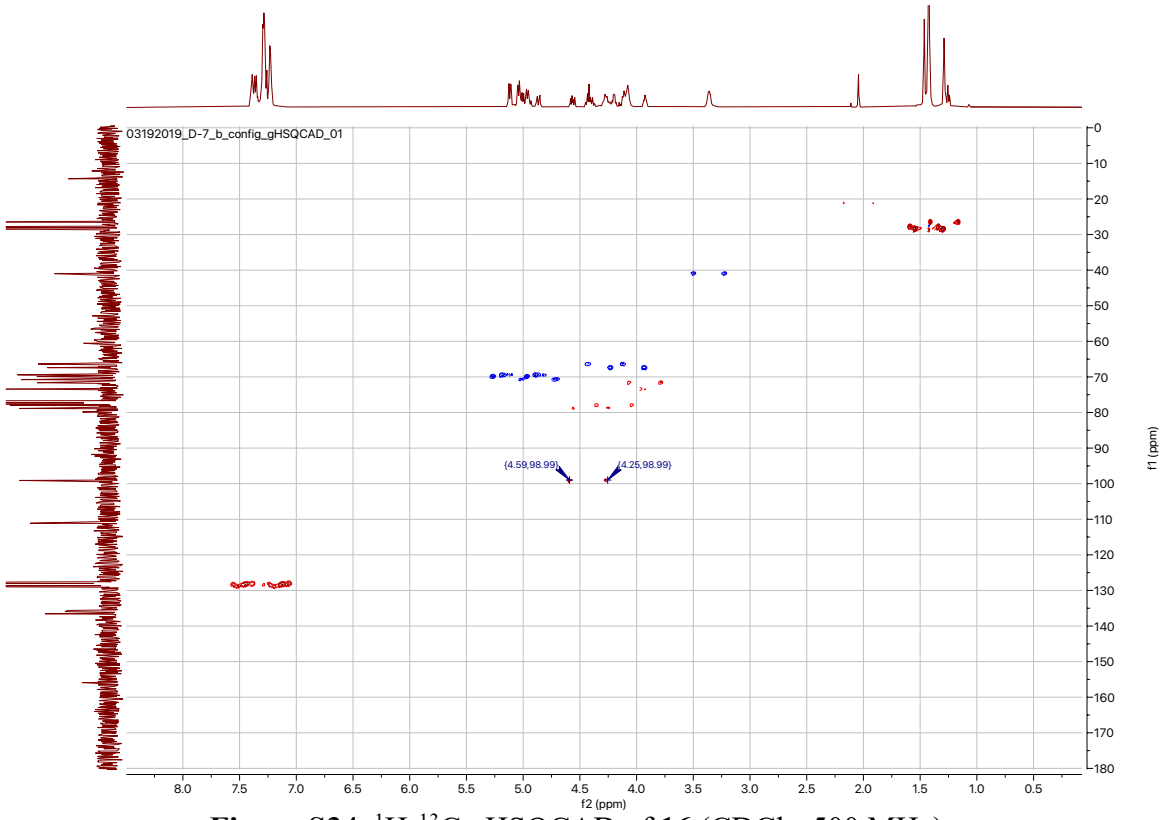

Figure S34. ^{1}H-^{13}C gHSQCAD of **16** ($CDCl_3$, 500 MHz).

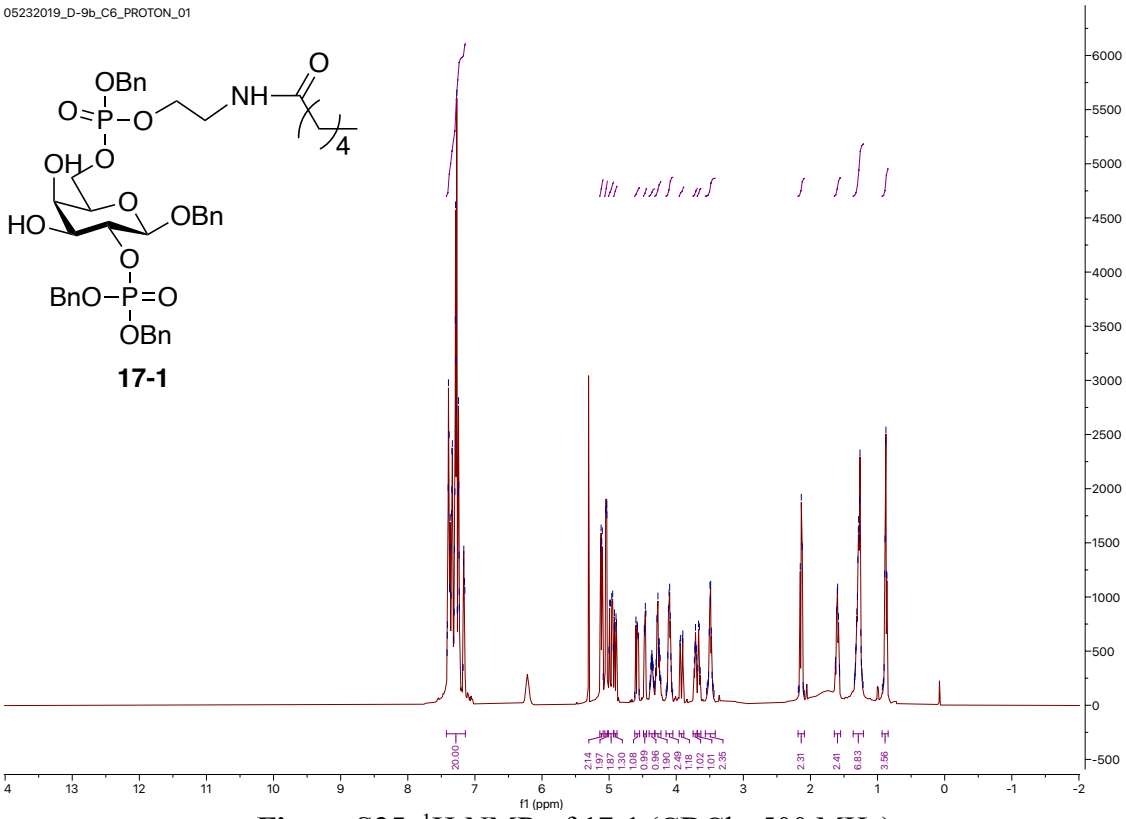

Figure S35. ^{1}H-NMR of **17-1** ($CDCl_3$, 500 MHz).

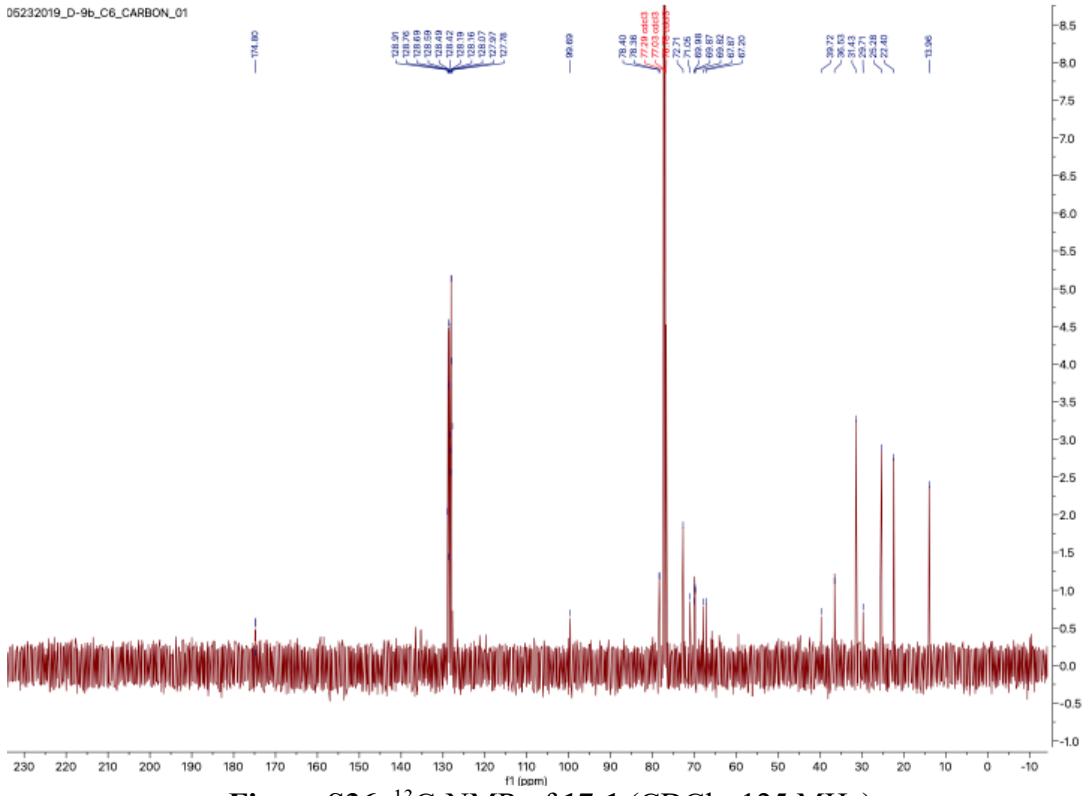

Figure S36. ^{13}C-NMR of **17-1** ($CDCl_3$, 125 MHz).

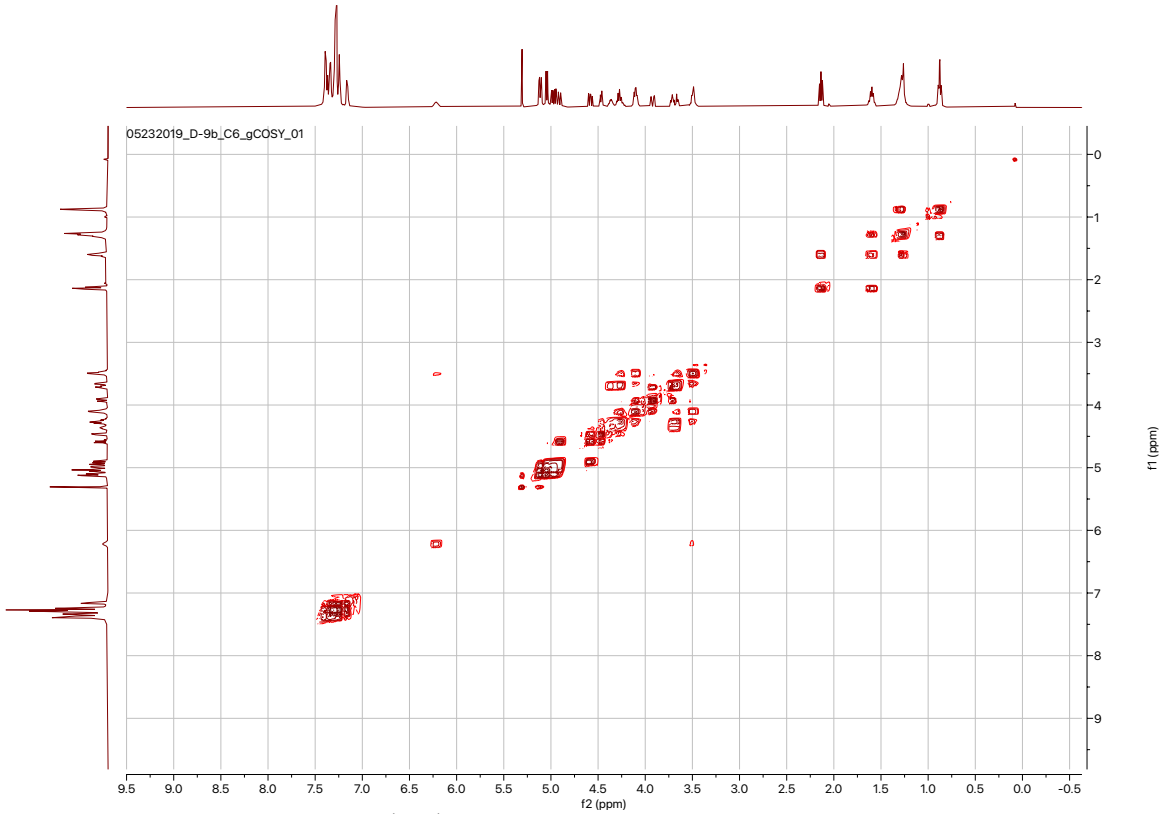

Figure S37. ^{1}H-^{1}H gCOSY of **17-1** ($CDCl_3$, 500 MHz).

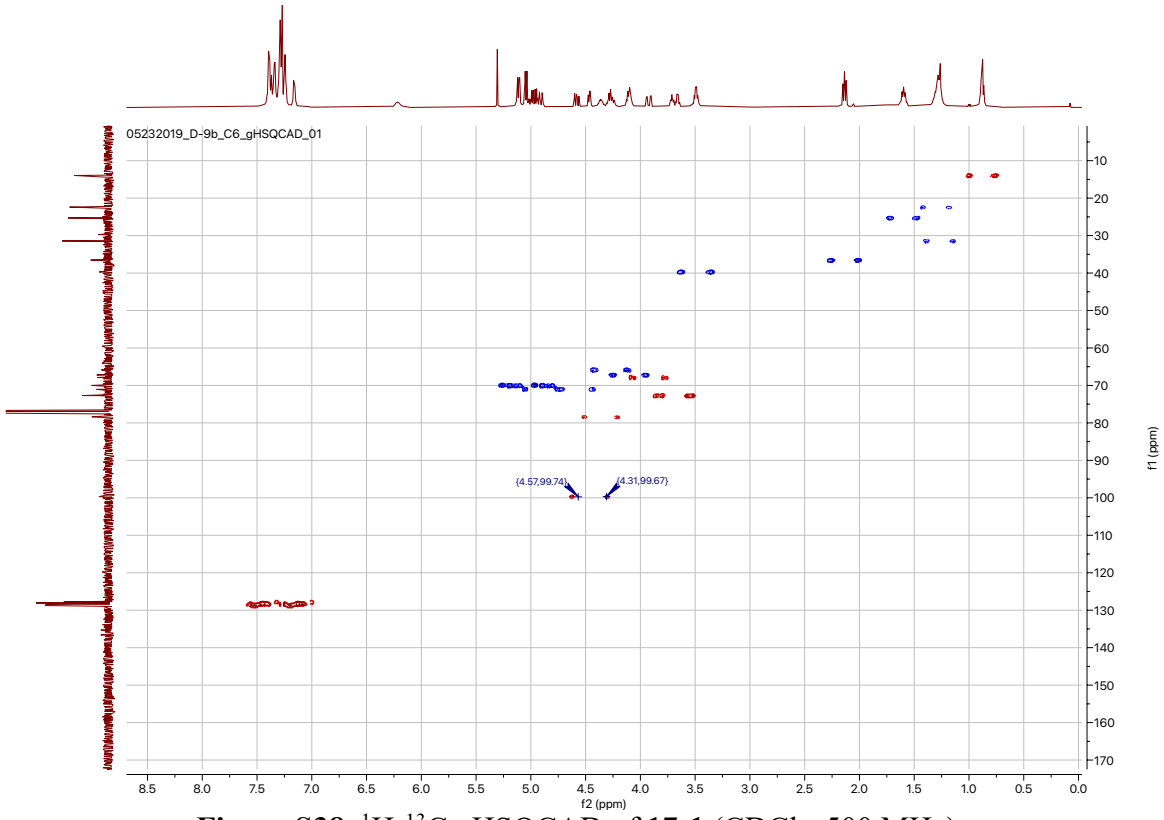

Figure S38. ^{1}H-^{13}C gHSQCAD of **17-1** ($CDCl_3$, 500 MHz).

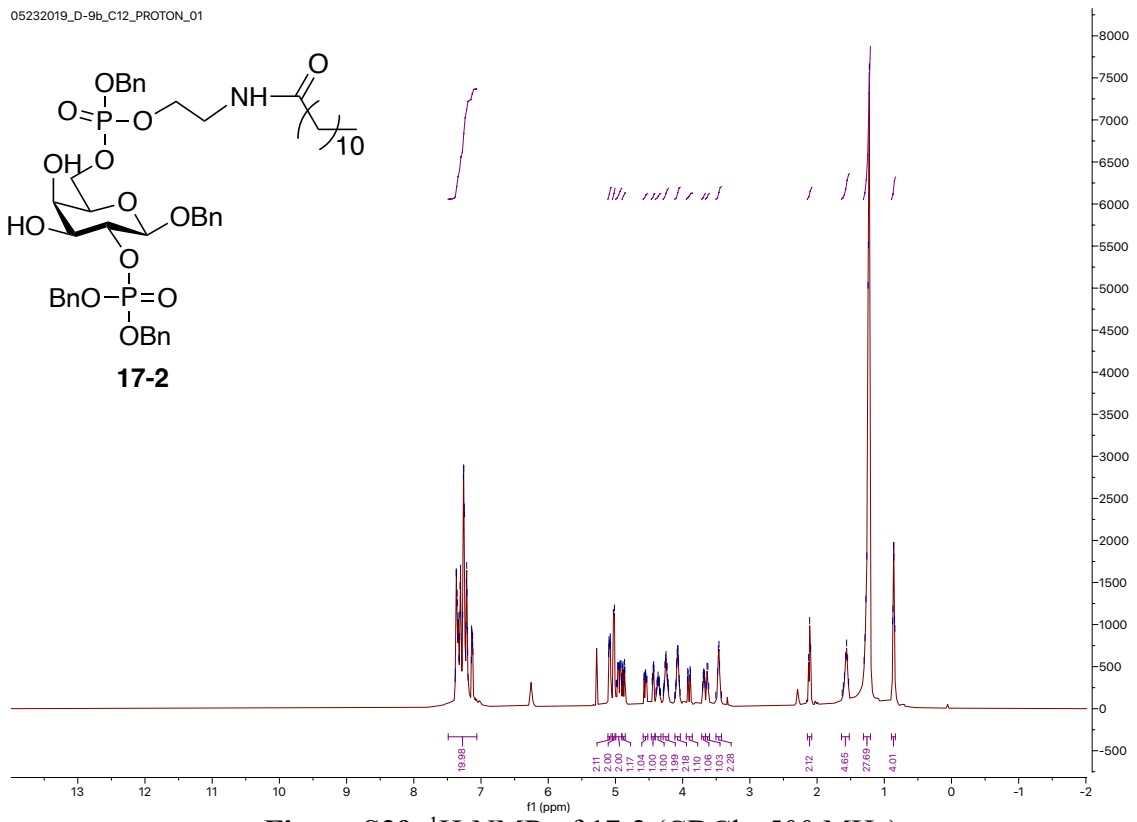

Figure S39. ^{1}H-NMR of **17-2** ($CDCl_3$, 500 MHz).

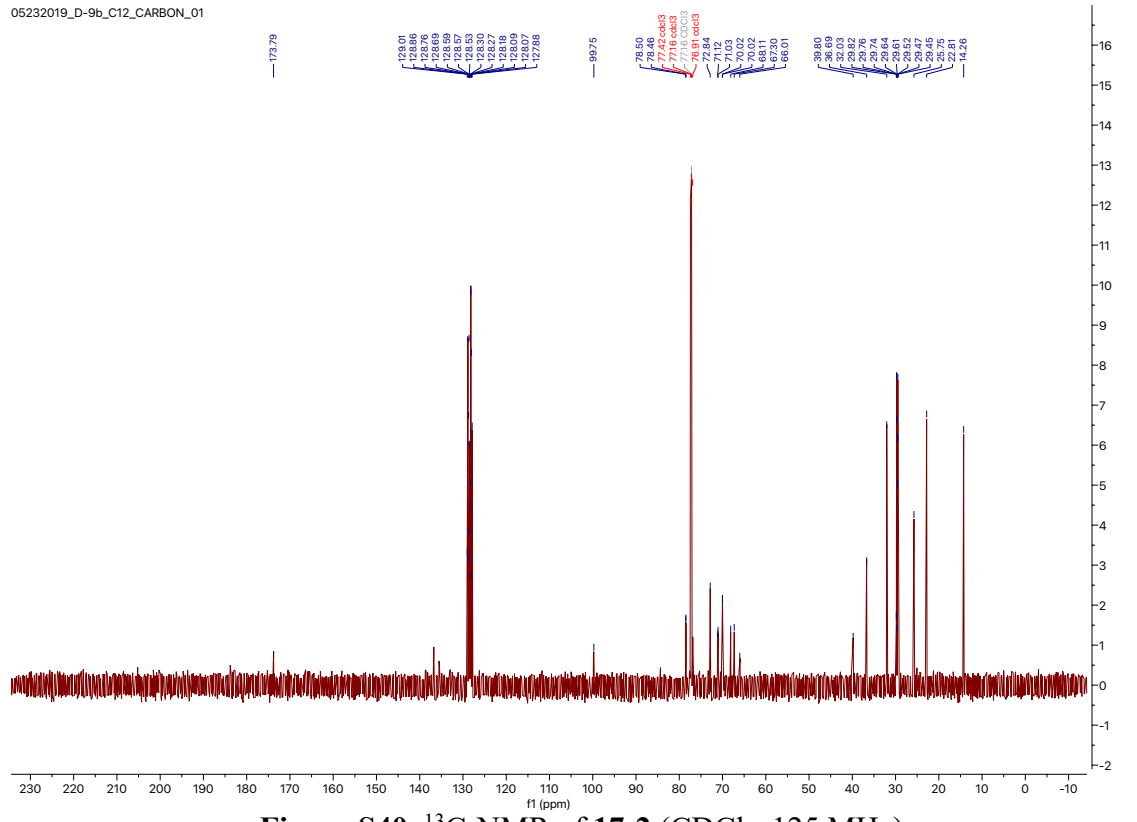

Figure S40. ^{13}C-NMR of **17-2** ($CDCl_3$, 125 MHz).

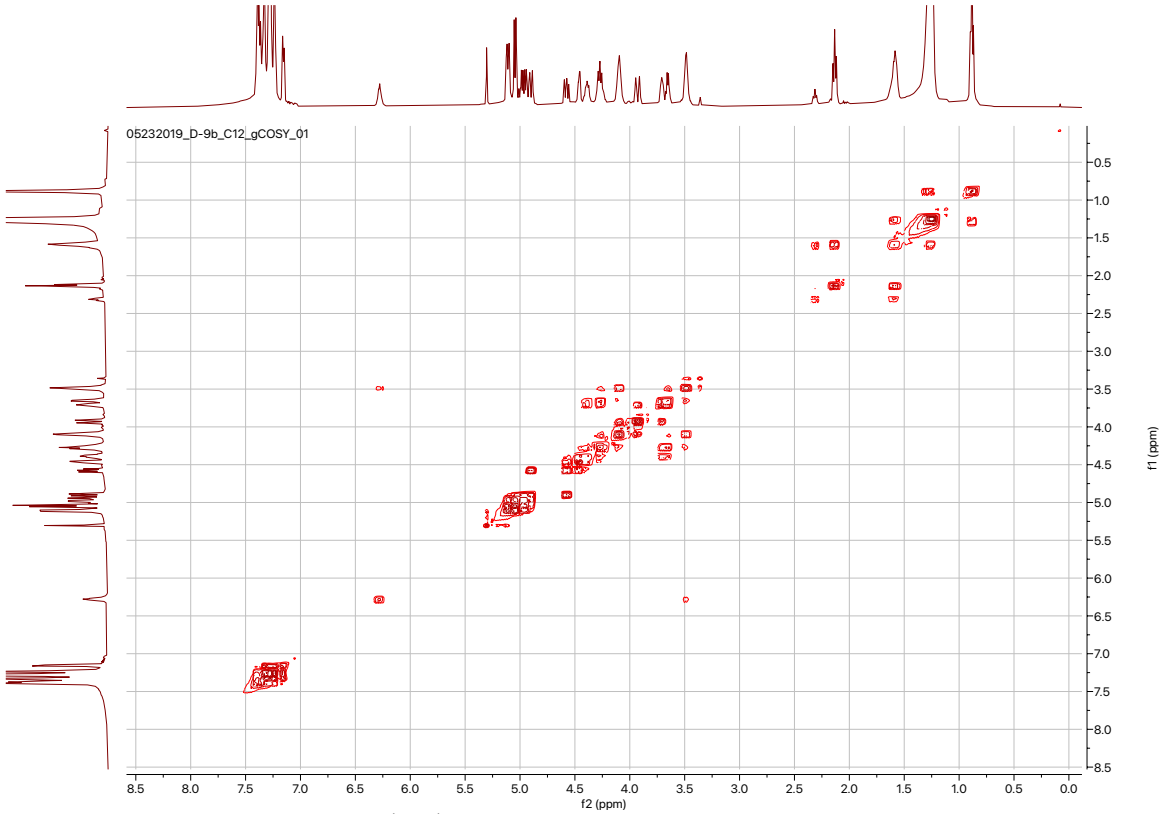

Figure S41. ^{1}H-^{1}H gCOSY of **17-2** ($CDCl_3$, 500 MHz).

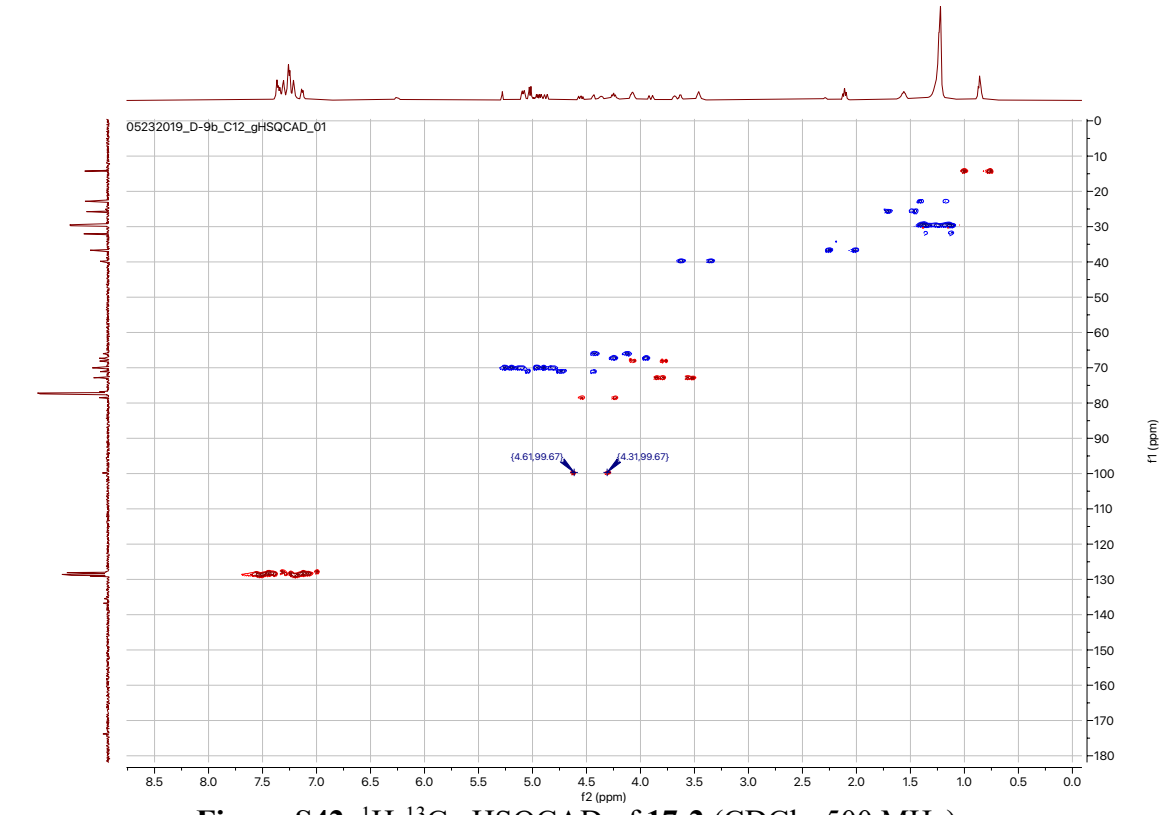

Figure S42. ^{1}H-^{13}C gHSQCAD of **17-2** ($CDCl_3$, 500 MHz).

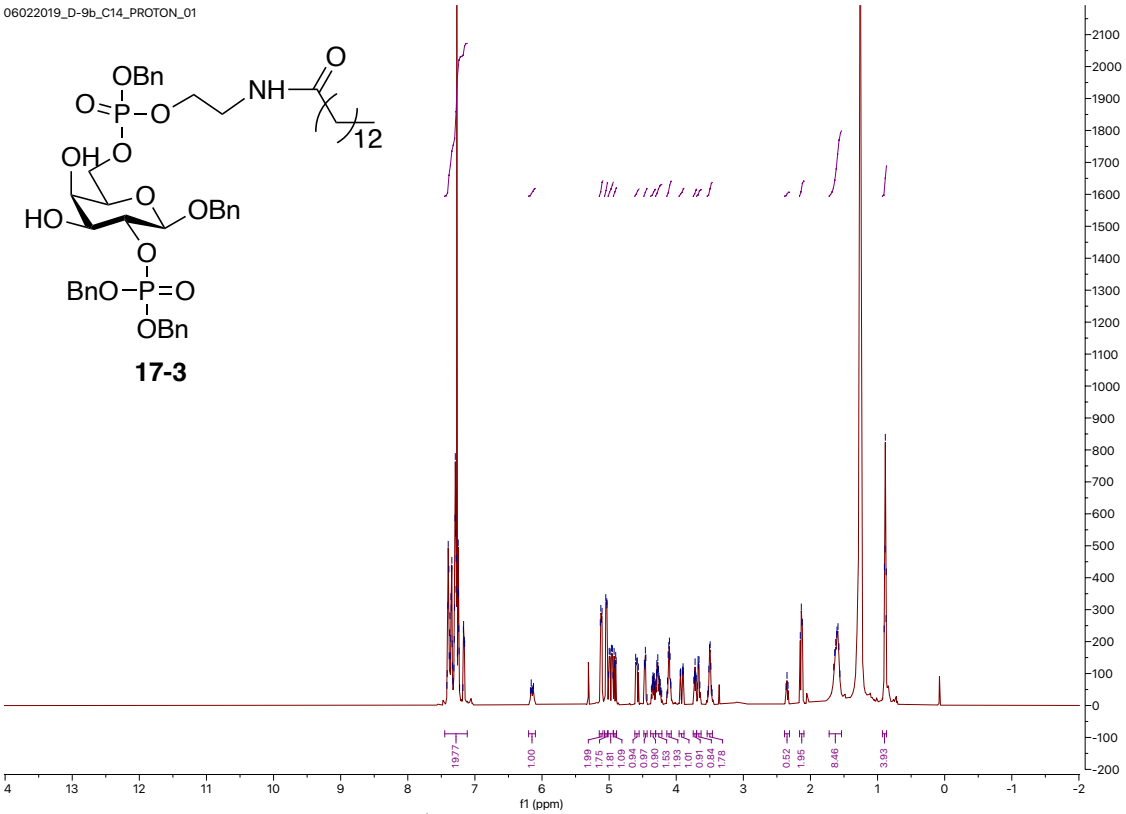

Figure S43. ^{1}H-NMR of **17-3** ($CDCl_3$, 500 MHz).

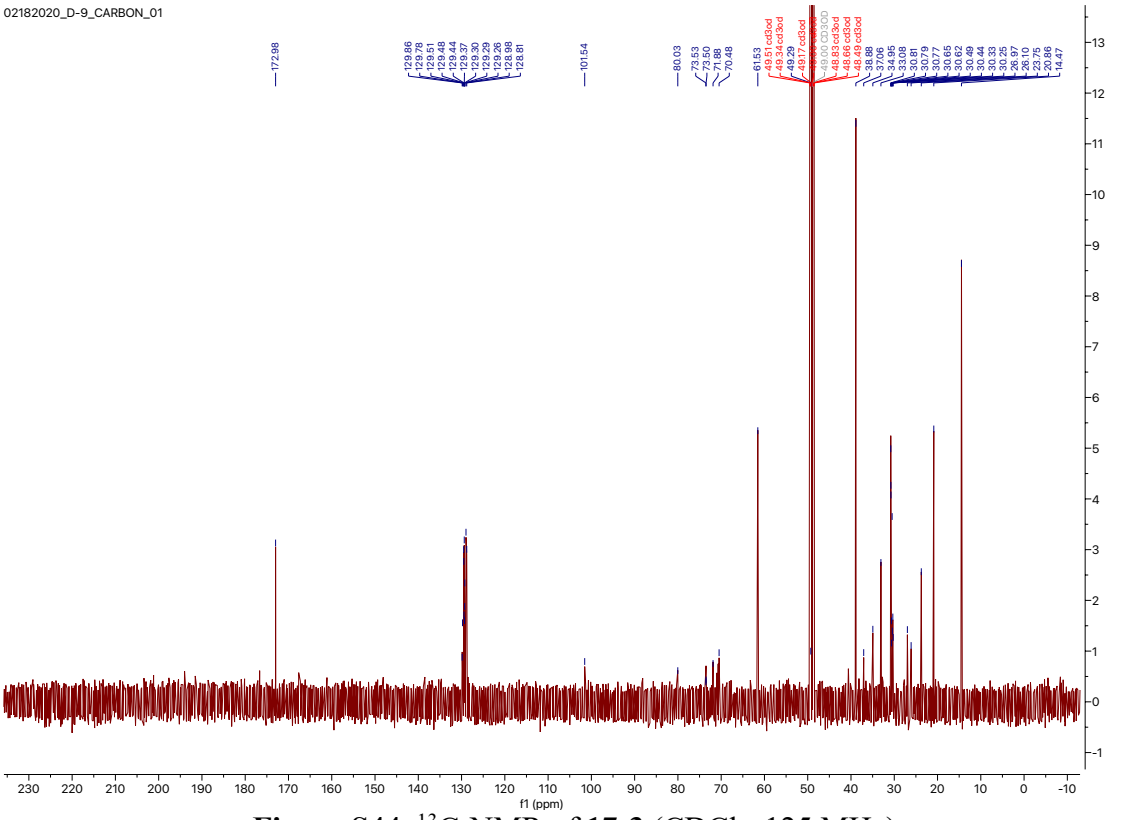

Figure S44. ^{13}C-NMR of **17-3** ($CDCl_3$, 125 MHz).

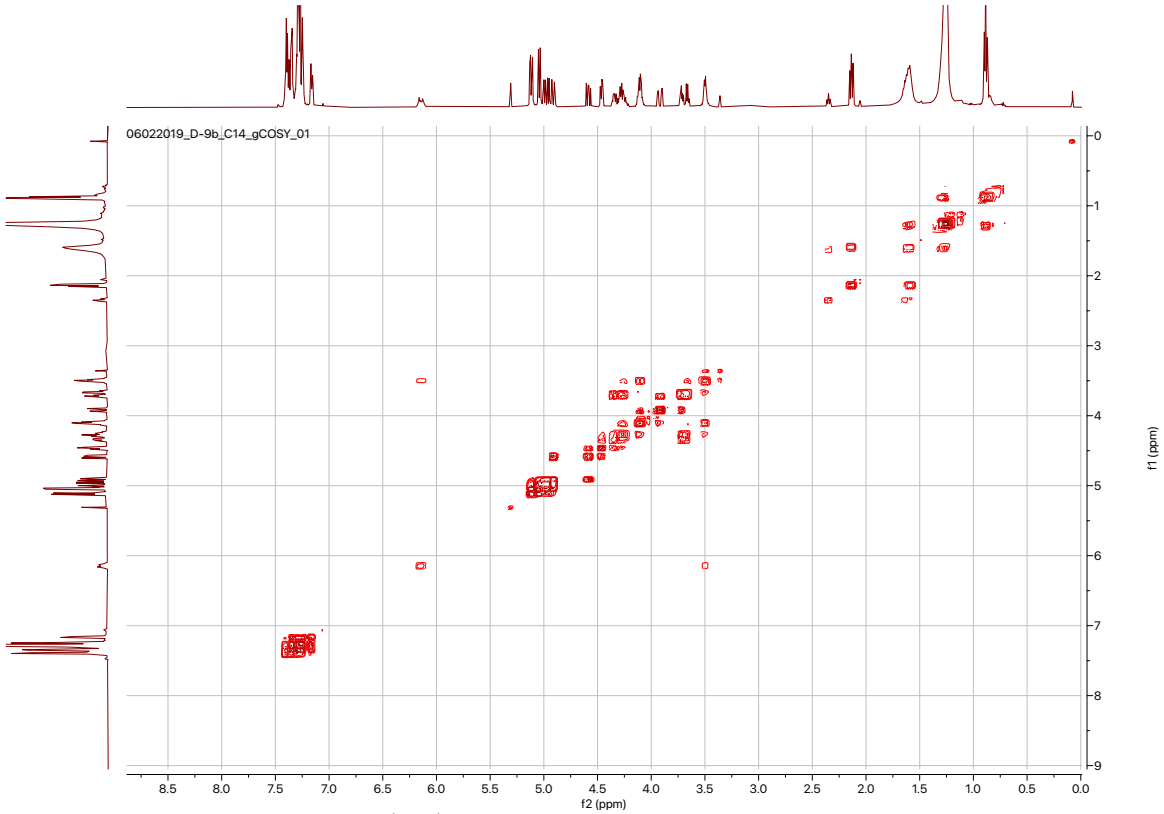

Figure S45. ^{1}H-^{1}H gCOSY of **17-3** ($CDCl_3$, 500 MHz).

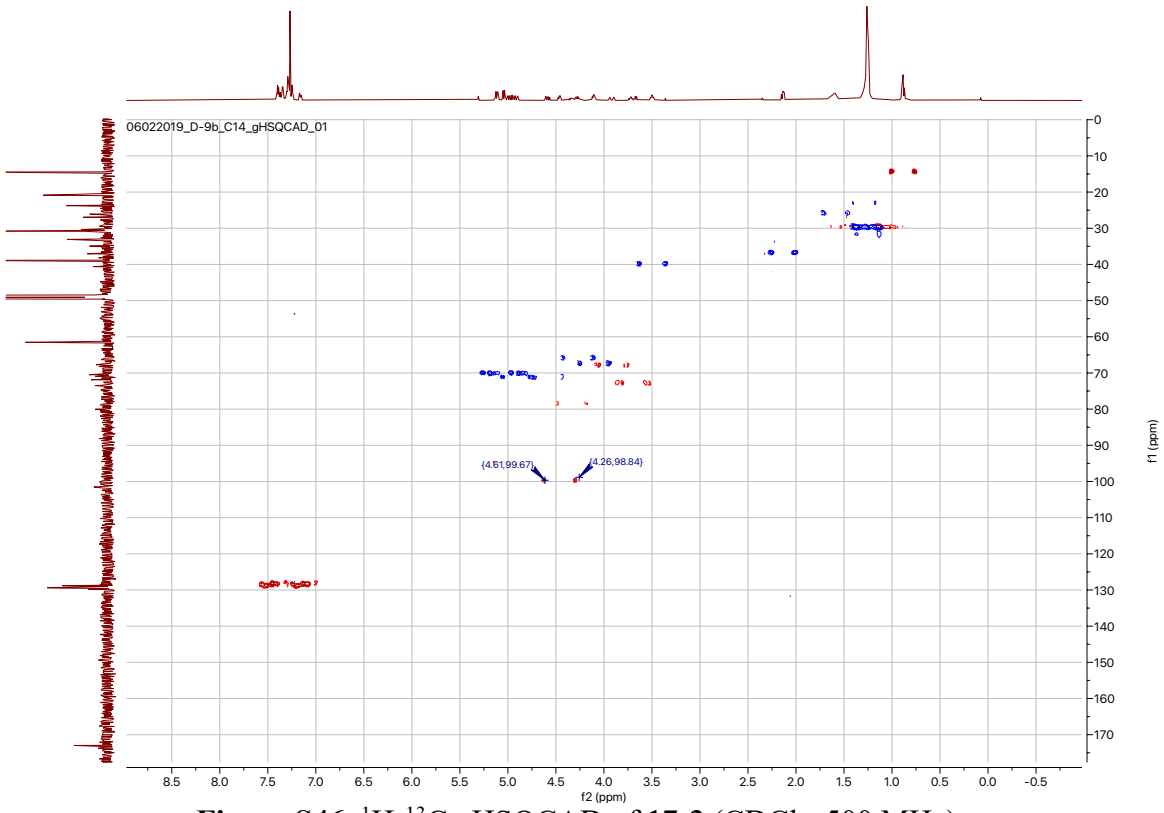

Figure S46. ^{1}H-^{13}C gHSQCAD of **17-3** ($CDCl_3$, 500 MHz).

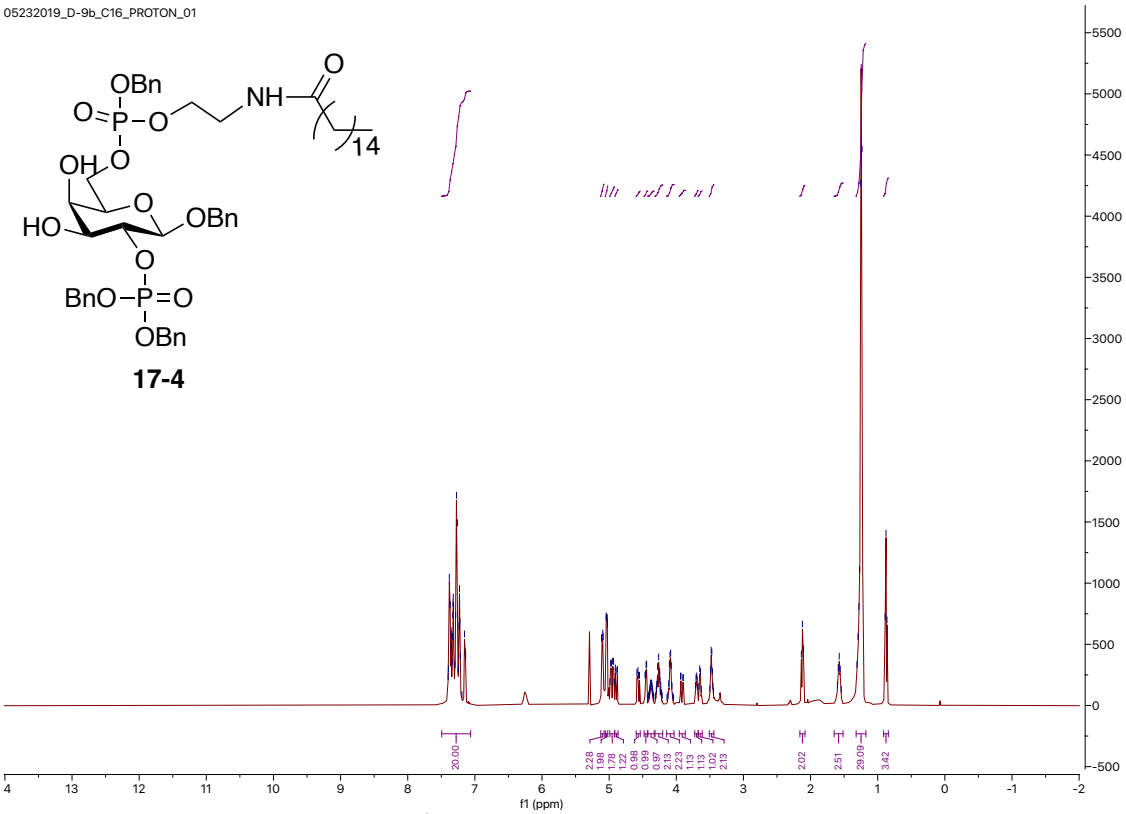

Figure S47. ^{1}H-NMR of **17-4** ($CDCl_3$, 500 MHz).

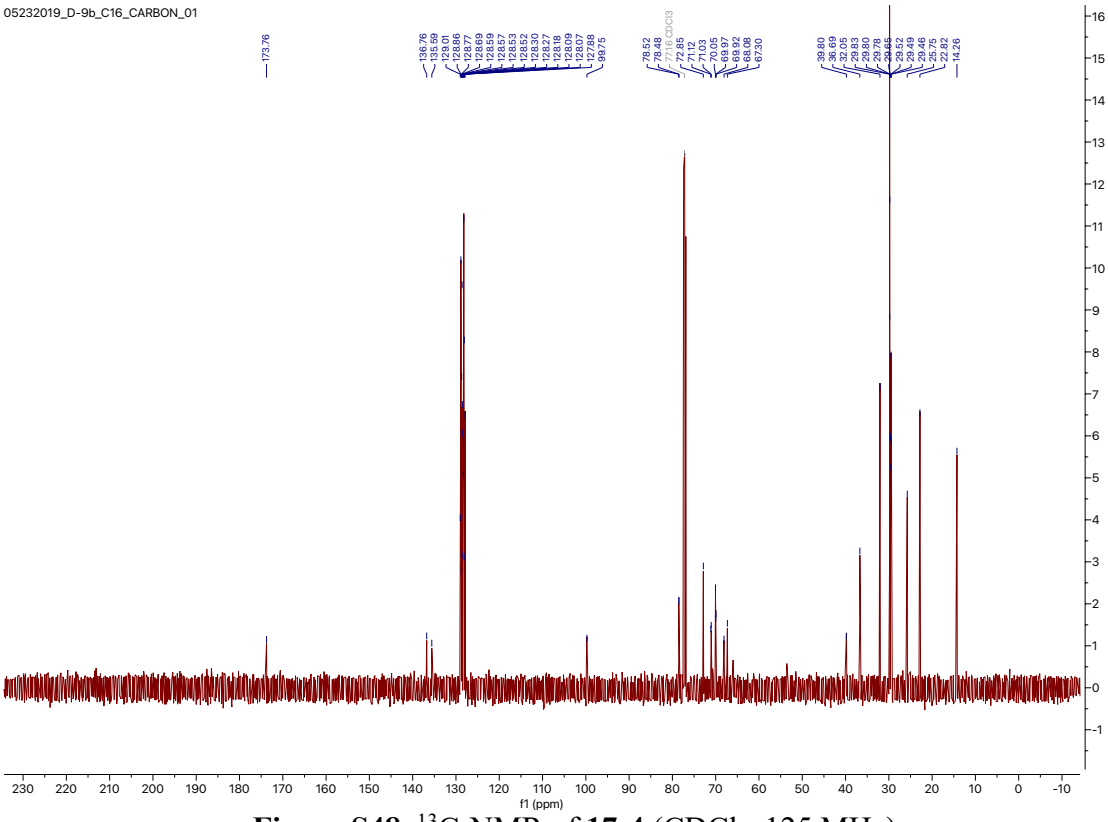

Figure S48. ^{13}C-NMR of **17-4** ($CDCl_3$, 125 MHz).

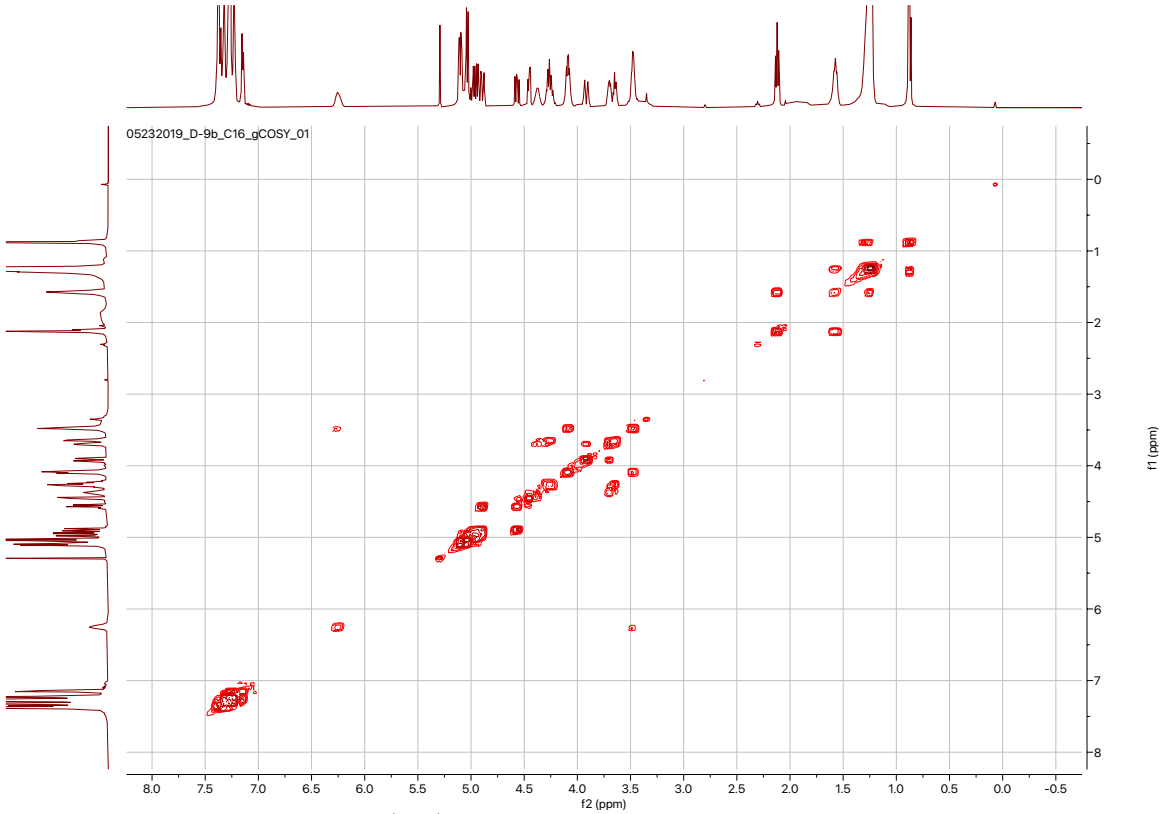

Figure S49. ^{1}H-^{1}H gCOSY of **17-4** ($CDCl_3$, 500 MHz).

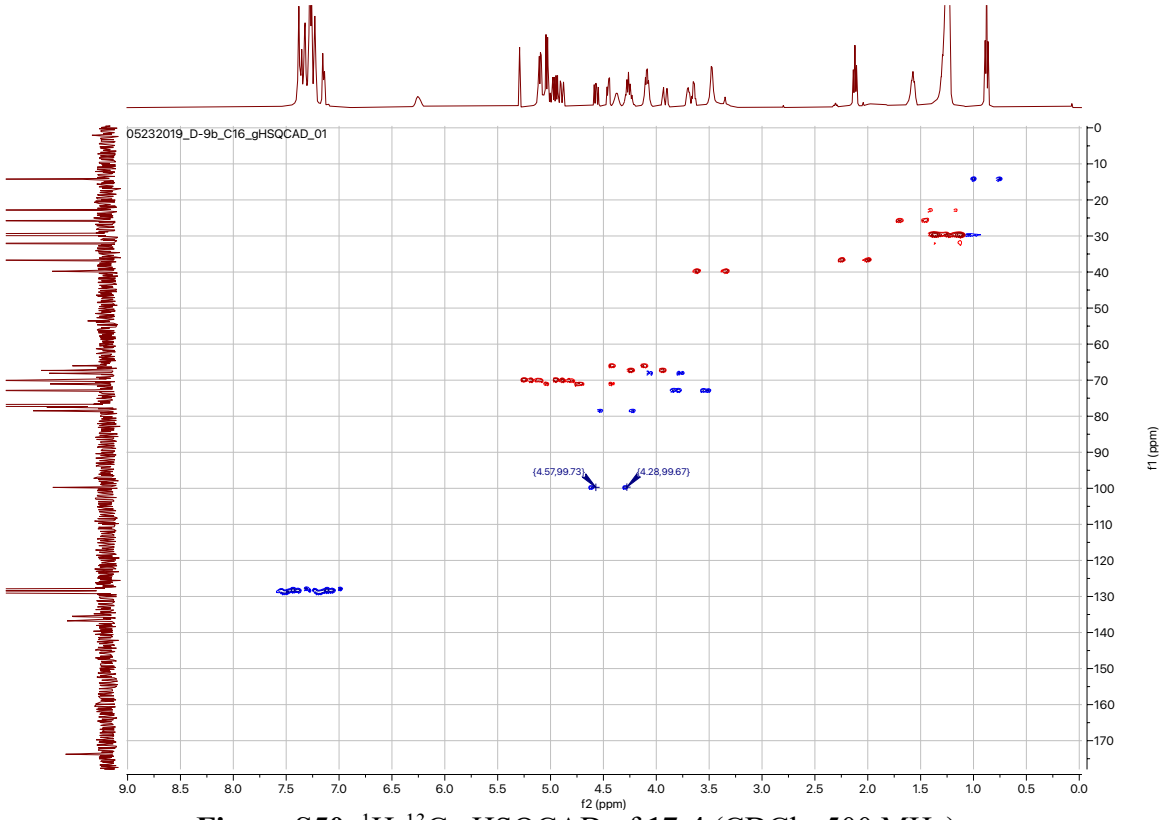

Figure S50. ^{1}H-^{13}C gHSQCAD of **17-4** ($CDCl_3$, 500 MHz).

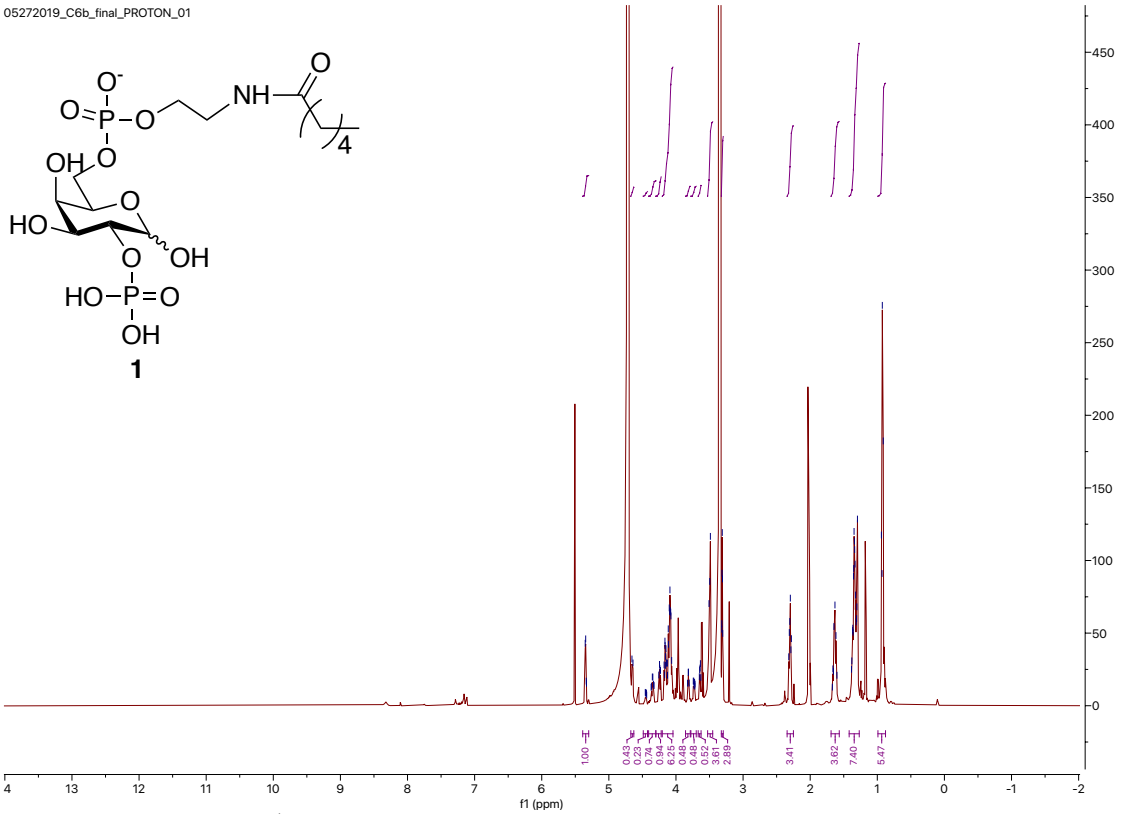

Figure S51. ^{1}H-NMR of **1** ($CDCl_3$: CD_3OD : D_2O 1 : 2 : 0.5, 500 MHz).

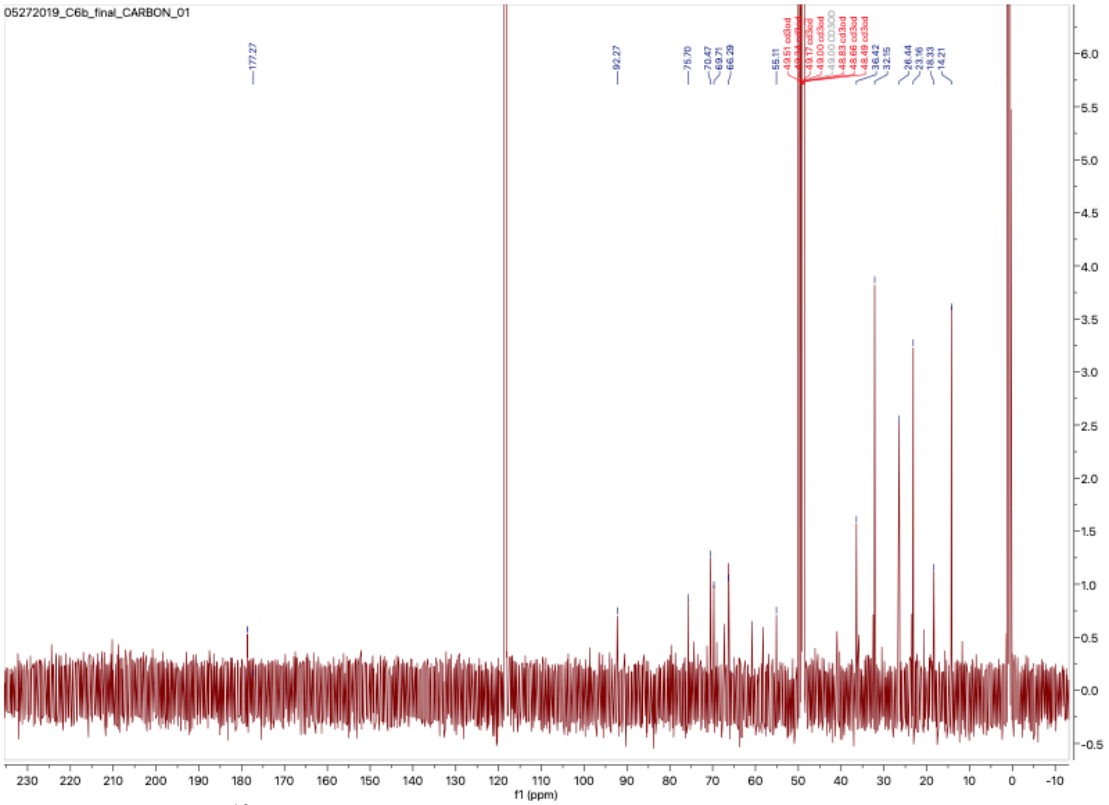

Figure S52. ^{13}C-NMR of **1** ($CDCl_3$: CD_3OD : D_2O 1 : 2 : 0.5, 125 MHz).

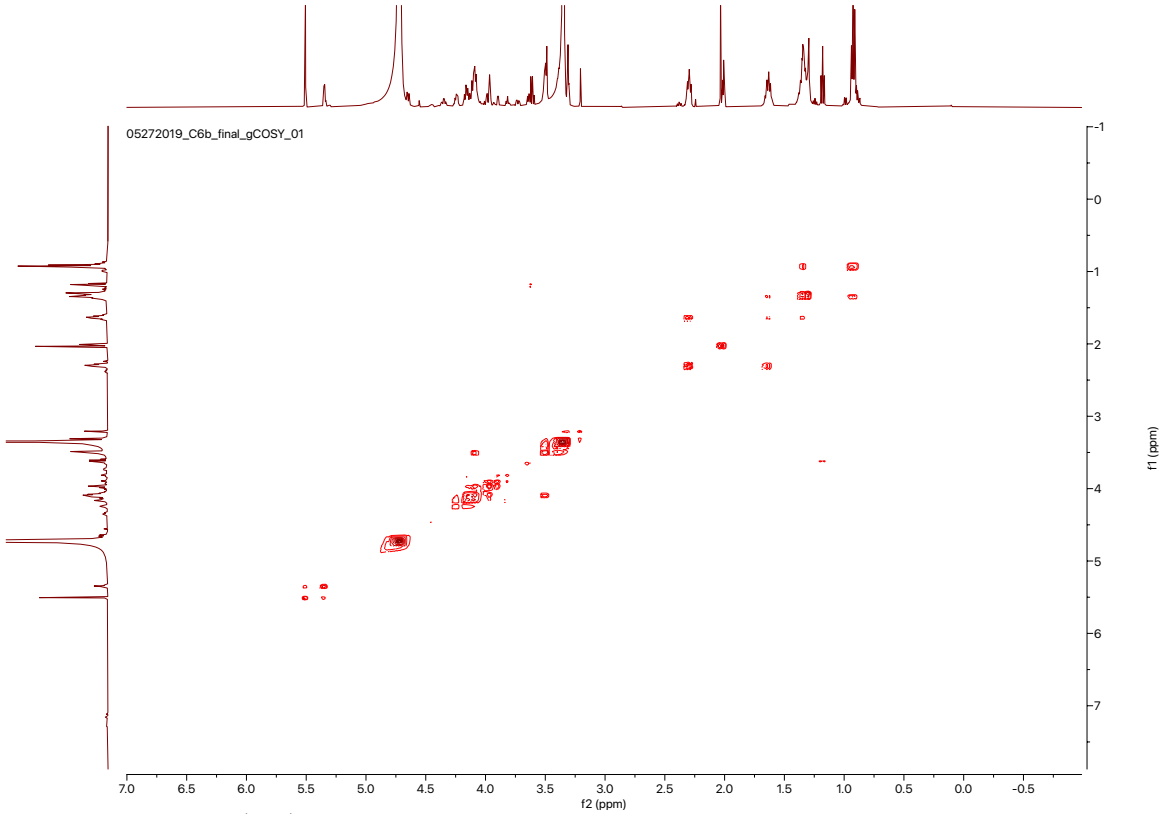

Figure S53. ^{1}H-^{1}H gCOSY of **1** ($CDCl_3$: CD_3OD : D_2O 1 : 2 : 0.5, 500 MHz).

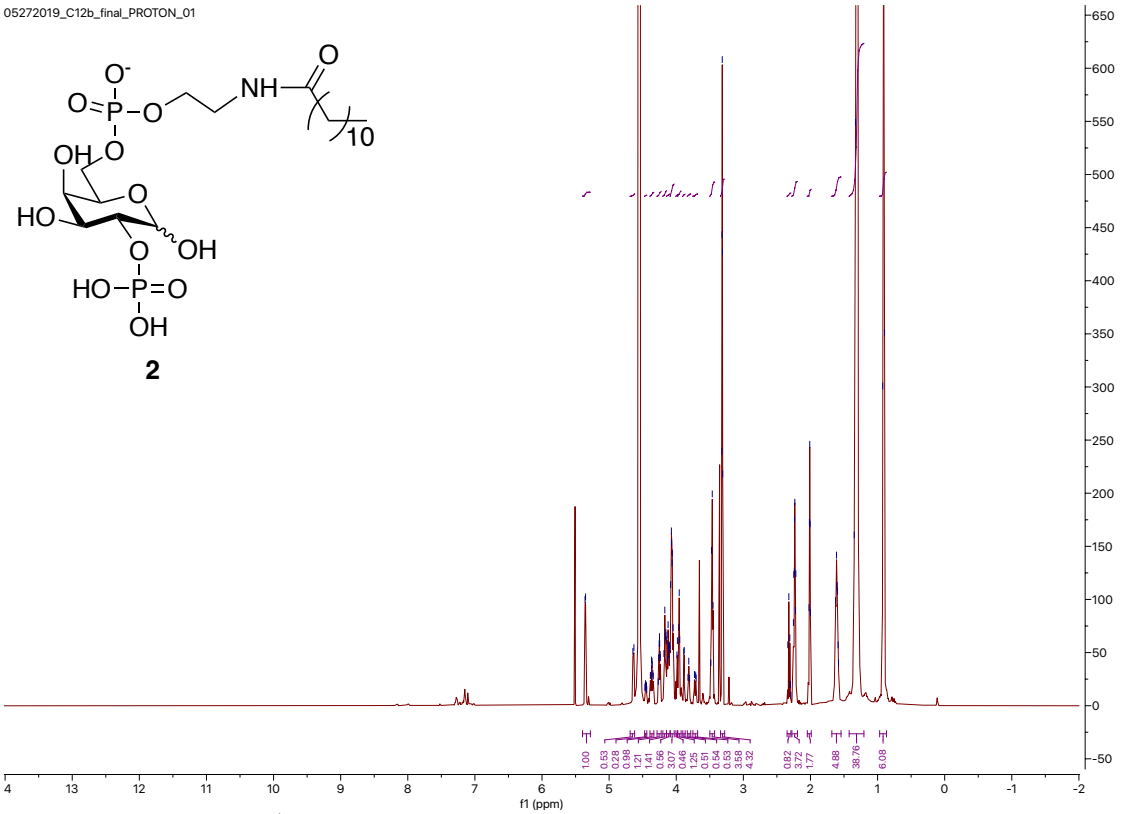

Figure S54. ^{1}H-NMR of **2** ($CDCl_3$: CD_3OD : D_2O 1 : 2 : 0.5, 500 MHz).

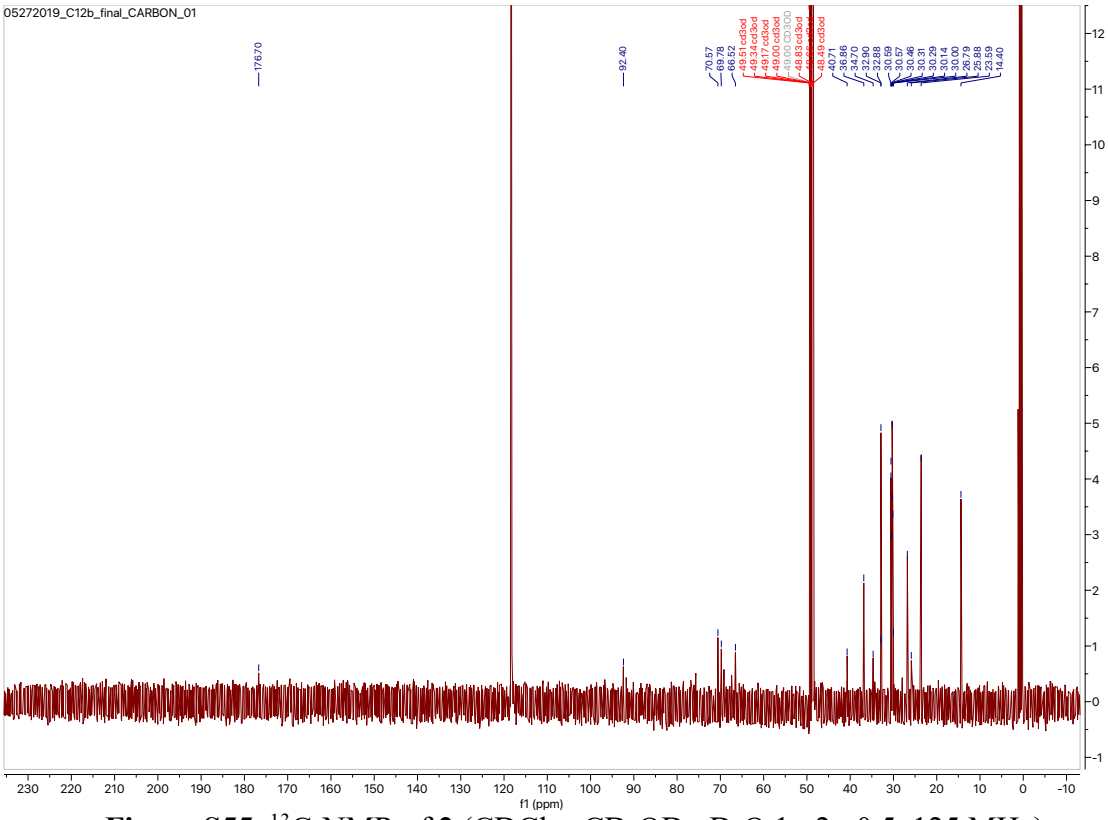

Figure S55. ^{13}C-NMR of **2** ($CDCl_3$: CD_3OD : D_2O 1 : 2 : 0.5, 125 MHz).

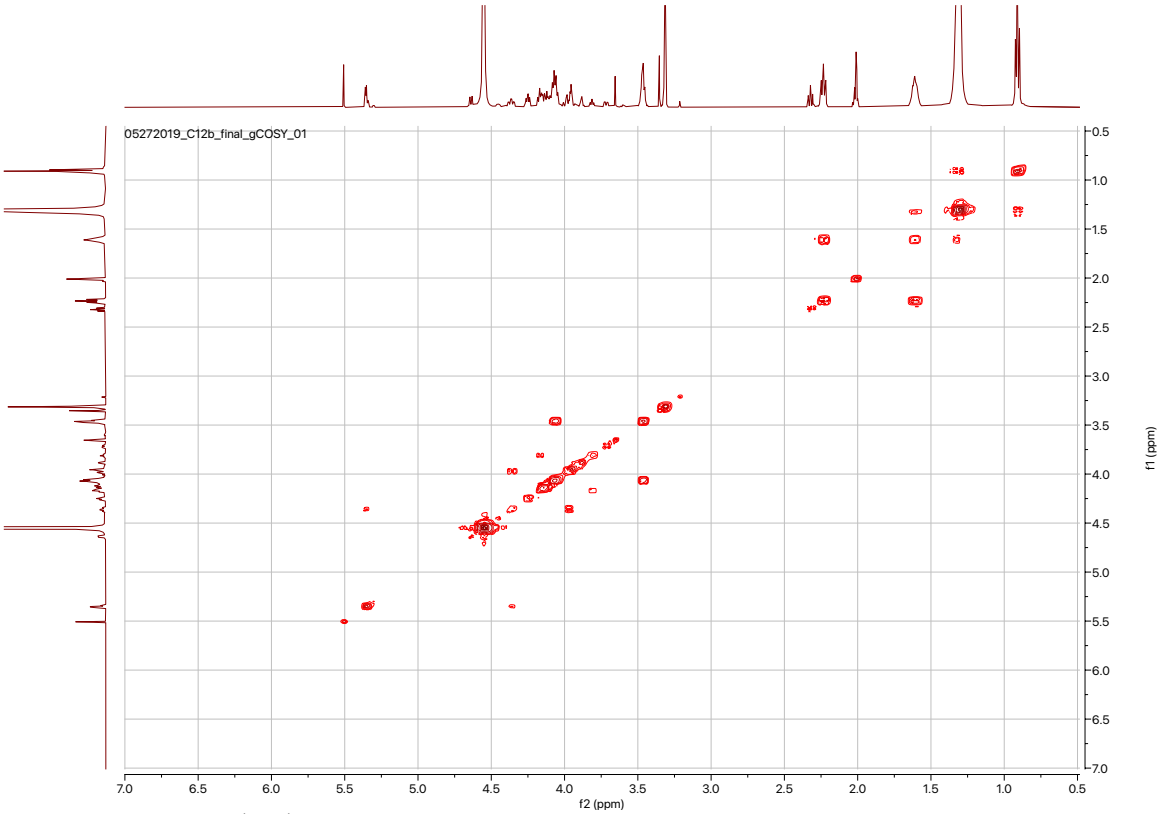

Figure S56. ^{1}H-^{1}H gCOSY of **2** ($CDCl_3$: CD_3OD : D_2O 1 : 2 : 0.5, 500 MHz).

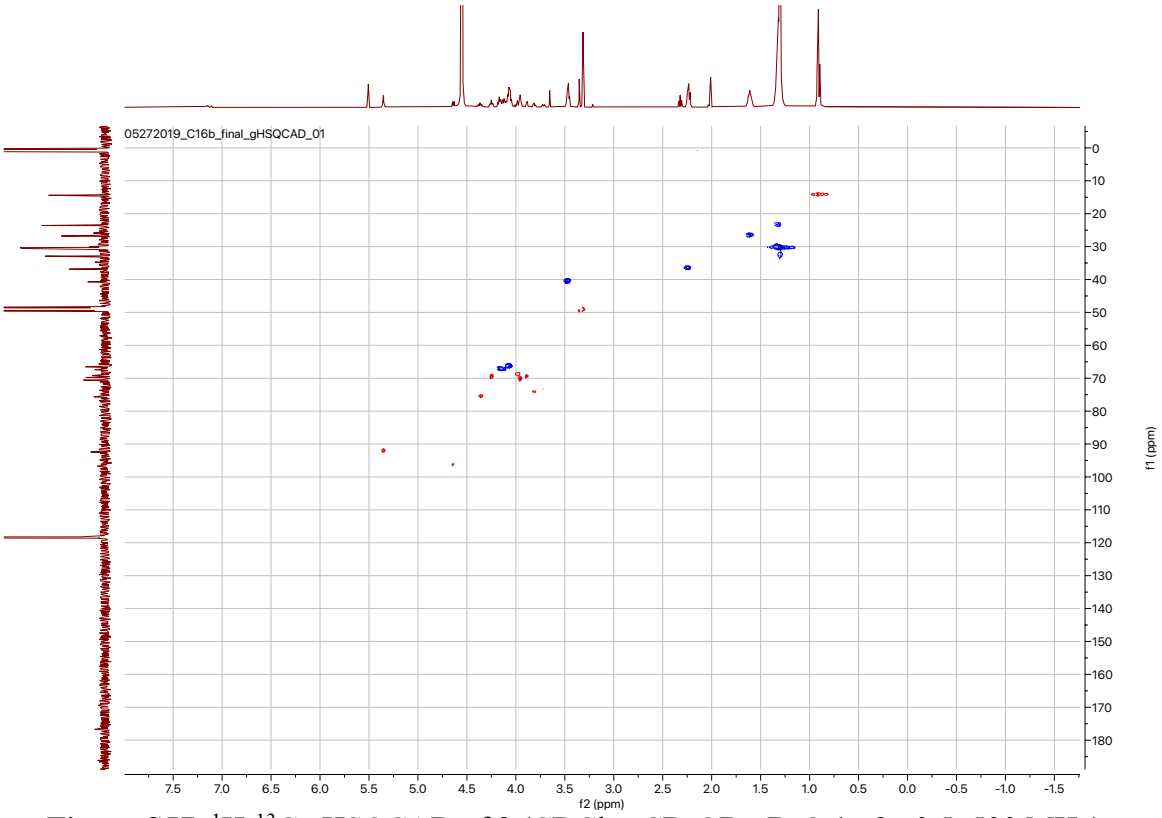

Figure S57. ^{1}H-^{13}C gHSQCAD of **2** ($CDCl_3$: CD_3OD : D_2O 1 : 2 : 0.5, 500 MHz).

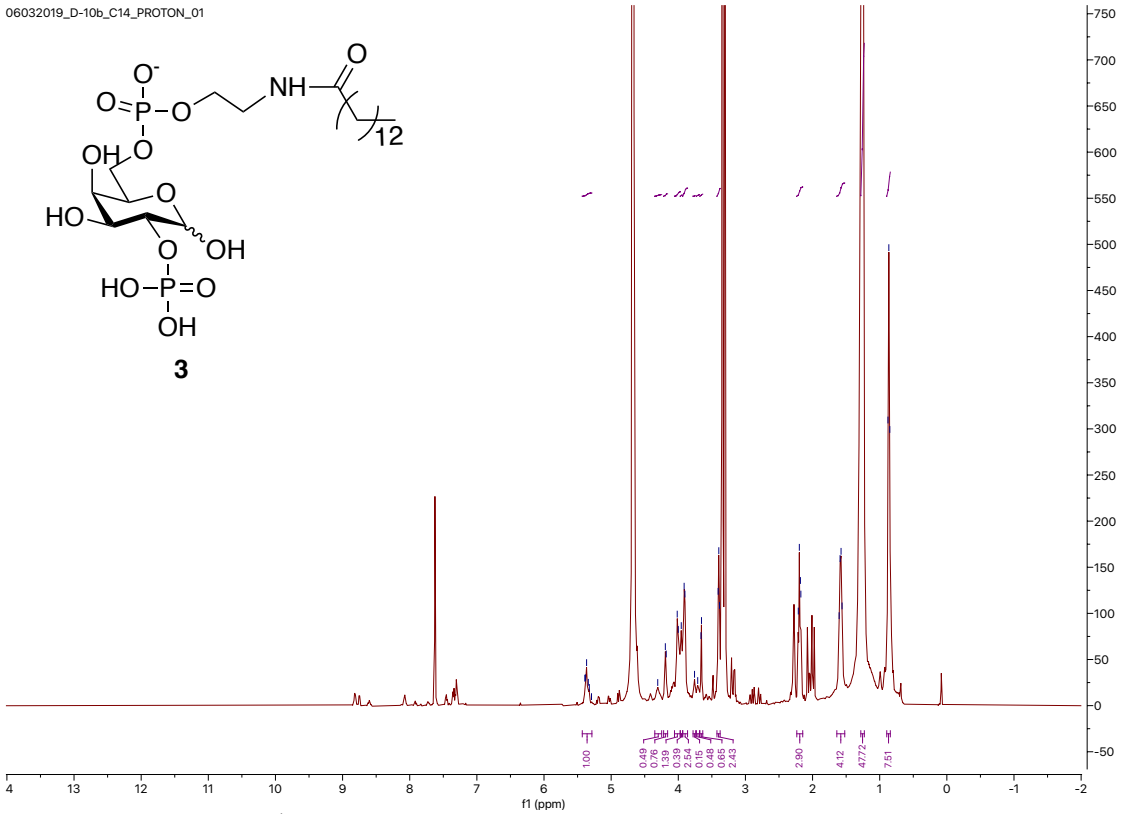

Figure S58. ^{1}H-NMR of **3** ($CDCl_3$: CD_3OD : D_2O 1 : 2 : 0.5, 500 MHz).

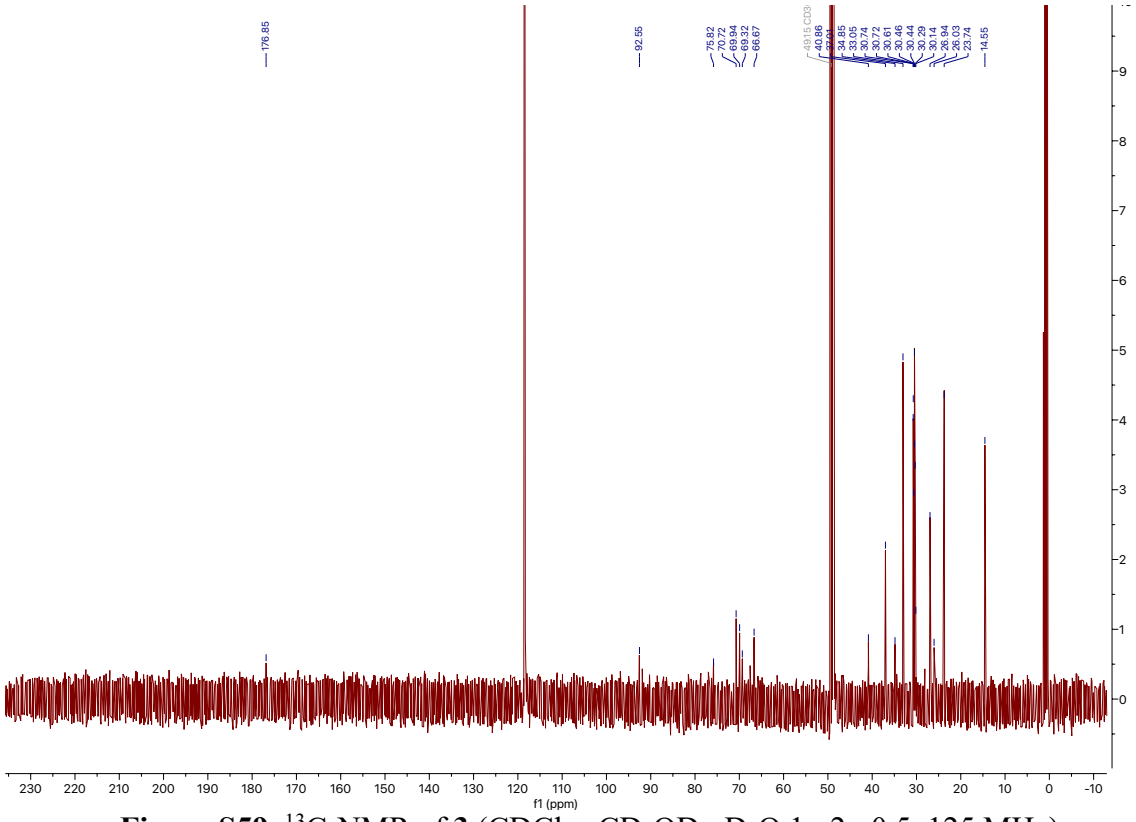

Figure S59. ^{13}C-NMR of **3** ($CDCl_3$: CD_3OD : D_2O 1 : 2 : 0.5, 125 MHz).

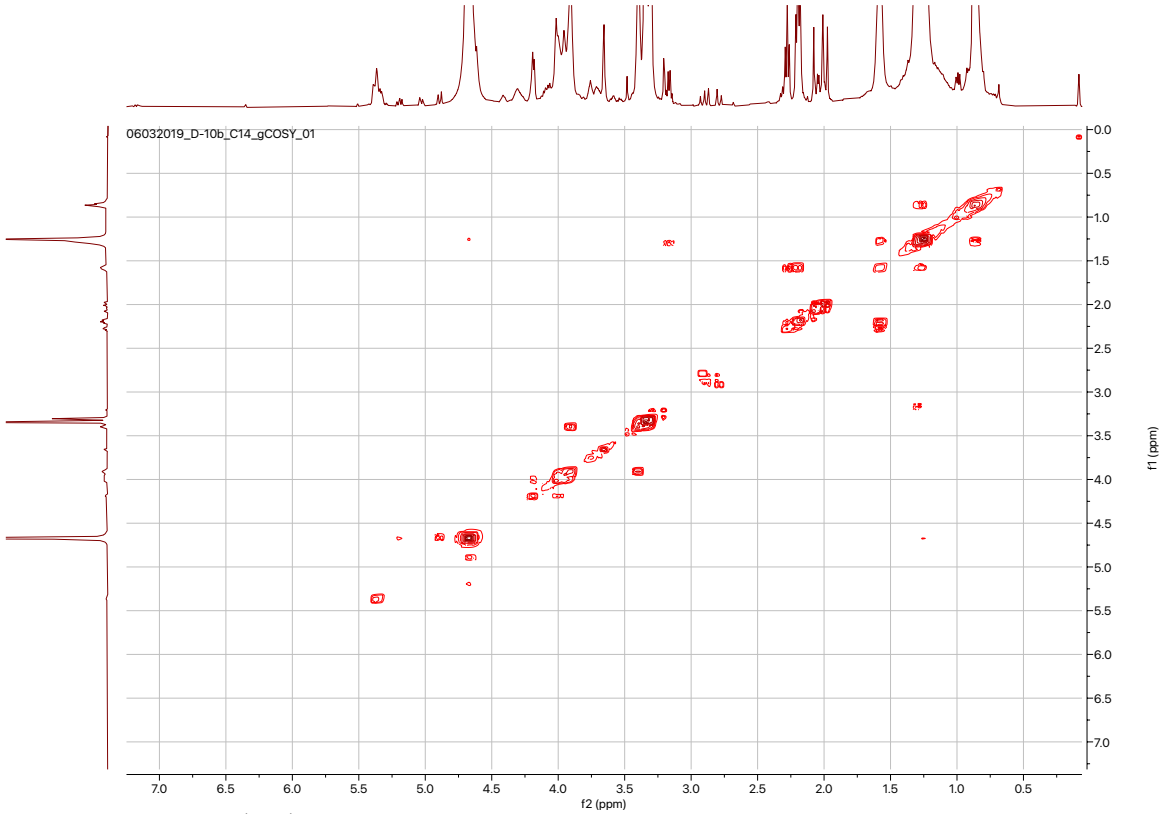

Figure S60. ^{1}H-^{1}H gCOSY of **3** ($CDCl_3$: CD_3OD : D_2O 1 : 2 : 0.5, 500 MHz).

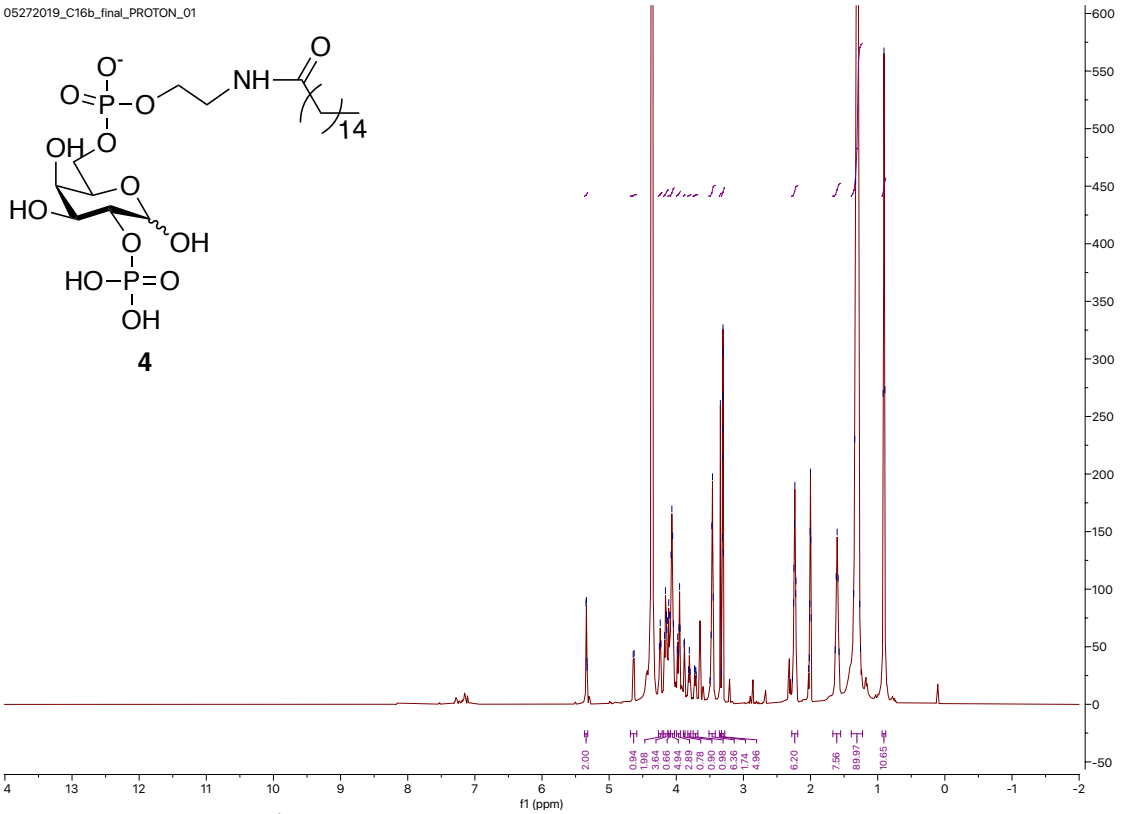

Figure S61. ^{1}H-NMR of **4** ($CDCl_3$: CD_3OD : D_2O 1 : 2 : 0.5, 500 MHz).

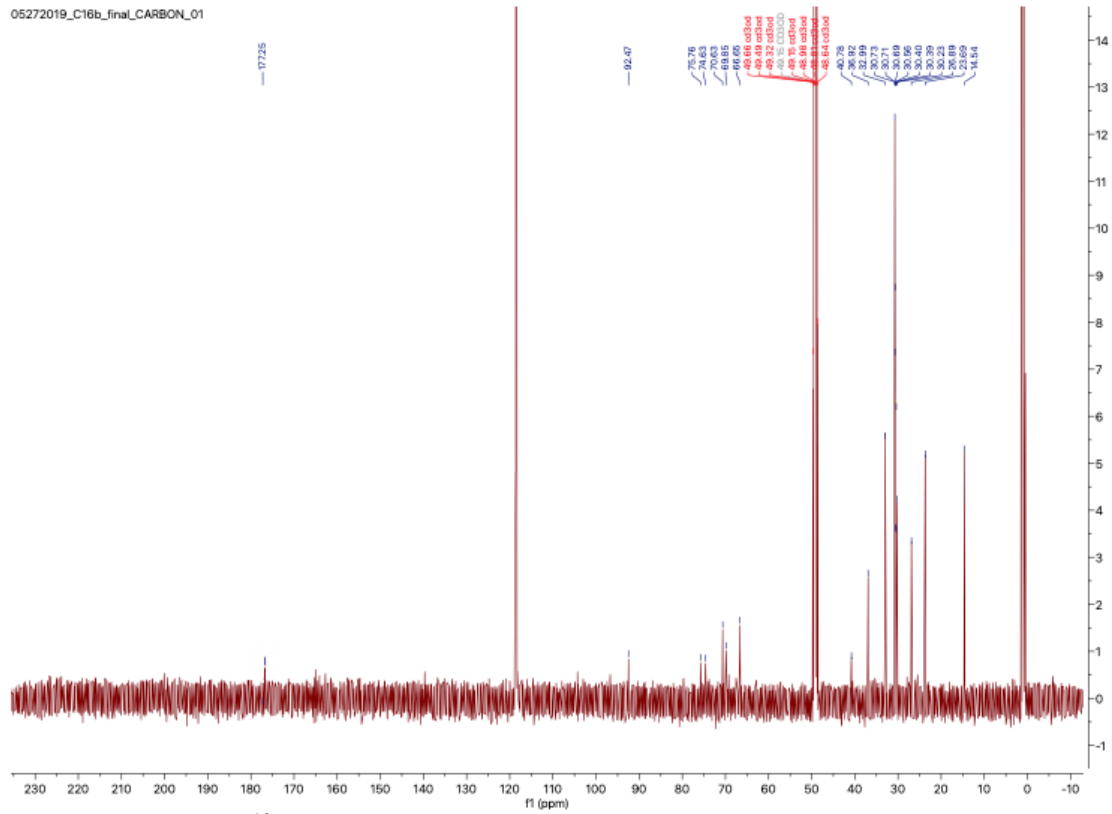

Figure S62. ^{13}C-NMR of **4** ($CDCl_3$: CD_3OD : D_2O 1 : 2 : 0.5, 125 MHz).

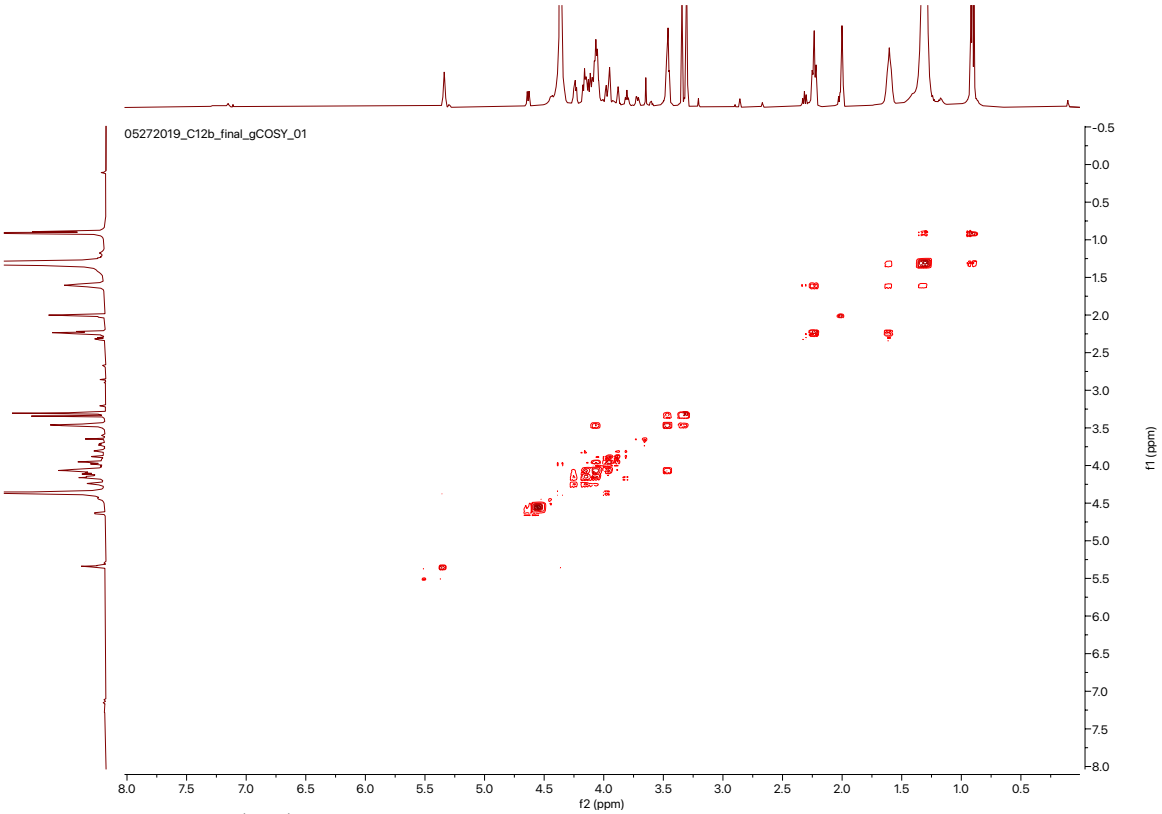

Figure S63. ^{1}H-^{1}H gCOSY of **4** ($CDCl_3$: CD_3OD : D_2O 1 : 2 : 0.5, 500 MHz).

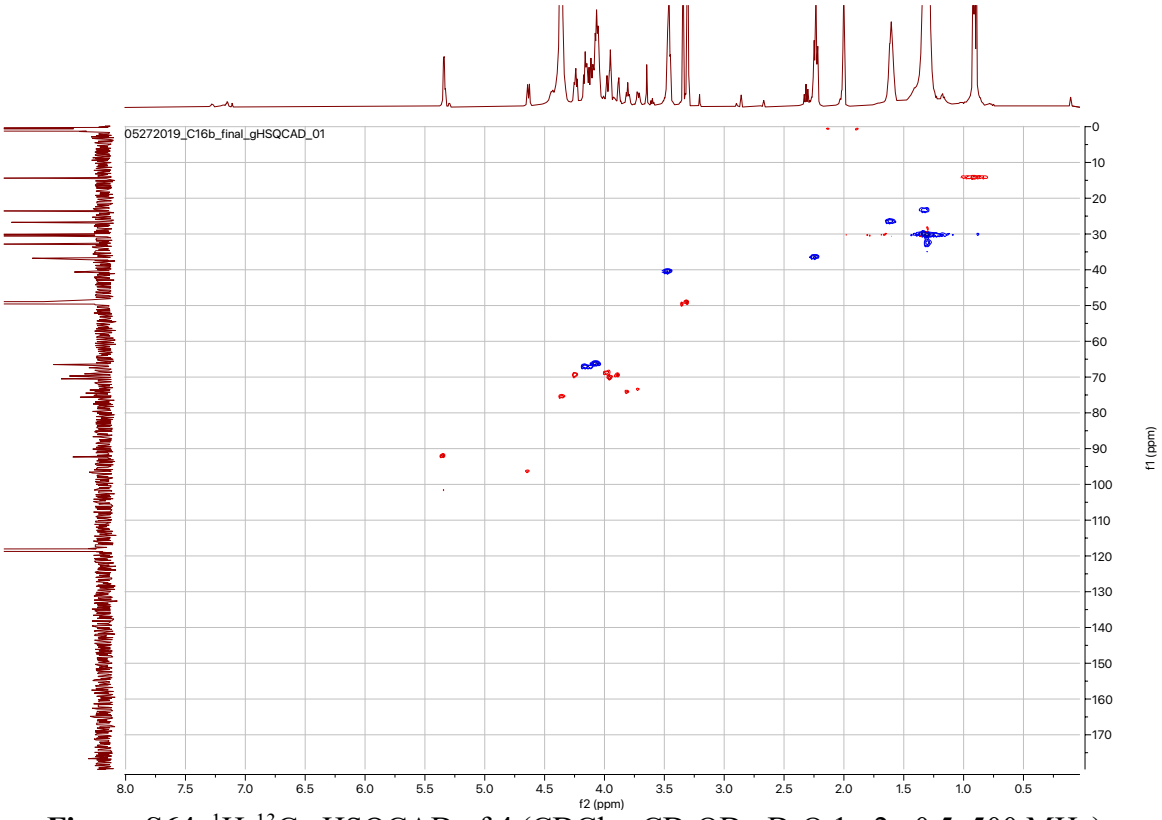

Figure S64. ^{1}H-^{13}C gHSQCAD of **4** ($CDCl_3$: CD_3OD : D_2O 1 : 2 : 0.5, 500 MHz).

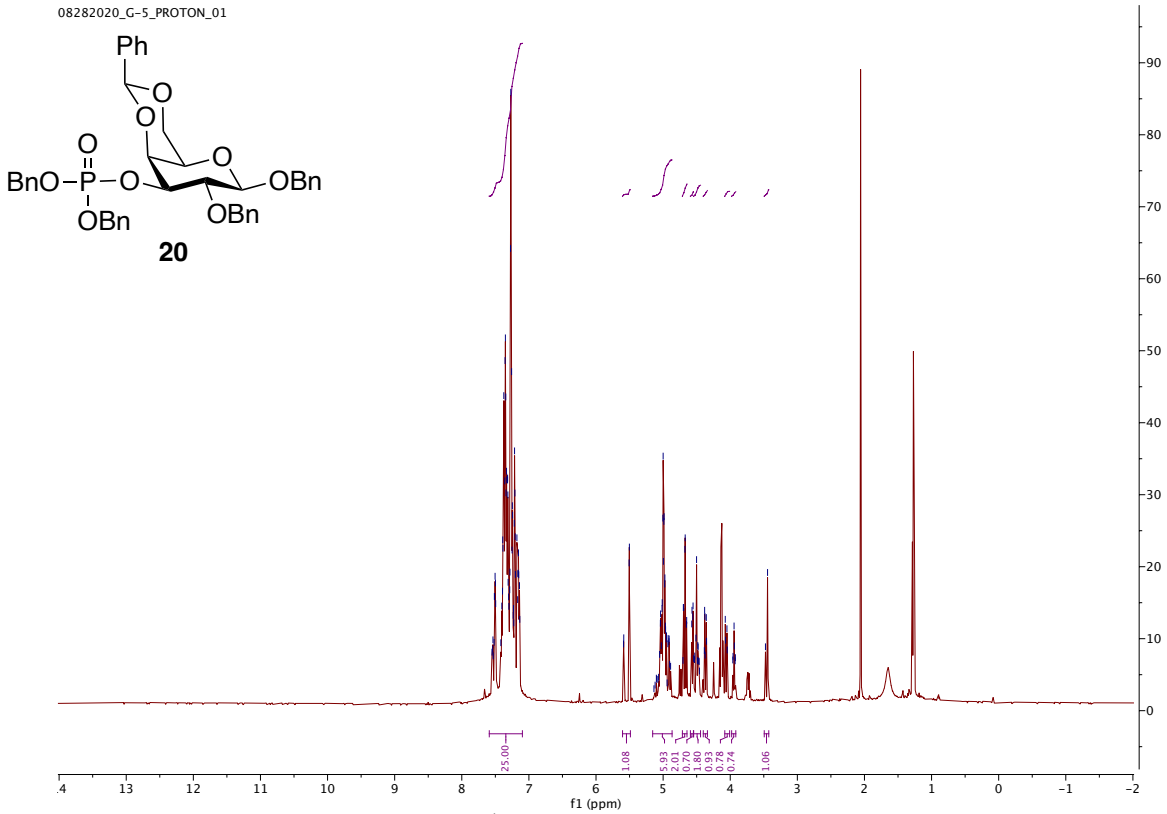

Figure S65. ^{1}H-NMR of **20** ($CDCl_3$, 500 MHz).

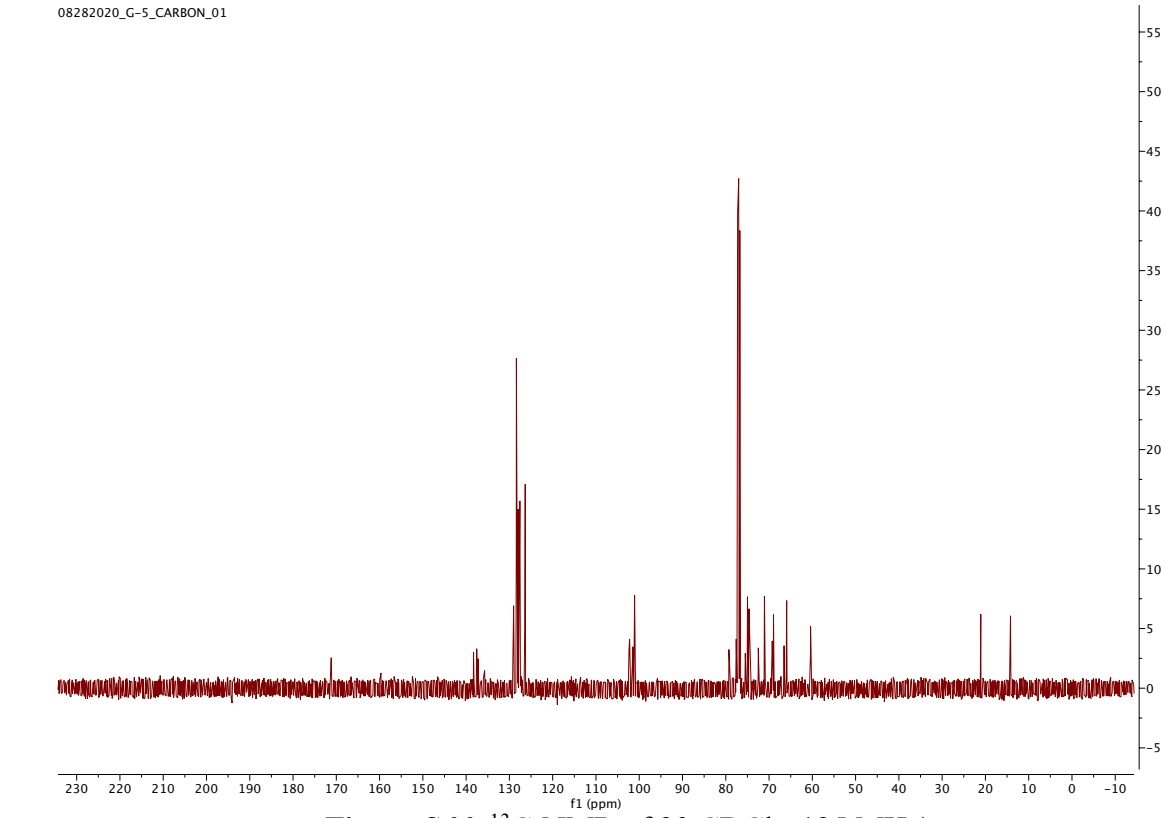

Figure S66. ^{13}C-NMR of **20** $CDCl_3$, 125 MHz).

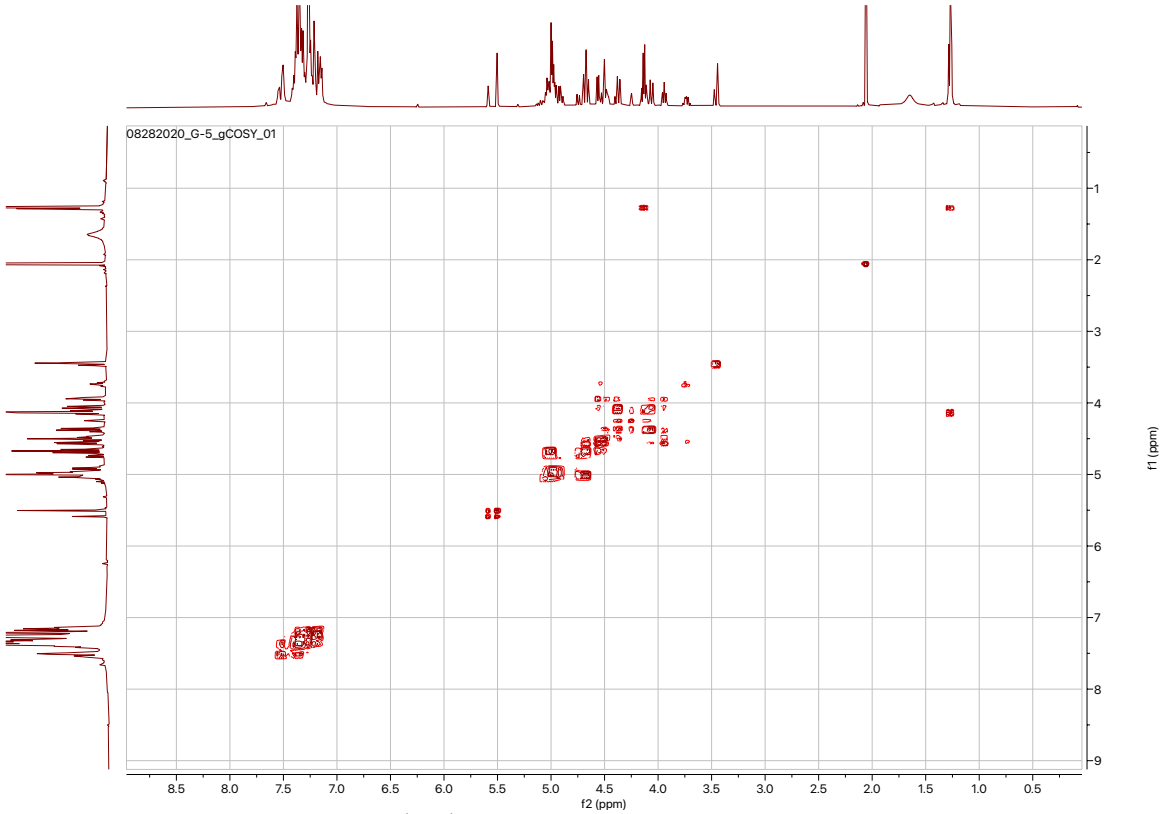

Figure S67. ^{1}H-^{1}H gCOSY of **20** ($CDCl_3$, 500 MHz).

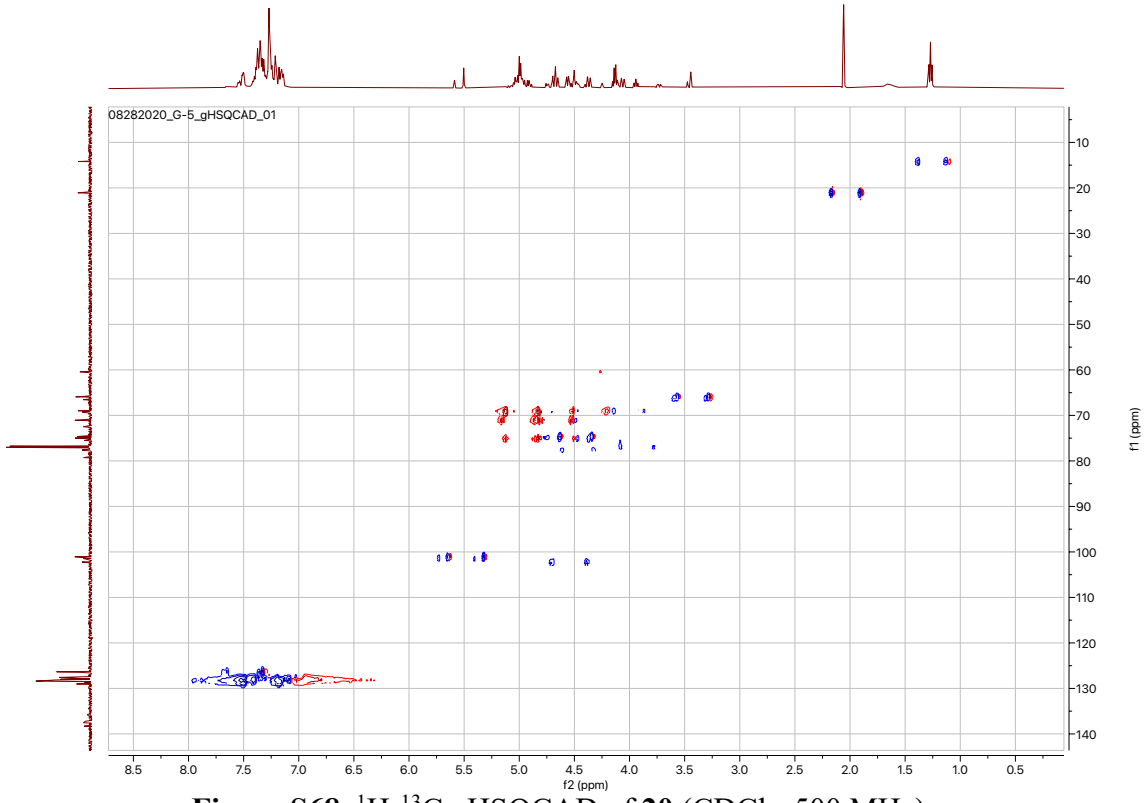

Figure S68. ^{1}H-^{13}C gHSQCAD of **20** ($CDCl_3$, 500 MHz).

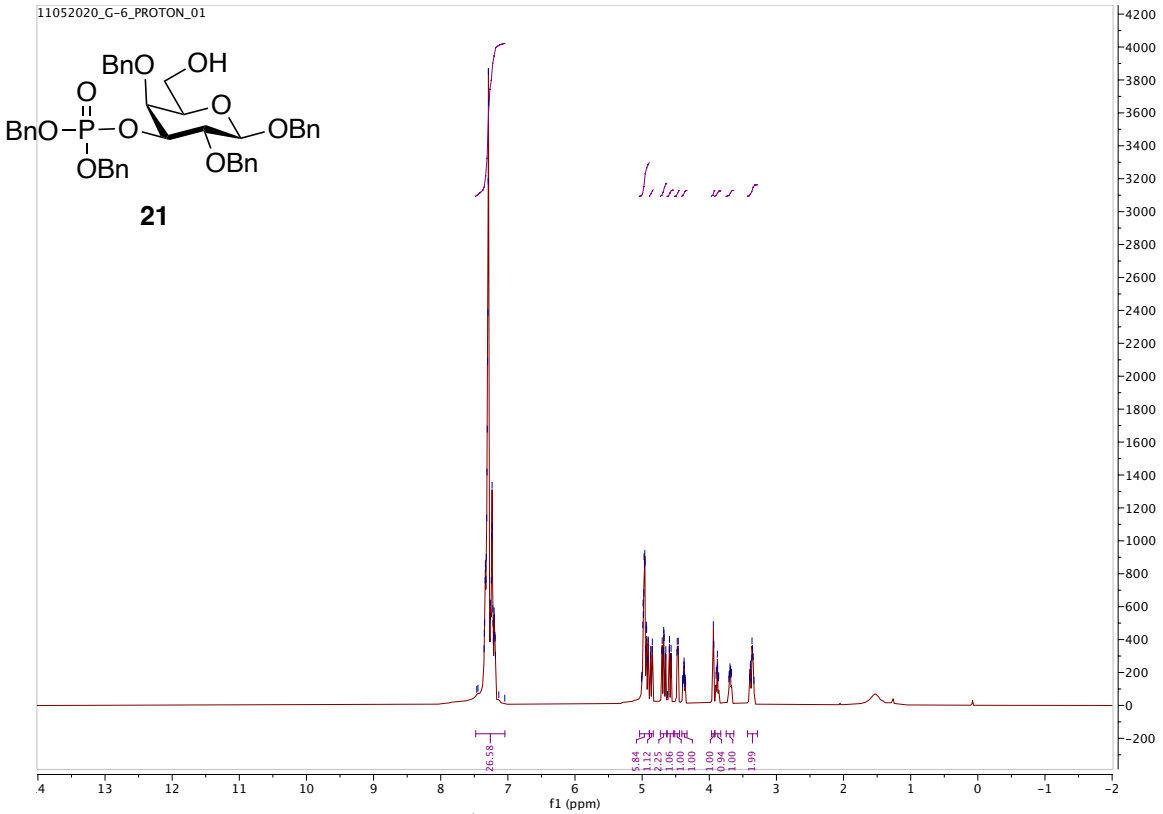

Figure S69. ^{1}H-NMR of **21** ($CDCl_3$, 500 MHz).

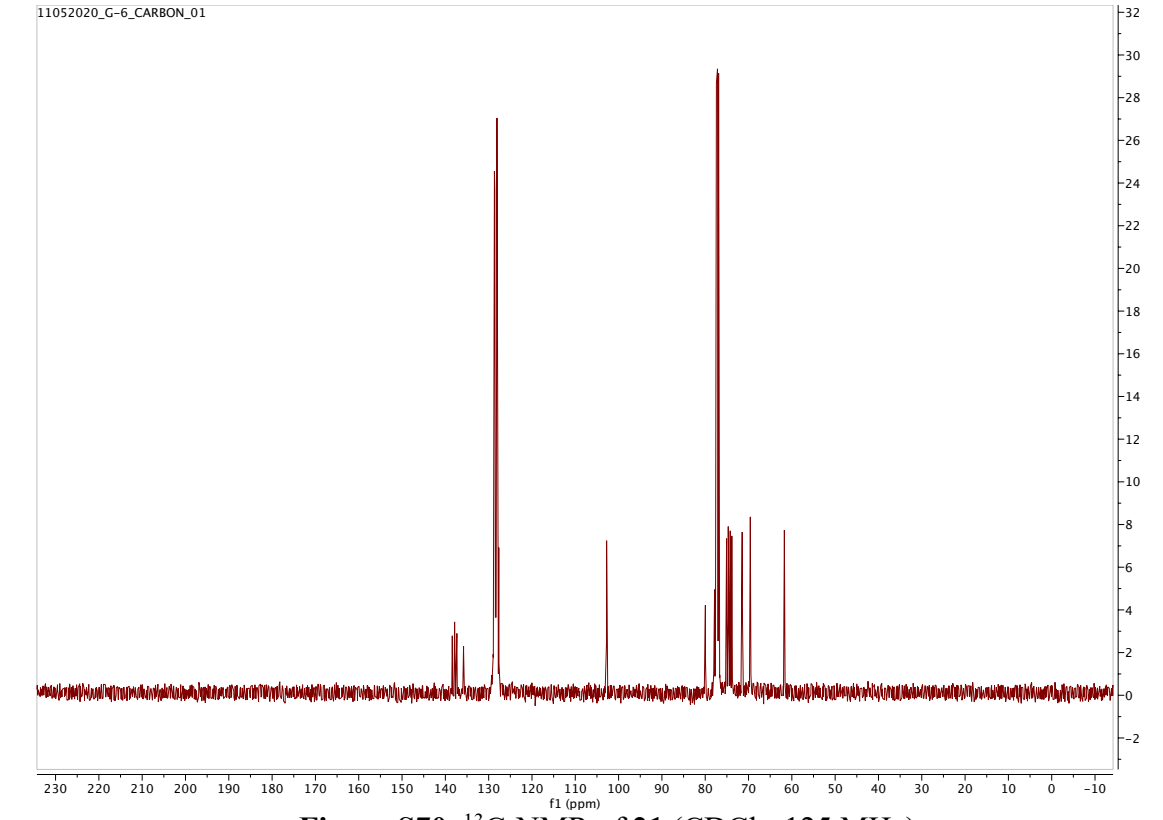

Figure S70. ^{13}C-NMR of **21** ($CDCl_3$, 125 MHz).

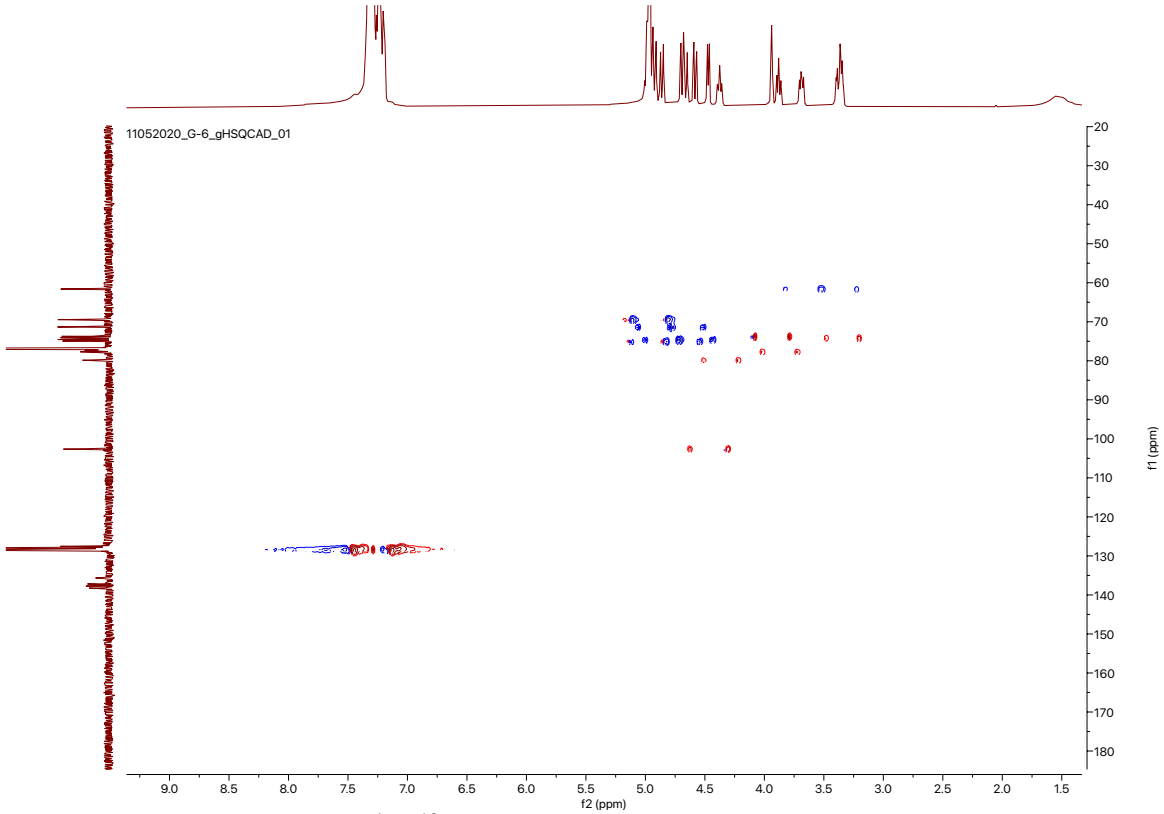

Figure S71. ^{1}H-^{13}C gHSQCAD of **21** ($CDCl_3$, 500 MHz).

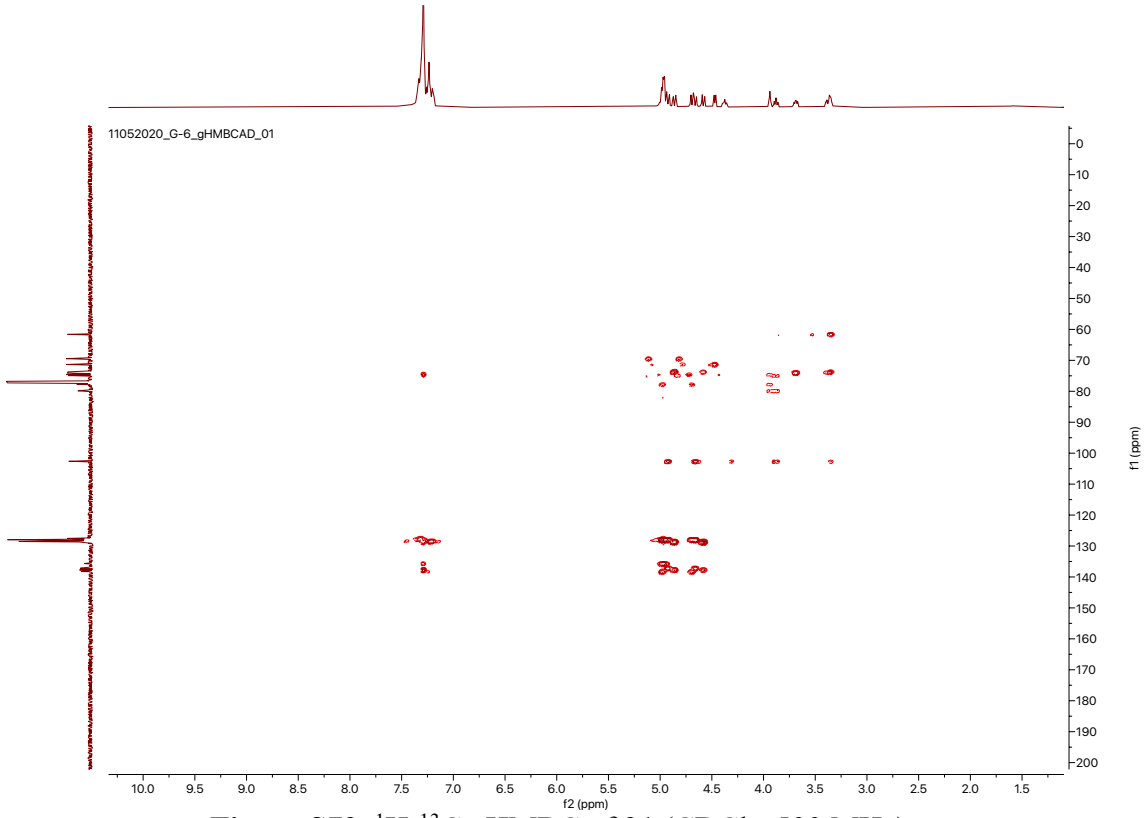

Figure S72. ^{1}H-^{13}C gHMBC of **21** ($CDCl_3$, 500 MHz).

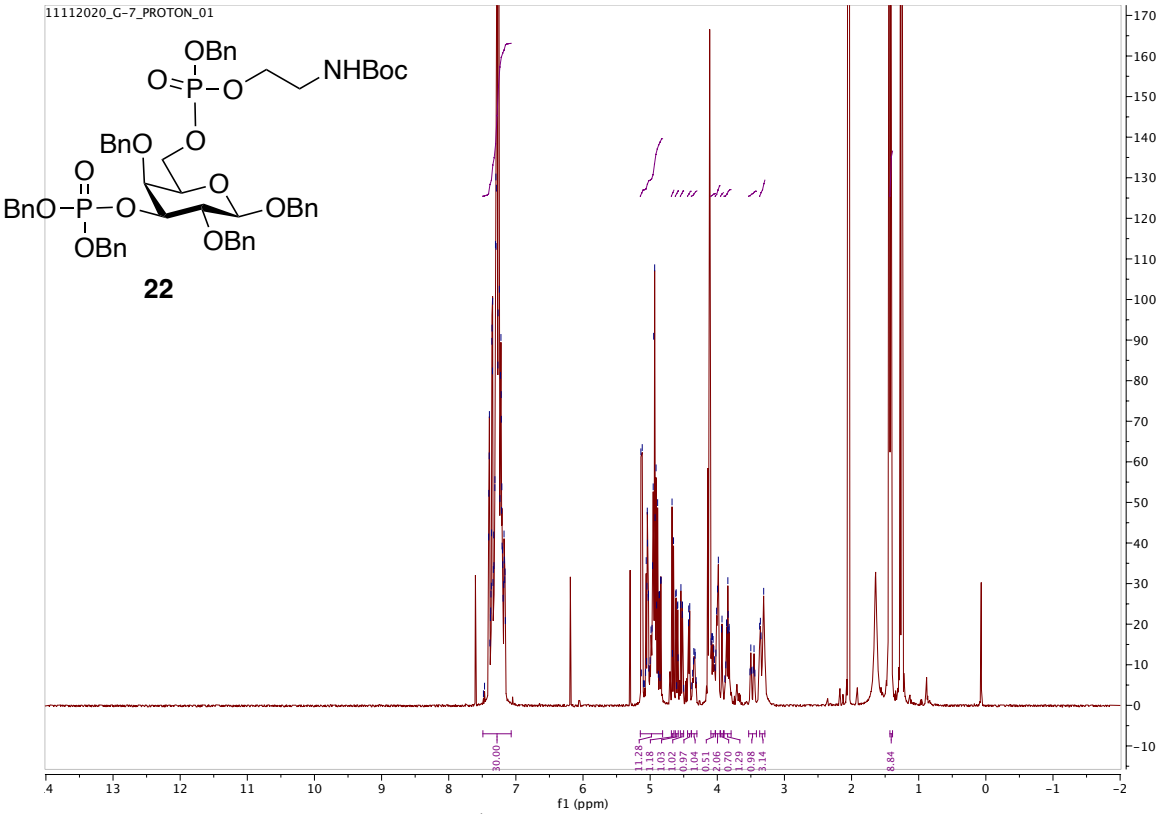

Figure S73. ^{1}H-NMR of **22** ($CDCl_3$, 500 MHz).

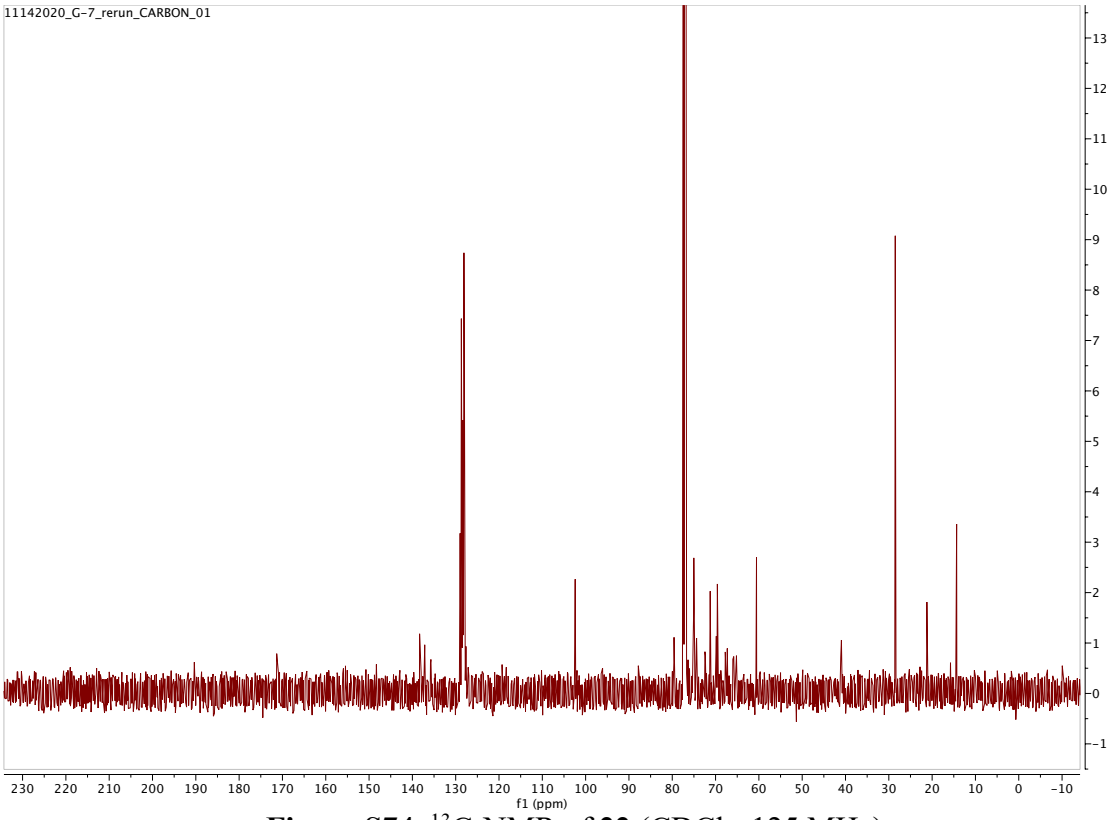

Figure S74. ^{13}C-NMR of **22** ($CDCl_3$, 125 MHz).

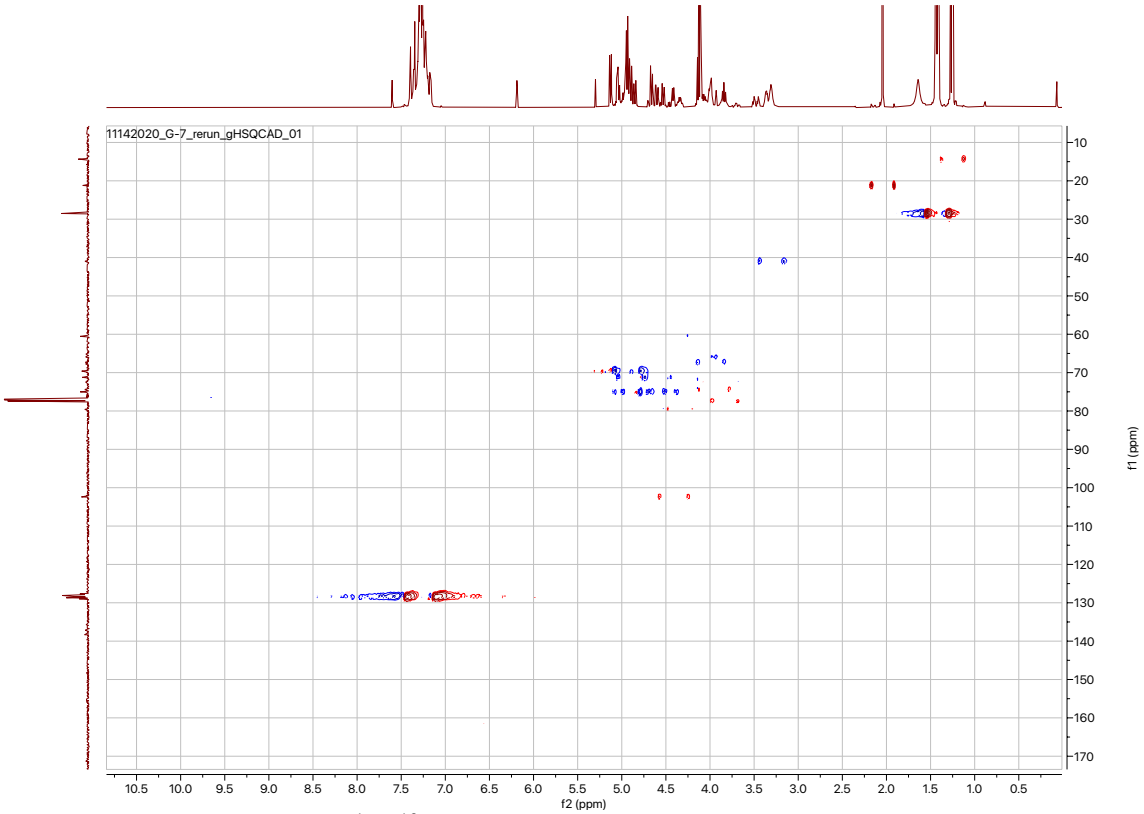

Figure S75. ^{1}H-^{13}C gHSQCAD of **22** ($CDCl_3$, 500 MHz).

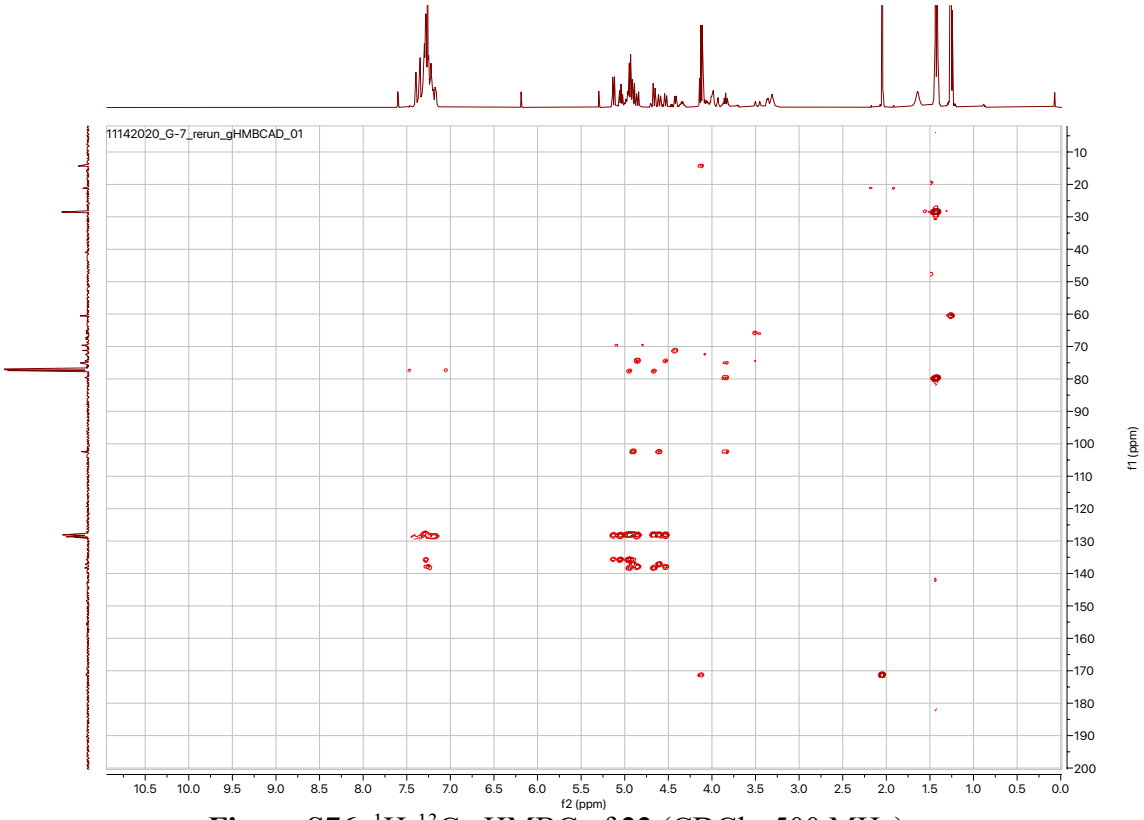

Figure S76. ^{1}H-^{13}C gHMBC of **22** ($CDCl_3$, 500 MHz).

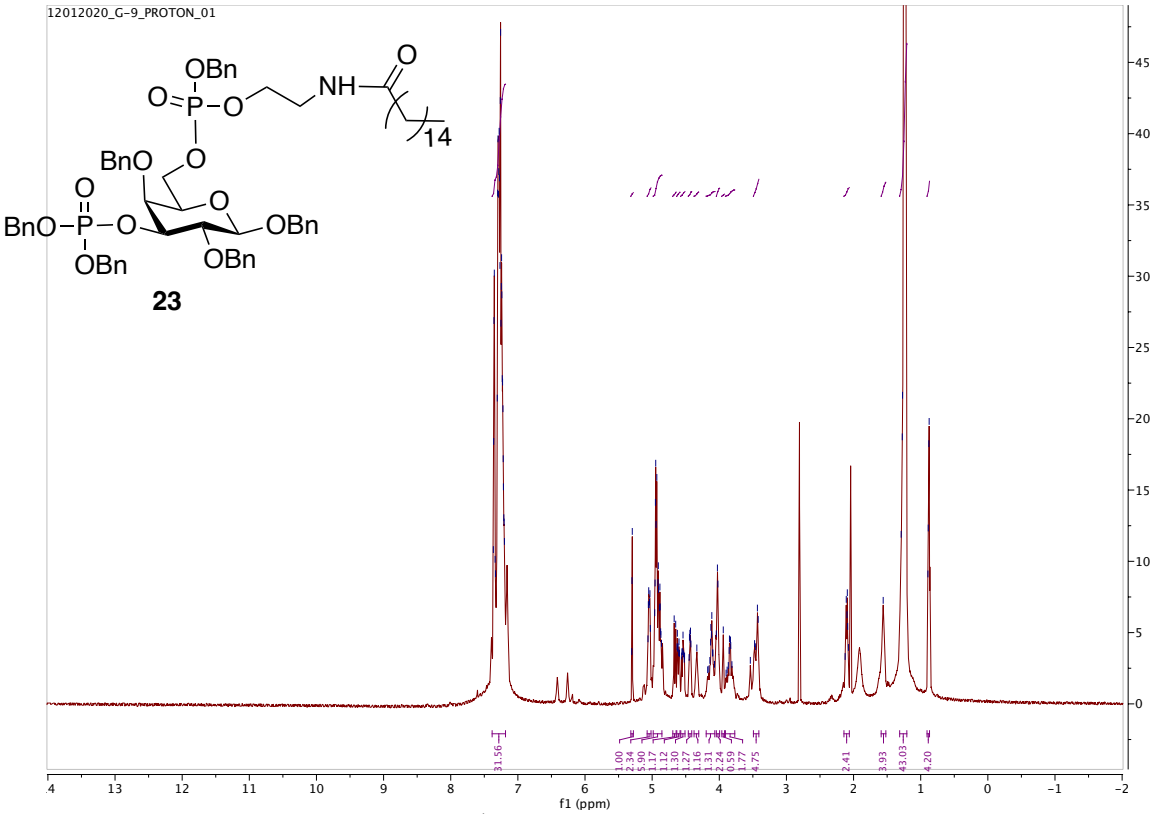

Figure S77. ^{1}H-NMR of **23** ($CDCl_3$, 500 MHz).

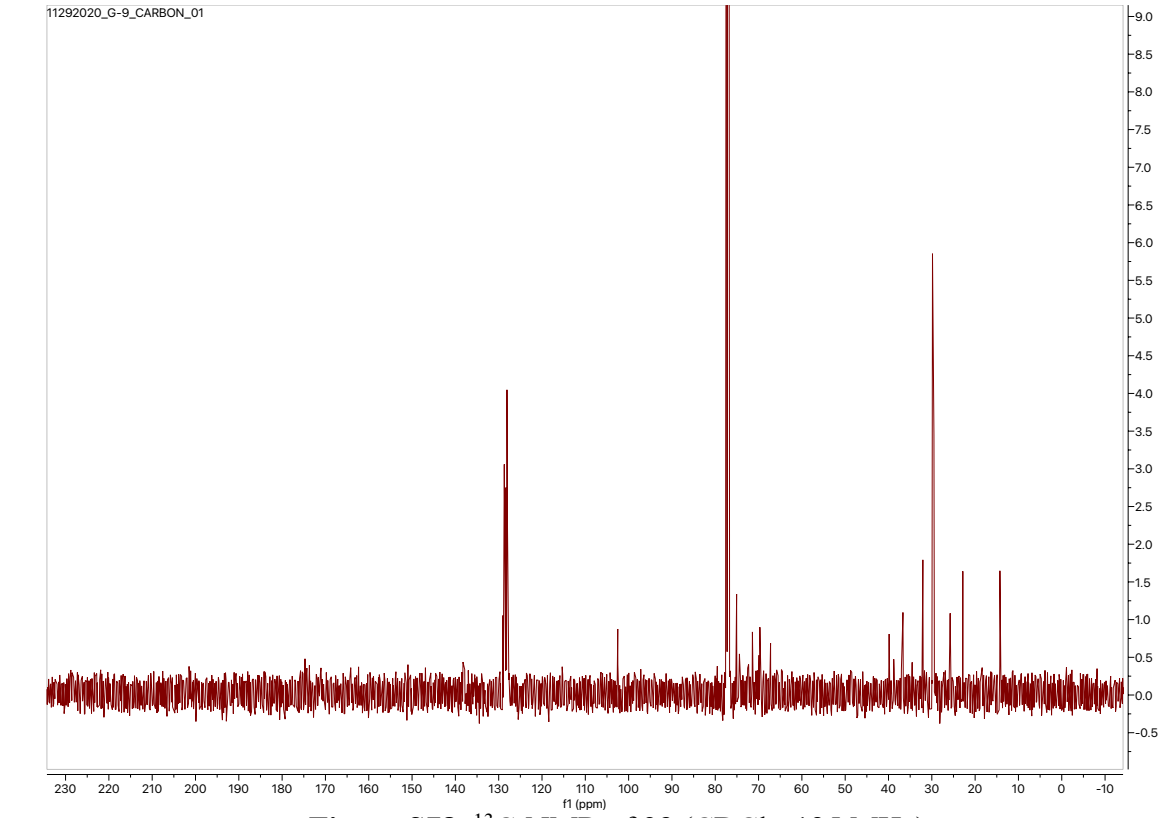

Figure S78. ^{13}C-NMR of **23** ($CDCl_3$, 125 MHz).

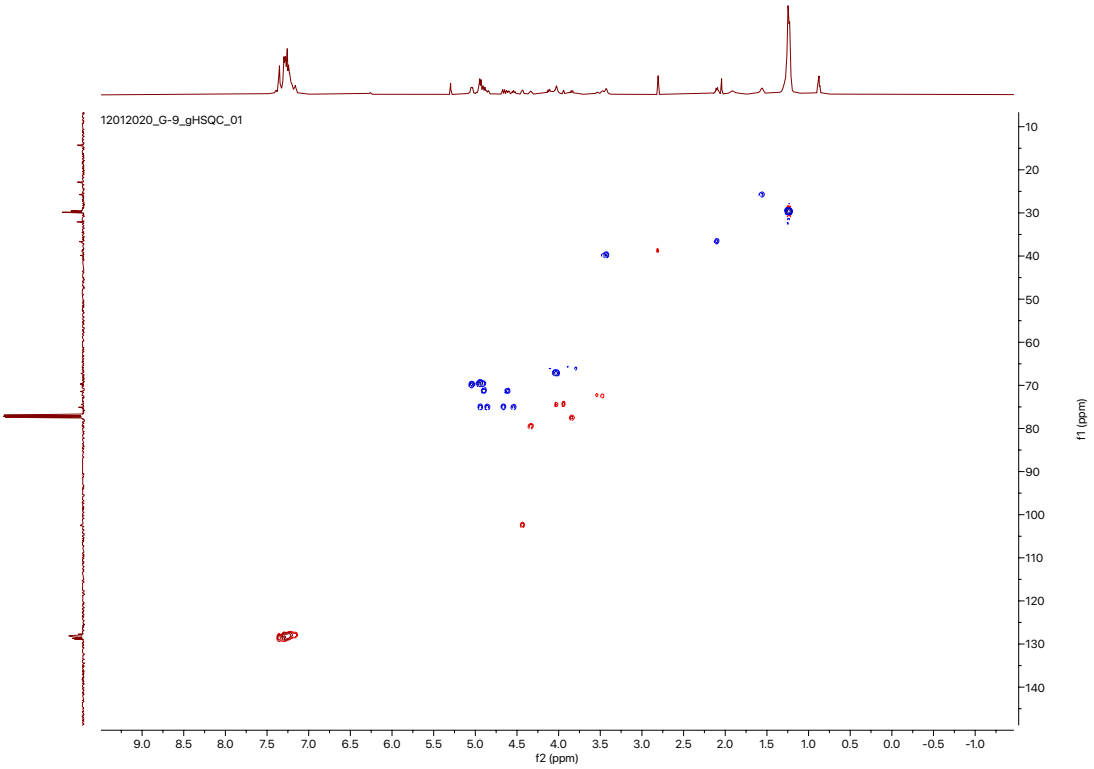

Figure S79. ^{1}H-^{13}C gHSQCAD of **23** ($CDCl_3$, 500 MHz).

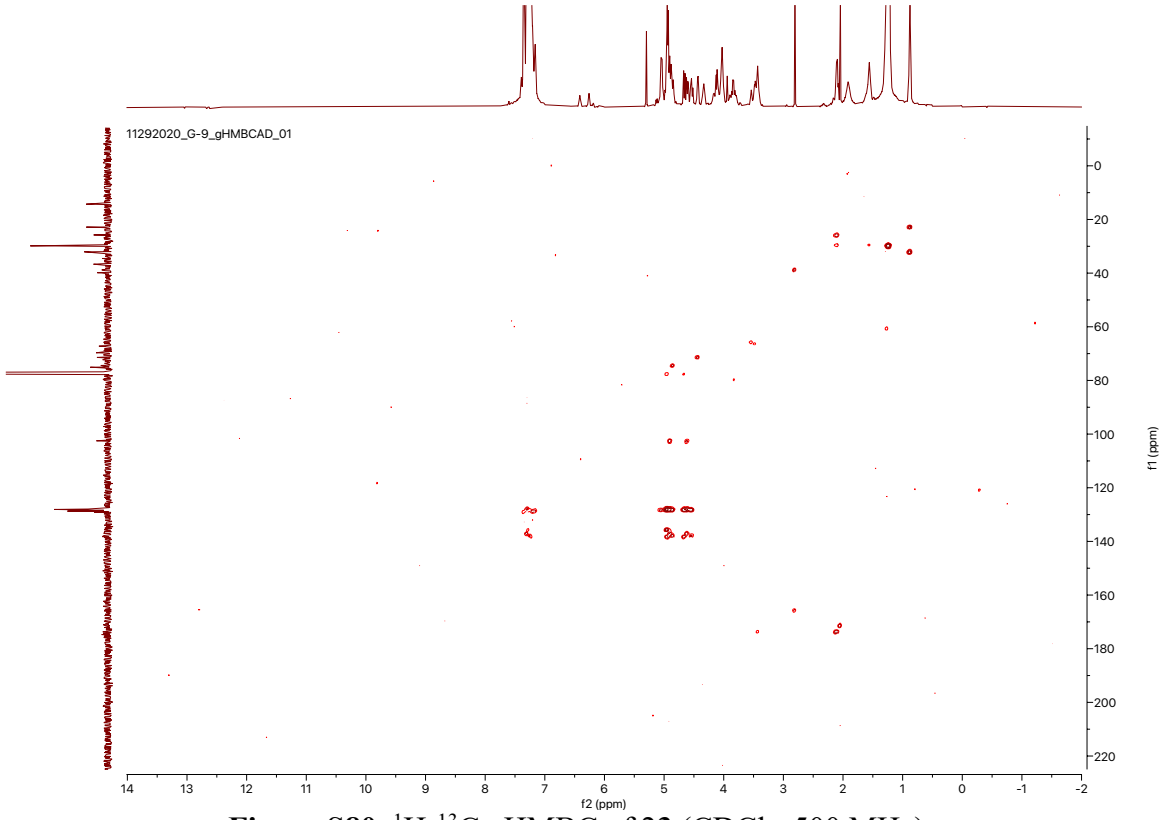

Figure S80. ^{1}H-^{13}C gHMBC of **23** ($CDCl_3$, 500 MHz).

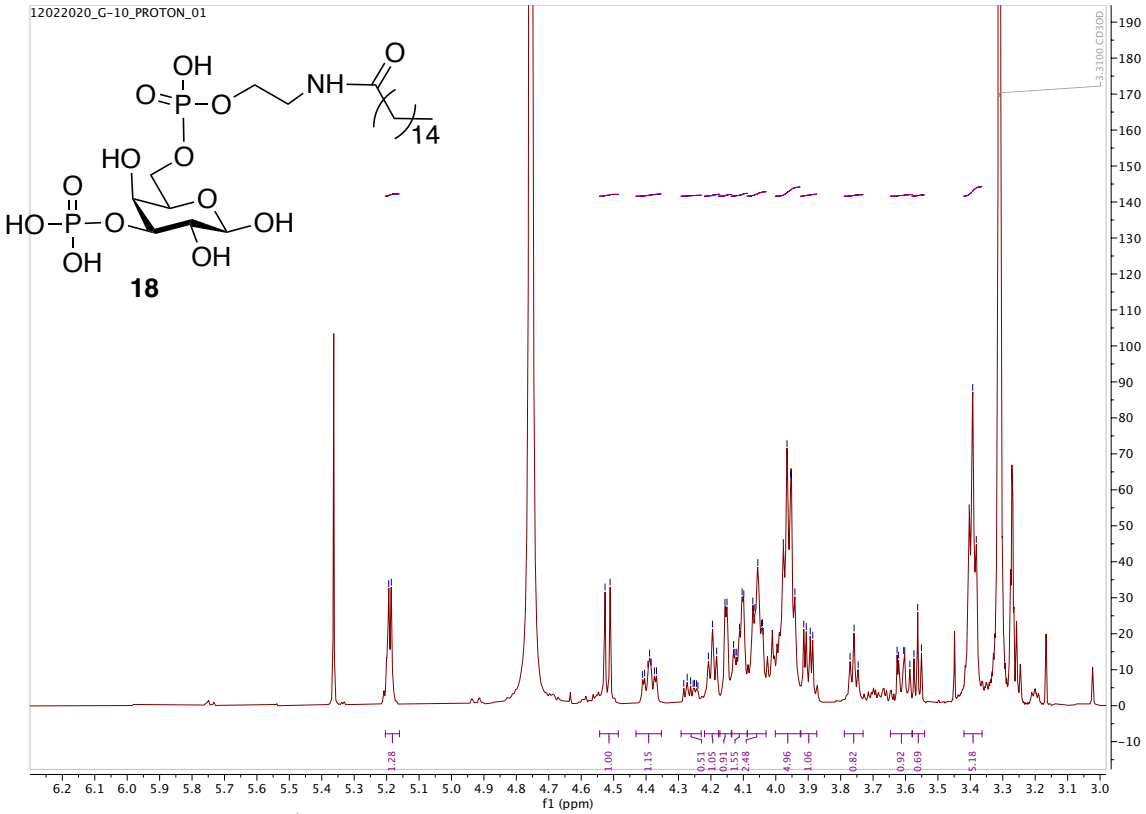

Figure S81. ^{1}H-NMR of **18** ($CDCl_3$: CD_3OD : D_2O 1 : 2 : 0.5, 500 MHz).

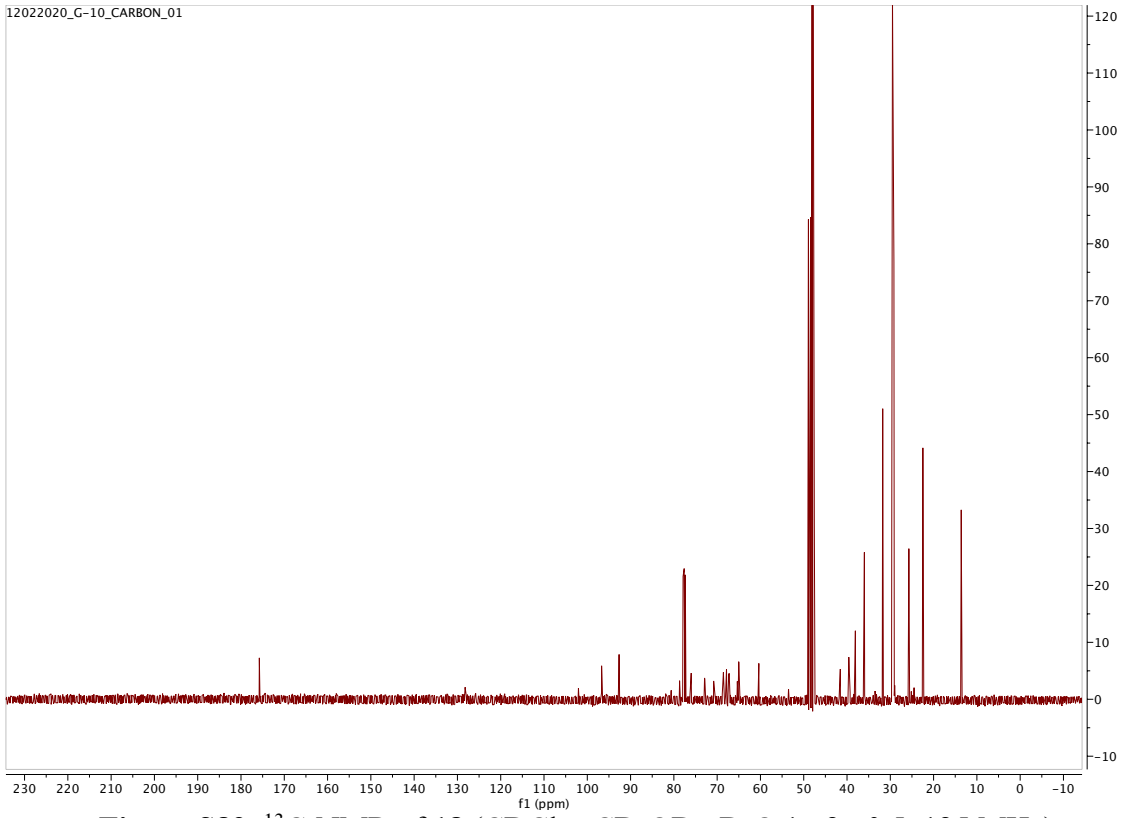

Figure S82. ^{13}C-NMR of **18** ($CDCl_3$: CD_3OD : D_2O 1 : 2 : 0.5, 125 MHz).

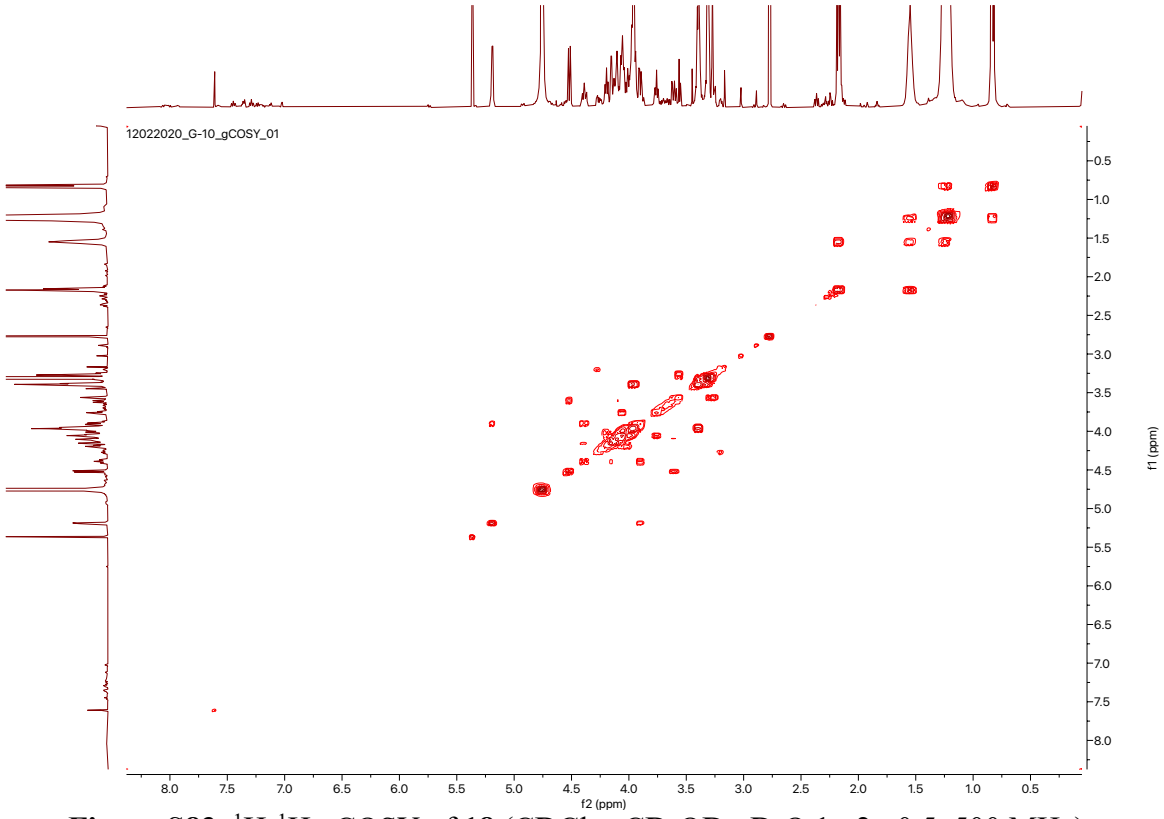

Figure S83. ^{1}H-^{1}H gCOSY of **18** ($CDCl_3$: CD_3OD : D_2O 1 : 2 : 0.5, 500 MHz).

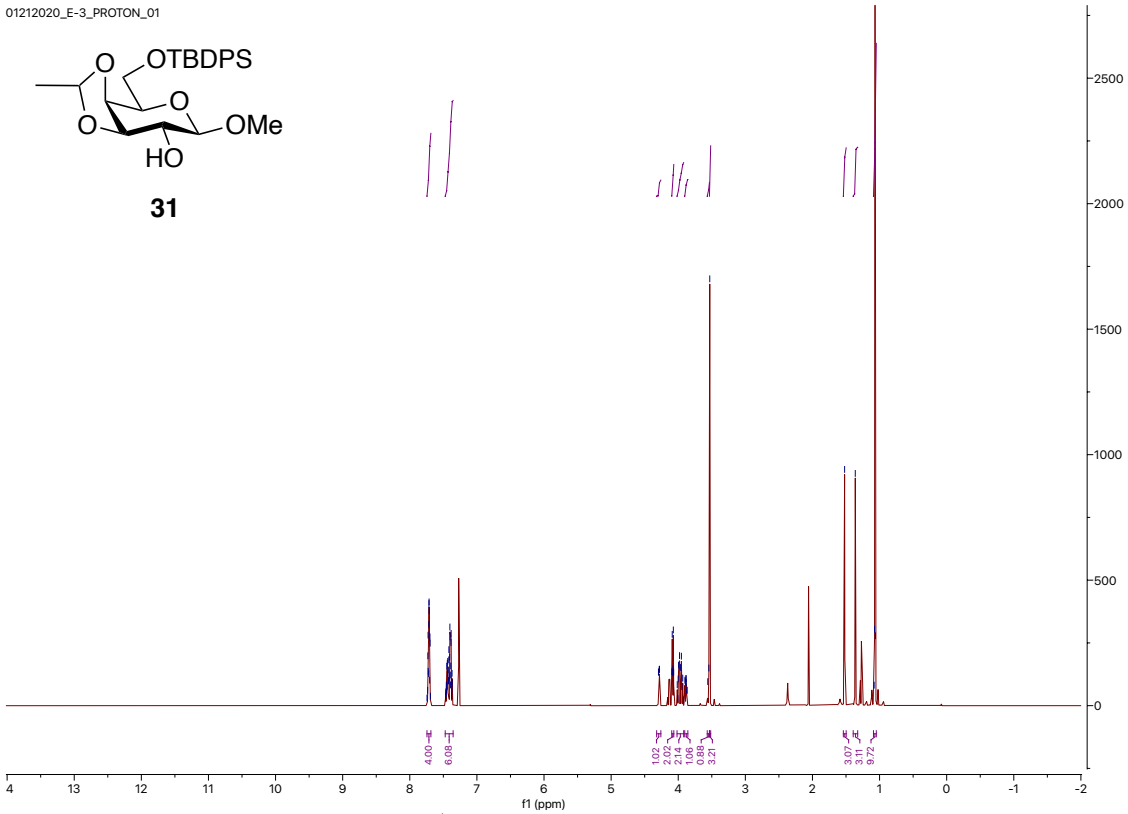

Figure S84. ^{1}H-NMR of **31** ($CDCl_3$, 500 MHz).

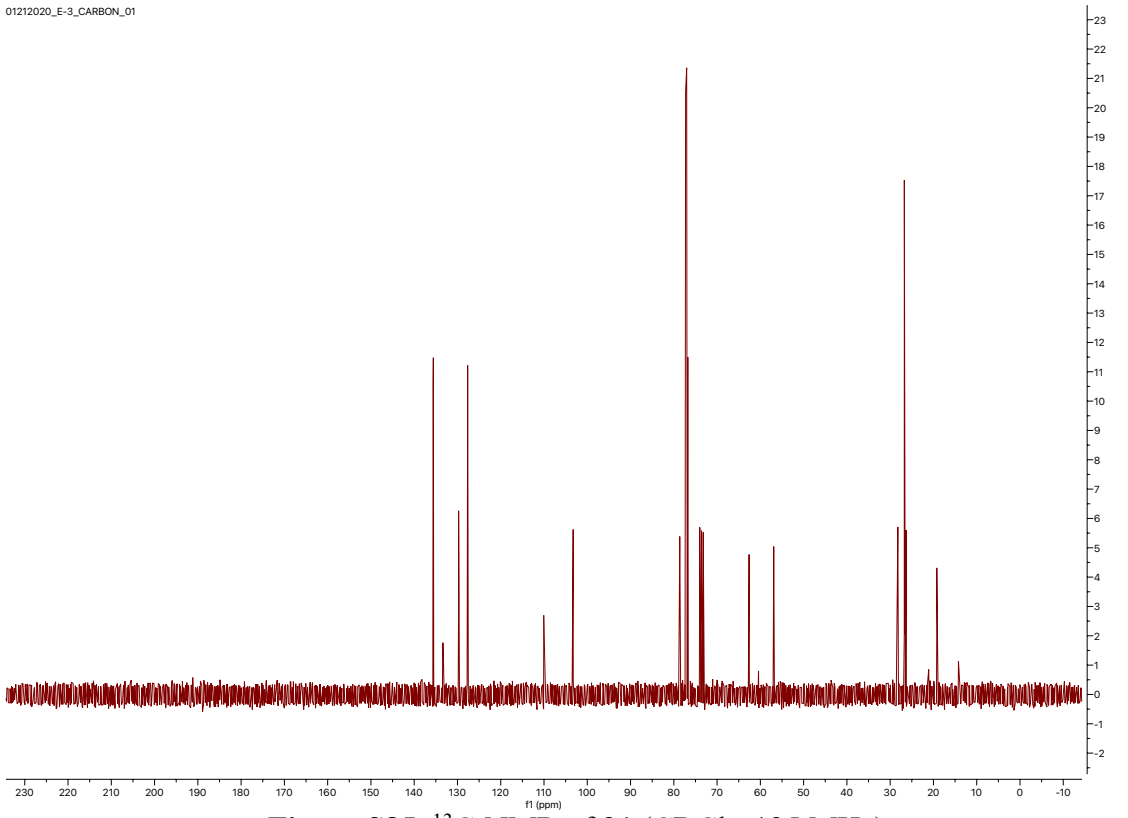

Figure S85. ^{13}C-NMR of **31** ($CDCl_3$, 125 MHz).

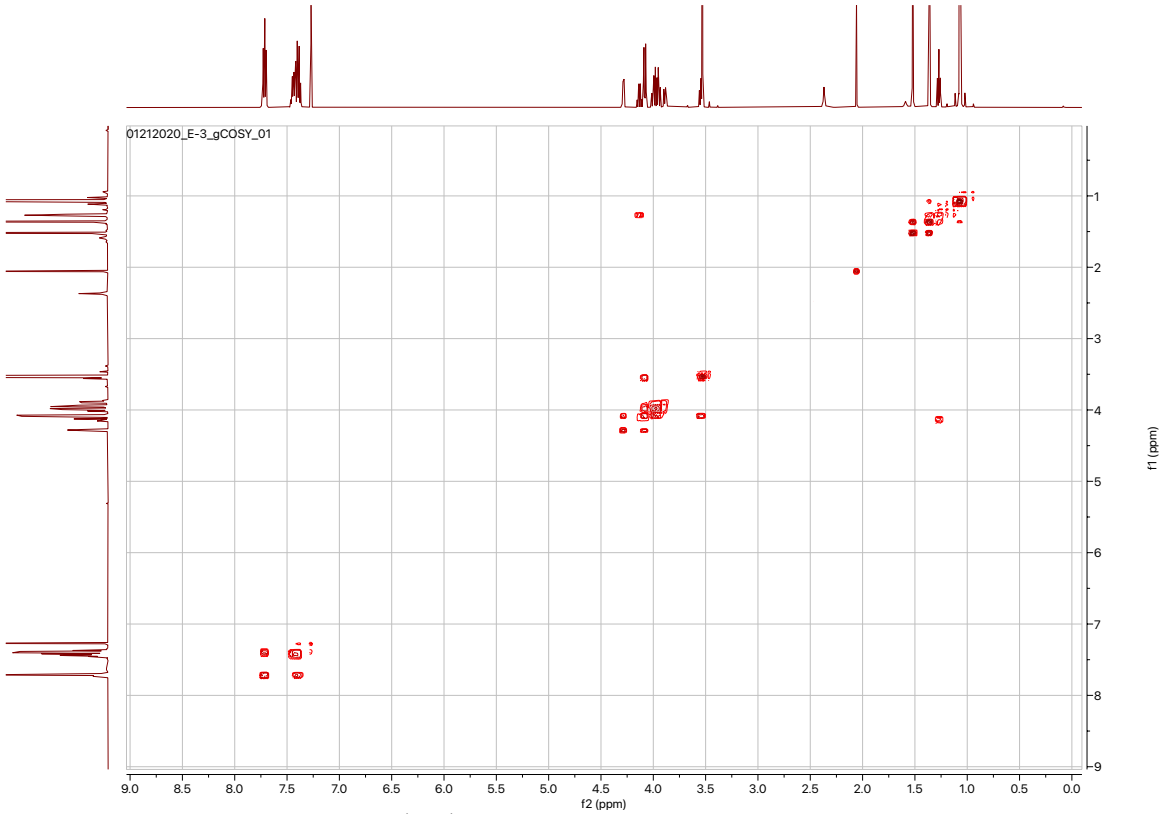

Figure S86. ^{1}H-^{1}H gCOSY of **31** ($CDCl_3$, 500 MHz).

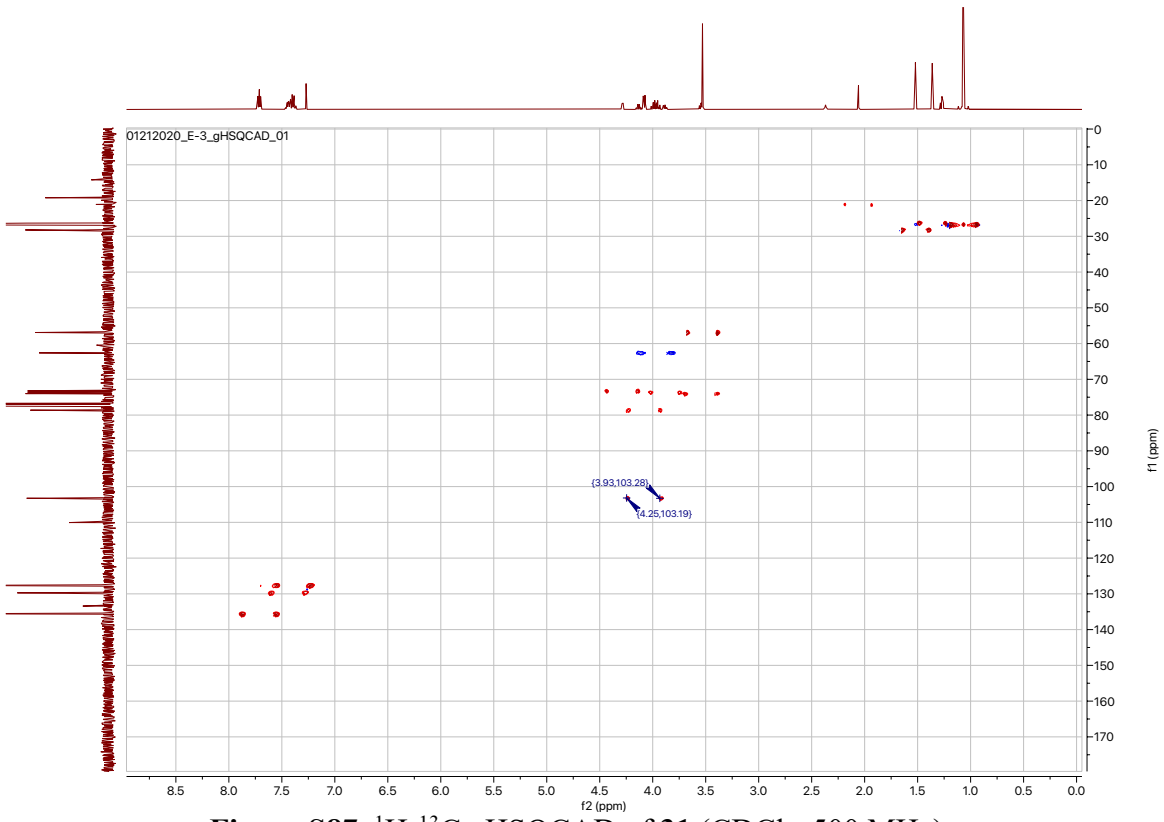

Figure S87. ^{1}H-^{13}C gHSQCAD of **31** ($CDCl_3$, 500 MHz).

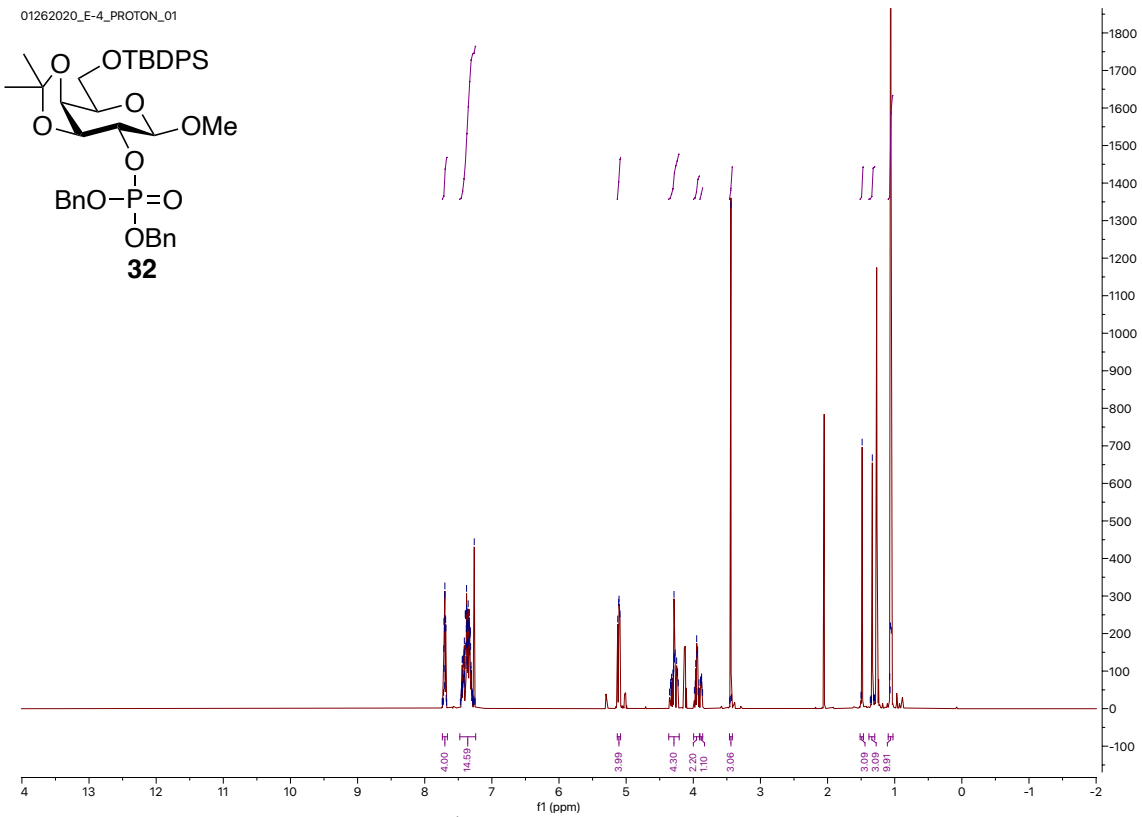

Figure S88. ^{1}H-NMR of **32** ($CDCl_3$, 500 MHz).

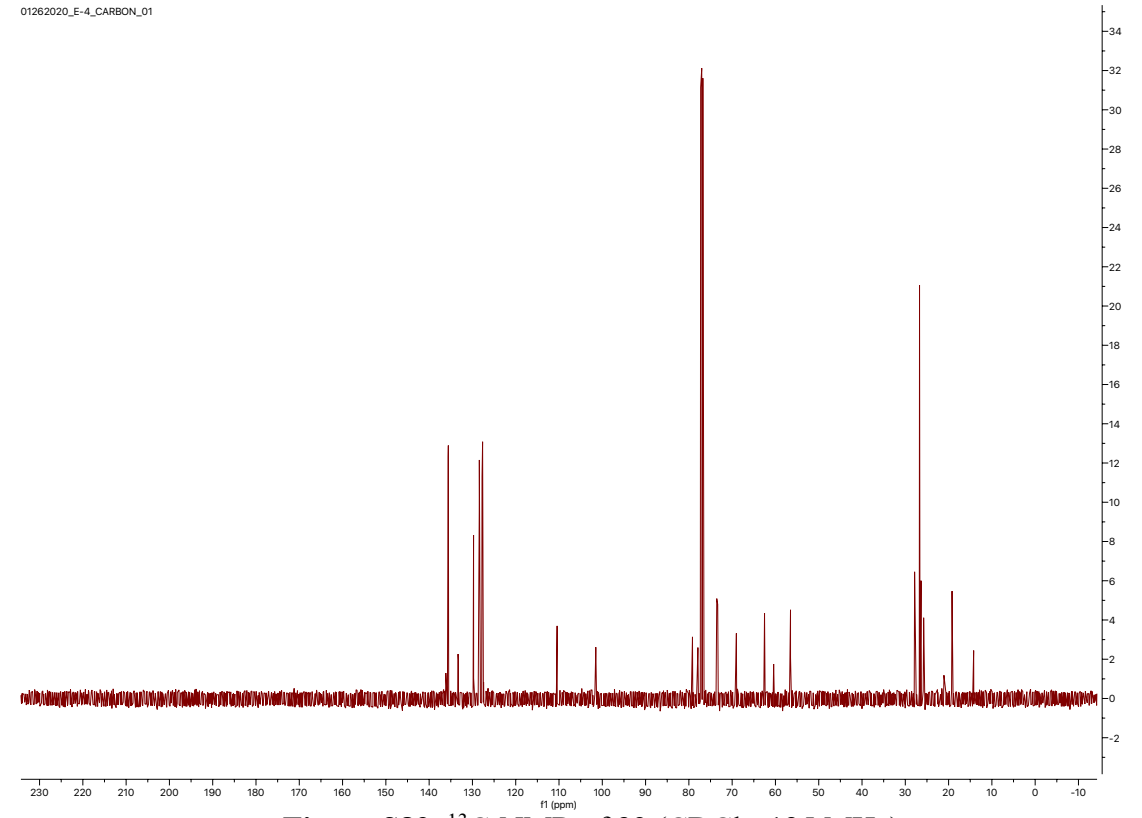

Figure S89. ^{13}C-NMR of **32** ($CDCl_3$, 125 MHz).

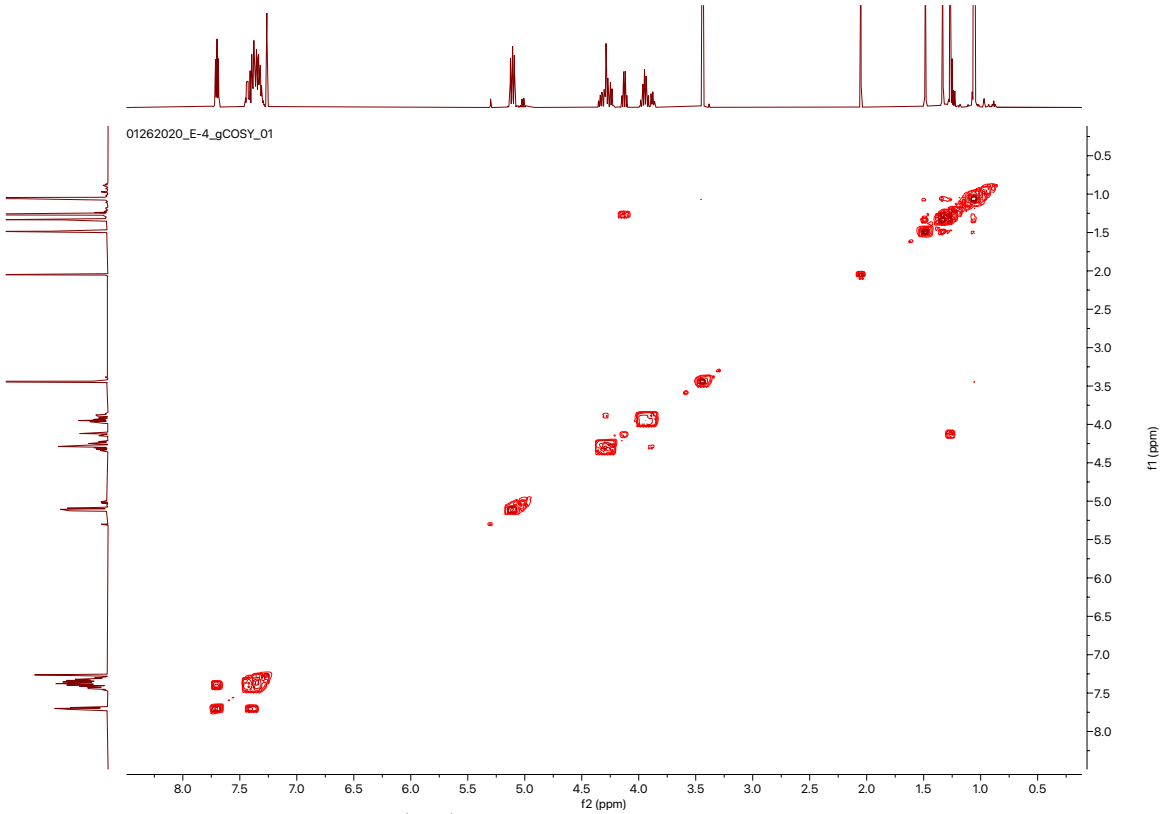

Figure S90. ^{1}H-^{1}H gCOSY of **32** ($CDCl_3$, 500 MHz).

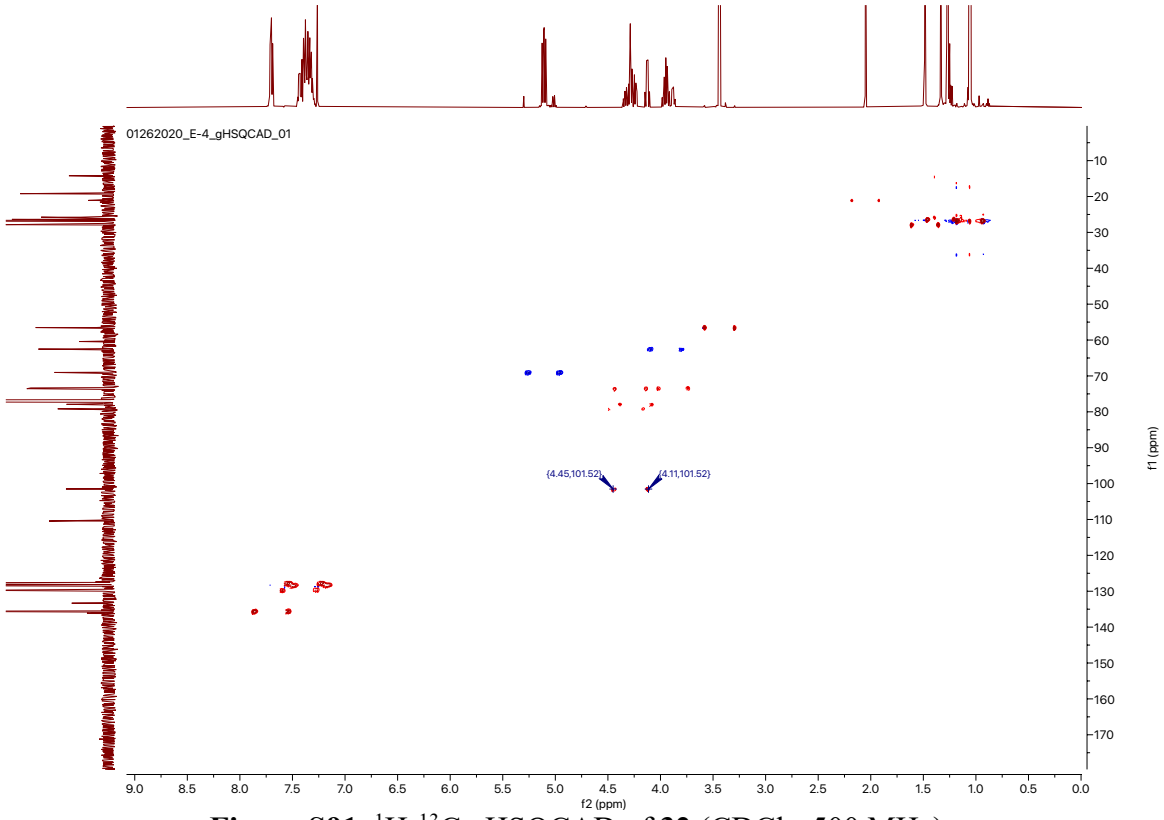

Figure S91. ^{1}H-^{13}C gHSQCAD of **32** ($CDCl_3$, 500 MHz).

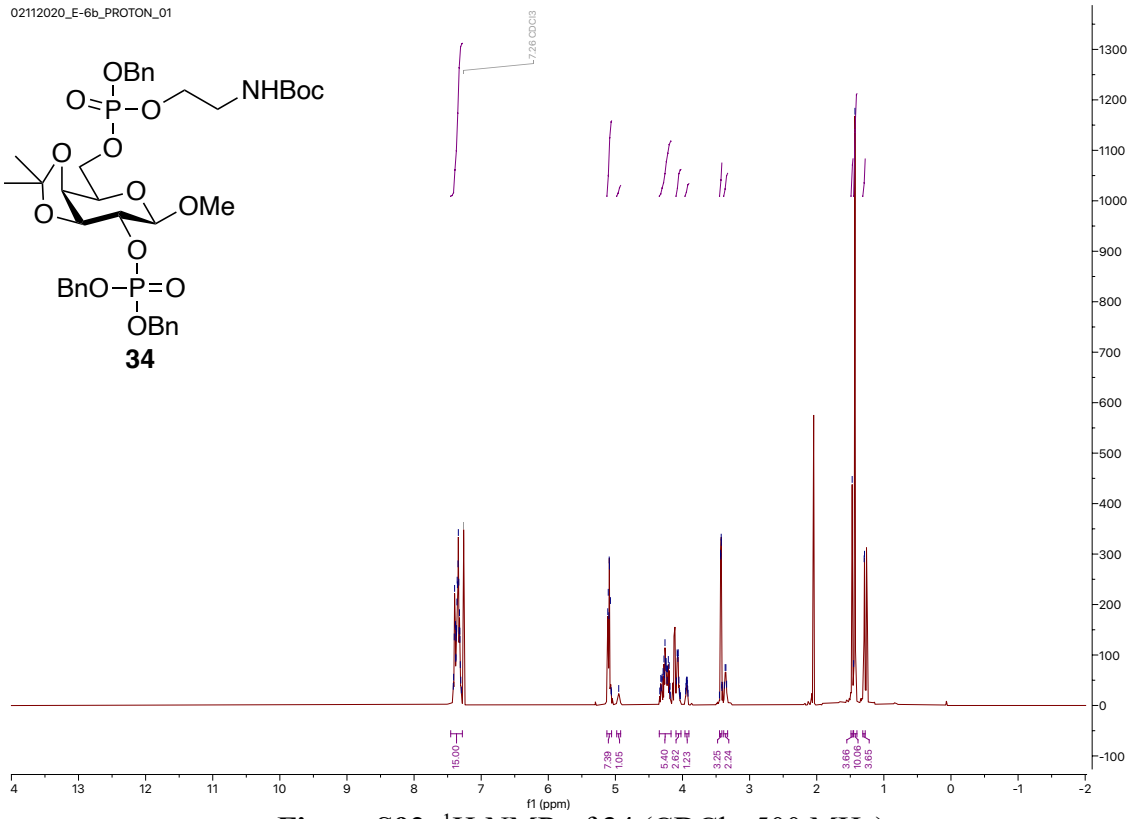

Figure S92. ^{1}H-NMR of **34** ($CDCl_3$, 500 MHz).

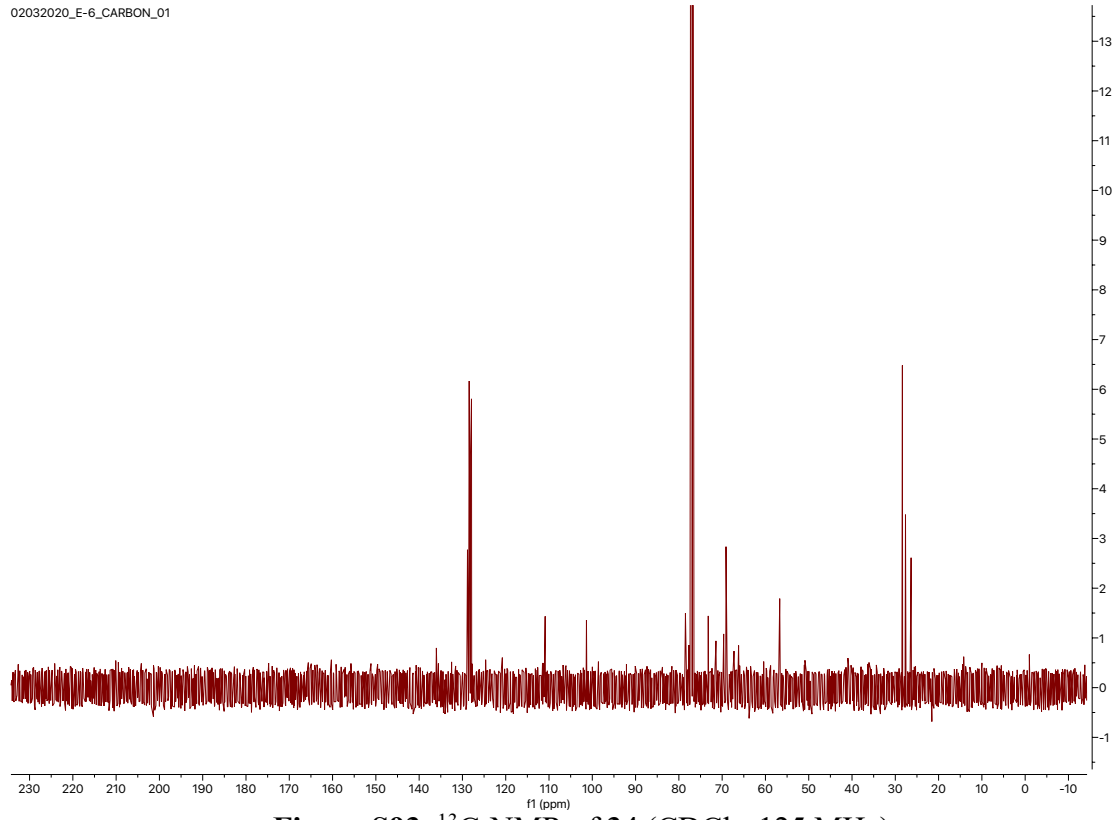

Figure S93. ^{13}C-NMR of **34** ($CDCl_3$, 125 MHz).

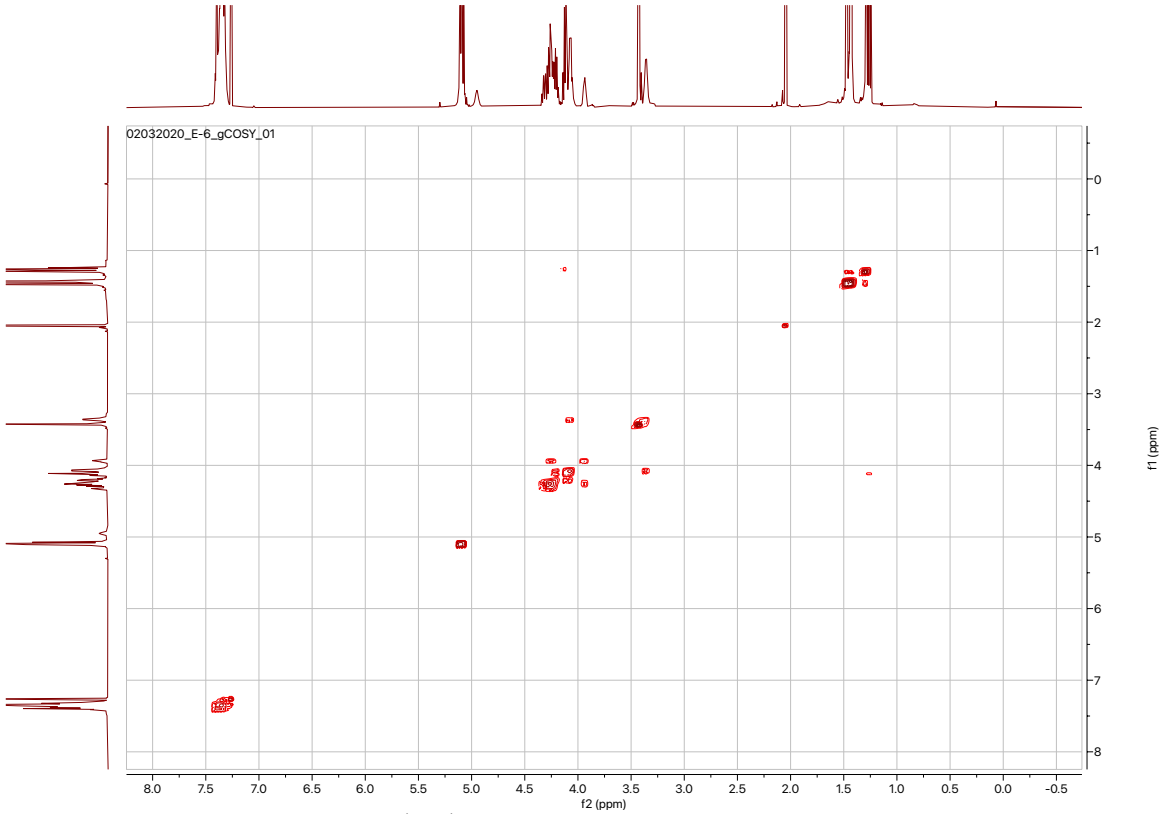

Figure S94. ^{1}H-^{1}H gCOSY of **34** ($CDCl_3$, 500 MHz).

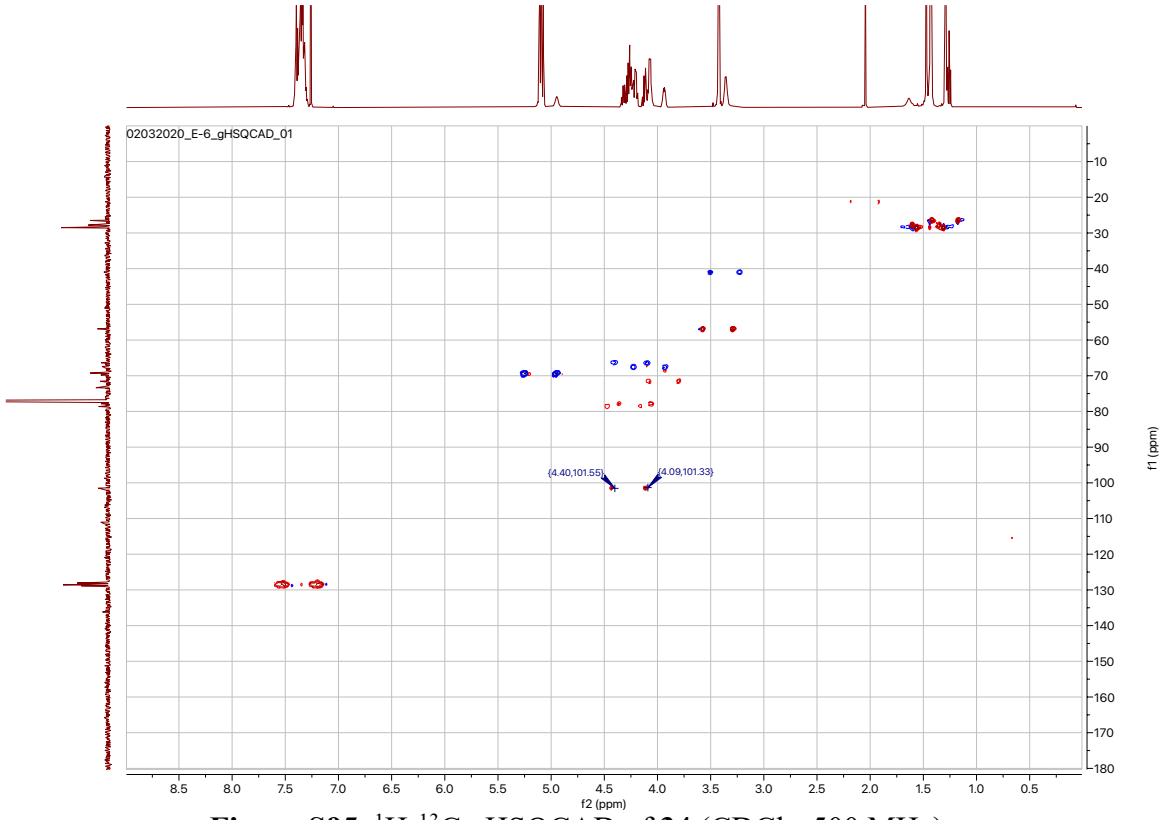

Figure S95. ^{1}H-^{13}C gHSQCAD of **34** ($CDCl_3$, 500 MHz).

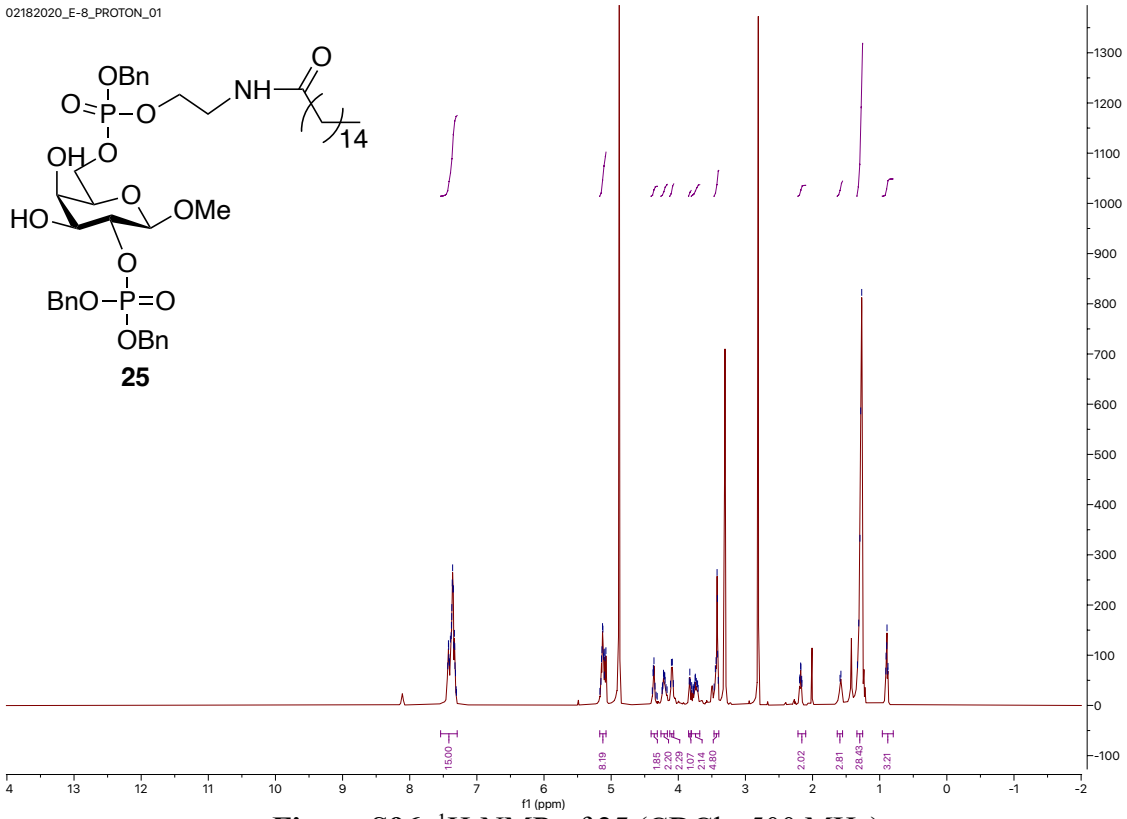

Figure S96. ^{1}H-NMR of **25** ($CDCl_3$, 500 MHz).

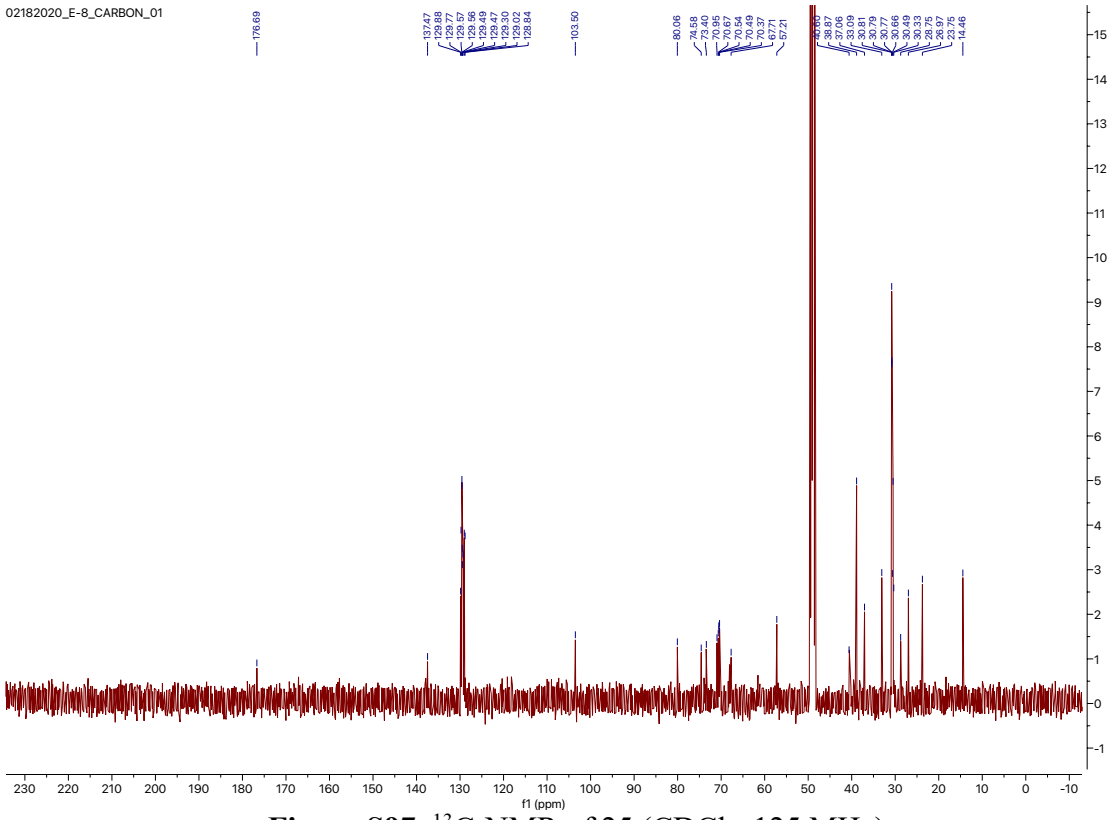

Figure S97. ^{13}C-NMR of 25 ($CDCl_3$, 125 MHz).

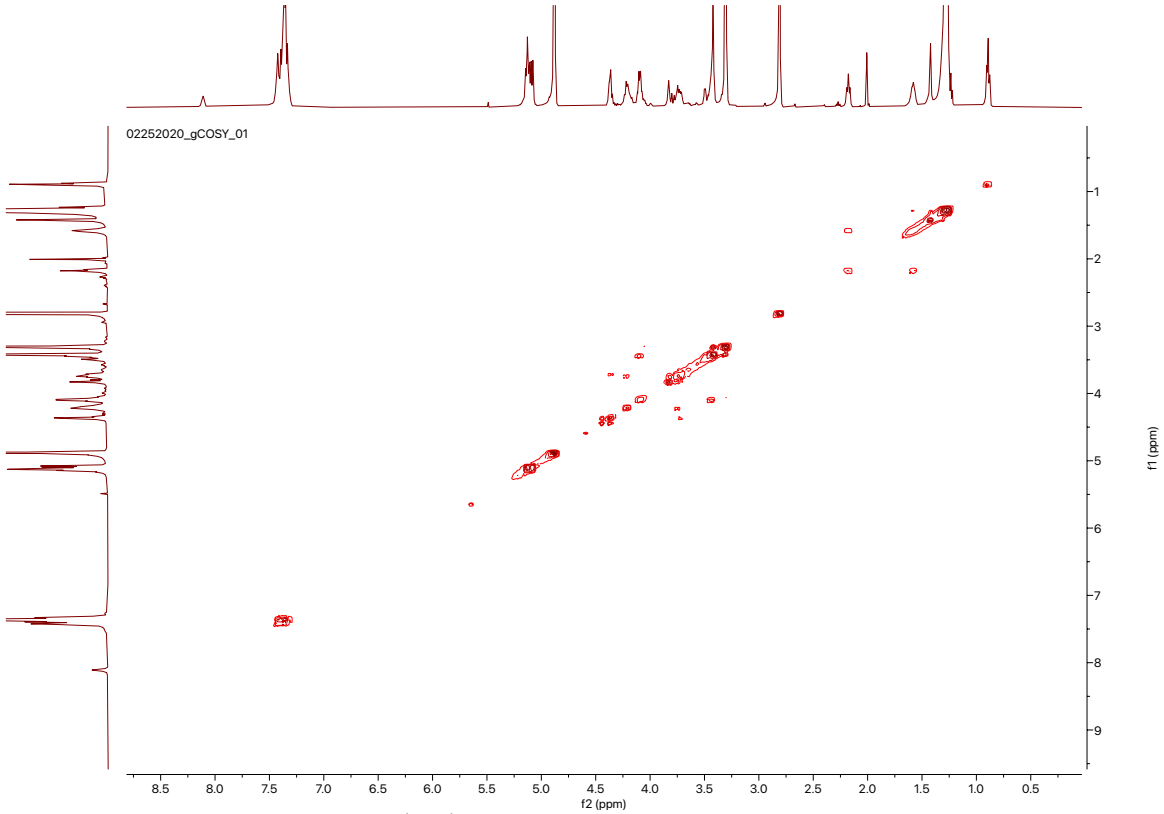

Figure S98. ^{1}H-^{1}H gCOSY of **25** ($CDCl_3$, 500 MHz).

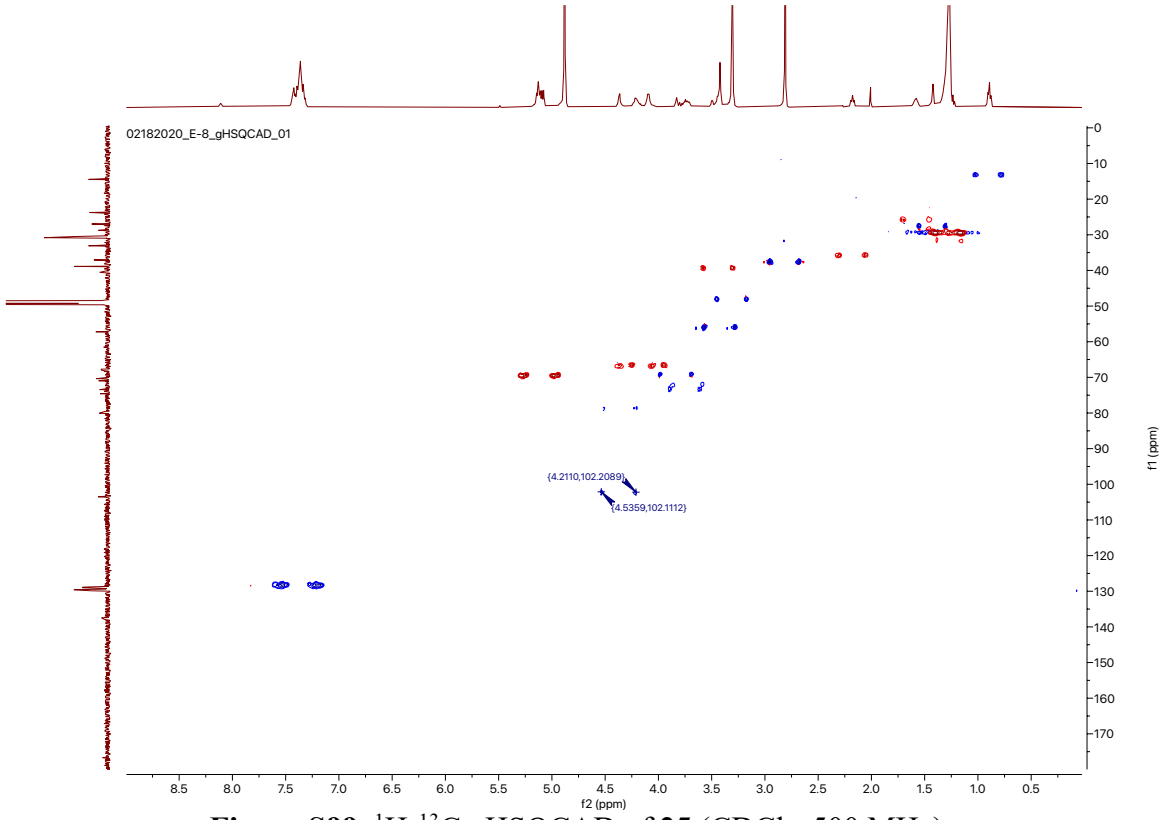

Figure S99. ^{1}H-^{13}C gHSQCAD of **25** ($CDCl_3$, 500 MHz).

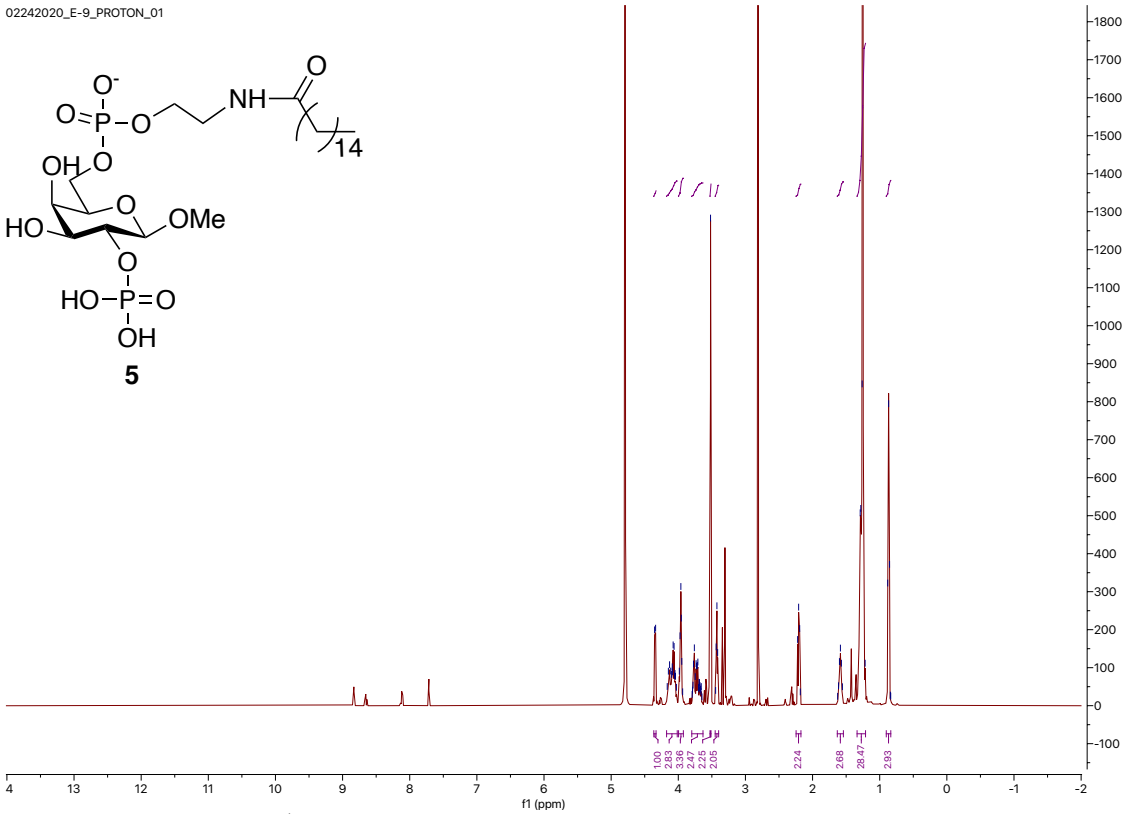

Figure S100. ^{1}H-NMR of **5** ($CDCl_3$: CD_3OD : D_2O 1 : 2 : 0.5, 500 MHz).

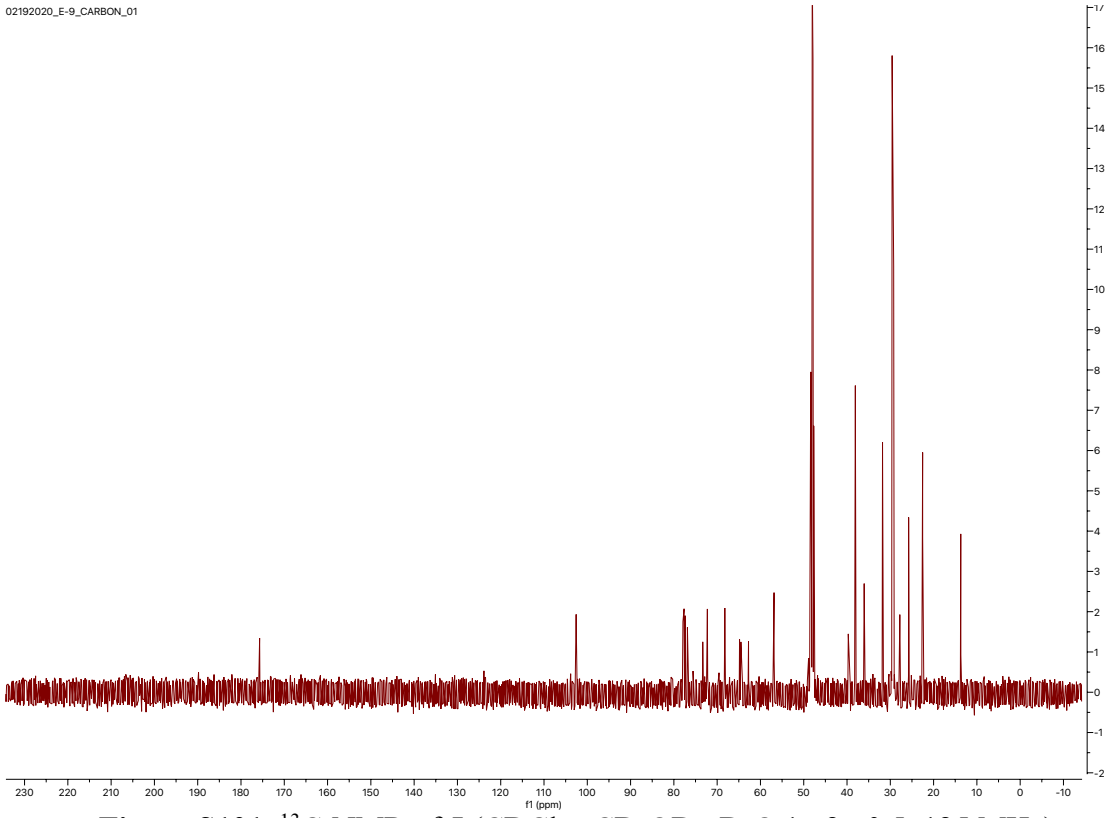

Figure S101. ^{13}C-NMR of **5** ($CDCl_3$: CD_3OD : D_2O 1 : 2 : 0.5, 125 MHz).

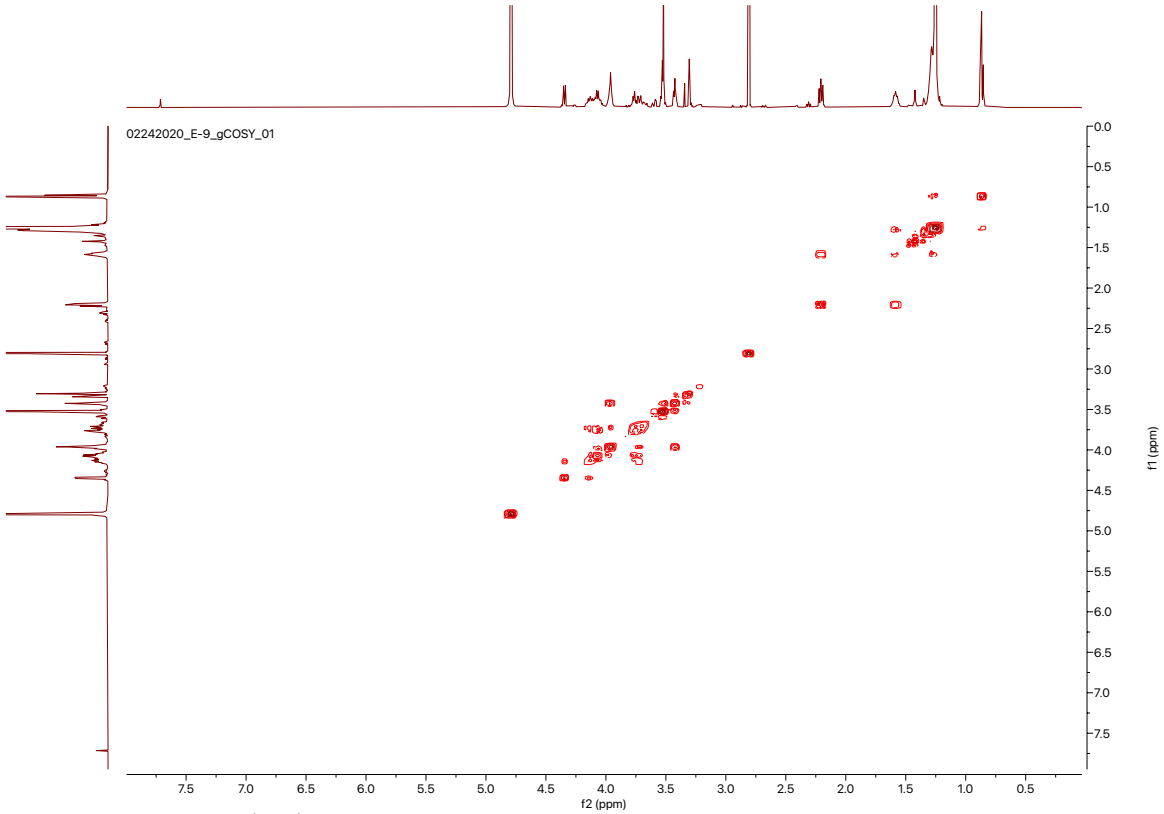

Figure S102. ^{1}H-^{1}H gCOSY of **5** ($CDCl_3$: CD_3OD : D_2O 1 : 2 : 0.5, 500 MHz).

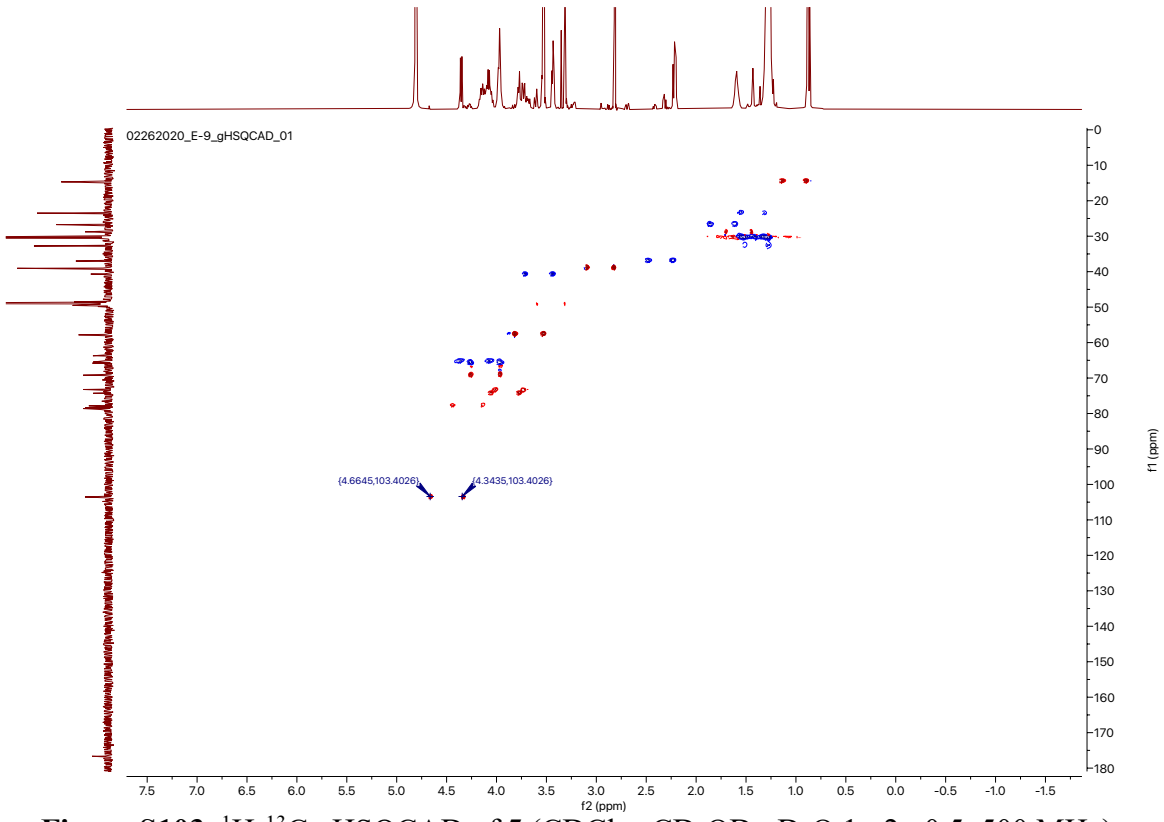

Figure S103. ^{1}H-^{13}C gHSQCAD of **5** ($CDCl_3$: CD_3OD : D_2O 1 : 2 : 0.5, 500 MHz).

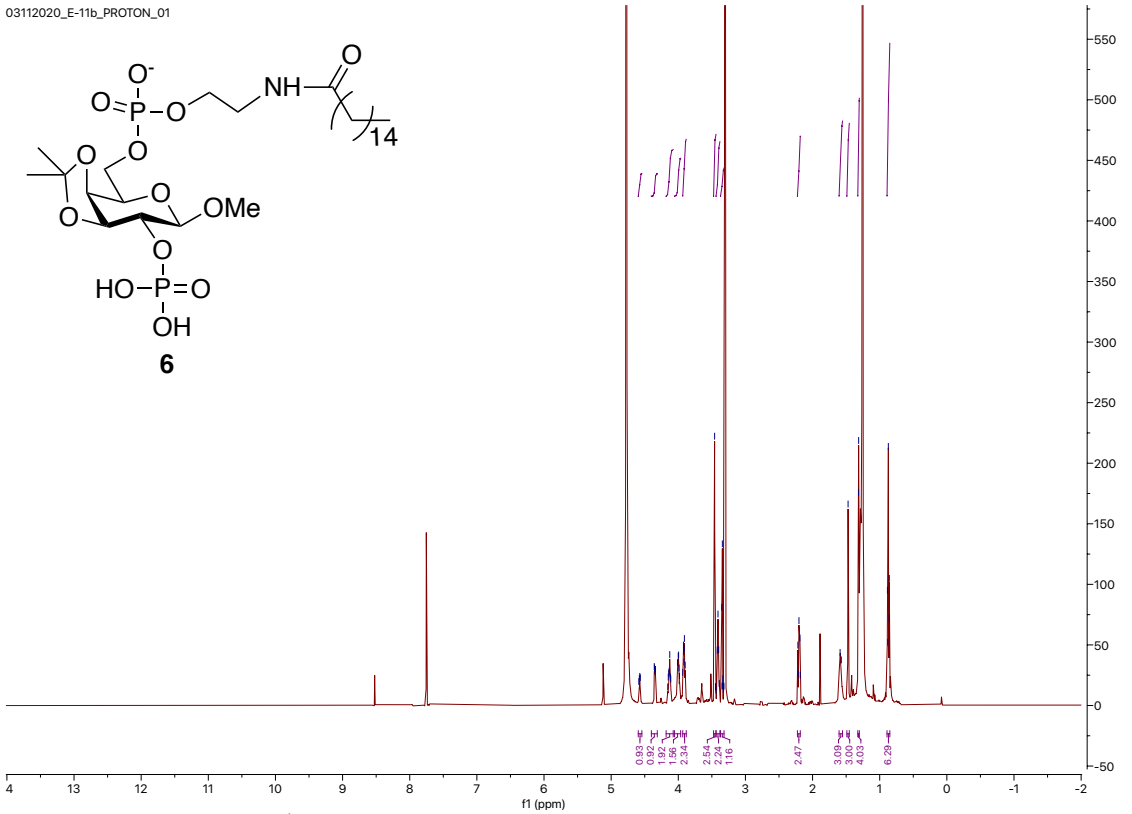

Figure S104. ^{1}H-NMR of **6** ($CDCl_3$: CD_3OD : D_2O 1 : 2 : 0.5, 500 MHz).

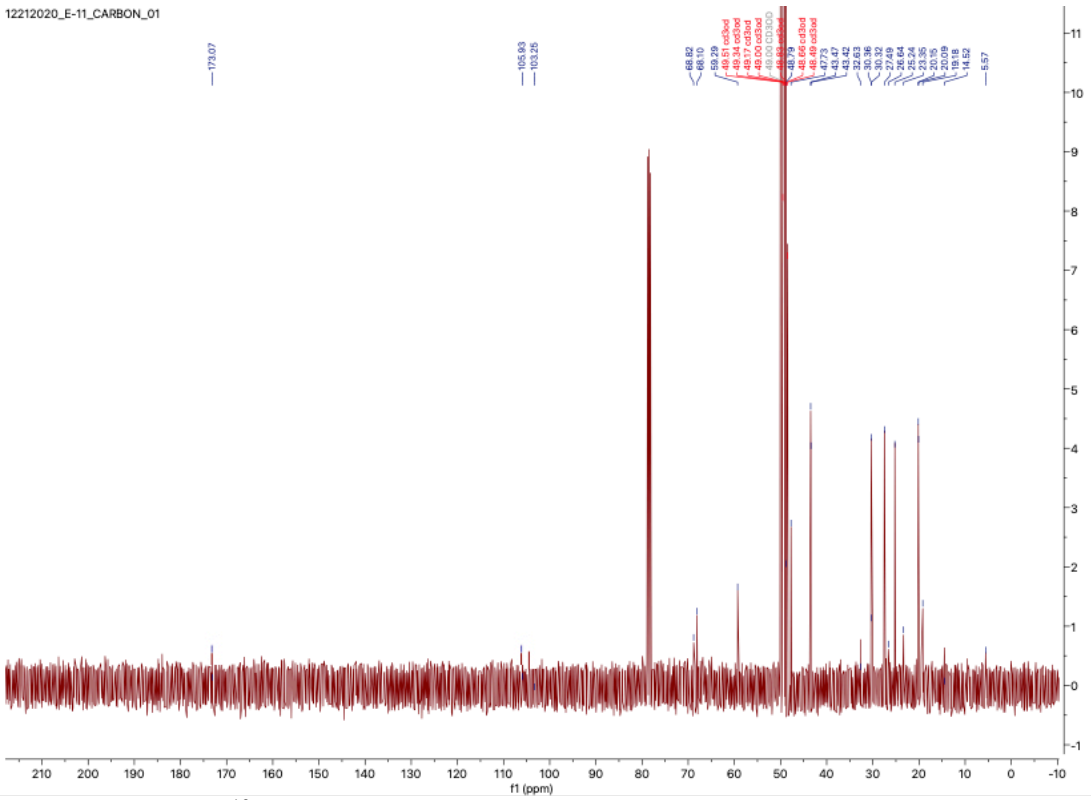

Figure S105. ^{13}C-NMR of **6** ($CDCl_3$: CD_3OD : D_2O 1 : 2 : 0.5, 125 MHz).

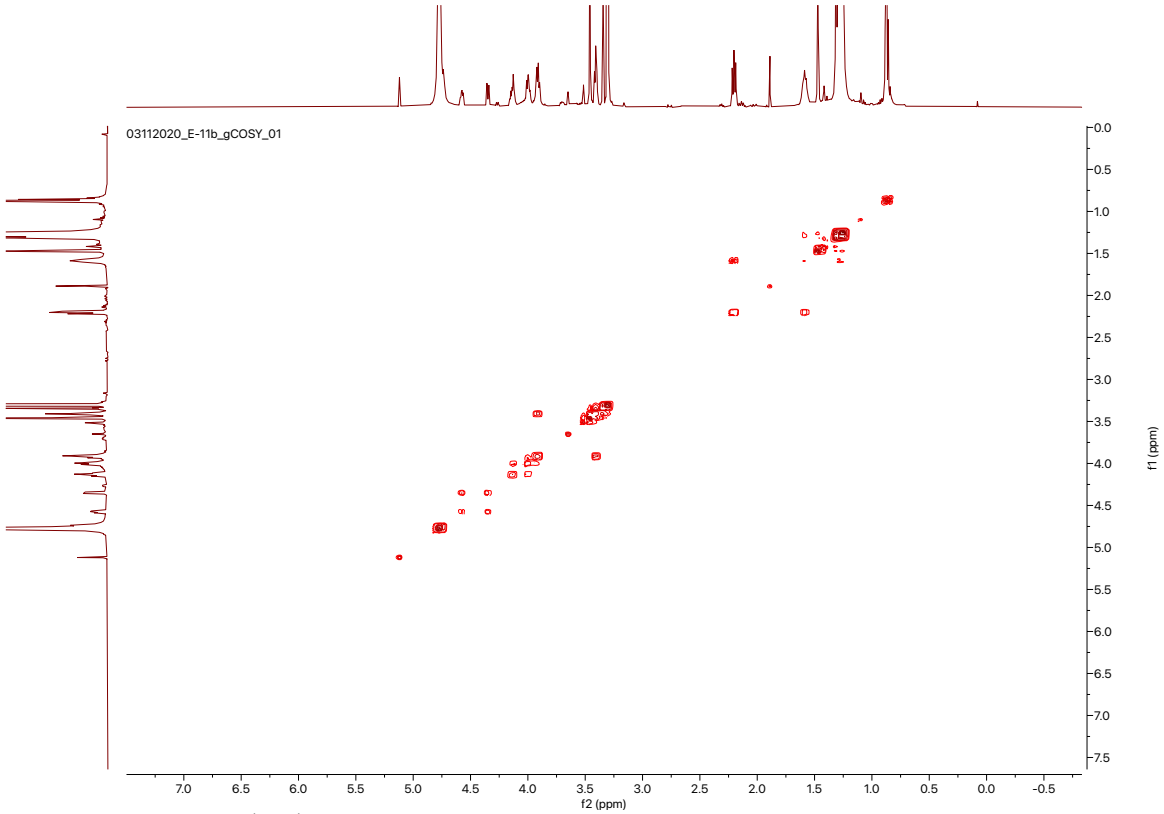

Figure S106. ^{1}H-^{1}H gCOSY of **6** ($CDCl_3$: CD_3OD : D_2O 1 : 2 : 0.5, 500 MHz).